Fibre-based Devices for Next Generation Photonics Communication Systems

YICHENG LAI

Doctor of Philosophy

ASTON UNIVERSITY

December 2003

Aston University

Fibre-based Devices for Next Generation Photonics Communication networks

Yicheng Lai

Doctor of Philosophy

December 2003

The future broadband information network will undoubtedly integrate the mobility and flexibility of wireless access systems with the huge bandwidth capacity of photonics solutions to enable a communication system capable of handling the anticipated demand for interactive services. Towards wide coverage and low cost implementations of such broadband wireless photonics communication networks, various aspects of the enabling technologies are continuingly generating intense research interest. Among the core technologies, the optical generation and distribution of radio frequency signals over fibres, and the fibre optic signal processing of optical and radio frequency signals, have been the subjects for study in this thesis.

Based on the intrinsic properties of single-mode optical fibres, and in conjunction with the concepts of optical fibre delay line filters and fibre Bragg gratings, a number of novel fibre-based devices, potentially suitable for applications in the future wireless photonics communication systems, have been realised. Special single-mode fibres, namely, the high birefringence (Hi-Bi) fibre and the Er/Yb doped fibre have been employed so as to exploit their merits to achieve practical and cost-effective all-fibre architectures.

A number of fibre-based complex signal processors for optical and radio frequencies using novel Hi-Bi fibre delay line filter architectures have been illustrated. In particular, operations such as multichannel flattop bandpass filtering, simultaneous complementary outputs and bidirectional nonreciprocal wavelength interleaving, have been demonstrated. The proposed configurations featured greatly reduced environmental sensitivity typical of coherent fibre delay line filter schemes, reconfigurable transfer functions, negligible chromatic dispersions, and ease of implementation, not easily achievable based on other techniques.

A number of unique fibre grating devices for signal filtering and fibre laser applications have been realised. The concept of the superimposed fibre Bragg gratings has been extended to non-uniform grating structures and into Hi-Bi fibres to achieve highly useful grating devices such as overwritten phase-shifted fibre grating structure and widely/narrowly spaced polarization-discriminating filters that are not limited by the intrinsic fibre properties.

In terms of the fibre-based optical millimetre wave transmitters, unique approaches based on fibre laser configurations have been proposed and demonstrated. The ability of the dual-mode distributed feedback (DFB) fibre lasers to generate high spectral purity, narrow linewidth heterodyne signals without complex feedback mechanisms has been illustrated. A novel co-located dual DFB fibre laser configuration, based on the proposed superimposed phase-shifted fibre grating structure, has been further realised with highly desired operation characteristics without the need for costly high frequency synthesizers and complex feedback controls.

Lastly, a novel cavity mode condition monitoring and optimisation scheme for short length, linear-cavity fibre lasers has been proposed and achieved. Based on the concept and simplicity of the superimposed fibre laser cavities structure, in conjunction with feedback controls, enhanced output performances from the fibre lasers have been achieved. The importance of such cavity mode assessment and feedback control for optimised fibre laser output performance has been illustrated.

Keywords: wireless photonics communication systems, fibre-based devices, optical fibre delay line filters, fibre Bragg gratings, superimposed gratings, fibre lasers.

To mum and dad

To my only and dearest *bro*

To my lovely little fat-legged *fish*

Acknowledgements

My utmost gratitude goes to my supervisor, Professor Ian Bennion, for his guidance, care, support, and encouragement throughout these years. There are no words I can find to express better my respect and sincere thanks to this great scientist, educator and mentor.

I would not have the strength and endurance to pursue this research course if not for the patience, understanding, encouragement and support from my parents, my brother and Fish. They have helped and supported me in many aspects of livelihood to allow me to be able to focus on my research.

I would like to acknowledge the efforts A/Prof. Cheng Tee Hiang and A/Prof Lu Chao went through some years back to support my overseas attachment to Aston University. Unaware to them, they have created a vital turning point of my life.

My sincere thanks go to Dr Wei Zhang for his dedicated guidance and discussions throughout my Ph.D. years. I owe much of my research results to him and really enjoyed every minute working with him.

Needless to mention, my sincere appreciations go to my '*quasi*' supervisor, Dr John Williams, for his inspirational and interesting discussions throughout the course of my research studies. Under his guidance, these three years of research had been both enjoyable and fulfilling.

I would also like to express my sincere appreciations to Bert, Dr Lin Zhang, Dr Xuewen Shu, Dr Zhijian Huang, Dr Kate Sugden, Dr Kaiming Zhou, Dr Tom Allsop, Dr Donghui Zhao and Dr Jinsong Leng. Their ideas, skills and willingness to give assistance every time were vital to the completion of my Ph.D. Their outstanding characters have also been great learning models for me.

Last but not least, my deepest gratitude goes out to all my friends. Life in Birmingham would have been miserable without them.

I gratefully acknowledge the studentship supports from Indigo Photonics Limited and the Overseas Research Students Awards Schemes.

CONTENTS

List of Figures

Chapter 1: Introduction

1.1 Future broadband photonics communication systems

The amount of information dealt with and required each day has been rapidly and continuously increasing. What is indispensable to support this trend in the future is the development of broadband information network systems. In particular, there is no doubt that wireless access systems will get more and more important because of their attractive nature: mobility, relocatability and cost effective network installation [1]. In fact, the use of wireless radio waves (microwave/millimetre waves) for future broadband service provision seems assured as bands around 60GHz have been identified for this purpose: for example, the European Radiocommunications Office has identified two sub-bands (62-63GHz and 65-66GHz) for mobile broadband applications and interactive multimedia services (IMS) are being tried out by operators worldwide including BT in the UK [2][3]. Electromagnetic waves of micro/millimetre wavelengths are therefore expected to play indispensable roles in the future broadband communication systems for the *wireless last hop* to provide the tetherless connectivity that is expected to be in great demand.

Towards wide coverage and low cost implementation of such broadband wireless communication networks, integration of photonics and conventional microwave/millimetre wave technologies, the concept commonly referred to as *microwave/millimetre wave photonics* is inevitable [4]. Photonics technology offers a possible breakthrough against difficulties in the conventional wireless technologies. It overcomes bandwidth limitations and opens up new possibilities to both broadband signal transmissions as well as signal processing [4].

Among the core technologies in microwave/millimetre wave photonics that attract huge interest, the fibre optic millimetre wave (mm-wave) link has witnessed intense research in the recent years [4][5]. The concept of future provision of broadband interactive services over the wireless media at mm-wave frequencies requires multiple antenna remote stations (RS) to provide the wireless connectivity to users via radio links. The antenna RSs are networked to a central office (CO) which performs all the switching, routing and various other signal processing functionalities [6]. Due to the large propagation losses at high radio frequencies, the coverage areas of the RSs are small, leading to a pico- or micro-cellular wireless network architecture. The small coverage areas in conjunction with high propagation losses provide a unique advantage in managing scarce radio bandwidth by utilizing efficient frequency reuse and by deploying sectorizations of the RS antennas' coverage areas [7]. The consequent increase in the number of antenna RSs in an area and the need for efficient, low cost broadband communication links between the multiple RSs and the CO becomes a challenge for the lossy, inflexible wired transmissions in coaxial cables. Optical fibre as an ultra broadband, flexible, low loss transmission link offers the best solution to date.

Optical fibre is well known as a transmission medium with an enormous bandwidth of about 4THz for the 1.55μm wavelength region where the erbium doped fibre amplifiers (EDFA) are most effective [2]. Their advantages in terms of low loss (fractional decibels/km), high immunity to electromagnetic interference and most importantly large bandwidth-length product (on the order of 100GHz·km for single-

mode fibres) enable effective deployment to provide the broadband interconnections of multiple antenna RSs with the CO [2][5]. In addition, scaleable and easy-to-manage fibre-fed network can be realised by incorporating wavelength division multiplexing (WDM) technology [8]. Optical fibres are of interest also due to their ability to process high-speed signals directly in the optical domain thus avoiding costly electro-optic or opto-electronic conversions that eventually create an electronic bottleneck [9]. Furthermore, various other photonics devices can be integrated into optical fibres for signal conditioning or filtering functions.

The merging of photonics and wireless technologies therefore opens up new perspectives to future broadband photonics communication systems that are capable of handling the anticipated demand for interactive services. Various aspects of the enabling technologies behind such a communication system are hence continuingly generating intense research interest.

1.2 Challenge: Radio over fibre

The restricted spectrum available at microwave frequencies has been a major problem for wireless communication and new frequency bands situated in the millimetre wave region between 30-70GHz have been considered [5][10]. In conjunction with the distribution of radio wave signals over optical fibres, it promises a low cost and low loss high capacity wireless communication network for the future [11]. For any wireless radio network systems to be viable, the cost of the infrastructure must be lower than is currently the case. Several technological choices for the distribution of radio signals to and from the remote stations are considered and they can be categorized into 1) radio frequency over fibre (radio-over-fibre) where the radio signals are transported to the RSs without the need for further upconversions; 2) intermediate frequency (IF) over fibre where lower frequency subcarriers are used to transport the radio channels with upconversions at the RSs; and 3) baseband transmission where the data is upconverted to the required radio frequency at the remote antenna sites [12].

In contrast with radio-over-fibre transmission, the use of IF or baseband transmissions allow signals to be transported over longer fibre distances without detrimental effects from the chromatic dispersion of optical fibres [12][13]. In addition, both IF and baseband transmissions can exploit the use of mature microwave and digital electronic hardware at the remote antenna station. However the subsequent need for a local oscillator for frequency upconversion increases the cost and complexity of the RS equipment.

On the other hand, radio-over-fibre signal transmission has the advantage that the RS architecture is simplified since the need for remote frequency up- and down converting mixers and local oscillators is eliminated. The reduction of equipment required at the remote antenna site leads to small, lightweight, low cost antenna units with low power consumptions. In addition, the generation, control, routing and processing of the radio wave signals are centralized where equipment can be shared between a number of antenna sites and where it can be protected from environmental factors [12][14]. Alleviation of the undesired fibre chromatic dispersion effects through, for example, single side band modulation using fibre grating filters have been proposed [15][16]. Optical radio frequency modulation and generation schemes that are tolerant to the effects of fibre dispersion are also being actively investigated [3][13][17].

Despite the fact that radio-over-fibre is most likely to be the cost-effective enabling technology for broadband wireless service provision, the deployment of the fibre infrastructure in these systems still rests primarily on the availability of a radio wave (micro/millimetre wave) optical transmitter. The transmission

technique requires radio signals to be placed on an optical carrier and distributed by means of the optical fibre network to the points of radiations (i.e. remote antenna sites). Millimetre wave modulation using currently available optical sources is not straightforward. Various techniques proposed to date, ranging from external modulations to injection locking as well as opto-electronic phase-locked loop configurations, involve relatively costly and complex feedback systems and/or special waveguide structures not commercially available in order to generate high performance radio frequency signals [18]-[20]. As a result, effective low cost techniques for optical generation of high spectral purity radio frequency signal remains a subject of intense research. This poses one of the key technology challenges in the future broadband photonics communication network systems.

1.3 Challenge: Signal processors

For successful implementation of fibre optic links in mass-market applications, a cost effective infrastructure is strongly required. Considering the architecture of the future fibre optic networks where a large number of remote antenna stations will be connected to a single central office, the simplicity of the RS is obviously a critical factor. Much research has been directed towards optimising the remote station, both in terms of the transmission technique as well as the signal processing [21][22] of the optical and radio wave signals.

Optical technologies, for many years, have been considered for a wide variety of signal processing tasks such as convolution, correlation, matrix operation and frequency filtering [9][23]. Optical filters, in particular, are of interest due to their ability to process high-speed signals, so removing the costly electro-optic/opto-electronic conversions and the electronic limitations for processing high-speed signals that are already in the optical domain [9]. Wide band processing of microwave and millimetre wave signals is limited by the modulation and detection frequency responses of currently available electronic technologies even though they are very effective at lower frequencies. Direct modulation of laser diodes may reach beyond 30GHz (40GHz with external modulators) for some special structures and available fastest detection devices are in the range of 60GHz [2][24].

While single-mode optical fibre has been used most often in connection with communication and sensing systems, it can also be used in configurations that are capable of processing broadband signals. Of special interest is an optical network built with fibre element devices that integrate seamlessly into the system fibre links. Using fibre optic based signal processors, direct interfacing of the devices with the high-speed communication system, in principle, can be achieved easily.

To date, key photonics technologies such as optical delay lines [22], fibre gratings [25] and waveguide technologies [26] have been continuingly explored to help realise the necessary components and infrastructure for an effective, efficient and low cost fibre optic network. Common objectives include low loss, reconfigurable transfer characteristics, low dispersion, wide operation bandwidth and good isolation. The photonics processing of optical and radio wave signals using fibre-based devices hence remains of considerable research interest.

1.4 Objectives

The objectives of this research can be broadly divided into two fields of interest:

1) To explore and realise fibre-based optical transmitters suitable for use in fibre wireless communication systems.

2) To explore and realise fibre-based signal processors suitable for both optical and radio frequency signals processing.

In terms of the fibre-based optical transmitters, it is the aim of this research to study and explore the use of fibre grating laser technology instead of the conventional approach based on semiconductor lasers. Emphasis is placed on studying the effectiveness of utilizing the lasing characteristics of fibre lasers. Furthermore, exploitation and integration of unique fibre grating structures in fibre laser configurations to achieve the desired high performance lasing operation are investigated. On the aspect of fibre optic signal processors, characteristics (in terms of physical and light-guiding properties) of special fibres are studied and utilized so as to realise different all-fibre device architectures with integrated desirable characteristics and which overcome common limitations imposed by current technologies on system designs. Overall, the focus in both aspects emphasizes exploitation of the various advantages of optical fibres and related technologies, taking into consideration issues like fabrication complexities and cost to realise some fibre-based devices potentially applicable in next generation broadband photonics communication systems.

1.5 Outline of thesis

This thesis consists of 8 Chapters and, overall, it covers the relevant aspects of single-mode optical fibres, its related technologies, and novel fibre devices based on these technologies realised in this research.

Following the brief introduction, in Chapter 1, to some of the key aspects of future broadband photonics communication network, and the motivations and objectives of this research, Chapter 2 seeks to highlight some of the important characteristics of single-mode optical fibres. Relevant properties of single-mode optical fibres to this research are emphasized and two special single-mode optical fibres that form the basis of the devices described in this thesis are highlighted.

Chapter 3 proceeds to discuss one of the key fibre device technologies known as the optical fibre delay line filter. Important concepts behind fibre optic delay line filter configurations are outlined. Experimental applications of such filter configurations using high birefringence (Hi-Bi) fibres for a number of different complex signal processing operations are illustrated and discussed.

Chapter 4 then introduces the fibre Bragg grating technology and the characteristics of various fibre grating structures adopted in this research. Novel fibre grating structures are further illustrated and form the basis of the fibre grating devices covered in subsequent Chapters.

Chapter 5 describes a novel tunable fibre grating transmission filter configuration utilizing pump-induced thermal effects in doped fibres. Detailed experimental results of various architectures based on this novel concept are illustrated and discussed.

Chapter 6 describes another important application of fibre grating technology – the fibre laser. A brief review of rare-earth doped fibre lasers is given and operating characteristics of distributed feedback

(DFB) fibre lasers are highlighted. Novel applications of the DFB fibre lasers for optical generation of high frequency signals are illustrated and discussed. A unique fibre laser configuration is further demonstrated.

Chapter 7 discusses the issues with mode stabilization and optimisation of fibre laser operations. A brief review of some of the wavelength monitoring and longitudinal mode stabilization schemes for fibre lasers is given. Some of the key factors influencing the output performance of fibre lasers are highlighted. A novel cavity mode condition monitoring and feedback scheme for fibre lasers is demonstrated. Experimental results based on two linear-cavity fibre laser configurations are illustrated and discussed.

Finally, Chapter 8 concludes the work carried out in the course of this research.

1.6 Major contributions of the thesis

Important results obtained in the course of this research are described in detail in Chapter 3 to Chapter 7. The major results achieved can be summarized as follows:

1) Novel Hi-Bi fibre delay line filter architectures for complex signal processing of optical and radio wave signals have been proposed and demonstrated. In particular, operations like multichannel flattop bandpass filtering, simultaneous complementary outputs and bidirectional nonreciprocal wavelength-interleaved filtering, not easily achievable based on other techniques, have been illustrated. The proposed configurations feature various advantages such as greatly reduced environmental sensitivity typical of coherent fibre delay line filter schemes, reconfigurable transfer function, negligible chromatic dispersion, and ease of implementation. An intuitive approach, based on a series of cross-sectional views and ray arrows, to analyse the filter transfer response has been further demonstrated.
2) Unique fibre grating structures based on superimposed phase-shifted fibre gratings and superimposed uniform fibre Bragg gratings in Hi-Bi fibre have been proposed and illustrated. The characteristics of these grating structures have been utilized to enable a novel fibre laser configuration for optical generation of high frequency signals in the millimetre wave regime and beyond. Besides its structural simplicity, ease of fabrication and flexibility in the frequency achievable, the proposed fibre laser, in contrary to conventional techniques, enables low phase noise, narrow linewidth beat signal without the need to employ high frequency electronic devices or complex feedback controls.
3) An optically tunable fibre grating transmission filter configuration based on pump-induced thermal effects in short sections of doped fibres has been proposed and demonstrated for the first time. Different architectures, namely, the single phase-shifted fibre grating, the dual phase-shifted fibre grating and the Fabry-Perot multichannel filter have been demonstrated with excellent spectral responses, requiring only very low power-distance product.
4) Based on the concept and simplicity of superimposed fibre gratings structures, a direct real-time cavity mode assessment and optimisation scheme for fibre laser has been proposed and demonstrated for the first time. The proposed scheme enables cavity mode conditions monitoring, stabilization and optimisation for enhanced output performance from the fibre laser. Optimisation of the operation of short linear cavity fibre laser configurations, namely,

the distributed feedback (DFB) fibre laser and the distributed Bragg reflector (DBR) fibre laser have been demonstrated for the first time.

1.7 References

[1] J.R. Forrest, "Communication networks for the new millennium", *IEEE Trans. Microwave Theory and Tech.*, 47(12), pp. 2195-2201, 1999.

[2] L. Noël, D. Wake, D.G. Moodie, D.D. Marcenac, L.D. Westbrook, D. Nesset, "Novel techniques for high capacity 60GHz fibre radio transmission systems", *IEEE Trans. Microwave Theory and Tech.*, 45(8), pp. 1416-1423, 1997.

[3] D. Wake, C.R. Lima, P.A. Davies, "Optical generation of millimetre wave signals for fibre-radio systems using a dual mode DFB semiconductor laser", *IEEE Trans. Microwave Theory and Tech.*, 43(9), pp. 2270-2276, 1995.

[4] M. Tsuchiya, T. Hoshida, "Nonlinear photodetection scheme and its system applications to fibre-optic millimetre-wave wireless down links", *IEEE Trans. Microwave Theory and Tech.*, 47(7), pp. 1342-1350, 1999.

[5] H. Ogawa, D. Polifko, S. Banba, "Millimeter-wave fibre optic systems for personal radio communication", *IEEE Trans. Microwave Theory and Tech.*, 40(12), pp. 2285-2292, 1992.

[6] J.J. O'Reilly, P.M. Lane, "Remote delivery of video services using mm-waves and optics", *J. Lightwave Technol.*, 12(2), pp. 369-375, 1994.

[7] A. Nirmalathas, D. Novak, C. Lim, R.B. Waterhouse, "Wavelength reuse in the WDM optical interface of a millimetre-wave fibre-wireless antenna base station", *IEEE Trans. Microwave Theory and Tech.*, 49(10), pp. 2006-2012, 2001.

[8] G.H. Smith, D. Novak, C. Lim, "A millimetre-wave full duplex fibre radio star tree architecture incorporating WDM and SCM", *IEEE Photon. Technol. Lett.*, 10, pp. 1650-1652, 1998.

[9] K.P. Jackson, S.A. Newton, B. Moslehi, M. Tur, C.C. Cutler, J.W. Goodman, H.J Shaw "Optical fibre delay-line signal processing", *IEEE Trans. Microwave Theory and Tech.*, 33(3), pp.193-209, 1985.

[10] E. Hashimoto, A. Takada, Y. Katagiri, "High frequency synchronized signal generation using semiconductor lasers", *IEEE Trans. Microwave Theory and Tech.*, 47(7), pp. 1206-1218, 1999.

[11] A.J. Cooper, "Fibre/radio for the provision of cordless/mobile telephony services in the access network", *Electron. Lett.*, 26, pp. 2054-2056, 1990.

[12] C. Lim, A. Nirmalathas, D. Novak, R. Waterhouse, G. Yoffe, "Millimeter-wave broadband fibre wireless system incorporating baseband data transmission over fibre and remote LO delivery", *J. Lightwave Technol.*, 18(10), pp. 1355-1363, 2000.

[13] H. Schmuck, "Comparison of optical millimetre wave system concepts with regard to chromatic dispersion", *Electron. Lett.*, 31, pp. 1848-1849, 1995.

[14] J. Park, K.Y. Lau, "Millimetre wave (39GHz) fibre-wireless transmission of broadband multichannel compressed digital video", *Electron. Lett.*, 32, pp. 474-476, 1995.

[15] J. Park, W.V. Sorin, K.Y. Lau, "Elimination of fibre chromatic dispersion penalty on 1550nm millimetre wave optical transmission", *Electron. Lett.*, 33, pp. 512-513, 1997.

[16] J. Marti, J.M. Fuster, R.I. Laming, "Experimental reduction of chromatic dispersion effects in lightwave microwave/millimetre wave transmissions employing tapered linearly chirped fibre gratings", *Electron. Lett.*, 33, pp. 1170-1171, 1997.

[17] C. Lim, A. Nirmalathas, D. Novak, "Techniques for multichannel data transmission using a multisection laser in millimetre wave fibre radio systems", *IEEE Trans. Microwave Theory and Tech.*, 47(7), pp. 1351-1357.

[18] Z. Ahmed, H.F. Liu, D. Novak, M. Pelusi, Y. Ogawa, D.Y. Kim, "Low phase noise millimetre wave signal generation using a passively modelocked monolithic DBR laser injection locked by an optical DSBSC signal", *Electron. Lett.*, 31(15), pp. 1254-1255, 1995.

[19] Y.J. Wen, H.F. Liu, D. Novak, Y. Ogawa, "Millimeter wave signal generation from a monolithic semiconductor laser via subharmonic optical injection", *IEEE Photon. Technol. Lett.*, 12(8), pp. 1058-1060, 2000.

[20] J.B. Georges, D.M. Cutrer, O. Solgaard, K.Y. Lau, "Optical transmission of narrowband millimetre wave signals", *IEEE Trans. Microwave Theory and Tech.*, 43(9), pp. 2229-2240, 1995.

[21] B. Moslehi, J.W. Goodman, M. Tur, H.J. Shaw, "Fibre optic lattice signal processing", *Proc. IEEE*, 72, pp. 909, 1984.

[22] M.Y. Frankel, R.D. Esman, "Fibre-optic tunable microwave transversal filter", *IEEE Photon. Technol. Lett.*, 7(2), pp. 191-193, 1995.

[23] M. Tur, J.W. Goodman, B. Moslehi, J.E. Bowers, H.J. Shaw, "Fibre optic signal processor with applications to matrix vector multiplication and lattice filtering", *Optics Lett.*, 7(9), pp. 463-465, 1982.

[24] S. Tedjini, A. Ho-Quoc, D.A.M. Khalil, "All-optical networks as microwave and millimetre wave circuits", *IEEE Trans. Microwave Theory and Tech.*, 43(9), pp. 2428-2434, 1995.

[25] C.R. Giles, "Lightwave applications of fibre Bragg gratings", *J. Lightwave Technol.*, 15(8), pp. 1391-1404, 1997.

[26] T. Suhara, H. Nishihara, "Integrated optics components and devices using periodic structures", *IEEE J. Quantum Electron.,* QE-22, pp. 845-867, 1986.

Chapter 2: Single-mode optical fibres

2.1 Overview

The use of optical fibre is revolutionizing many areas of science and engineering. Single-mode fibre (SMF), in particular, is capable of transmitting modulated signals with bandwidths exceeding 100GHz over long distances with losses typically less than 0.2dB/km [1]-[4]. Since only one mode is guided, its phase and polarization can potentially be determined, utilized or manipulated at any point along the length of the fibre. As a result, single-mode optical fibre is revolutionizing system links as well as device configurations. Various device technologies based on SMF have been proposed to date, all of which take advantage of the intrinsic superior physical and propagation properties of optical fibres. This chapter seeks to give a basic review of the key properties of single-mode optical fibre. Characteristics of two variants of conventional single-mode fibres (special fibres) are highlighted.

2.2 Single-mode optical fibre characteristics

The single-mode step-index fibre is the most widely adopted fibre in various communication systems and device configurations. It consists of a narrow dielectric core (diameter on the order of 9μm) of higher refractive index surrounded by a lower index cladding (diameter on the order of 125μm) such that the number of propagation modes within the wavelength range of interest (around 1.5μm) reduces to one. Various physical parameters determine the performance characteristics of the fibre and they include: the fibre geometry, concentrations of dopants within the core/cladding, types of dopants within the core/cladding, effective refractive index difference between the core and the cladding and the cross sectional index profile. The key performance parameters, namely the insertion loss, dispersion, and birefringence are important considerations and determine its application relevance in communication systems and device architectures. These important features of the single-mode optical fibre characterize the performance of the fibre-based devices discussed in this research. Due to the dependency of the fibre performance characteristics on the physical parameters, a large number of fibre variants for different applications have been conceived. Two commonly known special fibres types namely, rare-earth doped fibres and high-birefringence (Hi-Bi) fibres, are discussed.

2.2.1 Insertion loss

The premier feature of optical fibre is its extremely low loss, which has made it the dominant transmission medium for long link lengths. In fact, to date optical fibre links provide the lowest loss connection between two points in either digital- or analogue-formatted signal transmissions. The loss characteristics of optical fibres result from a number of wavelength-dependent mechanisms including scattering, absorption and wavelength-independent externally induced losses such as microbending. Rayleigh scattering is the dominant loss mechanism in optical fibres below a wavelength of about 1.6μm

[1][5]. This loss mechanism is due to the scattering of the propagating electromagnetic wave by small (on the order of a few tenths of a micron) irregularities in the medium. The attenuation coefficient per unit length for Rayleigh scattering is proportional to λ^{-4}, where λ denotes the optical wavelength, and as a result the attenuation is relatively lower at longer wavelengths than at shorter wavelengths.

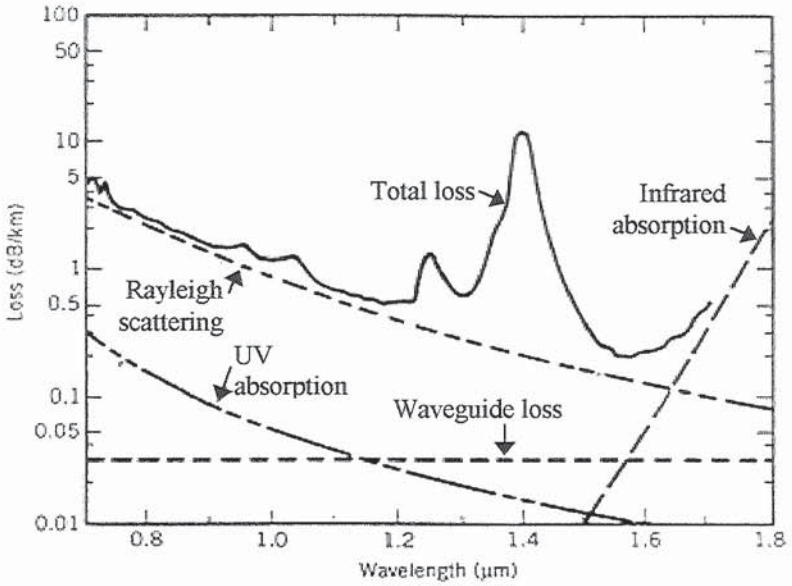

Figure 2.1 Variation of attenuation with wavelength for a single-mode optical fibre. Diagram obtained from [6].

At longer wavelengths, infrared absorption losses resulting from the vibrations of the bonds between the glass constituents limit most optical fibre systems to operation at wavelengths of about 1.6μm and below. Unwanted materials or impurities within the fibre then contribute to absorption losses. Molecular hydrogen and hydroxyl ions (OH-ions) formed by chemical interaction between diffused hydrogen and glass are the dominant impurities in typical single-mode optical fibres, generating loss peaks at wavelengths of 1.25 μm and 1.39 μm respectively [7][9]. Gross imperfections, microbends and waveguide scattering all give rise to additional wavelength-independent losses. Each of these losses is very small over a particular range of optical wavelengths. However the combined effect of these losses yields a composite loss profile as shown in Figure 2.1 that limits the operation of fibre systems to a spectral band from the visible to the near infrared (0.6μm-1.6μm) where the losses are low with a minimum of approximately 0.2dB/km near 1.5μm.

As well as being an important consideration in fibre link transmission, the loss characteristic of single-mode optical fibre in device applications demands equal attention. This is particularly so in terms of ionizing radiation-induced loss in some fibre-based device fabrication processes, the most notable example being fibre grating formation using intense UV radiation. In general, due to the fact the molecular bonds in multi-component optical fibres (doped fibres) are vulnerable, common single-mode fibres doped with GeO_2 or B_2O_2 are known to be more sensitive to the effects of radiation that those of pure silica [9]. In the case of the fibre grating fabrication process, the exposure of hydrogen-loaded optical fibres to intense UV radiation

leads to a dissociation of the molecules and the formation of Si-OH and/or Ge-OH bonds. This is accompanied by the formation of Ge oxygen-deficient centres that creates the desired index change. The presence of molecular hydrogen in optical fibres as mentioned above has been known to increase the absorption loss [7]. Furthermore, the formation of these OH^- ions due to UV radiation enhances peak loss associated with Si-OH at 1.39μm and Ge-OH at 1.42μm [7][10]. It is worth remarking that the overall loss induced through the presence of molecular hydrogen or hydroxyl ions is much less at the 1.5μm window, which is the key operation band that modern communication systems and devices are based on.

2.2.2 Dispersion

Aside from the loss characteristics of single-mode fibres that can limit the distance that an optical signal can propagate, a phenomenon known as chromatic dispersion can also limit the distance over which the fibre optic signal can travel without significant distortions. Chromatic dispersion describes the fact that the speed of signal propagation in the fibre depends on the wavelength of the light. The dominant dispersive mechanism depends on the waveguide properties of the fibre and the spectrum of the optical source [5]. Since the single-mode optical fibre supports one propagation mode only, unlike multimode fibres, it does not suffer from the effect of inter-modal dispersion. Single-mode fibre, however, does exhibit an amount of dispersion (on the order of 17ps/nm.km) as a result of material dispersion and waveguide dispersion [11]. Waveguide dispersion arises because the way in which the waves match the boundary conditions at the core-cladding interface depends on their frequencies. As a result, the propagating phase velocity is a function of the wave frequency. Material dispersion on the other hand relates to the fact that the speed of transmission of the electromagnetic waves through a transparent material is influenced by the interaction of the waves with the atoms of the material. Because the interaction is a function of the wave frequency, the velocity of propagation of the waves hence depends on the wave frequency as well. Although the relationship between material dispersion and waveguide dispersion is quite complex, to a first approximation they may be added algebraically to yield the total dispersion commonly called chromatic dispersion.

The overall dispersion characteristic of a standard single-mode fibre is as shown in Figure 2.2 [11]. It is evident that the major contribution to the dispersion of standard fibre comes from the material dispersion. More importantly, the resultant chromatic dispersion (Trace D) passes through a point of minimum dispersion at λ_0 (~1.3 μm) around which is defined commonly as the second telecommunication window. The waveguide dispersion contribution is negligible except near the zero-dispersion wavelength λ_0 where the two dispersion effects become comparable. The dispersion value changes sign about λ_0 hence giving rise to two distinct regimes, the normal regime where D is negative and the anomalous regime where D is positive. In the anomalous dispersion regime, short wavelengths travel faster than long wavelengths and so light propagating through a fibre with anomalous dispersion will emerge with the blue end of the spectrum leading the red. The opposite is true for the normal dispersion regime.

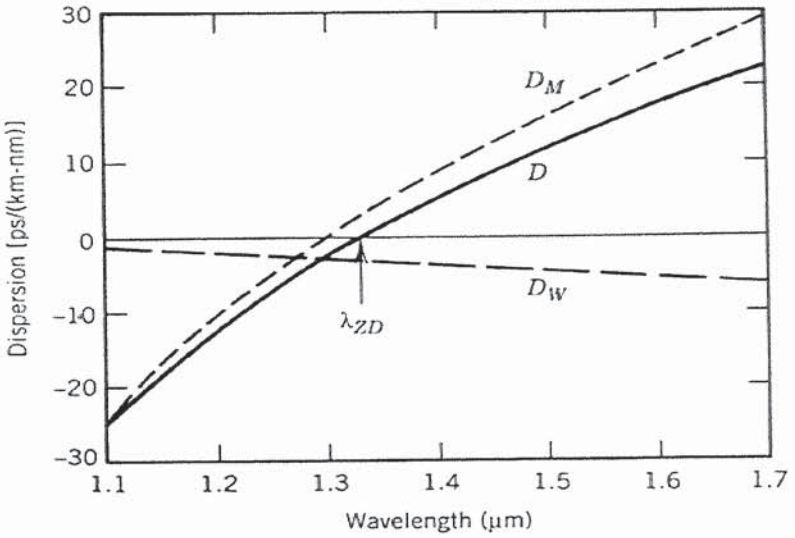

Figure 2.2 Dispersion characteristics of a standard single-mode fibre. Trace D_M denotes the material dispersion while Trace D_W denotes the waveguide dispersion. The resultant dispersion (Trace D) characteristic exhibits a point of zero dispersion at wavelength λ_0. Diagram obtained from [12].

Despite the fact that standard single-mode fibre exhibits a low loss region around 1.5μm, it suffers from a noticeable amount of dispersion of 17ps/nm·km as shown in Figure 2.2. Efforts to modify the dispersion characteristics of single-mode fibre saw the realisation of dispersion-shifted fibre, dispersion compensated fibre as well as dispersion flattened fibre [11][13]. The technologies behind these fibres are essentially based on the fact that modification of the waveguide parameters like geometry, cross sectional index profiles as well as core dopants modifies the waveguide or material dispersion contributions and thereby influences the resultant dispersion characteristics [14].

In terms of device applications, the low amount of dispersion over short fibre lengths (few hundred metres) poses little concern for many single-mode fibre device architectures. In applications like fibre delay line structures, the absence of any significant dispersion effect is attractive for implementation of wide bandwidth complex signal processing functions. Consider, for example, a 100GHz free spectral range delay line filter based on fibre length of 10m: the dispersion incurred over a 20nm (2.5THz) operation bandwidth is 3.4ps (taking the fibre dispersion = 17ps/nm·km) which amounts to a negligible fractional free spectral range (FSR) distortion of <0.4% over the entire operation bandwidth. Detailed description and analysis of the fibre delay line device is covered in Chapter 3.

In terms of transmission, due to the length of the fibre involved, the dispersion effect plays a significant role in determining the maximum transmission bandwidth-distance possible. For an input optical source, the maximum modulation bandwidth is limited by the fact that its constituent spectral components over the occupied wavelength spectral range σ (root mean square linewidth) suffer differential delay after propagating over a fibre of length L. It can be shown that the bandwidth-distance product $\Delta f \cdot L$ is given by [15]

$$\Delta f \cdot L = \frac{250}{\sigma |D|} \tag{2.1}$$

where $\Delta f \cdot L$ is in GHz·km, σ is in nm and dispersion coefficient D is in ps/nm·km. Through operating at the optimal dispersion wavelength or by reducing the dispersion at the optical carrier frequency (by means of dispersion shifted fibre etc.), single-mode fibre offers bandwidth-distance products capable of exceeding 100GHz·km.

Chromatic dispersion has an important implication to radio-over-fibre transmission links in a wireless photonics communication system [16]. Conventionally, using external modulators (intensity modulation schemes), the propagation of the modulated signal in the fibre as a function of time, t and distance, z can be described by the electric field $\bar{E}(t, z)$

$$\bar{E}(t,z) = \bar{E}_0 \cdot \left\{ \cos(\omega_0 t - \beta_0 z) + \frac{m}{2} \{ \cos[(\omega_0 + \omega_m)t - \beta_+ z] + \cos[(\omega_0 - \omega_m)t - \beta_- z] \} \right\} \tag{2.2}$$

where ω_0 denotes the angular carrier frequency and the last two terms are the sidebands at frequencies $\pm\omega_m$ relative to the carrier frequency. β_0, β_- and β_+ denote the propagation constants at the respective frequencies. Since the refractive index of the fibre is a function of the wavelength, the propagation constants for the two sidebands are different. The propagation constant $\beta(\omega)$ around the optical carrier frequency can be expressed by the Taylor expansion given by [17]

$$\beta(\omega) = \beta_0 + \beta_1(\omega - \omega_0) + \frac{1}{2}\beta_2(\omega - \omega_0)^2 + ... \tag{2.3}$$

where higher order dispersion terms are neglected and β_i denotes the i^{th} derivative of the propagation constant with respect to the frequency. The optical signal propagates in the fibre with the group velocity $1/\beta_1$ and the fibre dispersion D is related to the group velocity dispersion parameter β_2 by [17]

$$D = -\frac{2\pi c}{\lambda^2}\beta_2 \tag{2.4}$$

where dispersion D is in ps/nm·km. At the receiver end, the sidebands and the carrier are mixed generating a heterodyne signal component at the modulation frequency. From (2.2) through (2.4), the magnitude of the detected radio frequency (RF) current component at the modulation frequency, $I_{\omega m}$, after a transmission distance L can be expressed by [17]

$$I_{\omega m} = I_0 \cos(\frac{1}{2}\beta_2 L \omega_m^2) \tag{2.5}$$

where I_0 denotes a constant proportional to the average optical power. Evidently, the amplitude of the signal component varies with a cosine function and reaches a null whenever the argument is an odd multiple of $\pi/2$. This implies that at modulation frequencies given by

$$f_m = f_0\sqrt{\frac{N}{2 \cdot L \cdot c \cdot D}} \quad \text{where N = 1, 3, 5.....} \tag{2.6}$$

the dispersion-length product causes the components of the beat signal between the carrier and the sidebands to be in counter phase resulting in a cancellation of the photocurrents that manifest as dips in the frequency response as shown in Figure 2.3.

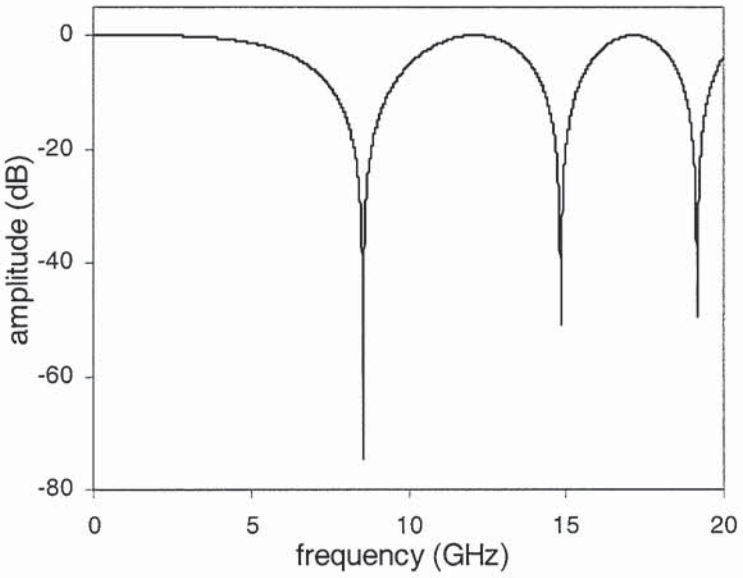

Figure 2.3 Simulated frequency response for a dual sideband signal transmission over 50km of fibre with a group delay dispersion of 17ps/nm·km.

The chromatic dispersion in fibres, hence, presents an important limiting factor for consideration in optical generation and distribution of radio wave signals, in particular where direct modulation of laser source or external amplitude modulation are concerned. It is worth remarking that various techniques have been proposed to date to overcome this dispersion-induced power fading using techniques like single sideband modulation [18], phase diversity [19] and a self-heterodyne coherent scheme [16]. The dispersion-induced impairment forms one of the key considerations in radio wave signal generation and distribution over fibres. It follows that the absence of the chromatic dispersion effects in the heterodyne technique plays a key role in the choice for high frequency RF generation and distribution over fibres. Further details are presented in Chapter 6.

2.2.3 Birefringence

Despite the name, light actually propagates within a single-mode fibre in two polarization modes corresponding to the two degenerate orthogonal eigen-modes. For an ideal single-mode fibre with a perfect circular core and uniform cross-sectional refractive index distribution, the polarization modes are degenerate with identical propagation constants and phase velocities such that the injected light propagates through the fibre without suffering any changes in its state of polarization. In reality, single-mode fibre exhibits some degree of refractive index asymmetry, an artifact largely due to variation in the fibre drawing and cabling processes, that breaks the circular symmetry and causes the polarization modes to propagate with slightly different phase velocities. Consequently, the two orthogonal modes slip out of phase relative to each other during propagation and distort the input state of polarization. These polarization components exit the fibre with a time delay between them commonly known as the differential group delay (DGD). The term birefringence refers to the physical asymmetry in the index of refraction that allows different polarization modes to travel at different speeds. It is a measure of the difference in refractive index experienced by the two polarization modes propagating within the fibre. Due to birefringence, two principal propagation axes aligned along the propagation paths of the two polarized eigen-modes are formed, commonly referred to as the fast and slow axes respectively.

Birefringence exists in all optical fibres and varies unpredictably along the length of a standard single-mode fibre. The amount of birefringence in single-mode fibres is on the order of 10^{-8} [20] and is highly dependent on the thermal and mechanical stresses on the fibre. The varying birefringence along the length of the fibre leads to polarization mode coupling which repeats many times along a long fibre communication link. Thus, the polarization state of light within the fibre evolves as it propagates through the fibre such that the output polarization state no longer correlates to the input state of polarization. More importantly, the differential group delay between the two polarization modes in long single-mode fibre links shows a dependency upon wavelength and environmental conditions.

One of the adverse effects of birefringence in optical fibres for communication applications relates to a phenomenon called polarization mode dispersion (PMD). The resulting difference in propagation time between the degenerate polarization modes of an input light signal, along with its dependency upon wavelength and environmental factors, can cause transmission impairments similar in character to chromatic dispersion-induced pulse broadening or splitting. In contrast to chromatic dispersion, PMD in long fibre links at any given wavelength is a stochastic process due to the random polarization mode coupling. The distribution of the DGD values measured over a wide wavelength range or over a long period of time statistically follows a Maxwell distribution [21]. Even though modern single-mode fibres typically exhibit a low value of polarization mode dispersion coefficient ($\sim 0.5\text{ps}/\sqrt{\text{km}}$), in high-speed long-haul fibre communication systems, the mean amount of DGD incurred should be kept below one-tenth of a bit period (e.g. 10ps for a 10Gbps system) for minimal effect on the fidelity of the transmitted short pulses [22]. Hence, the maximum transmission distance, L_{PMD}, for a particular data rate, B, as a function of the PMD coefficient, $\Delta\tau_{PMD}$, can be expressed by

$$L_{PMD} \leq \frac{1}{100 \cdot B^2 \cdot \Delta\tau_{PMD}^2} \tag{2.7}$$

Evidently the transmission distance achievable decreases with the square of the data rate and with the square of the PMD coefficient as depicted in Figure 2.4. Various techniques [23][24] to compensate PMD effects in long haul transmission systems have been proposed and it remains a topic of intense research.

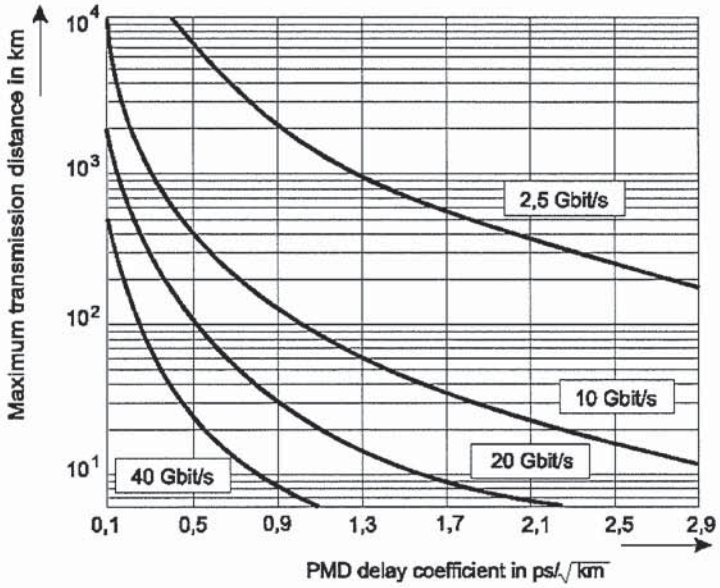

Figure 2.4 Diagram depicting dependency of maximum transmission distances for different data rates on the PMD coefficients. Diagram obtained from [25].

In contrast with long fibre links, birefringence effects in fibre optic components are generally deterministic, predictable, reproducible and controllable, in many cases. Owing to the short fibre length, polarization mode coupling in fibre devices is generally negligible and the DGD is constant as a function of wavelength, since there is only one effective axis of birefringence. Under such circumstances, the differential index between the degenerate polarization modes remains constant. For devices like the fibre Bragg grating, where the wavelength response is a function of the effective core index, the birefringence introduces a deterministic polarization-dependent transfer response. This is illustrated in Figure 2.5 where the wavelength spectral response of a fibre grating is clearly dependent on the state of polarization (SOP) of the input light. The birefringence in this case measured ~9.3×10^{-6}, which is much higher than the intrinsic fibre birefringence due to asymmetry in the UV irradiation in the fabrication process [26]. The fibre Bragg grating, which is covered in detail in Chapter 4, essentially consists of periodic refractive index perturbations within the core of the optical fibre. A phase shift can be introduced into the grating by simply creating a refractive index disruption in the grating structure. The introduction of a phase shift within the fibre Bragg grating enables a sharp resonance feature (transmission peak) in the spectral response of the grating. Due to the birefringence, the phase shift characteristics in fibre grating devices can be similarly affected and exhibit polarization dependency. As shown in Figure 2.6, the resonance transmission peak in a phase-shifted fibre Bragg grating is influenced by the index anisotropy which causes polarization splitting in the transmission peak. The birefringence-induced differential phase shift measured 0.14π leading to a corresponding wavelength splitting of 9pm.

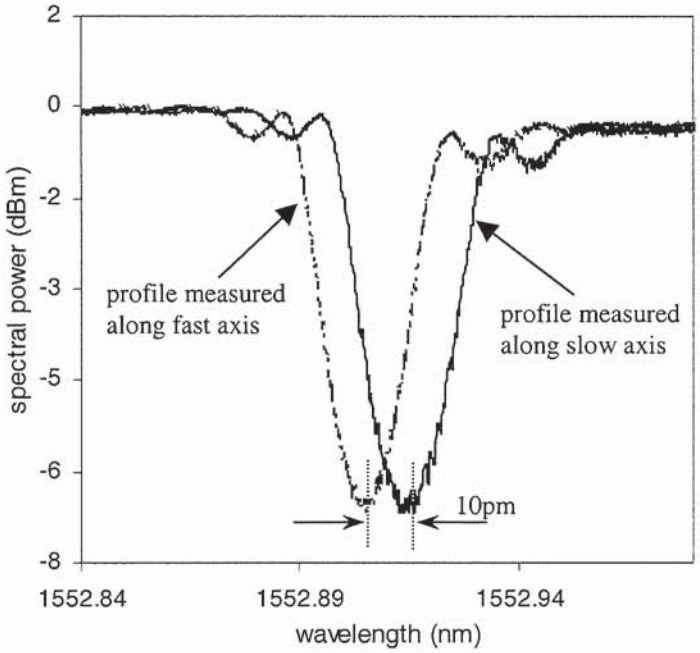

Figure 2.5 Superimposed spectral profiles of a fibre Bragg grating along different input polarization axes. The index anisotropy (i.e. birefringence) here measured ~ $9.3x10^{-6}$.

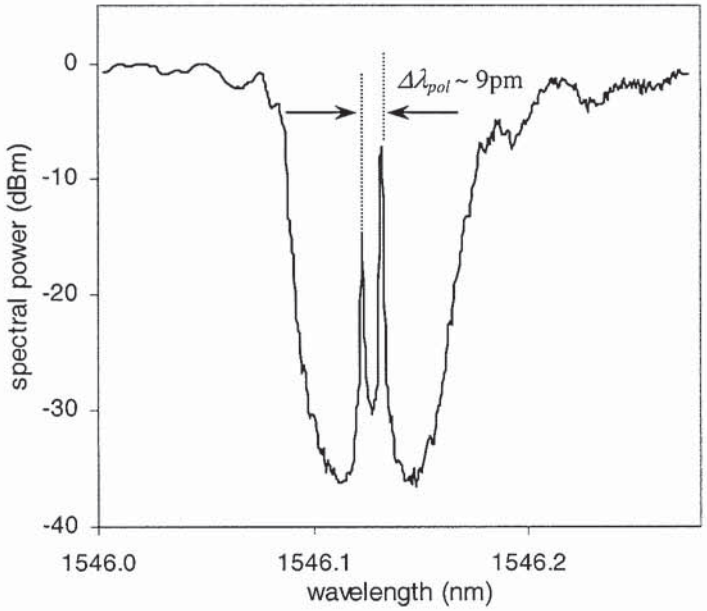

Figure 2.6 Spectral profile of a phase-shifted fibre grating. The birefringence-induced polarization-dependent phase shift induced split polarization peaks in transmission, separated by ~9pm.

The effect of birefringent phase shifts has considerable significance in some device applications, perhaps most notably in intra-cavity fibre grating lasers [27]. Birefringence-induced polarization splitting leads to dual polarization mode operation in single-mode fibre lasers. Apart from the fact the polarization modes propagate and emerge at slightly different wavelengths, they also generate a beat signal in the low

frequency range (<3GHz) generally considered as a low frequency noise [28]. In all cases, the effective birefringence is largely determined by the photo-induced index anisotropy since the intrinsic birefringence in single-mode fibre is very low. In the case of the phase-shifted fibre grating, as shown in Figure 2.6, the wavelength spacing, $\Delta\lambda_{pol}$, between the polarization transmission peaks can be related to the effective birefringence by the following expressions:

$$\frac{2\Delta n \cdot \pi}{\lambda} L = \Delta\varphi \tag{2.8}$$

$$\frac{\Delta\varphi}{\pi} = \frac{\Delta\lambda_{pol}}{\Delta\lambda_{FSR}} \tag{2.9}$$

where Δn denotes the effective birefringence at the phase shift region of length L, $\Delta\varphi$ the birefringent phase shift, and $\Delta\lambda_{FSR}$ the cavity free spectral range. It is evident that the polarization transmission peak spacing is directly proportional to the amount of birefringence. Much study has been devoted to both characterization and suppression of the induced birefringence [29][30] in fibre devices. It is worth noting that the amount of the birefringent phase shift can be manipulated/adjusted through intense UV irradiation. Birefringence in fibre devices has further enabled various useful applications, such as in fibre lasers and polarimetric sensors [31][32]. On the basis of utilizing and manipulating the birefringence effect in fibre grating devices, novel fibre laser configurations for microwave/millimetre wave signal generations have been realised and are described in detail in Chapter 6.

2.2.4 High birefringence (Hi-Bi) fibre

Effectively, fibre based components can exhibit different sections of fixed birefringence where the axes are not necessarily aligned. Strong polarization mode coupling as a result occurs as light propagates through the fibre structure, and the DGD between the polarization modes varies strongly as a function of the wavelength. The mode coupling dictates the evolution of the SOP as light propagates through the device and a transfer function can be mapped out relating the SOP at the input and output as a function of wavelength. Unlike the case of long fibre links, the polarization transfer function in this case, despite the strong polarization mode coupling, remains deterministic and by using some polarization discriminating device, the output response can be readily manipulated. This technique forms the basis of many birefringent filter configurations [33][34]. Fibre devices based on this principle rely on the control and use of the phase or polarization state in the fibre. The stringent requirement on the integrity of the SOP, in the presence of environmental perturbations, calls for fibres that are resistant to surrounding perturbations on the SOP of light propagating through it. This has led to a special type of fibre commonly known as polarization-maintaining (PM) or high-birefringence (Hi-Bi) fibre.

Conventional or standard single-mode fibre belongs to a class of fibre known as low-birefringence fibre, and the SOP of light propagating through it is sensitive to external perturbations such as transverse pressure, bend, strain and temperature. In various applications, including coherent optical transmission systems and fibre optic sensing systems, the SOP of light along the fibre is critical and measures to counter birefringence variations due to environmental perturbations are necessary.

Hi-Bi fibre allows linearly polarized light to propagate in unstable environmental conditions without the need for polarization state controller. The birefringence of Hi-Bi fibre is much larger and more uniform than the residual birefringence of ordinary single-mode fibre. Because the birefringence is associated with a systematic physical asymmetry of the fibre cross-section, Hi-Bi fibre exhibits distinct fast and slow principal optical axes. Light coupled into a length of Hi-Bi fibre will resolve into two orthogonal linearly polarized modes with different propagation velocities according to how the input electric field projects onto the fast and slow axes of the fibre. The Hi-Bi fibre is only polarization-maintaining when the electric field of the input light is aligned with either the fast or the slow axis. Otherwise, due to the difference in the refractive index between the two axes, the respective electric fields are phase shifted relative to one another in proportion to the distance travelled, resulting in the SOP of the propagating light evolving periodically as it travels along the fibre. It is important to note that the polarized modes are maintained along the fibre and energy does not couple between the modes (in the linear low intensity regime).

Birefringence in Hi-Bi fibres may be stress-induced by placing the core between or within glass elements of different physical composition, or may originate in a deliberate asymmetry of the core geometry. In all cases, the result is a difference in the index of refraction between the orthogonal axes. The most widely known Hi-Bi fibres are the Panda, Bow tie, elliptical stress, and elliptical core types, and their cross sections are illustrated in Figure 2.7.

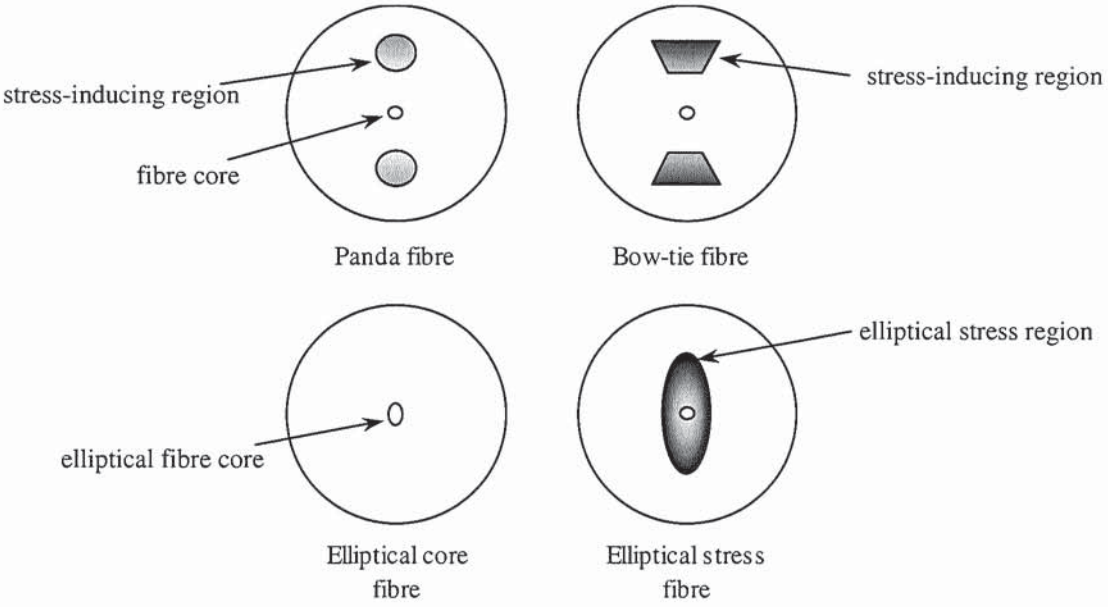

Figure 2.7 Cross-sectional profiles of various common high-birefringence (Hi-Bi) fibres.

The characteristics of Hi-Bi fibres are most commonly described using three parameters, namely, the beat length, L_B, the holding parameter, h, and the transmission loss. When the input light to the Hi-Bi fibre is not aligned to either of the propagation axes, the SOP propagating down the fibre evolves periodically: the distance over which it completes a full polarization evolution cycle, corresponding to the distance over which the differential phase shift between polarization modes reaches 2π, is known as the beat length, L_B, which can be expressed by

$$L_B = \frac{\lambda}{\Delta n} = \frac{2\pi}{\Delta\beta} \tag{2.10}$$

where λ denotes the wavelength, $\Delta\beta$ the differential propagation constant between the polarized modes, and Δn is the birefringence of the fibre. L_B is especially convenient for comparing different polarization-maintaining fibres for different wavelengths since it is directly proportional to the operation wavelength.

In addition to the amount of the birefringence, another important factor for polarization-maintaining fibre, in particular where long lengths are involved, is how well they hold a given polarization. In other words, the average rate at which the perturbation-induced power coupling out of the desired SOP into the orthogonal state is a significant parameter. There are many factors that degrade the polarization-maintaining capabilities of the Hi-Bi fibre and they include intrinsic factors like structural imperfections, nonlinear effects, and extrinsic environmental factors such as temperature or mechanical deformations like bending and twist. These influences result in random mode couplings as the induced birefringence varies in strength and orientation [35]. Consequently the polarization extinction ratio (ER) of the Hi-Bi fibre degrades with length. The parameter h characterizing the random perturbation is connected to the ER as follows [22]:

$$\mathrm{ER} = 10\log[\tanh(h \cdot l)] \; ; \; \mathrm{ER} = 10\log\frac{P_{xy}}{P_{xx}} \tag{2.11}$$

where h is measured in m^{-1}, l is the length of the fibre, P_{xx} denotes the power component along the launched axis and P_{xy} is the cross-coupled power component which leads to a polarization extinction ratio of ER.

Temperature fluctuation is one of the most severe degradation factors in the performance of Hi-Bi fibres. To reduce the influence of temperature on the performance integrity of the fibre, thick nylon coating [36] of 500μm (twice the normal coating thickness) has been found to reduce thermal sensitivity effectively. Furthermore, a thicker layer of coating is also effective against undesirable induced birefringence as a result of transverse pressure at kinks, in particular in coiled fibres [36]. Hi-Bi fibre is significantly resistant to induced birefringence due to mechanical perturbations like bending (bending radius >10cm), pure axial tension, and small twist. However transverse pressure, in particular at 45^0 azimuth, can create drastic mode coupling [37]. Commercially available Hi-Bi fibres achieve reduced crosstalk due to external perturbations (temperature and transverse pressure) with a 400μm coating, which significantly reduces induced birefringence by several orders compared to a bare Hi-Bi fibre. A method to minimize the temperature and strain sensitivities without increasing the fibre size or weight (due to additional coating) has also been proposed [38]. By selecting suitable fibre parameters including the core ellipticity, refractive index difference, thickness of inner cladding, and the ratio of the major axes of the core and the cladding, temperature and strain insensitive Hi-Bi fibre for a particular range of wavelength can be designed.

With increasing need and improved technology for manufacturing long (>25km) Hi-Bi fibres with high polarization-maintaining capabilities (i.e. high h parameter), considerable progress has been made in minimizing transmission loss as well. In [39], for example, optimised design parameters have led to 5 km of PANDA type Hi-Bi fibre with a transmission loss of 0.22dB/km in the 1.5μm window with an h parameter of $4 \times 10^{-7} m^{-1}$ (i.e. crosstalk of –27dB). Thus, optimisation has led to Hi-Bi fibre with transmission loss comparable to that of conventional single-mode fibre, which has been successfully demonstrated in coherent optical transmission, and in bidirectional polarization-discriminating optical transmission [40]. In general, commercially available PM fibres are capable of achieving h values between 10^{-6} and 10^{-7} corresponding to polarization crosstalk better than -40dB in a 1km fibre with typical loss <0.8dB/km.

Hi-Bi fibres are essentially single-mode fibres with maximized modal birefringence and accompanying this feature is the ability to perform polarization-differentiating operations and filtering. Furthermore, due the ability to harness and manipulate its SOP and the degenerate polarization modes with ease and stability -not easily achievable in conventional single-mode fibres- a number of useful fibre-based devices can be realised. By utilizing such advantages in Hi-Bi fibres, novel fibre device architectures and applications have been demonstrated and are discussed in detail in Chapter 3, Chapter 4 and Chapter 6.

2.2.5 Dopants and rare-earth doped fibres

Since the advent of fibre optic technology, apart from improving the characteristics of optical fibres for communication links, increasing efforts are made to design and fabricate special fibres to perform specific, important functions. Approaches based on modifications of the geometrical parameters offer an obvious way to improve, for example, the polarization-holding properties or the dispersion characteristics. Modifications to the chemical composition of the fibre similarly can yield changes/improvements to the performance of optical fibres.

Early interest in the material composition of fibres was mainly to identify the optimum dopants (oxide impurities) like Boria (B_2O_3), Alumina (Al_2O_3), Germania (GeO_2) and Phosphorus Pentoxide (P_2O_5) for increasing or lowering the refractive index of the core and cladding respectively [41]. Subsequent interest in doping fibre with rare-earth ions increased rapidly due to the prospect for realising both active and passive devices in these fibres [42][43]. Improvements in the fabrication techniques, and in the host glass compositions, have since yielded high consistency doped fibres [44]. These special fibres enable elegant solutions to many device architectures, particularly when coupling loss and size are important.

Within the context of this thesis, emphasis is placed on rare-earth doped fibre, particularly the Er/Yb doped fibre, and subsequently its applications in fibre grating filters and laser applications, which are discussed in detail in Chapter 5 to Chapter 7. Among the various types of rare-earth doped fibres, Erbium (Er^{3+}) doped and Erbium/Ytterbium (Er/Yb) doped fibres are of particular importance since optical amplifiers and lasers based on such fibres have operating wavelengths that coincide with the third window for optical communication (1.5μm). Early demonstrations of Erbium doped fibre amplifiers (EDFA) [45] and Erbium doped fibre lasers [46] illustrated their great potential for communication systems operating in the 1.5μm window. With the availability of semiconductor pump laser diode with high output power [47][48], EDFA and fibre lasers can be potentially made practical during applications and thus there have been intense research and development activities in fibre amplifiers and lasers based on rare-earth doped fibres.

The energy transition diagram of Er^{3+} fibre is shown in Figure 2.8. The fluorescence spectrum of Er^{3+} doped fibre, which corresponds to the transition from the $^4I_{13/2}$ to the $^4I_{15/2}$ ground level, covers the useful wavelength range from 1520nm to 1580nm. The precise shape and magnitude of the absorption and fluorescence spectra depend on the host glass environment, which modifies the ion energy structure [49]. Several pump wavelengths are available to populate the upper energy state $^4I_{13/2}$ of the Er^{3+} fibre. In fact besides 1480nm and 980nm, pump wavelengths at 532nm, 810nm and 670nm have been utilized and demonstrated [50]-[52]. The use of 980nm pump band offers the best amplifier noise performance [53]. Results also indicate that 980nm pump offers the advantage of operating in a region free of pump excited state absorption [54]. Furthermore higher gain and efficiency are obtained compared to using other pump wavelengths [55][56]. As a result, 980nm pump laser diode is the most commonly adopted pump module for both Erbium-based fibre amplifiers and lasers.

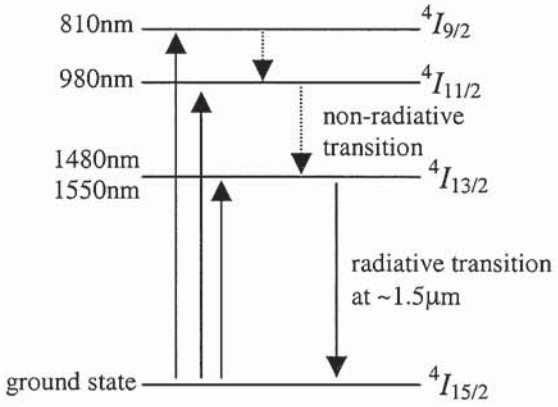

Figure 2.8 Partial energy diagram for Erbium doped fibre.

The pure engineering simplicity of a practical fibre laser based on Er^{3+} fibre for use in the 1.5μm regime promoted the initial interest and development of the Er^{3+} doped fibre laser [57]-[59]. The extensive emission bandwidth of Er^{3+} fibre further led to the development of broadly tunable continuous wave Er^{3+} fibre lasers [60]. Despite the significant success in rare-earth doping of silica-based fibres [61] and the encouraging number of reports on fibre lasers, operation of Er^{3+} fibre laser was not without undesired effects. Of substantial importance was the sustained self-pulsing phenomenon commonly observed in Er^{3+} doped fibre lasers [41][62]-[65]. This is generally linked to the high Er^{3+} ion concentration, which results in the formation of ion pairs and clusters. The ions interactions result in rapid energy transfers through cross relaxation, and tend to degrade the output and intensity noise performance or even destabilize the laser operation. Since the percentage of clusters increases with concentration, the problem plagued realisation of short, robust fibre lasers where highly doped Er^{3+} fibres were needed.

The use of Yitterbium (Yb^{3+}) codoping in Erbium doped fibre initially was to relax the tolerance on the usable pump wavelength [66] since the operating wavelength of the 980nm laser diode is temperature dependent and the $^4I_{15/2}$ -$^4I_{11/2}$ absorption band for Er^{3+} in silica fibre is spectrally narrow [67]. With Ytterbium-sensitisation, the optical pump excites the Er^{3+} ions indirectly, via energy transfer from the Yb^{3+} ions. As depicted in Figure 2.9, the Yb^{3+} absorbs the pump light and cross relaxation between adjacent $Er^{3+}$and Yb^{3+} allows the energy to be transferred to the Er^{3+} system. Further studies revealed that Ytterbium codoping in heavily Erbium doped fibre lasers effectively suppresses self-pulsating effects [68] and reduces low frequency intensity noise, thereby relaxing the requirement on pump diode power stability [69]. Er/Yb doped fibre has been shown to be effective in increasing the small signal gain of EDFA as well [70][71].

In contrast to Er^{3+} ions, the Yb^{3+} ions offer a broad absorption band from 800nm to 1100nm, with a particularly high peak-absorption cross-section. Moreover, Ytterbium doped fibre is not prone to concentration quenching and offers two orders of magnitude higher absorption at 980nm than non-sensitised Er^{3+} doped fibre. The increase in pump absorption reduces the need to increase Er^{3+} ion concentration in short cavity fibre lasers. Several highly efficient fibre lasers based on Er/Yb doped fibres with lengths on the order of just a few centimetres have been reported [72][73]. Based on such Er/Yb doped fibres, fibre laser applications and novel monitoring schemes have been realised in this research and are described in Chapter

7. Interestingly, by taking the advantage of the high 980nm pump absorption of the Er/Yb doped fibre, a new tunable fibre grating filter configuration has been conceived and is described in detail in Chapter 5.

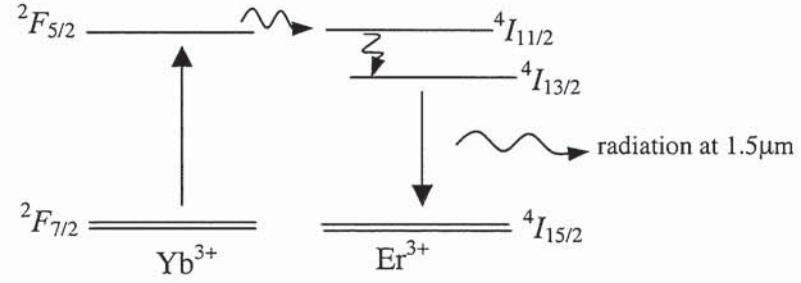

Figure 2.9 Relevant energy levels for Er/Yb co-doped system.

With the advent of the wavelength division multiplexed (WDM) communication systems, the demand for narrow linewidth optical sources has generated interest in the design and realisation of stable single-mode fibre lasers [74]. Apart from using a reduced cavity length, wavelength-selective filters/reflectors are required to enhance the mode-selectivity within the fibre laser cavity. An early demonstration of spectral selectivity using an integral fibre grating [58][75] successfully reduced the output spectral linewidth and multimode operation. With the subsequent development of non-invasive formation of intra-cavity grating structures [76], an all-fibre robustly single-mode Er^{3+} doped fibre laser configuration has been achieved [77]. Efforts to further realise such intra-cavity fibre grating feedback single-mode laser configurations using Er/Yb doped fibre in order to increase its output efficiency and power, however, are inhibited by the difficulty in inscribing fibre gratings into the Er/Yb fibre. The energy transfers between the Yb^{3+} and Er^{3+} ions are efficient provided the electrons relax preferentially to the Er^{3+} upper laser state $^4I_{13/2}$ rather than back to the $^2F_{5/2}$ level of the Yb^{3+} ion. This is enforced through the use of phosphosilicate glass host. The use of Phosphorous doping was however known to reduce fibre photosensitivity even with incorporation of Germanium [78][72]. Most fibre grating feedback Er/Yb fibre lasers overcome the problem through splicing which consequently introduces intracavity splice loss [72][73].

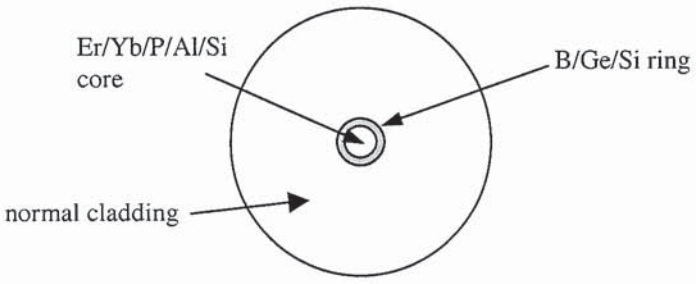

Figure 2.10 Cross-sectional profile of the Er/Yb doped fibre with a photosensitive ring.

The development of highly photosensitive Er/Yb fibre was finally realised in mid-1997 by L.Dong *et al* without modifications to the host glass for Er^{3+} and Yb^{3+} ions [49]. A highly photosensitive B/Ge doped silica cladding was used to surround a standard Er/Yb doped phosphosilicate core as shown in Figure 2.10. The Er/Yb doped core was not affected by the B/Ge doped silica cladding, which allowed strong gratings to be achieved despite the reduced overlap between the gratings and the guided optical field. The fibre combines the advantages of Yb^{3+}-sensitization with the unique features fibre grating offers. It exhibits a typical small-signal absorption ~230dB/m at 980nm and ~25dB/m at 1535nm with a cutoff wavelength of 1470nm and numerical aperture (NA) of 0.18. It can be spliced to any standard fibres with minimal loss without special adjustment required to the fusion splicer. Without resorting to hydrogenation or splicing to integrate intra-cavity strong reflectors in the fibre, high performance single-frequency fibre grating laser was realised [79] with cavity length in the order of centimetres and output power in the order of mW.

Based on such photosensitive Er/Yb doped fibres, fibre laser configurations and applications have been realised in this research. More importantly, due to the ability to inscribe and trim fibre Bragg grating structures in this fibre, unique fibre laser configurations designed for wireless photonics applications have been achieved and are detailed in Chapter 6.

2.3 Conclusions

Various characteristics of single-mode optical fibres have been outlined. Fibre insertion loss, dispersion and birefringence effects have been discussed with emphasis on their implications to long fibre links as well as fibre-based device applications. For fibre-based devices, the insertion loss and dispersion generally pose negligible concerns. Birefringence, however, can cause its transfer response to exhibit significant polarization dependency. The advances in fibre engineering and doping techniques in rare-earth doped fibres have been outlined with particular attention on Erbium doped and Erbium/Ytterbium doped fibres. Two special fibres namely, the Hi-Bi fibre and the photosensitive Er/Yb doped fibre, highlighted in this chapter subsequently formed the basis for a number of fibre-based devices discussed in the following chapters of this thesis.

2.4 References

[1] K. Kirayama, N. Uesugi, M. Ohashi, S. Seikai, K. Ishihara, "Design and performance of ultra low loss single-mode fibre cable in 1.5μm wavelength region", *J. Lightwave Technol.*, LT3(3), pp. 579-585, 1985.

[2] P.D. Lazay, A.D. Pearson, "Developments in single-mode fibre design, materials and performance at Bell Laboratores", *IEEE J. Quantum Electron.*, QE18(4), pp. 504-510, 1982.

[3] P.D. Lazay, A.D. Pearson, W.A. Reed, P.J. Lemaire, "An improved single-mode fibre design exhibiting low loss high bandwidth and tight mode confinement simultaneously", *IEEE J. Quantum Electron.*, 17(12), pp. 2566-2567, 1981.

[4] D. Marcuse, C. Lin, "Low dispersion single-mode fibre transmission- The question of practical versus theoretical maximum transmission bandwidth", *IEEE J. Quantum Electron.*, QE17(6), pp. 869-878, 1981.

[5] K.P. Jackson, S.A. Newton, B. Moslehi, M. Tur, C.C. Cutler, J.W. Goodman, H.J. Shaw, "Opticsl fibre delay line signal processing", *IEEE Trans. Microwave Theory and Tech.*, MTT33(3), pp. 193-209, 1985.

[6] A. Ghatak, K. Thyagarajan, "Introduction to fiber optics", Cambridge University Press, pp. 5, 1998.

[7] A. Iino, M. Kuwabara, K. Kokura, "Mechanisms of hydrogen induced losses in silica based optical fibres", *J. Lightwave Technol.*, 8(11), pp. 1675-1679, 1990.

[8] H. Itoh, Y. Ohmori, M. Nakahara, "Germanium dopant effect on hydroxyl loss increase in optical fibres", *J. Lightwave Technol.*, LT4(2), pp. 116-120, 1986.

[9] J. Gowar, "Optical communication systems, Second Edition", Prentice Hall, pp. 102-103, 1993.

[10] P.J. Lemaire, R.M. Atkins, V.Mizrahi, W.A. Reed, "High pressure H_2 loading as a technique for achieving ultra high UV photosensitivity and thermal sensitivity in $Ge0_2$ doped optical fibres", *Electron. Lett.*, 29(13), pp. 1191-1193, 1993.

[11] J. Gowar, "Optical communication systems, Second Edition", Prentice Hall, pp. 82-85, 1993.

[12] A. Ghatak, K. Thyagarajan, "Introduction to fiber optics", Cambridge University Press, pp. 189, 1998

[13] A. Sugimura, K. Daikoku, N. Imoto, T. Miya, "Wavelength dispersion characteristics of single-mode fibres in low loss region", *IEEE J. Quantum Electron.*, QE16(2), pp. 215-224, 1980.

[14] P. Francois, "Tolerance requirements for dispersion free single-mode fibre design: Influence of geometrical parameters, dopants diffusion and axial dip", *IEEE Trans. Microwave Theory and Tech.*, MTT30(10), pp. 1478-1487, 1982.

[15] J. Gowar, "Optical communication systems, Second Edition", Prentice Hall, pp. 69-73, 1993.

[16] H. Shmuck, "Comparison of optical millimetre wave system concepts with regard to chromatic dispersion", *Electron. Lett.*, 31(21), pp. 1848-1849, 1995.

[17] B. Chrstensen, J. Mark, G. Jacobsen, E. Bodtker, "Simple dispersion measurement technique with high resolution", *Electron. Lett.*, 29(1), pp. 132-133, 1993.

[18] G.H. Smith, D. Novak, Z. Ahmed, "Overcoming chromatic dispersion effects in fibre wireless systems incorporating external modulators", *IEEE Trans. Microwave Theory and Tech.*, 45(8), pp. 1410-1415, 1997.

[19] S.A. Havstad, A.B. Sahin, O.H. Adamczyk, Y. Xie, A.E. Willner, "Distance independent microwave and millimetre wave power fading compensation using a phase diversity configuration", *IEEE Photon. Technol. Lett.*, 12(8), pp. 1052-1054, 2000.

[20] H. Schneider, H. Harms, A. Rapp, H. Aulich, "Low birefringence single-mode fibres: Preparation and polarization characteristics", *Applied Optics*, 17(19), pp. 3035-3037, 1978.

[21] T.E. Darcie and C.D. Poole, "Polarization induced performance variables", *Communication Engineering and Design*, 1992.

[22] Profile Optische Systeme, "Basic notes on PMD and polarization", Application notes, BN9000, 2000.

[23] S. Lanne, W.Idler, J.P. Thiery, J.P. Hamaide, "Fully automatic PMD compensation at 40Gbit/s", *Electron. Lett.*, 38(1), 2002.

[24] R. Khosravani, S.A. Havstad, Y.W. Song, P. Ebrahimi, A.E. Willner, "Polarization mode dispersion compensation in WDM systems", *IEEE Photon. Technol. Lett.*, 13(12), pp. 1370-1372, 2001.

[25] Profile Inc., "Basic note PMD and polarization", Application notes, BN9000, pp. 15, 2000.

[26] T. Erdogan, V. Mizrahi, "Characterization of UV-induced birefringence in photosensitive Ge-doped silica optical fibres", *J. Opt. Soc. Am. B*, 11(10), pp. 2100-2105, 1994.

[27] M Douay, T. Feng, P. Bernage, P. Niay, E. Delevaque, T. Georges, "Birefringence effect of optical fibre laser with intracore fibre Bragg grating", *IEEE Photon. Technol. Lett.*, 4(8), pp. 844-846, 1992.
[28] L. Xu, I. Glesk, D. Rand, V. Baby, P.R. Prucnal, "Suppression of beating noise of narrow-linewidth erbium doped fibre ring lasers by use of a semiconductor optical amplifier", *Optics Lett.*, 28(10), pp. 780-782, 2003.
[29] A.M. Vengsarkar, Q. Zhong, D. Inniss, W.A. Reed, P.J. Lemaire, S.G. Kosinski, "Birefringence reduction in side-written photoinduced fibre devices by a dual exposure method", *Optics Lett.*, 19(16), pp. 1260-1262, 1994.
[30] R. Gafsi, M.A. El-Sherif, "Analysis of induced birefringence effects on fibre Bragg gratings", *Optical Fibre Technology*, 6, pp. 299-323, 2000.
[31] H.K. Kim, S.K. Kim, B.Y. Kim, "Polarimetric fibre laser sensors", *Optics Lett.*, 18(4), pp. 317-319, 1993.
[32] J. Hernandez-Cordero, V.A. Kozlov, A.L.G. Carter, T.F. Morse, "Fibre laser polarization tuning using a Bragg grating in a Hi-Bi fibre", *IEEE Photon. Technol. Lett.*, 10(7), pp. 941-943, 1998.
[33] T. Ozeki, "Optical equalizers", *Optics Lett.*, 17(5), pp. 375-377, 1992.
[34] H.D. Ford, R.P. Tatam, "Birefringent-fibre Solc wavelength filters", *10th Optical Fibre Sensors Conference*, pp. 560-563, 1995.
[35] S.C. Rashleigh, W.K. Burns, R.P. Moeller, "Polarization holding in birefringent single-mode fibres", *Optics Lett.*, 7(1), pp. 40-42, 1982.
[36] J. Noda, K. Okamoto, Y. Sasaki, "Polarization-maintaining fibres and their applications", *J. Lightwave Technol.*, LT4(8), pp. 1071-1089, 1986.
[37] A. Kumar, R. Ulrich, "Birefringence of optical fibre pressed into a V groove", *Optics Lett.*, 6(12), pp. 644-646, 1981.
[38] F. Zhang, J.W.Y. Lit, "Temperature and strain sensitivities of high-birefringence elliptical fibres", *Applied Optics*, 31(9), pp.1239-1243, 1992.
[39] Y.Sasaki, T. Hosaka, M. Horiguchi, J. Noda, "Design and fabrication of low loss and low crosstalk polarization maintaining optical fibres", *J. Lightwave Technol.*, LT-4, (8), pp. 1097-1102, 1986.
[40] Y. Sasaki, "Long length low loss polarization maintaining fibres", *J. lightwave Technol.*, LT5(9), PP. 1139-1146, 1987.
[41] J. Gowar, "Optical communication systems", 2nd Edition, pp. 64-68, 1993.
[42] S.B. Poole, D.N Payne, M.E. Fermann, "Fabrication of low loss optical fibres containing rare-earth ions", *Electron. Lett.*, 21, pp. 737-738, 1985.
[43] S.B. Poole, D.N Payne, R.J. Mears, M.E. Fermann, R.I. Laming, "Fabrication and characterization of low loss optical fibres containing rare-earth ions", *J. Lightwave Technol.*, LT-4(7), pp. 870-876, 1986.
[44] B.J. Ainslie, "A review of the fabrication and properties of Erbium doped fibres for optical amplifiers", *J. Lightwave Technol.*, 9(2), pp. 220-227, 1991.
[45] R.J. Mears, L. Reekie, I.M. Jauncy, D.N. Payne, "High gain rare-earth doped fibre amplifier at 1.54μm," *Proc. Optical Fibre Communication Conference (OFC)*, WI1, 1987.
[46] R.J. Mears, L. Reekie, S.B. Poole, D.N. Payne, "Low threshold tunable CW and Q-switched fibre laser operating at 1.55μm," *Electron. Lett.*, 22, pp.159-160, 1986.
[47] K.Yamada, "More than 3000hr stable CW operation of 1.48μm laser diodes for erbium doped fibre amplifier pumping source", *Topical Meet. Optical Amplifiers and Applications*, Monterey, CA, WA3, 1990.
[48] A. Larsson, S.Forouhar, J. Cody, R.J. Lang, P.A. Andrekson, "A 980nm pseudomorphic single quantum well laser for pumping erbium doped optical amplifiers", *Topical Meet. Amplifiers and Applications*, Monterey, CA, WA2, 1990.
[49] B.J. Ainslie, A.P. Craig, S.T. Davey, "The absorption and fluorescence spectra of rare-earth ions in silica-based monomode fibre", *J. Lightwave Technol.*, 6(7), pp.287-292, 1988.
[50] M. Horiguichi, M. Shimizu, M. Yamada, K. Yoshino, H.Hanafusa, "Highly efficient optical fibre amplifier pumped by 0.8μm band laser diode", *Electron. Lett.*, 26(21), pp. 1758-1759, 1990.
[51] M. Horiguichi, M. Yoshino, M. Shimizu, M.Yamada, "670nm semiconductor laser diode pump erbium-doped fibre amplifiers", *Electron. Lett.*, 29(7), pp. 593-595, 1993.
[52] M.C. Farries, P.R.Morkel, R.I. Laming, T.A. Birks, D.N. Payne, E.J. Tarbox, "Operation of Erbium doped fibre amplifiers and lasers pumped with frequency doubled Nd:YAG lasers", *J. Lightwave Technol.*, 7(10), pp.1473-1477, 1989.
[53] M. Yamada, M. Shimizu, M. Okayasu, T. Takeshita, M. Horiguchi, Y. Tachikawa, E. Sugita, "Noise characteristics of Er^{3+} doped fibre amplifiers pumped by 0.98 and 1.48μm laser diodes", *IEEE Photon. Technol. Lett.*, 2(3), pp. 205-207, 1990.

[54] R.I. Laming, S.B. Poole, E.J. Tarbox, "Pump excited state absorption in erbium doped fibres", *Optics Lett.*, 13(12), pp. 1084-1086, 1988.
[55] R.I. Laming, M.C. Farries, P.R. Morkel, L. Reekie, D.N. Payne et al, "Efficient pump wavelengths of erbium doped fibre optical amplifier", *Electron. Lett.*, 25, pp.12-14, 1989.
[56] M. Yamada, M. Shimizu, T. Takeshita, M. Okayasu, M. Horiguchi, S. Uehara, E. Sugita, "Er^{3+} doped fibre amplifier pumped by 0.98μm laser diodes", *IEEE Photon. Technol. Lett.*, 1(12), pp. 422-424, 1989.
[57] Y. Kimura, M. Nakazawa, "Lasing characteristics of Er^{3+} doped silica fibres from 1553 up to 1603nm", *J. Applied Physics*, 64(2), pp. 516-520, 1988.
[58] I.M. Jauncey, L. Reekie, R.J. Mears, C.J. Rowe, "Narrow linewidth fibre laser operating at 1.55μm", *Optics Lett.*, 12(3), pp. 164-165, 1987.
[59] Y. Kimura, K. Suzuki, M. Nakazawa, "Laser diode pumped mirror free Er^{3+} doped fibre laser", *Optics Lett.*, 14(18), pp.999-1001, 1989.
[60] L. Reekie, R.J. Mears, S.B. Poole, D.N. Payne, "Tunable single-mode fibre lasers", *J. Lightwave Technol.*, LT-4(7), pp. 956-960, 1986.
[61] B.J. Ainslie, A.P. Craig, S.T. Davey, B. Wakefield, "The fabrication, assessment and optical properties of high-concentration Nd^{3+} and Er^{3+} doped silica based fibres", *Material Lett.*, 6(6), pp.139-143, 1988.
[62] J.L. Zyskind, V. Mizrahi, D.J. DiGiovanni, J.W. Sulhof, "Short single frequency erbium doped fibre laser", *Electron. Lett.*, 28(15), pp. 1385-1387, 1992.
[63] J.L. Wagener, P.F. Wysocki, M.J.F. Digonnet, H.J. Shaw, "Effects of concentration and clusters in erbium doped fibre lasers", *Optics Lett.*, 18(23), pp. 2014-2016, 1993.
[64] F. Sanchez, P.L. Boudec, P.L. François, G. Stephan, "Effects of ion pairs on the dynamics of erbium-doped fibre lasers", *Physics Review*, 48, 1993.
[65] H.L.An, E.Y.B.Pun, H.D.Liu, X.Z.Lin, "Effects of ion clusters on the performance of a heavily doped erbium doped fibre laser", *Optics Lett.*, 23(15),pp. 1197-1199, 1998.
[66] D.C. Hanna et al, "Efficient operation of an Yb sensitised Er fibre laser pumped in the 0.8μm region", *Electron. Lett.*, 24, pp. 1068-1069, 1988.
[67] W.L. Barnes, S.B. Poole, J.E. Townsend, L. Reekie, D.J. Taylor, D.N. Payne, "Er^{3+}-Yb^{3+} and Er^{3+} doped fibre lasers", *J. Lightwave Technol.*, 7(10), pp. 1461-1465, 1989.
[68] M. Ding, P.K. Cheo, "Effects of Yb:Er-codoping on suppressing self-pulsing in Er-doped fibre lasers", *IEEE Photon. Technol. Lett.*, 9(3), pp.324-326, 1997.
[69] H.L. An, X.Z. Lin, H.D. Liu, "Intensity noise suppression by ytterbium codoping in heavily erbium doped fibre lasers with partly clustered erbium ions", *Optics Lett.*, 25(24), pp. 1747-1749, 2000.
[70] J. Nilsson, P. Scheer, B. Jaskorzynska, "Modeling and optimisation of short Yb^{3+} sensitized Er^{3+} doped fibre amplifiers", *IEEE Photon. Technol. Lett.*, 6(3), pp.383-385, 1994.
[71] J.E. Townsend, W.L. Barnes, K.P. Jedrzejewski, "Yb^{3+} sensitised Er^{3+} doped silica optical fibre with ultrahigh transfer efficiency and gain", *Electron. Lett.*, 27(21), pp.1958-1959, 1991.
[72] J.T. Kringlebotn, J.L. Archambault, L. Reekie, J.E. Townsend, G.G. Vienne, D.N. Payne, "Highly efficient low noise grating feedback Er^{3+}:Yb^{3+} codoped fibre laser", *Electron. Lett.*, 30(12), pp.972-973, 1994.
[73] J.T. Kringlebotn, P.R. Morkel, L. Reekie, J.L. Archambault, D.N. Payne, "Efficient diode pumped single frequency Erbium:Ytterbium fibre laser", *IEEE Photon. Technol. Lett.*, 5(10), pp.1162-1164, 1993.
[74] G.A. Ball, W.H. Glenn, "Design of a single-mode linear cavity erbium fibre laser utilizing Bragg reflectors", *J. Lightwave Technol.*, 10(10), pp. 1338-1343, 1992.
[75] I.M. Jauncey, L. Reekie, J.E. Townsend, D.N. Payne, "Single longitudinal mode operation of an Nd^{3+} doped fibre laser", *Electron. Lett.*, 24(1), pp. 24-26, 1988.
[76] G. Meltz, W.W. Morey, W.H. Glenn, "Formation of Bragg gratings in optical fibres by a transverse holographic method", *Optics Lett.*, 14(15), pp. 823-825, 1989.
[77] G.A. Ball, W.W. Morey, W.H. Glenn, "Standing wave monomode erbium fibre laser", *IEEE Photon. Technol. Letters*, 3(7), pp. 613-615, 1991.
[78] L. Dong, W.H. Loh, J.E. Caplen, J.D. Minelly, "Efficient single frequency fibre laser with novel photosensitive Er/Yb optical fibres", *Optics Lett.*, 22(10), pp.694-696, 1997.
[79] W.H. Loh, B.N. Samson, L. Dong, G.J. Cowle, K. Hsu, "High performance single frequency fibre grating based Erbium:Ytterbium codoped fibre lasers", *J. Lightwave Technol.*, 16(1), pp. 114-118, 1998.

Chapter 3: Optical fibre delay line filters

3.1 Overview

In fibre optics communication systems, including wireless (microwave/millimetre wave) photonics communication networks, it has been recognised that it is advantageous to perform signal processing in the optical domain. Performing signal processing directly in the optical domain overcomes the limitations (e.g. loss, efficiency and cost) of electro-optic and opto-electronic signal conversion, as well as the electronic bottleneck for processing high-speed signals that are already in the optical domain. As detailed in Chapter 2, optical fibre possesses various favourable characteristics like low loss (fractional decibels/km), large bandwidth-distance product (on the order of 100GHz·km), large time-bandwidth product and low dispersion for both transmission links and device applications. Among the various forms of fibre-based signal processors, the fibre optic delay line filter scheme in particular exploits these superior characteristics for vast numbers of applications and various complex signal processing operations, notably microwave/millimetre wave signal processing [1]-[5]. This chapter seeks to highlight some of the key concepts behind fibre delay line filter schemes and the determining factors influencing the operation of such filters. Based on the concept of fibre delay line structure, the Hi-Bi fibre delay line filter scheme is discussed. Various complex optical and radio wave signal-processing operations based on the Hi-Bi fibre delay line structure are demonstrated.

3.2 Key concepts of the optical delay line filter

An optical delay line processor generally comprises 4 key elementary operations: optical branching, tap weighting, differential time delay and summing. The basic concept of the delay line signal processing configuration can be illustrated by Figure 3.1.

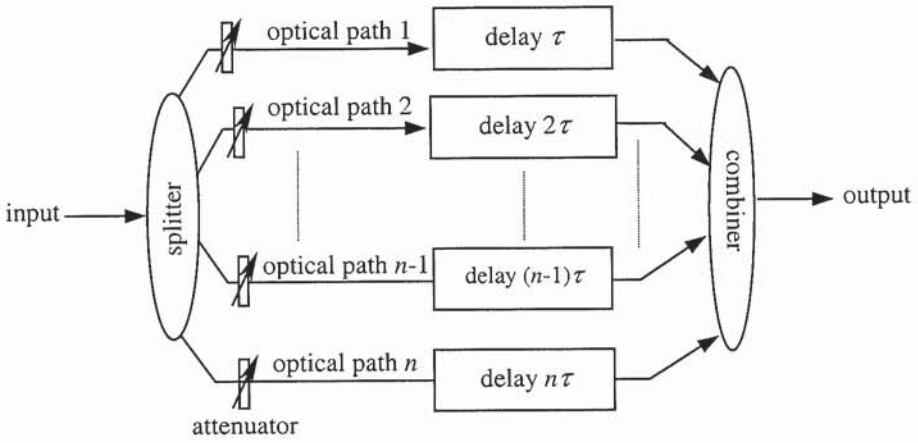

Figure 3.1 Figure illustrating the basic concept behind the optical delay line filter configuration.

As shown in Figure 3.1 the incoming optical signal is split into various paths (known as optical taps) through the process of optical branching. The magnitude of each individual signal path is attenuated appropriately and a differential time delay of τ is introduced between the optical taps. The output response of the filter is obtained by recombining the optical signals on a square-law photodetector. This form of tapped-delay line filter scheme, otherwise known as the transversal filter, is adopted for frequency domain signal processing where the tap weights are adjusted to realise the desired filtering operation [6][7].

An alternative approach for the filter form is the lattice structure configuration where the filter device consists of cascaded modules of elementary delay line filter blocks. Each basic building block consists of a delay line configuration as shown in figure 3.2. Higher order lattices are simply linear extensions of the basic sections as shown in Figure 3.3. By varying the coupling ratios between the optical taps in the elementary modules and combining the lattice sections in some prescribed ways, the system transfer function can be adjusted for different frequency responses. It should be noted that the transfer function of the non-recursive lattice filter is similar to that of the transversal filter [1][6].

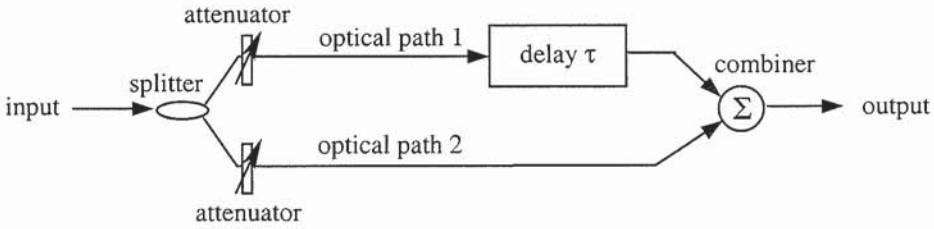

Figure 3.2 The basic delay line filter structure as the building block for lattice configuration.

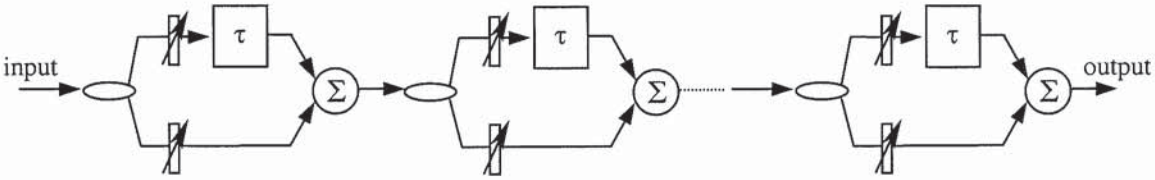

Figure 3.3 Schematic of an optical delay line lattice structure filter configuration.

The transfer function of the lattice structure can be represented with a system response matrix. Each elementary filter section can be expressed by a transfer matrix formulation whose elements relate the input and output terminals. The resultant response of the composite structure is simply the product of the individual transfer matrices [8].

As described in Chapter 2, the optical fibre is an excellent delay medium for broadband signal processing. Apart from its low loss and dispersion characteristics, fibre length can provide precise time delay of 4.87 ns/m, assuming an effective refractive index of 1.46. Components necessary to realise optical branching and summation in optical fibres can be readily achieved using N x N couplers. Most important of

all, by confining all optical taps within an optical fibre, it simplifies the detection scheme and also increases the light-collection efficiency.

A basic fibre delay line filter section of the lattice structure can be realised by cascading two 2x2 couplers with a delay section of $\Delta\tau$ along one of the cascaded optical path as illustrated in Figure 3.4.

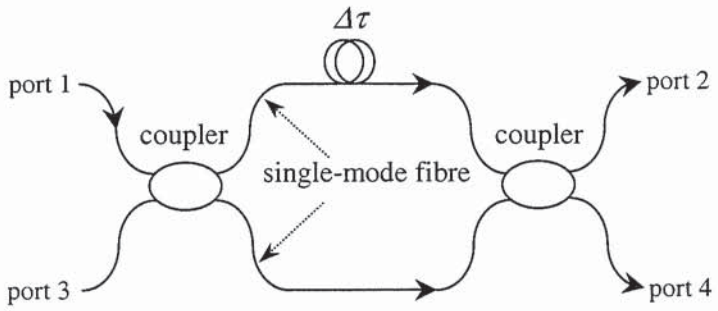

Figure 3.4 Schematic illustrating a basic fibre delay line filter block using cascaded 2x2 couplers.

Each filter module composes of two basic component matrices. The first being the delay time difference whose matrix representation can be given by

$$M_d = \begin{pmatrix} e^{-j\omega\frac{\Delta\tau}{2}} & 0 \\ 0 & e^{j\omega\frac{\Delta\tau}{2}} \end{pmatrix} \tag{3.1}$$

where $\Delta\tau$ denotes the relative time delay between the two optical arms and ω is the optical angular frequency. The coupler with intensity coupling coefficient of a on the other hand can be expressed by [9]

$$M_c = \begin{pmatrix} \sqrt{a} & j\sqrt{(1-a)} \\ j\sqrt{(1-a)} & \sqrt{a} \end{pmatrix} \tag{3.2}$$

where $\sqrt{a}$ denotes the amplitude coupling coefficient and $j = \sqrt{-1}$ is the 90^0 phase shift for the coupled signal. Therefore, the resultant transfer matrix, M_{sect}, for the filter section is simply given by

$$M_{sect} = M_c \cdot M_d \cdot M_c \tag{3.3}$$

With N stages, the resultant filter characteristic can be expressed by the product of all the basic transfer matrices and is given by

$$M_{filter} = M_N \cdot M_{N-1} \cdots\cdots M_2 \cdot M_1 \cdot M_0 \tag{3.4}$$

such that the output E-fields, denoted by E_2 and E_4 from port 2 and port 4 of the N^{th} section are given by

$$\begin{pmatrix} E_2 \\ E_4 \end{pmatrix} = M_{filter} \begin{pmatrix} E_1 \\ E_3 \end{pmatrix} \tag{3.5}$$

where E_i denotes the E-field at i^{th} port. For each input through port 1(or port 3) into an N stage lattice structure, there will be 2^N output optical taps from port 2(or port 4) with delay time difference of 0 to $N\Delta\tau$. Hence the impulse response of the lattice structure can be expressed as

$$x(t) = \sum_{k=0}^{N} x_k \delta(t - k\Delta\tau) \tag{3.6}$$

where $\delta(t)$ denotes the Delta function and the coefficients x_k denote the complex amplitude coefficient of the k^{th} optical tap with a delay $k\Delta\tau$. The frequency response is then obtained by conducting Fourier transformation [10] given by

$$X(\omega) = \sum_{k=0}^{N} x_k e^{-j\omega k\Delta\tau} \tag{3.7}$$

From the above equation, it is evident that the frequency response of the filter structure is periodic with a period given by $\Delta\tau$, thereby giving a free spectral range (FSR) of $1/\Delta\tau$. The intensity response is then the square of the magnitude of the frequency response, $X(\omega)$, given in (3.7).

In the above analysis, apart from the assumptions that all components are lossless and dispersion-less, which can be valid for most optical fibre delay line filter structures that adopt standard single-mode fibres and couplers, the operation represents that of an optically coherent optical delay line filter architecture. In principle, a delay line structure that coherently combines the tapped signals enables both phase and amplitude controls over the output transfer response. However, to maintain the relative phase integrity of the optical taps in each path requires stringent stabilization as well as isolation from environmental perturbations. Thus, in general, coherent detection that depends on the phase of the optical carrier is avoided in fibre delay line filters. Optical sources with coherence times less than the shortest relevant time delay in the system are generally adopted so as to avoid environmentally sensitive optical interference effects. The signals are added on an intensity basis and hence the transfer matrix for M_c is expressed by its intensity coupling coefficient as follows

$$M_c = \begin{pmatrix} a & 1-a \\ 1-a & a \end{pmatrix} \tag{3.8}$$

where a denotes the intensity coupling coefficient of the coupler.

The incoherent summing in fibre delay line filters (i.e. without the phase term j) consequently makes negative weighting of optical taps not achievable. These architectures are generally referred to as *positive systems* where all the optical taps are positive quantities and add on an intensity basis. The power extracted from a fibre delay line can be weighted by attenuation or amplification before detection. However, since power is an inherently positive quantity, it cannot be optically manipulated to sum to zero with other incident optical taps if the effects of coherence interference are eliminated. This feature of incoherent fibre delay line filter restricts its applications to bandpass and high pass filtering [1].

A number of signal processing filter schemes based on incoherent operation of fibre delay line architectures have been proposed and demonstrated e.g. [11]-[16]. Some of these techniques adopt high dispersion fibre to create variable delay with optical wavelength [11][12] while others adopt reflectively tapped transversal filter scheme using in-fibre reflective elements like fibre gratings [13]-[16]. In all cases, the unit time delay relies on the tap optical wavelength or spatial separation of individual tapping element, or a combination of both. Regardless of the technique involved, all the proposed schemes adopt a low-coherence source (i.e. broadband optical source), or a multimode optical source, or a multiple of uncorrelated wavelength sources so as to generate a series of non-interacting taps necessary for incoherent operation. If a low coherence optical source is unavailable, the unit time delay between the optical taps then has to be large to ensure incoherence and this consequently limits the frequency response to a small free spectral range.

On the other hand, a coherent fibre optic delay line processor has been illustrated [17] where the source coherence exceeded the smallest differential delay in the device. In this case the optical phase was retained during operation and a complex-valued tap coefficient operation was realised. Due to the all-fibre circuit, there was no limitation on data rate imposed by any electronic operation [18]. Expectedly, since the phase coherence was maintained, the system sensitivity to environmental fluctuation disturbed the relative phase between the first and last signal path, and isolation containment was necessary to reduce the coherence noise effects. Evidently the degree of environmental isolation limited the maximum differential delay that could be provided by the system.

An alternative approach to realise coherent optical delay line filter was achieved in miniature planar lightwave circuits [19][20] using silica-based single-mode waveguide monolithically integrated on a silicon substrate. Optical signals introduced to the filter (fabricated on a 3-inch silicon wafer) were tapped, weighted and coherently summed without inherent power loss [20]. The filter architecture allowed arbitrary complex tap coefficients by utilizing phase information of the optical signals and thereby allowed arbitrary frequency responses. Interesting optical signal processing functions like multichannel selection, low pass as well as high pass filtering were illustrated [21], confirming that coherent delay line filter schemes could realise arbitrary signal processing functions not possible in incoherent systems.

Efforts to overcome limitations imposed by the incoherent nature of the fibre delay line filter schemes on the other hand have been explored [22]-[25]. These methods involved the use of bipolar taps where instead of allowing arbitrary phase for each optical path, the relative phase between the optical taps were either 0 or π. Enabling techniques include the use of differential detection schemes [22][26] where each transfer function was implemented by a separate structure with a differential photodetector employed at the filter output in order to perform electronic signal subtraction. All-optical techniques through the use of

cross gain saturation in a semiconductor amplifier or cross intensity modulation of the longitudinal modes of the Fabry-Perot (FP) laser diode were also illustrated [23]-[25].

To effectively realise a coherent fibre delay line filter scheme, the use of the non-interfering orthogonal polarized modes in a high birefringence (Hi-Bi) fibre was proposed and demonstrated [27]. The fibre delay line filter based on Hi-Bi fibre overcomes the limitations imposed by the optical source coherence without stringent requirement on environmental isolation. The following sections in this chapter seek to, firstly, highlight the Hi-Bi fibre delay line filter scheme and its operating principle. Following on, by further cascading such Hi-Bi fibre delay lines in sequence, it is demonstrated that bipolar operation can be enabled without the need of additional components. On the basis of this bipolar Hi-Bi fibre delay line architecture, a number of interesting signal processing functions, for example, multichannel flattop bandpass filtering, dual complementary output operation, and bidirectional non-reciprocal wavelength-interleaved filtering have been realised and are discussed in detail.

3.3 High birefringence (Hi-Bi) fibre delay line filter

Consider an input light at an azimuth θ with respect to the birefringence axes of the Hi-Bi fibre. The input light will degenerate into two non-interfering orthogonal polarized modes which propagate within the core of the fibre with a differential delay determined by the birefringence, Δn and the length of the fibre, L. The detected intensity at the output end of the Hi-Bi fibre after passing through a mixer (i.e. polarizer) depends strongly on the relative phase of the two polarization modes since they coherently interfere at the detector. The phase difference $\Delta\varphi$ and the time delay τ between the two polarization modes can be expressed by

$$\Delta\varphi = \frac{2\Delta n \cdot \pi}{\lambda} L \; ; \; \tau = \frac{\Delta n}{c} L \tag{3.9}$$

respectively where Δn denotes the fibre birefringence, L is the fibre physical length and c is the velocity of light. Analogous to the Mach-Zehnder (MZ) filter, the output response from the fibre exhibits periodic intensity variation against the input wavelength. The output response, $|E_o|^2$, given by the magnitude of the coherent sum of the electric field can be expressed as

$$|E_o|^2 = \left| \sum_{i=1}^{2} u_i \cdot \exp\left\{ j\left(\frac{2n_i\pi}{\lambda} L \right) \right\} \right|^2 \tag{3.10}$$

where u_i denotes the amplitude of the i^{th} polarized mode with corresponding refractive index n_i and λ denotes the optical wavelength. The time varying term in the expression for the polarized mode electric field is left out. The values of u_i are related directly to the relative angular orientation between the input light and the birefringence axes of the fibre and can be expressed by, coordinate orientation, as

$$\begin{bmatrix} u_1 \\ u_2 \end{bmatrix} = \begin{bmatrix} \cos\theta \\ \sin\theta \end{bmatrix} \tag{3.11}$$

where the relative orientation between the input polarization and the birefringence axes is as shown in Figure 3.5.

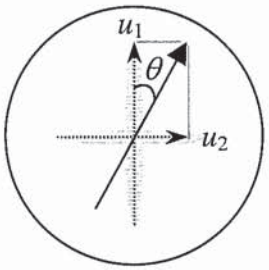

Figure 3.5 Cross-sectional profile depicting the input light orientation with respect to the birefringence axes of the Hi-Bi fibre.

The optical path difference (OPD) between the two polarization optical branches is directly related to the birefringence and length of the fibre and simply given by

$$OPD = \Delta nL \tag{3.12}$$

The simulated output intensity response of the Hi-Bi fibre delay line, based on (3.10), against input wavelength at different launched azimuths θ is as shown in Figure 3.6. The frequency separation between consecutive notches in the output response is known as the free spectral range (FSR) and is given by

$$FSR = \frac{c}{\Delta n \cdot L} \tag{3.13}$$

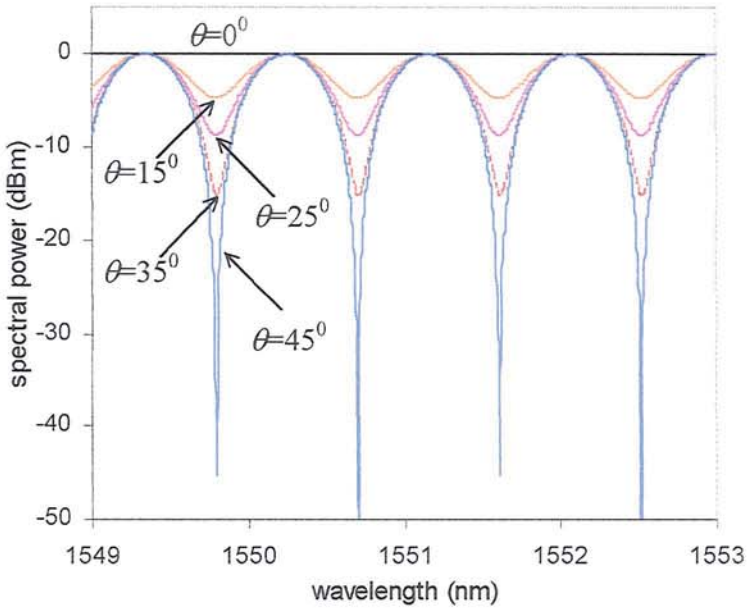

Figure 3.6 Simulated output responses of a Hi-Bi fibre for input light at different launched azimuths θ. Simulation parameters used: L=4m, $\Delta n=4.6x10^{-4}$.

It is evident that the response as shown in Figure 3.6 is analogous to that from a common Mach-Zehnder (MZ) filter configuration. Each degenerate polarization mode corresponds to an optical branch with the relative delay or phase difference determined by the fibre length and birefringence only. Contrary to the common MZ architecture, the two optical signals propagate within a single optical fibre and the single-line structure allows efficient packaging and isolation if necessary. The amplitude ratio between the polarization modes is determined by the coupling angle between the input polarization azimuth and the birefringence axes. Since the birefringence fluctuation associated with environmental perturbation can be minimized in Hi-Bi fibres (through thick coating and avoiding sharp external mechanical stress), relative phase stability can be achieved easily without stringent environmental conditioning. This single-line fibre Mach-Zehnder architecture using Hi-Bi fibre allows coherent operation not limited by the optical source coherence. Its simplicity (compared to all other fibre delay line architectures), stability and feasibility as demonstrated in [27] offers a new approach to realise more complex coherent fibre delay line designs applicable in optical as well as microwave/millimetre wave signal processing.

3.3.1 Cascaded Hi-Bi fibre delay line filter

The higher order lattice filter structure based on a linear extension of the basic delay line filter block enables complex system transfer functions not achievable by individual elementary modules. The cascading of multiple basic modules creates a larger number of optical taps and depending on the way the elementary delay line filter blocks are combined, different transfer response can be obtained. Considering a single Hi-Bi fibre section as an elementary fibre delay line module, a Hi-Bi fibre lattice delay line filter structure is conceived to perform complex signal processing functions.

Firstly, consider a cascaded two section Hi-Bi fibre delay line filter structure such that the angular offset between the birefringence axes of the Hi-Bi fibres is θ. Polarization mode degeneration occurs as light couples from one Hi-Bi fibre to the other. The cross coupling of the polarization modes at the Hi-Bi fibres interface resembles that of light coupling through a directional coupler. For the case of polarization mode coupling, the amplitude split ratio of the two optical paths is purely determined by the angular alignment θ. The transfer matrix representing such coupling, commonly known as optical axis rotation [28], can be expressed as

$$M_{rot} = \begin{pmatrix} \cos\theta & \sin\theta \\ -\sin\theta & \cos\theta \end{pmatrix} \tag{3.14}$$

where θ represents the relative angle between the two birefringence axes. Hence for a two-section Hi-Bi fibre delay line filter, its transfer matrix relating the input E-fields ($E_{i\text{-}f}$ and $E_{i\text{-}s}$) to the output E-fields ($E_{0\text{-}f}$ and $E_{0\text{-}s}$) can be expressed as

$$\begin{pmatrix} E_{o-f} \\ E_{o-s} \end{pmatrix} = M_{filter} \begin{pmatrix} E_{i-f} \\ E_{i-s} \end{pmatrix};$$

$$M_{filter} = \begin{bmatrix} \cos\theta_2 & \sin\theta_2 \\ -\sin\theta_2 & \cos\theta_2 \end{bmatrix} \begin{bmatrix} 1 & 0 \\ 0 & \exp\left(j\frac{2\Delta n\pi}{\lambda} L_1\right) \end{bmatrix} \begin{bmatrix} \cos\theta_1 & \sin\theta_1 \\ -\sin\theta_1 & \cos\theta_1 \end{bmatrix} \tag{3.15}$$

where θ_1 and θ_2 denote the coupling angles for polarization modes into Hi-Bi fibre 1 and Hi-Bi fibre 2 respectively. For a linearly polarized input light,

$$\begin{pmatrix} E_{i-f} \\ E_{i-s} \end{pmatrix} = \begin{pmatrix} 1 \\ 0 \end{pmatrix} \tag{3.16}$$

Hence the output E-fields along the fast and slow axes of the second Hi-Bi fibre for linearly polarized input light at an azimuth θ_1 is given by

$$\begin{bmatrix} E_{o-f} \\ E_{o-s} \end{bmatrix} = \begin{bmatrix} \cos\theta_2 & \sin\theta_2 \\ -\sin\theta_2 & \cos\theta_2 \end{bmatrix} \begin{bmatrix} 1 & 0 \\ 0 & \exp\left(j\frac{2\Delta n\pi}{\lambda}L_1\right) \end{bmatrix} \begin{bmatrix} \cos\theta_1 & \sin\theta_1 \\ -\sin\theta_1 & \cos\theta_1 \end{bmatrix} \begin{bmatrix} 1 \\ 0 \end{bmatrix}$$

$$= \begin{bmatrix} \left(\cos\theta_2 \cdot \cos\theta_1 - \sin\theta_2 \cdot \sin\theta_1 \cdot \exp\left(j\frac{2\Delta n\pi}{\lambda}L_1\right)\right) & \left(\cos\theta_2 \cdot \sin\theta_1 + \sin\theta_2 \cdot \cos\theta_1 \cdot \exp\left(j\frac{2\Delta n\pi}{\lambda}L_1\right)\right) \\ \left(-\sin\theta_2 \cdot \cos\theta_1 - \cos\theta_2 \cdot \sin\theta_1 \cdot \exp\left(j\frac{2\Delta n\pi}{\lambda}L_1\right)\right) & \left(-\sin\theta_2 \cdot \sin\theta_1 + \cos\theta_2 \cdot \cos\theta_1 \cdot \exp\left(j\frac{2\Delta n\pi}{\lambda}L_1\right)\right) \end{bmatrix} \begin{bmatrix} 1 \\ 0 \end{bmatrix}$$

$$= \begin{bmatrix} \cos\theta_2 \cdot \cos\theta_1 - \sin\theta_2 \cdot \sin\theta_1 \cdot \exp\left(j\frac{2\Delta n\pi}{\lambda}L_1\right) \\ -\sin\theta_2 \cdot \cos\theta_1 - \cos\theta_2 \cdot \sin\theta_1 \cdot \exp\left(j\frac{2\Delta n\pi}{\lambda}L_1\right) \end{bmatrix} \tag{3.17}$$

The output response, essentially taking a similar form as in (3.7), is the magnitude of the coherent sum of the optical taps, conveniently expressed as

$$|E_o(\lambda)|^2 = \left|\sum_{k=0}^{1} u_k \cdot \exp\left\{j\left(\frac{2\Delta n\pi}{\lambda}kL_1\right)\right\}\right|^2$$

$$\text{where } \begin{bmatrix} u_0 \\ u_1 \end{bmatrix} = \begin{bmatrix} \cos\theta_2 \cdot \cos\theta_1 \\ -\sin\theta_2 \cdot \sin\theta_1 \end{bmatrix} \text{ or } \begin{bmatrix} u_0 \\ u_1 \end{bmatrix} = \begin{bmatrix} -\sin\theta_2 \cdot \cos\theta_1 \\ -\cos\theta_2 \cdot \sin\theta_1 \end{bmatrix} \tag{3.18}$$

depending on whether the output response is obtained along the fast or the slow axis respectively. It is evident that as a result of the degeneration of the polarized modes propagating through the cascaded Hi-Bi fibre structure, bipolar optical taps are created. These optically created negated taps hence enable the filter structure to perform periodic complex transfer functions like flattop band pass filtering not possible with purely positive structures [22].

The determination of the tap coefficients, apart from the above matrix expressions, can be intuitively arrived through a series of cross sectional views as depicted in Figure 3.7.

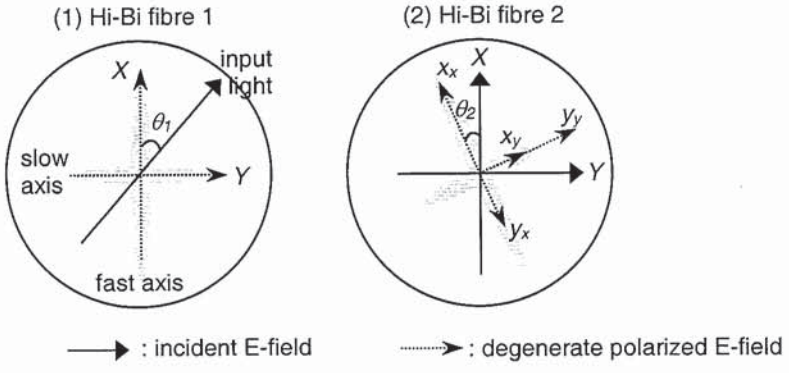

Figure 3.7 Diagrams depicting the degenerations of light propagating through the two-section cascaded Hi-Bi fibre delay line filter structure.

The advantage of such representation allows one to deduce and observe the order and polarity of the optical taps. The magnitude of the degenerate E-fields along the fast axis and the slow axes, represented by dotted traces x_i and y_i respectively (where subscript i denotes the axis the E-field couples onto), can be obtained simply by following the degenerations of the ray arrows onto the birefringence axes as they propagate through the structure. As an example, consider a 3-section cascaded Hi-Bi fibre delay line filter structure where the length ratio Hi-Bi fibre 1: Hi-Bi 2 is 2:1.

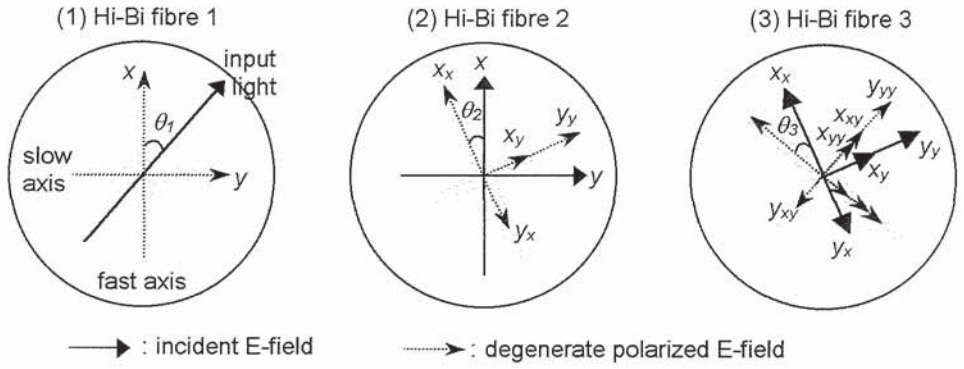

Figure 3.8 Diagrams illustrating the degenerations of the E-fields propagating through a 3-section cascaded Hi-Bi fibre delay line structure. Degenerate modes along the fast axis of Hi-Bi 3 are labelled only for clarity.

As shown Figure 3.8, the linearly polarized input light at an azimuth θ_1 to the birefringence axes of Hi-Bi 1 degenerates into polarized modes x, y which propagate down Hi-Bi fibre 1 with a differential delay given by $\Delta\tau_1 = \frac{\Delta n \cdot L_1}{c}$. The magnitudes of x and y are simply given by $\cos\theta_1$ and $\sin\theta_1$ respectively. The polarized modes in turn couple onto the birefringence axes of Hi-Bi 2 at an angle θ_2 (relative to birefringence axes of Hi-Bi 2) to generate x_x, x_y, y_x , y_y sequentially at the exit end of Hi-Bi 2 with tap magnitudes $\cos\theta_1 \cdot \cos\theta_2$; $\cos\theta_1 \cdot \sin\theta_2$; $\sin\theta_1 \cdot \sin\theta_2$; $\sin\theta_1 \cdot \cos\theta_2$ respectively. The relative delay between the 4 optical taps is given by $\Delta\tau_2 = \frac{\Delta n \cdot L_2}{c}$ and $\Delta\tau_1 = 2\Delta\tau_2$ due to the fibre length ratio. Considering the output taps along the birefringence axes of the third Hi-Bi fibre section, the 4 resultant optical taps x_{xy}, x_{yy}, y_{xy}, y_{yy} (or x_{xx}, x_{yx}, y_{xx}, y_{yx}) will then have amplitude coefficients given by

$$X_m = \begin{bmatrix} x_{xy} \\ x_{yy} \\ y_{xy} \\ y_{yy} \end{bmatrix} = \begin{bmatrix} \cos\theta_1 \cdot \cos\theta_2 \cdot \sin\theta_3 \\ \cos\theta_1 \cdot \sin\theta_2 \cdot \cos\theta_3 \\ -\sin\theta_1 \cdot \sin\theta_2 \cdot \sin\theta_3 \\ \sin\theta_1 \cdot \cos\theta_2 \cdot \cos\theta_3 \end{bmatrix} \text{ or } X_m = \begin{bmatrix} x_{xx} \\ x_{yx} \\ y_{xx} \\ y_{yx} \end{bmatrix} = \begin{bmatrix} -\cos\theta_1 \cdot \cos\theta_2 \cdot \cos\theta_3 \\ \cos\theta_1 \cdot \sin\theta_2 \cdot \sin\theta_3 \\ \sin\theta_1 \cdot \sin\theta_2 \cdot \cos\theta_3 \\ \sin\theta_1 \cdot \cos\theta_2 \cdot \sin\theta_3 \end{bmatrix} \quad (3.19)$$

where the tap coefficient associated with y_{xy} (or x_{xx}) is of opposite polarity to the rest of the group as exemplified by the opposite-pointing ray arrow in Figure 3.8. The four resultant optical taps are temporally

spaced evenly with unit delay $\Delta\tau_2$ and the output response utilizing the 4 resultant optical taps along the slow axis of Hi-Bi 3 is given by

$$X(\omega)=\sum_{m=0}^{3} X_m e^{j\omega(m\Delta\tau_2)} \tag{3.20}$$

The evaluation yields the same result as obtained through the similar matrix computation process given in (3.15)-(3.17). On the basis of such an approach, the frequency response of various Hi-Bi fibre lattice delay line filter schemes can be analysed and are presented in the following sections.

3.3.2 Multichannel flattop optical bandpass filter

Wavelength division multiplexed (WDM) technology has proven to offer cost effectiveness and higher capacity in optical communication networks. Ever increasing demand on transmission capacity has led to dense wavelength division multiplexed (DWDM) techniques that reduce channel spacing to increase the channel counts. Consequently optical filters such as multi/demultiplexer, optical add/drop, and interleaver are of special interest for optical communication systems. In these optical devices, various parameters like channel crosstalk, flatness in passband, insertion loss, dispersion and stability of wavelength spectral characteristics are always of concern.

Multi-passband optical transmission filters have numerous applications in WDM optical communications. In particular, they can be used for selecting and add/dropping optical channels. To avoid penalties in transmission, high data rate systems require transmission filters with flattened passbands (<1dB ripple) and linear in-band phase responses (i.e. constant group delay, zero dispersion) [29][30][31]. To achieve these functions with good performance, various techniques have been explored. These include fibre-based devices [29][32][33], planar waveguide configurations [34] as well as thin film interference filter schemes [35]. Filter devices based on fibre grating technology are attractive due to its intrinsic advantages like low insertion loss, compactness and fibre compatibility. Considerable efforts however are needed, to date, to tailor their amplitude responses and corresponding phase characteristics to the desired features for WDM systems [32]. Fibre grating devices are also intrinsically reflective and design considerations are needed to enable operation in transmission. Other fibre-based device schemes include the cascaded Mach-Zehnder structure using fibre fused couplers [36][37] of varying coupling ratios. Exploiting the ultra low dispersion characteristics of conventional single-mode fibre over short lengths (order of metres), they exhibit excellent group delay characteristics, low insertion loss and engineering simplicity. Their wavelength transfer stability however can only be achieved under proper environmental isolation. Alternative technologies based on cascaded Mach-Zehnder interferometers (MZI) [38] on planar lightwave circuits (PLC) or waveguide technology on the other hand show promising results [39][40][41]. Apart from the relative fabrication complexity, technologies like deep ridge waveguide and high-index SiON are required to achieve sufficient index contrast to reduce the minimum bend radius and to enhance the achievable FSR [40][42] for these fibre-matched waveguides. In addition, careful fibre alignment and integration are necessary to reduce fibre in/out coupling losses.

The approach to realise various signal processing functions based on the birefringence properties of fibres [43] was demonstrated using the Solc filter concept [44]. These filters, commonly known as birefringent filters, make use of the variation of retardation with wavelength of the birefringent medium, in conjunction with input and output polarization-selective devices, e.g. polarizers, to produce a desired transmission function. Such filters produced in fibres offer greater control on the transmission function than bulk-optic schemes or thin films [43][44]. Early demonstrations using mechanically induced birefringence (twisting, coiling) undermine the practicality during implementations because of the complexity and difficulty to construct the right amount and orientation of birefringence within the single-mode fibre. Approaches based on high-birefringence fibres as fibre analogues of bulk-optic waveplates were then illustrated [45][46]. Sagnac interferometric based configurations were further demonstrated [47][48].

Here, a new approach based on a fibre delay line configuration using a single-line cascaded Hi-Bi fibre architecture is proposed. Conceptually similar to the cascaded Mach-Zehnder structure realised using fibre couplers [36][38] or on waveguides [34][49], the Hi-Bi fibre equivalent architecture differs most notably in the fact that all the optical paths, made up by the degenerate polarization modes, propagate within a single fibre core. Since all the optical taps travel within the same fibre, environmental perturbations imposed on all signal taps within the fibre are identical. The large birefringence within the Hi-Bi fibre further ensures negligible coupling between the orthogonal polarization modes, thus removing any interferometric intensity noise arising from surrounding disturbances. The filter hence exhibits stable long-term operation without stringent measures required to isolate it from its surroundings. The high immunity against environmental disturbance allows the filter to operate stably in the coherent regime thereby exploiting the bipolar taps operation.

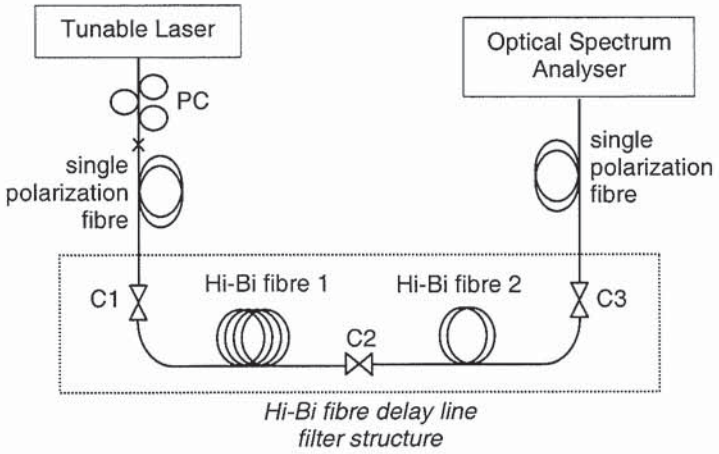

Figure 3.9 Experimental setup for the multichannel flattop bandpass filter.

The experimental setup for the delay line filter structure is as shown in Figure 3.9. Two pieces of Hi-Bi fibre with lengths 4.53m and 2.265m were used in the experiment. The beat length of the Hi-Bi fibre was 2.3mm corresponding to a birefringence of ~6.7 x 10^{-4}. The cleaved ends of the fibres were butted together (at C1, C2 and C3) such that by rotating the fibre ends with respect to each other, the orientation of the input light with respect to the birefringence axes could be varied. The input light was optimised and aligned to Hi-Bi fibre 1 through a combination of a fibre polarization controller (PC) and a single-polarization fibre (or commonly known as polarizing fibre) [50][51]. The polarizing fibre effectively transmits one linear polarization component with very low loss (<2dB/km) while attenuating the orthogonal component. No special attention was required to isolate the set-up from surrounding environmental perturbations.

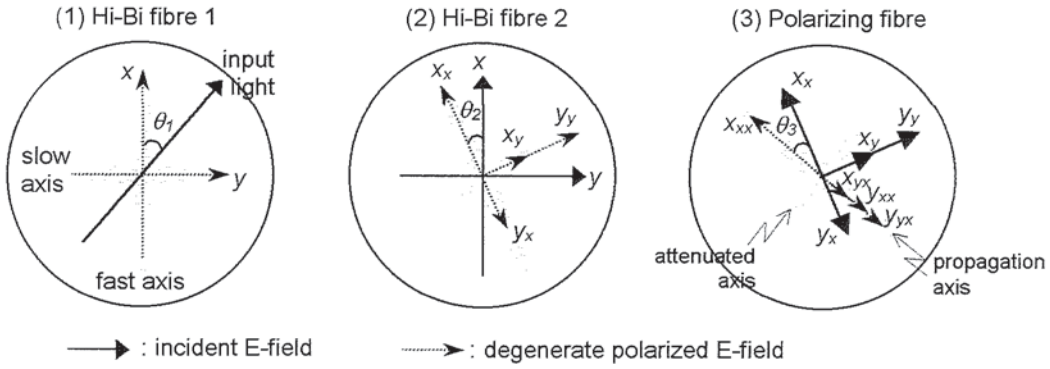

Figure 3.10 Diagrams showing the degenerations of light in the cascaded Hi-Bi fibre delay line filter structure.

Through the series of polarization modes degeneration as detailed in section 3.3.1, the resultant optical taps array X_m coupled into the propagation axis of the polarizing fibre as depicted in Figure 3.10 are given by, in temporal sequence,

$$X_m = \begin{bmatrix} x_{xx} \\ x_{yx} \\ y_{xx} \\ y_{yx} \end{bmatrix} = \begin{bmatrix} -\cos\theta_1 \cdot \cos\theta_2 \cdot \cos\theta_3 \\ \cos\theta_1 \cdot \sin\theta_2 \cdot \sin\theta_3 \\ \sin\theta_1 \cdot \sin\theta_2 \cdot \cos\theta_3 \\ \sin\theta_1 \cdot \cos\theta_2 \cdot \sin\theta_3 \end{bmatrix} \tag{3.21}$$

The output response measured at the exit end of the polarizing fibre is given by

$$|X(\omega)|^2 = \left| \sum_{m=0}^{3} X_m e^{jm\omega\Delta\tau} \right|^2 \tag{3.22}$$

where $\Delta\tau = \frac{\Delta n L_2}{c}$ =5.06ps. The output response of the filter when $\theta_1 = 0^0$; $\theta_2 = 0^0$; $\theta_3 = 45^0$ and $\theta_1 = 0^0$; $\theta_2 = 45^0$;$\theta_3 = 45^0$ are superimposed as shown in Figure 3.11. The filter response with $\theta_1 = 0^0$; $\theta_2 = 0^0$; $\theta_3 = 45^0$ was flat, expectedly from (3.22), since there were no degenerate polarization modes as light propagated along the aligned birefringence axes of the Hi-Bi fibres. By setting $\theta_1 = 0^0$; $\theta_2 = 45^0$;$\theta_3 = 45^0$, linearly polarized degenerate light along Hi-Bi fibre 2 formed two optical tap signals, creating a notch filter response. The FSR measured was ~1.6nm with notch depth >25dB.

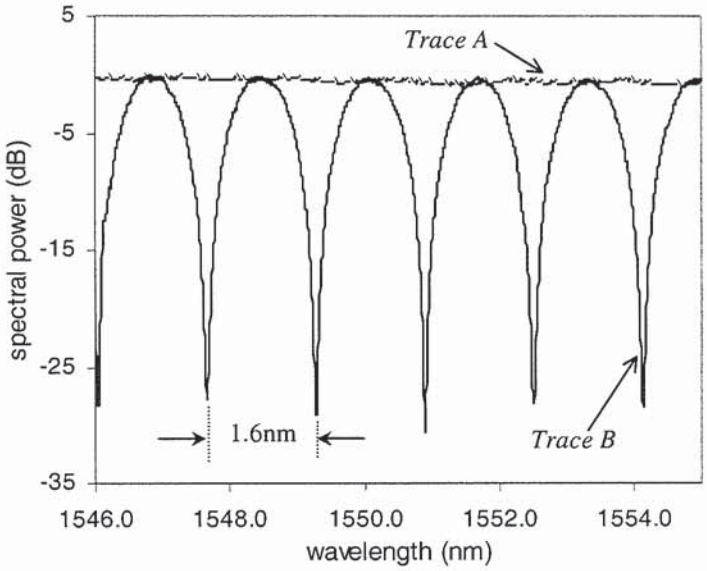

Figure 3.11 Superimposed filter responses when $\theta_1 = 0^0$; $\theta_2 = 0^0$; $\theta_3 = 45^0$ (Trace A) and $\theta_1 = 0^0$; $\theta_2 = 45^0$; $\theta_3 = 45^0$ (Trace B).

Since the delay interval between the optical taps in the filter structure is a function of both the length and the birefringence of the fibre, switching the angular alignment to $\theta_1 = 45^0$; $\theta_2 = 0^0$; $\theta_3 = 45^0$ reconfigured the filter notch response to a smaller FSR defined by the new $\Delta\tau$ given by $\Delta\tau = \frac{\Delta n(L_1 + L_2)}{c} = 15.18$ps. This led to a FSR of $1/\Delta\tau$ given by 0.528nm which corresponded closely to the experimental results as shown in Figure 3.12.

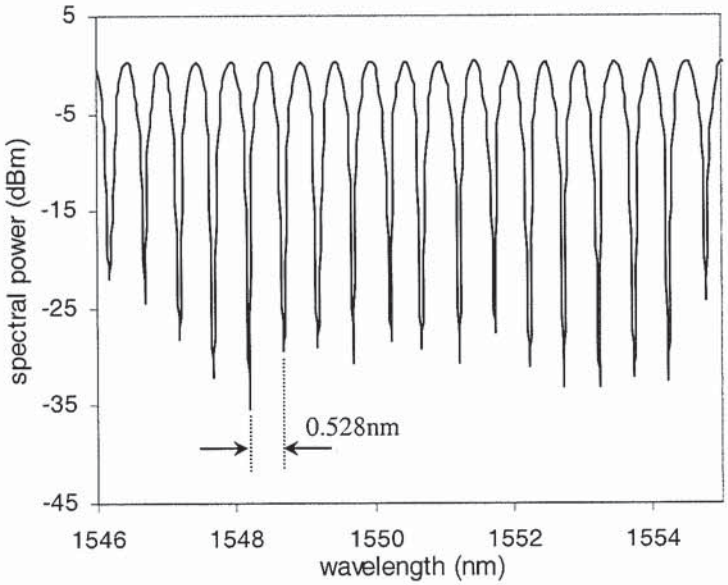

Figure 3.12 Filter notch response at $\theta_1 = 45^0$; $\theta_2 = 0^0$; $\theta_3 = 45^0$. Result highlighted that the FSR could be reconfigured simply by changing angular alignments θ_1 and θ_2.

Similarly, using $\theta_1 = 45^0$; $\theta_2 = 45^0$; $\theta_3 = 0^0$ the resultant $\Delta\tau$ of the filter structure was given by $\Delta\tau = \frac{\Delta n L_1}{c}$=10.12ps corresponding to a FSR of 0.8nm as shown in Figure 3.13. Evidently, with an increased number of cascaded sections, N, of different lengths, the number of different FSRs achievable is simply given by (2^N-1). In all cases, the spectral responses of the filter were highly stable under normal laboratory environment conditions without environmental isolation.

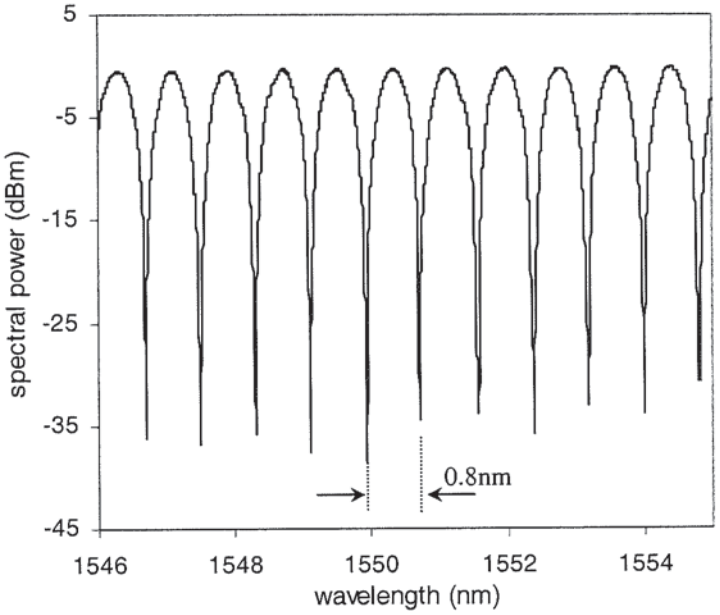

Figure 3.13 Notch filter response when $\theta_1 = 45^0$; $\theta_2 = 45^0$; $\theta_3 = 0^0$.

By setting $\theta_1 = 75^0$; $\theta_2 = 59^0$; $\theta_3 = 45^0$, the corresponding tap coefficients were given by [-0.094, 0.157, 0.585, 0.352] which indicated a flattop response based on simulation. The obtained spectrum agreed well with the superimposed simulation result (dotted trace) as shown in Figure 3.14. The measured side mode suppression was >30dB with ripples in the passband <0.15dB. The flattened passband width was 0.35nm with an FSR of 1.6nm. The measured ripple was attributed to the fluctuations in the measurement laser. Slight Hi-Bi fibre length ratio and angular discrepancies accounted for the less than ideal side lobe suppressions. The length ratio mismatch can be thermally compensated over a small, isolated section of the Hi-Bi fibre.

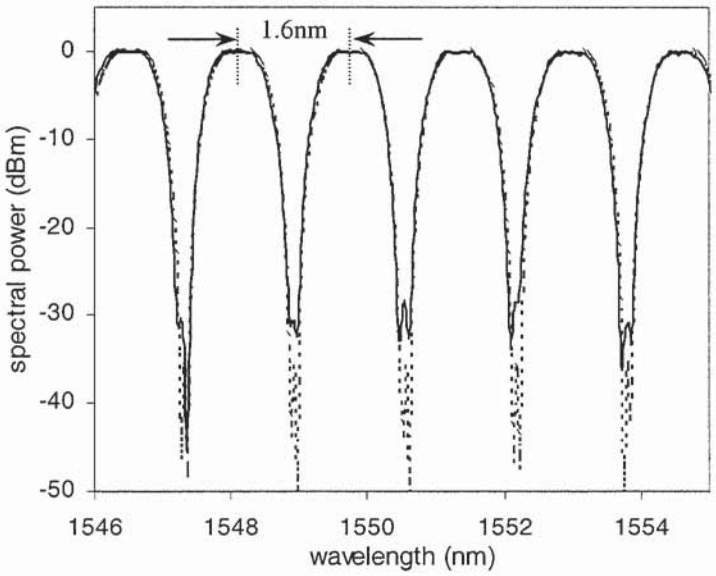

Figure 3.14 Flattop passband filter response when $\theta_1 = 75^0$; $\theta_2 = 59^0$; $\theta_3 = 45^0$. The dotted trace shows the simulated response.

The concept of the optical transversal filter scheme applies equally for greater number of cascaded sections. The increased number of Hi-Bi fibre sections corresponds to an increased number of polarization mode couplings/degenerations that subsequently lead to a greater number of optical taps in the filter structure. For a 3-section cascaded Hi-Bi fibre filter structure, the resultant bipolar optical tap coefficients, as depicted in Figure 3.15, are given by, in temporal sequence,

$$X_m = \begin{bmatrix} x_{xxx} \\ x_{xyx} \\ x_{yxx} \\ x_{yyx} \\ y_{xxx} \\ y_{xyx} \\ y_{yxx} \\ y_{yyx} \end{bmatrix} = \begin{bmatrix} -\cos\theta_1 \cdot \cos\theta_2 \cdot \cos\theta_3 \cdot \cos\theta_4 \\ \cos\theta_1 \cdot \cos\theta_2 \cdot \sin\theta_3 \cdot \sin\theta_4 \\ \cos\theta_1 \cdot \sin\theta_2 \cdot \sin\theta_3 \cdot \cos\theta_4 \\ \cos\theta_1 \cdot \sin\theta_2 \cdot \cos\theta_3 \cdot \sin\theta_4 \\ \sin\theta_1 \cdot \sin\theta_2 \cdot \cos\theta_3 \cdot \cos\theta_4 \\ -\sin\theta_1 \cdot \sin\theta_2 \cdot \sin\theta_3 \cdot \sin\theta_4 \\ \sin\theta_1 \cdot \cos\theta_2 \cdot \sin\theta_3 \cdot \cos\theta_4 \\ \sin\theta_1 \cdot \cos\theta_2 \cdot \cos\theta_3 \cdot \sin\theta_4 \end{bmatrix} \tag{3.23}$$

A total of 8 bipolar optical taps are generated within the structure of which 2 are of opposite polarity to the rest.

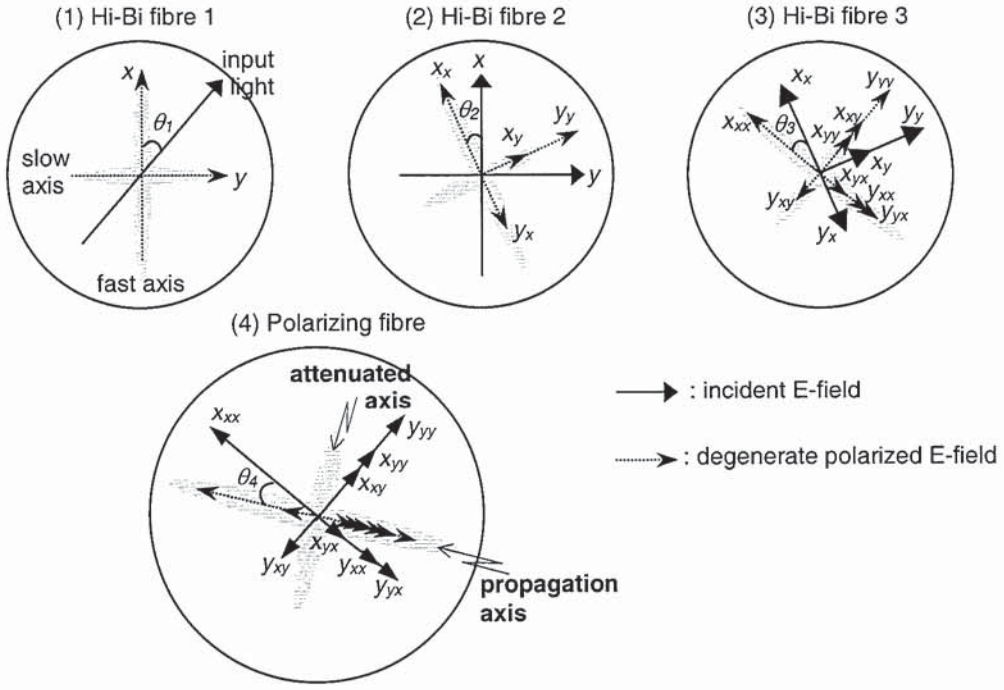

Figure 3.15 Diagrams depicting the degenerations of light propagating through a 3-section Hi-Bi fibre delay line filter structure.

In the experiment, a filter consisting of 3 Hi-Bi fibre sections with lengths of 4.53m, 2.265m and 1.133m were used. Based on simulation, a 3 section delay line filter with length ratios of 4:2:1 and angular orientation of $\theta_1 = 8^0$; $\theta_2 = 82^0$; $\theta_3 = 45^0$; $\theta_4 = 45^0$, at the interfaces produced a wide flattop channel passband of 0.82nm with enhanced side lobe suppression. The corresponding tap coefficients were [-0.069; 0.069; 0.49; 0.49; 0.069; -0.069; 0.01; 0.01] which corresponded to a truncated sinc function with negative coefficients that led to the flattop response [22].

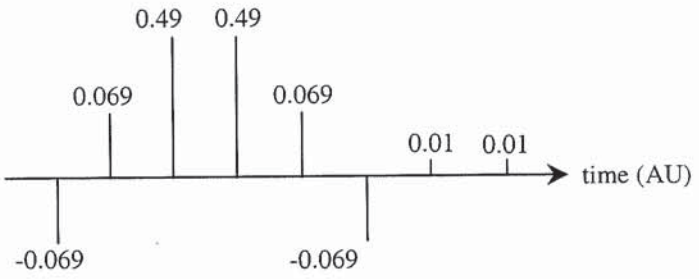

Figure 3.16 Hi-Bi fibre delay line filter tap coefficients corresponding to a truncated sinc function.

The measured spectrum superimposed with simulation results (dotted) is as shown in Figure 3.17. The measured response showed a FSR of 3.2nm and flattened passband width of 0.82nm with ripples <0.1nm. It should be pointed out that in the simulation result, the passband was almost ripple-free. We

attributed part of the measured ripples to the fluctuations of the measurement laser power. Furthermore, although the optical path length ratios between the Hi-Bi fibre sections could be trimmed through thermal conditioning over a Peltier device, a slight length ratio mismatch still existed and accounted for the ripple and the non-ideal side mode suppressions.

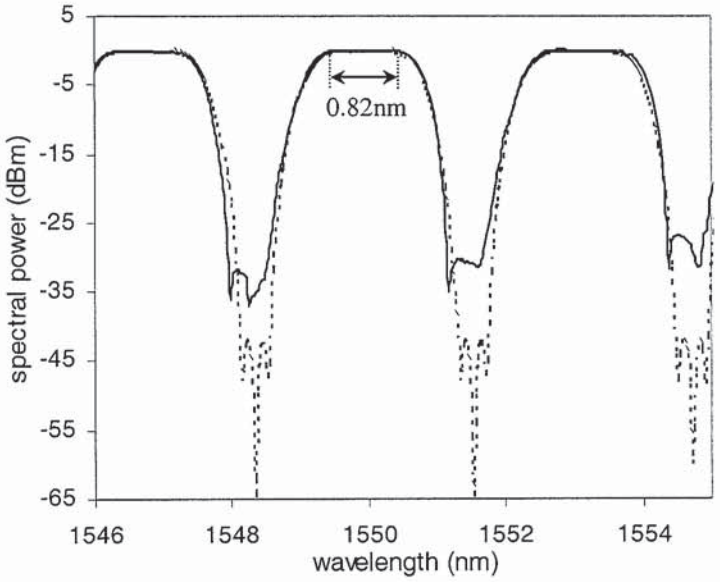

Figure 3.17 Simulated and measured responses of the 3-section Hi-Bi fibre delay line filter when $\theta_1 = 8^0$; $\theta_2 = 82^0$; $\theta_3 = 45^0$; $\theta_4 = 45^0$.

The dispersion characteristic of the filter was measured using the modulation phase shift technique [51]. A tunable laser in parallel with a Lightwave Component Analyser (LCA) was adopted for the measurement as shown in Figure 3.18.

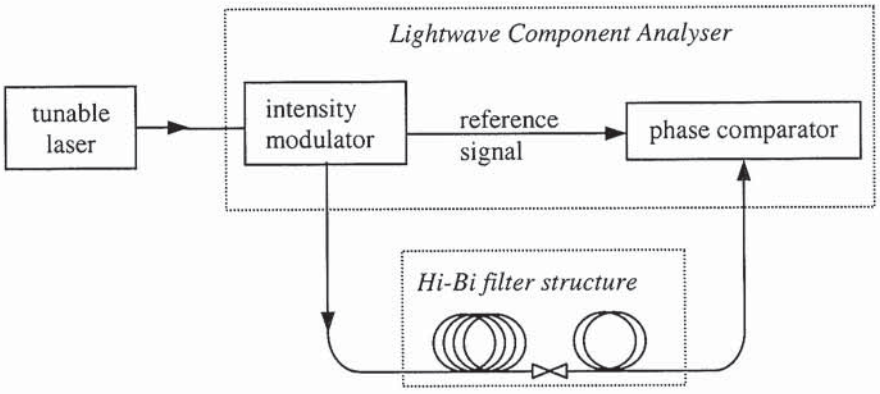

Figure 3.18 Group delay measurement setup to characterize the filter passband dispersion response.

The well-established modulation phase shift technique relates the measured electrical phase $\theta(\nu_0)$ of the intensity-modulated light to the group delay $\tau_{GD}(\nu_0)$ by the well-known equation

$$\tau_{GD}(\nu_0) = \frac{\theta(\nu_0)}{2\pi f_m} \tag{3.24}$$

where f_m is the modulation frequency and ν_0 is the optical carrier frequency. The group delay characteristics as a function of wavelength are obtained and the chromatic dispersion response is simply the derivative. It is evident that the modulation frequency used determines the frequency separation of the sidebands in the modulated signal. The phase measurement is in actual fact made by sampling two points at f_m away from the optical carrier frequency (despite $\nu_0 \gg f_m$). It has been recognized [52] that for devices with group delay characteristics that vary significantly with wavelength, the modulation phase shift technique using high modulation frequency (1 to 5 GHz) results in a smoothing-out effect and a well-known reduction in the actual peak-peak delay ripple measurement value. Hence, to maintain the desired wavelength accuracy and reliability of the group delay measurement, a low modulation frequency is preferred even though the timing resolution is reduced.

In the experiment, a modulation frequency of 200MHz and wavelength step of 5pm were adopted. The phase measurement accuracy achievable from the LCA was 0.01^0 leading to a timing resolution of 0.14ps. The group delay characteristic across a passband of the 2-section Hi-Bi fibre delay line filter structure when $\theta_1 = 75^0$; $\theta_2 = 59^0$; $\theta_3 = 45^0$ is as shown in Figure 3.19.

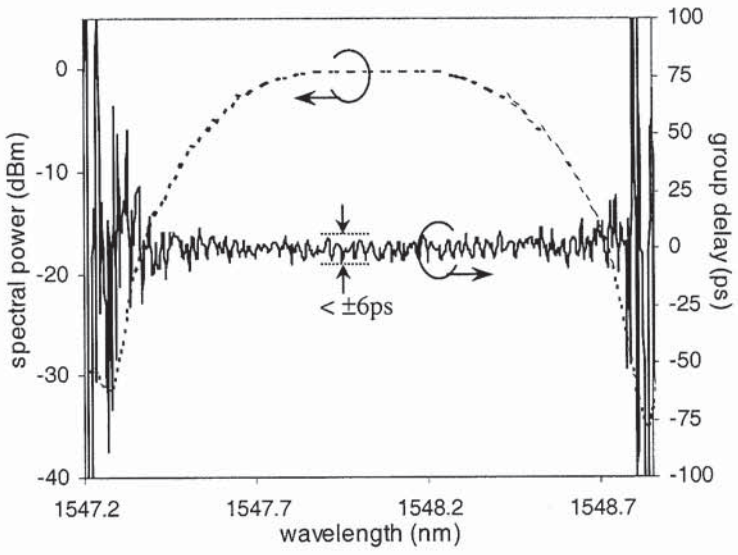

Figure 3.19 Measured group delay characteristics across a passband channel of the filter. The angular alignments between the cascaded Hi-Bi fibre sections were $\theta_1 = 75^0$; $\theta_2 = 59^0$; $\theta_3 = 45^0$.

From the results obtained, it was evident that the filter exhibited only a small amount of chromatic dispersion. The peak-to-peak group delay ripple across the passband of the filter response was < ±6ps at the modulation frequency of 200MHz. It is important to note that the system noise contribution during characterization process was measured to be of the same order of magnitude. The ultra-low dispersion

characteristics extend to all wavelength channels highlighted by Figure 3.20. Random group delay noise values outside the passband of the filter response were attributed to the low transmitted optical power.

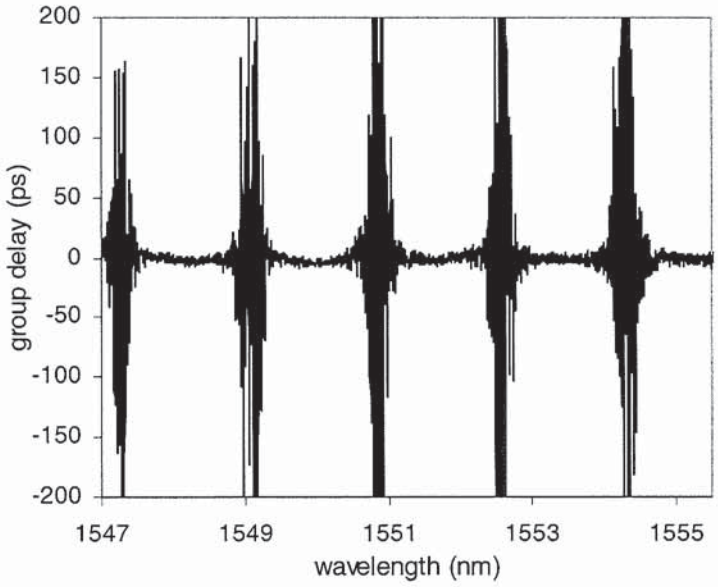

Figure 3.20 Measured filter group delay characteristics across a number of passbands.

It is important to note that the flattop passband response is a characteristic feature of a delay line filter architecture with bipolar taps [22]. Such transfer response is not achievable on a positive system. Since the single-line Hi-Bi fibre delay line architecture exhibits immunity to optical coherence interference noise, its practical implementation does not impose additional requirements on the optical source coherence. The stability of the filter was further exemplified by the long measurement time during the group delay characterization. The filter scheme, apart from its engineering simplicity, exploits the merits of optical fibres like low dispersion and ultra-wide operation bandwidth. In contrast to transversal form filters [19]-[21][53] on silica waveguides, the tap weightings can be determined easily without the need for an impulse response measurement. Furthermore, with commercially available Hi-Bi fibre keyed connectors and precision rotators, coupling angles (θ_1 to θ_4) can be, in practice, set to an accuracy of $<0.1^0$. Since the configuration does not employ mechanically induced twist or the use of fibre waveplates/free-space optics, it exhibits negligible insertion loss. To effectively enhance the filter isolation/sidelobe suppression, two or more of the filter structures can be concatenated during operation.

As in all delay line filter schemes, the optical taps form the key to the operation, hence output transfer function of the filter structure. Variations to the orientations between the fibre ends and/or lengths of the cascaded sections in the Hi-Bi fibre delay line filter structure alter the tap coefficients and a variety of transfer responses can be flexibly set. On a similar basis, further manipulations to the optical taps using some off-the-shelf components can enable interesting and useful filter responses like complementary outputs and directional isolation functionality, which are detailed in the following sections.

3.3.3 Simultaneous complementary output filter

An important trend in the next generation of fibre optical communication systems, apart from the higher speed and longer transmission distance, is the better utilization of the available spectrum. The obvious choice of reduction of channel spacing to increase the channel count poses technical challenges around insertion loss, chromatic dispersion etc to the component design [35]. An effective way to achieve denser channel spacing is to interleave wavelength channels that have wider spacing. Such components, known as interleavers, enable the practical implementation of dense wavelength division multiplexed (DWDM) systems by transforming the tougher task of separating or combining a single set of very closely spaced channels into an easier solution of separating or combing multiple sets of widely spaced channels. Their main functions include multiplexing (MUX), demultiplexing (DEMUX), optical add/drop and Rayleigh noise reduction in bi-directional systems [54]. To meet the requirement of next generation optical communication systems, such passive DWDM components must posses low dispersion, low loss, high isolation as well as flattened passbands [41]. Realisations of interleavers based on MZ interferometers out of fused fibres, planar lightwave circuits (PLC) and bulk optics configurations have been demonstrated [36] [40][55][56].

As mentioned in the previous section, the Hi-Bi fibre delay line filter response depends on the optical taps generated within the structure. With reference to Figure 3.10, the resultant output tap coefficients along the propagation axis of the polarizing fibre evidently depend on the coupling angle θ_3. Interestingly, by orientating the propagation axis of the polarizing fibre by a further 90^0, the output tap coefficients will be given by

$$X_m = \begin{bmatrix} x_{xy} \\ x_{yy} \\ y_{xy} \\ y_{yy} \end{bmatrix} = \begin{bmatrix} \cos\theta_1 \cdot \cos\theta_2 \cdot \sin\theta_3 \\ \cos\theta_1 \cdot \sin\theta_2 \cdot \cos\theta_3 \\ -\sin\theta_1 \cdot \sin\theta_2 \cdot \sin\theta_3 \\ \sin\theta_1 \cdot \cos\theta_2 \cdot \cos\theta_3 \end{bmatrix} \tag{3.25}$$

instead of (3.21) for the case depicted for Figure 3.10.

$$X_m = \begin{bmatrix} x_{xx} \\ x_{yx} \\ y_{xx} \\ y_{yx} \end{bmatrix} = \begin{bmatrix} -\cos\theta_1 \cdot \cos\theta_2 \cdot \cos\theta_3 \\ \cos\theta_1 \cdot \sin\theta_2 \cdot \sin\theta_3 \\ \sin\theta_1 \cdot \sin\theta_2 \cdot \cos\theta_3 \\ \sin\theta_1 \cdot \cos\theta_2 \cdot \sin\theta_3 \end{bmatrix} \tag{3.26}$$

Notably, the magnitude and order of occurrence of the negated tap differ between the two cases and the simulation results for both cases are as shown in Figure 3.21.

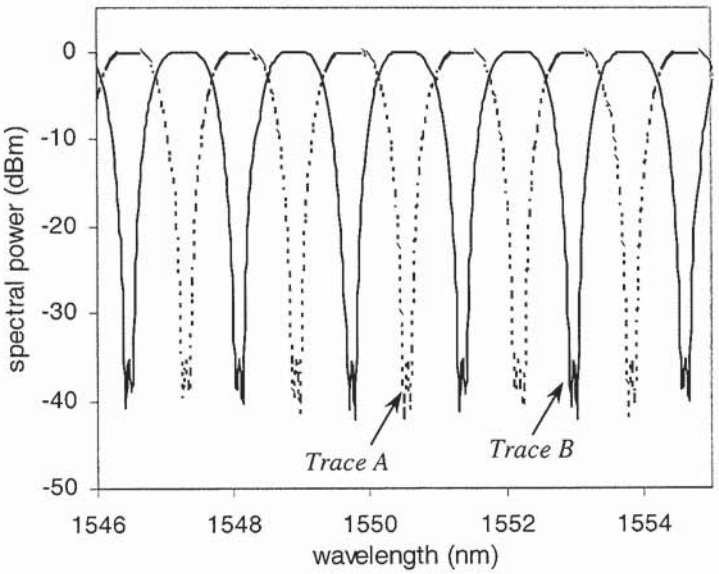

Figure 3.21 Simulated output filter responses for the two sets of orthogonal tap coefficients corresponding to angular alignments at $\theta_1 = 75^0$; $\theta_2 = 59^0$; $\theta_3 = 45^0$ (Trace A) and $\theta_1 = 75^0$; $\theta_2 = 59^0$; $\theta_3 = 135^0$ (Trace B).

From the results shown in Figure 3.21, it can be observed that the output responses along orthogonal axial directions are complementary to each other. This response characteristic applies to all angular arrangements (θ_1, θ_2) as exemplified by the similar response behaviours between $\theta_1 = 45^0$; $\theta_2 = 90^0$; $\theta_3 = 45^0$ and $\theta_1 = 45^0$; $\theta_2 = 90^0$; $\theta_3 = 135^0$, as shown in Figure 3.22. The wavelength-interleaved output response shows that a multichannel demultiplexer may be realised where the transfer function depends on the coupling angles and the free spectral range largely determined by the birefringence and the lengths of the Hi-Bi fibre sections adopted.

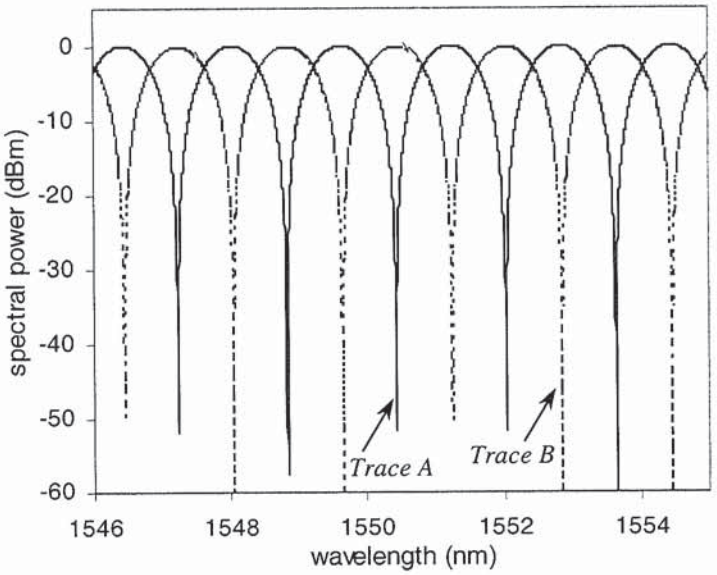

Figure 3.22 Simulated complementary notch filter responses from orthogonal output axes at $\theta_1 = 45^0$; $\theta_2 = 90^0$; $\theta_3 = 45^0$ (Trace A) and $\theta_1 = 45^0$; $\theta_2 = 90^0$; $\theta_3 = 135^0$ (Trace B).

In the experiment, in order to obtain simultaneous complementary outputs from the filter architecture along orthogonal propagation axes, a commercially available fibre-pigtailed polarization beam splitter was employed in place of the polarizing fibre. This is illustrated in Figure 3.23.

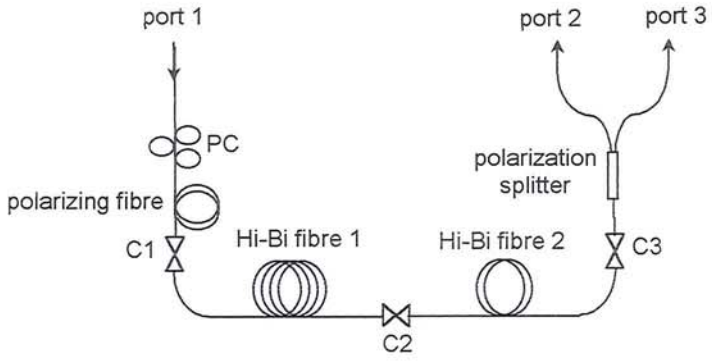

Figure 3.23 Experimental setup for the dual complementary output Hi-Bi fibre delay line filter.

The output arms of the polarization splitter, namely port 2 and port 3, corresponded to propagation paths for light along the fast and slow axes of the polarization beam splitter. Based on the same set of experiment parameters in section 3.3.2 (Figure 3.9), the output FSR of 1.6nm led to an interleaved channel spacing of 0.8nm (100GHz) and the measured response when $\theta_1 = 45^0$; $\theta_2 = 90^0$; $\theta_3 = 45^0$ and $\theta_1 = 75^0$; $\theta_2 = 59^0$; $\theta_3 = 45^0$ are as shown in Figure 3.24 and Figure 3.25.

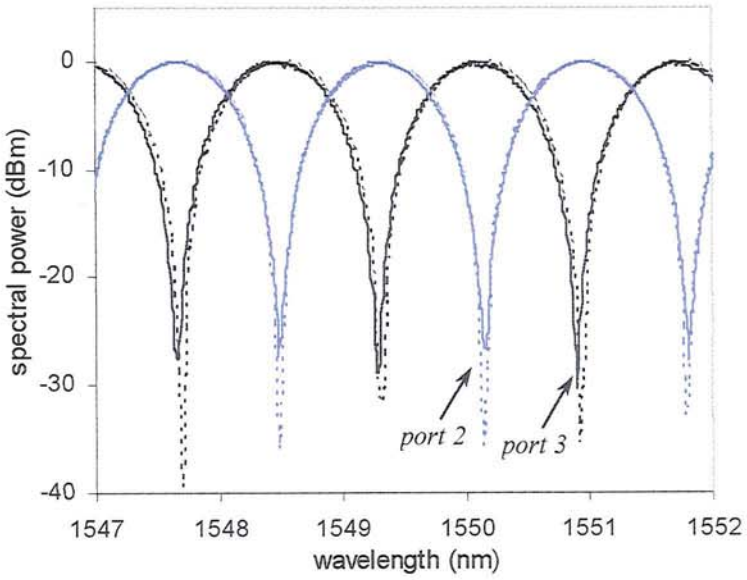

Figure 3.24 Measured (solid traces) and simulated (dotted traces) notch responses from output port 2 and port 3 when $\theta_1 = 45^0$; $\theta_2 = 90^0$; $\theta_3 = 45^0$.

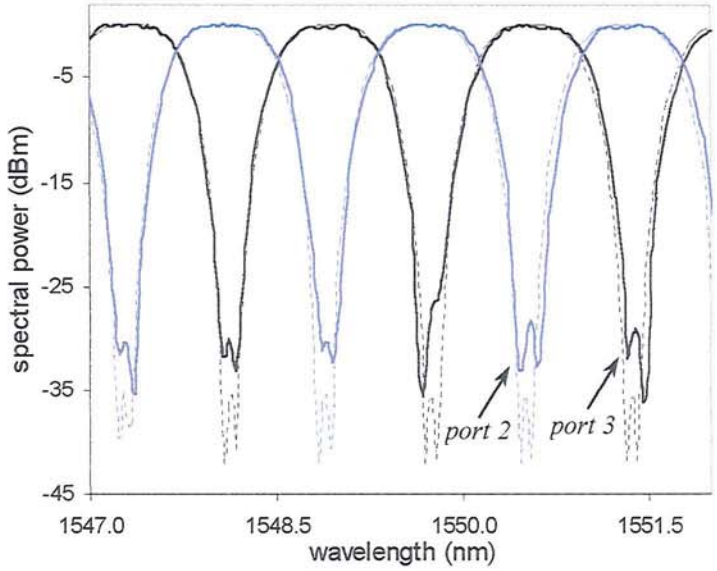

Figure 3.25 Measured (solid traces) and simulated (dotted traces) notch responses from output port 2 and port 3 when $\theta_1 = 75^0$; $\theta_2 = 59^0$; $\theta_3 = 45^0$.

In a similar context, an identical polarization splitter was adopted at the front end of the filter structure so as to transform the architecture into a 4-port device as shown in Figure 3.26.

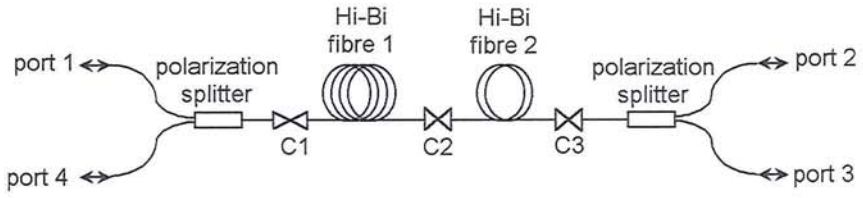

Figure 3.26 Hi-Bi fibre delay line filter with dual input and dual output ports by adopting an additional polarization splitter at the front end of the filter structure.

It is important to note that the filter configuration, in the absence of nonreciprocal optical elements, exhibited reciprocal responses such that the wavelength transfer characteristics between port 1↔ port 2 are identical to port 4↔ port 3. Denoting the interleaved channels as odd (λ_1, λ_3, λ_5) and even (λ_2, λ_4, λ_6) wavelength sets, the operation of the filter can be illustrated by the block diagram as shown in Figure 3.27.

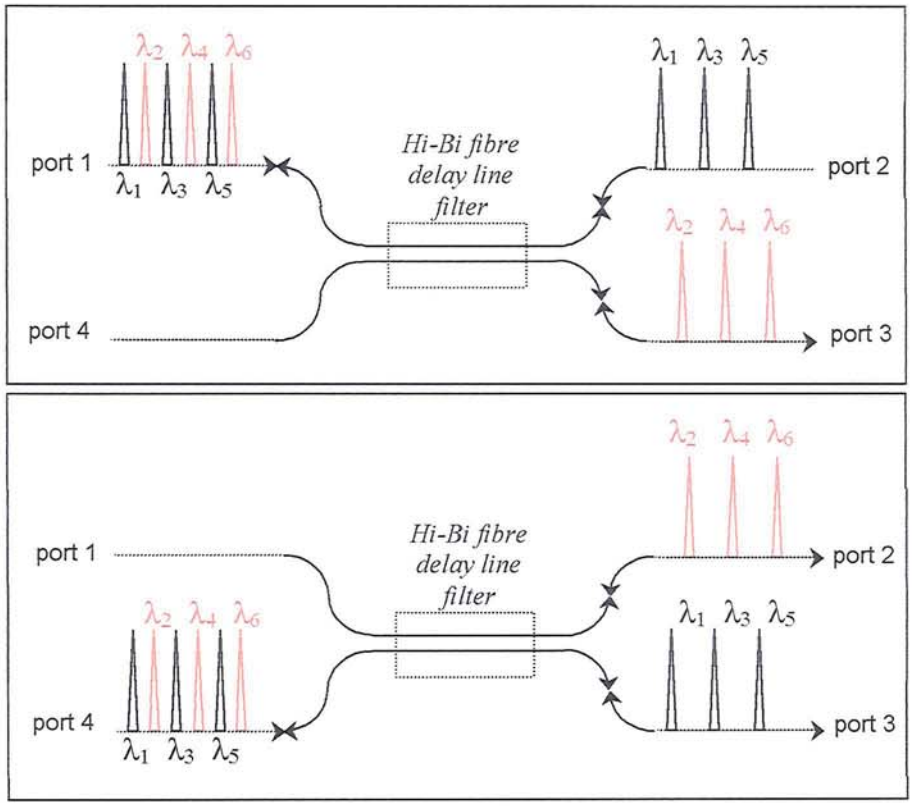

Figure 3.27 Block diagram illustrating the operations of the 4-port Hi-Bi fibre delay line filter structure.

The reciprocal response between successive ports (i.e. port 1↔ port 2; port 3↔ port 4) and complementary response between exit ports enables the 4-port configuration to realise channel add/drop functions. With reference to Figure 3.27, for a transmission link between port 1 and port 2, even channels propagating from port 1 towards port 2 are separated from odd channels and drop off at port 3. Adopting port 4 as an input path, even channels can then be re-introduced into the transmission link without the need of additional coupler or wavelength multiplexers. The 4-port filter scheme hence effectively operates as a wavelength interleaver for both multichannel multiplexing as well as demultiplexing, which is highly desired in DWDM optical communication systems.

3.3.4 Bidirectional nonreciprocal wavelength-interleaved filter

As highlighted in the previous section, the rapid advancement of optical fibre communication systems has raised considerable interest towards techniques that enable higher bandwidth usage efficiency. Apart from wavelength channels interleaving, a bidirectional transmission technique potentially enables doubling of the spectral efficiency by using the same set of optical frequencies for both upstream and down stream transmissions. Bidirectional WDM transmission over a single fibre, compared to unidirectional transmission, effectively reduces the use of fibre infrastructure by a factor of two and its feasibility has been demonstrated [57][58]. Such transmission systems however suffer drastic penalties due to back reflections [59]-[61][62]. Furthermore, in the presence of optical gain and the close proximity of the densely spaced wavelength channels, nonlinear interactions between the adjacent channels and backreflections from processes like stimulated Brillouin scattering (SBS) and Rayleigh backscattering [63]-[67] can cause signal distortion, increased crosstalk and EDFA noise figure degradation. To alleviate undesirable nonlinear interactions between adjacent channels and to prevent signal degradation and oscillations by optical backreflections, a bidirectional non-reciprocal wavelength-interleaved transmission scheme has been proposed and demonstrated [68][69]. This form of bidirectional transmission technique increases adjacent channel spacing by assigning a set of wavelength channels for one transmission direction while allocating an interleaved set of wavelength channels for the opposing transmission direction. This wavelength allocation and isolation scheme for the opposing transmitted wavelength channels (denoted as odd and even channels) effectively reduces channel cross talk as well as preventing oscillations in bidirectional amplifiers.

On the other hand, to effectively isolate backreflections from opposing WDM optical channels, optical devices that exhibit complementary periodic wavelength transfer functions between opposing transmission ports are needed. These devices enable wavelength interleaving while providing directional isolation to the interleaved channels. In conjunction with common bidirectional amplifiers such as the EDFA, they effectively allow bidirectional signal amplifications not limited by backscattering and optical reflections. Desirable device features for high level of performance include low loss, low dispersion, good isolation, and reconfigurable transfer responses. Implementations involving optical path separations through circulators, multiplexer/demultiplexer modules and filters have been demonstrated [68]-[70]. However such schemes can be restricted in the channel count and scalability by the operation bandwidth of the optical components adopted. Furthermore, the use of these components to separate optical paths can compromise noise figure performance [71]. Alternative approaches based on unique birefringent crystals and waveplates configurations have also been proposed e.g. [71][72].

It has been highlighted in the previous section that the resultant optical taps derived from orthogonal output propagation axes differ in the magnitude and order of occurrence of the negated tap. Consequently the filter responses are complementary between the two output propagation axes. In a similar context, by introducing polarization plane rotation on light propagating in one direction but not the other, the Hi-Bi fibre delay line filter structure will be able to perform bidirectional, nonreciprocal wavelength-interleaving transfer operation. In practice, this is achieved simply by incorporating an off-the-shelf fibre-pigtailed Faraday rotator within the filter architecture as shown in Figure 3.28.

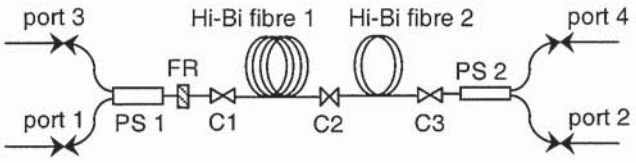

Figure 3.28 Hi-Bi fibre delay line configuration to perform bidirectional nonreciprocal wavelength interleaving filter function. PS: Polarization splitter; FR: Faraday rotator.

The configuration of the filter is similar to Figure 3.26 with the exception of the inclusion of a Faraday rotator (FR). Hi-Bi fibre 1 and 2 of length ratio 2:1 forms the wavelength-selective element while polarization splitters PS 1 and PS 2 couple light to and from its input/output ports onto the propagation axes of the Faraday rotator and Hi-Bi fibre 2 respectively. The off-the-shelf fibre-pigtailed Faraday rotator creates a 90^0 polarization plane rotation on light that propagates in the reverse direction (port 2→port 1).

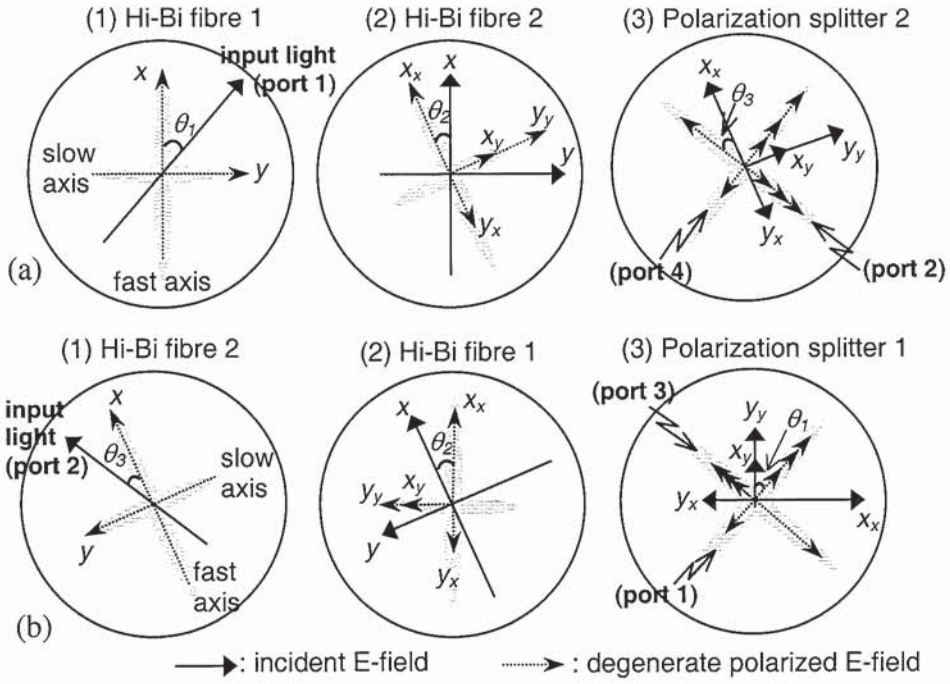

Figure 3.29 Figures depicting degenerations of E-fields in the (a) forward operation and (b)reverse operation of the filter structure.

Depicted in Figure 3.29a, in the forward operation (port 1→port 2), the port 1 input light (after the FR) launched into Hi-Bi fibre 1 at an azimuth θ_1 degenerates into two orthogonal polarized modes x, y. These optical taps with a delay interval τ_1 given by $\tau_1 = \Delta n \cdot L_1/c$ where c is the speed of light, L_1 is the length of Hi-Bi 1 and Δn is the fibre birefringence, couple into Hi-Bi fibre 2 at an azimuth θ_2 and degenerate to form polarized modes x_x, x_y, y_x, y_y sequentially. The delay interval τ_2 between these temporally evenly

spaced signal taps is given by $0.5\tau_1$ due to the Hi-Bi fibre length ratio. Subsequently, these polarized modes couple into the propagation axes of polarization splitter PS 2 to form the signal taps that determine the wavelength transfer characteristics at output ports 2 and 4.

In the reverse operation, as depicted in Figure 3.29b, similar polarization mode degeneration occurs as the input light propagates from port 2 towards port 1. The only difference lies in the 90^0 polarization plane rotation (with respect to propagation axes of PS 1) by the Faraday rotator before the optical taps x_x, y_x, x_y, y_y couple from Hi-Bi 1 into the propagation axes of PS 1. Note that the degenerate polarized modes x, y from the port 2 input light are temporally spaced at τ_2 and the delay interval between subsequent degenerate modes x_x, x_y or y_x, y_y in Hi-Bi 1 is given by $2\tau_2$ as a result of the Hi-Bi fibre length ratio. Consequently, the temporal sequence, in increasing order of time, of the output signal taps is x_x, y_x, x_y, y_y with delay interval similarly given by $0.5\tau_1$.

It is evident that the electric field amplitudes of all the polarized modes (hence tap coefficients) are only determined by coupling angles θ_1, θ_2 and θ_3. Based on Figure 3.29, the electric field amplitudes (tap coefficients) at output port 2 in the forward operation and output port 1 in the reverse operation can be expressed as

$$\begin{bmatrix} x_x \\ x_y \\ y_x \\ y_y \end{bmatrix} = \begin{bmatrix} -\cos\theta_1 \cdot \cos\theta_2 \cdot \cos\theta_3 \\ \cos\theta_1 \cdot \sin\theta_2 \cdot \sin\theta_3 \\ \sin\theta_1 \cdot \sin\theta_2 \cdot \cos\theta_3 \\ \sin\theta_1 \cdot \cos\theta_2 \cdot \sin\theta_3 \end{bmatrix} \text{ and } \begin{bmatrix} x_x \\ y_x \\ x_y \\ y_y \end{bmatrix} = \begin{bmatrix} \sin\theta_1 \cdot \cos\theta_2 \cdot \cos\theta_3 \\ -\sin\theta_1 \cdot \sin\theta_2 \cdot \sin\theta_3 \\ \cos\theta_1 \cdot \sin\theta_2 \cdot \cos\theta_3 \\ \cos\theta_1 \cdot \cos\theta_2 \cdot \sin\theta_3 \end{bmatrix} \tag{3.27}$$

respectively. Evidently, there is 1 tap negated with respect to the rest in each output group and of a different magnitude at a different order of occurrence. On a similar context to previous section, the resultant output responses from the two sets of tap coefficients are mutually complement. Nonreciprocal response is hence achieved between the output ports for the counter-propagating operations. Since the tap coefficient is a function of the coupling angles, a variety of wavelength transfer characteristics can be achieved by simply varying θ_1, θ_2 and θ_3. The free spectral range (FSR) of the output response, determined by the tap interval, is given by $1/(0.5\tau_1)$. Accurate alignment to the desired FSR can be achieved by suitable choice of Hi-Bi fibre length and birefringence. Similar analysis extends to port 3↔port 4, port 3↔port 2, and port 1↔port 4. The operation of the filter between different ports can be illustrated by the propagation paths of the odd and even channels as shown in Figure 3.30.

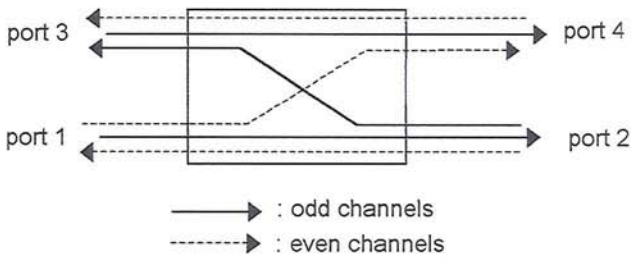

Figure 3.30 Equivalent block diagram showing the operation of the filter scheme.

In the experiment, under two special cases: $\theta_1 = 45°$; $\theta_2 = 0°$; $\theta_3 = 45°$ and $\theta_1 = 45°$; $\theta_2 = 90°$; $\theta_3 = 45°$, the relative orientations between the birefringence axes of Hi-Bi fibre 1 and 2 were aligned and orthogonal respectively. These reconfigured the structure to a 2-tap optical notch filter with maximum tap time interval for the former and minimum tap time interval for the latter. Figure 3.31 shows the superimposed measured forward and reverse filter responses between port 1 and port 2 at θ_1=45°; θ_2=0°; θ_3= 45° while the filter response at θ_1=45°; θ_2=90°; θ_3= 45° is as shown in Figure 3.32.

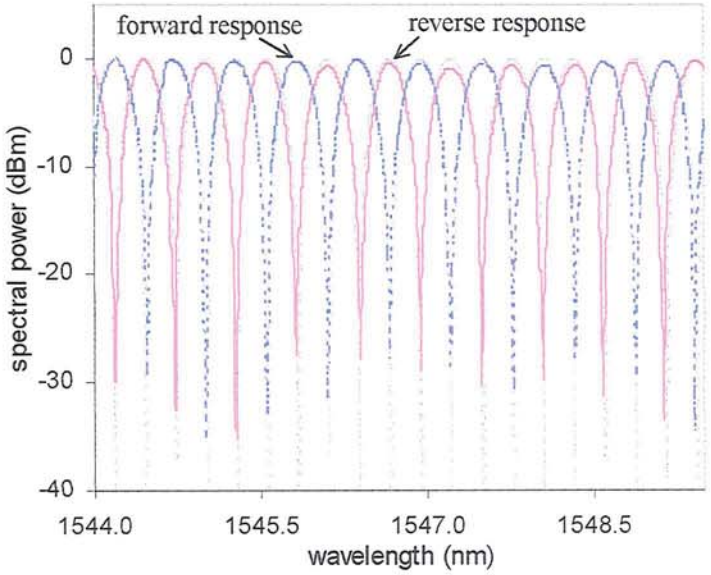

Figure 3.31 Simulation (grey traces) and measured forward and backward responses of the filter at port 1 and port 2 when θ_1=45°; θ_2=0°; θ_3=45°.

The obtained spectrum agreed well with the simulation results. The measured FSR were 0.53nm and 1.6nm respectively with notch depth measured to be >30dB. Nonreciprocal wavelength-interleaving filter characteristics were clearly evident. Similarly, by setting θ_1=75°; θ_2=58°; θ_3 = 45° a flattop bandpass response as shown in Figure 3.33 was realised. The characteristic feature of bipolar operation was evident through the flattened passbands measured 0.32nm with ripples <0.1dB for both forward and reverse operations. The measured FSR of 1.6nm consequently resulted in interleaved channel spacing of 0.8nm.

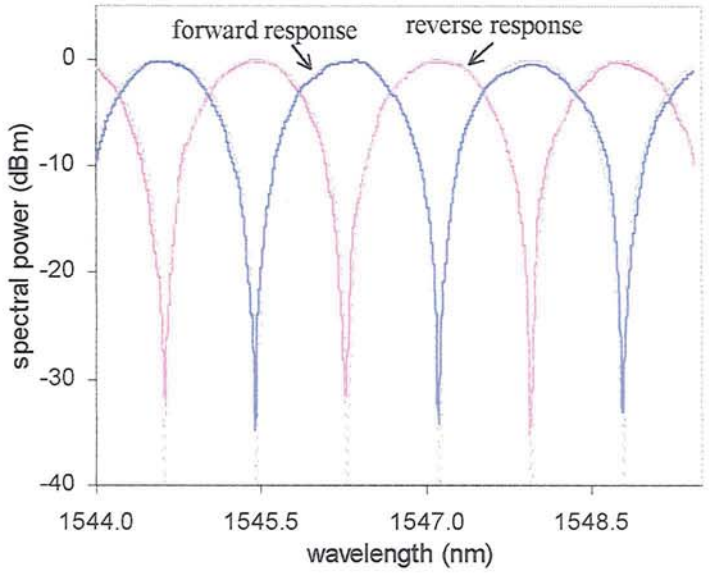

Figure 3.32 Simulation (dotted trace) and measured forward and backward responses of the filter at port 1 and port 2 when θ_1=45°; θ_2=90°; θ_3=45°.

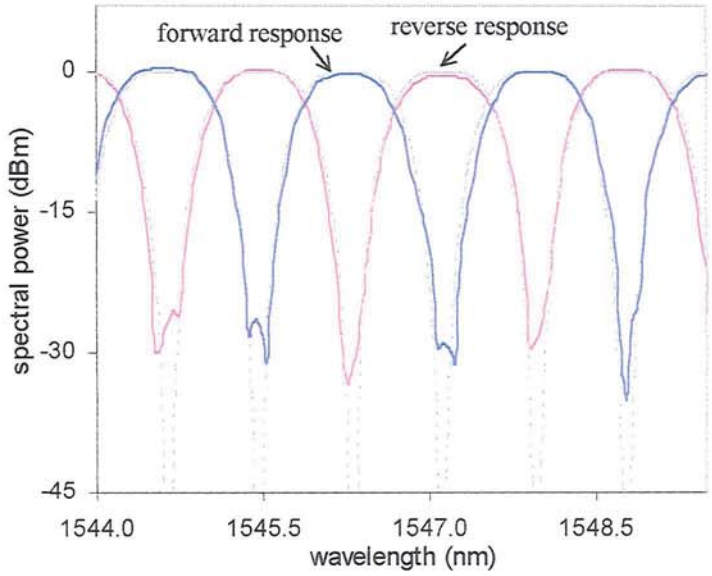

Figure 3.33 Simulation (dotted trace) and measured forward and backward responses of the filter at port 1 and port 2 when θ_1=75°; θ_2=59°; θ_3=45°.

The bidirectional nonreciprocal wavelength-interleaver based on coherent fibre delay line filter has several advantages over proposed schemes described in [71]-[73]. Most notably, without the use of bulk optics and/or expensive birefringent crystal-based inner stages, the architecture avoids critical optics alignment to achieve low loss performance and ease of implementation. More importantly, the operating bandwidth and the wavelength transfer response of the filter scheme are not limited by the low dispersion characteristics of the wavelength-selective element. In many crystal/bulk optics-based filter schemes, Calcite

blocks exhibiting dispersion on the order of 1.5ps/nm over a length of 17mm (an order higher than that in the fibre delay line filter scheme), are often adopted. Due to its fibre based configuration and engineering simplicity, the filter offers reconfigurable wavelength transfer function (by varying angular alignments θ_1, θ_2, θ_3), wide operation bandwidth and negligible chromatic dispersion across all wavelength channels. Since the material dispersion of the Hi-Bi fibre is very small, the wavelength transfer characteristics of the transversal filter extend without distortion across the entire C-band. Contrary to reported schemes [68]-[74], excess loss within the device is not attributed to the wavelength-selective filter element (i.e. Hi-Bi fibre sections) but due to the insertion losses of the polarization rotator and splitters measured <1dB. Since the concept of the delay line filter applies to a greater number of cascaded Hi-Bi fibre sections, enhanced filter response (e.g. higher side lobe suppression, widened passband width) can hence be realised without compromising insertion loss. Equivalent fibre technology of the Faraday rotator and polarization splitter e.g. [75][76] can be alternatively adopted in practice to realise a truly all-fibre configuration. On the basis of its fibre-based configuration, the filter scheme can potentially enable bidirectional, nonreciprocal wavelength-interleaving amplification by adopting Hi-Bi rare-earth doped fibres. Contrary to all reported schemes, such Hi-Bi fibre delay line amplifier architecture will not require additional cascaded unidirectional amplifiers or circulars to enable high performance, low noise figure bidirectional amplification.

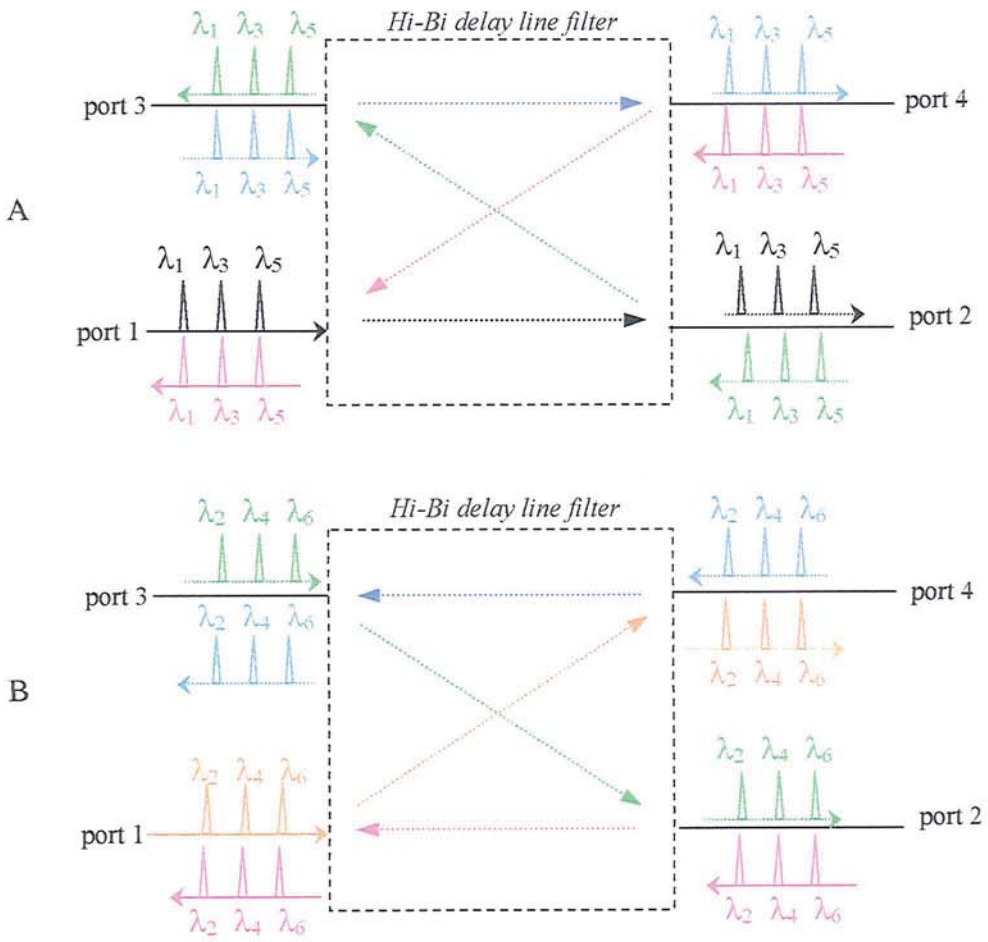

Figure 3.34 Schematic diagrams showing the filter operating as a circulator.

Conceptually similar to [74], it is interesting to note that the filter scheme can be adapted to perform a bidirectional circulator function as depicted in Figure 3.34. Wavelength channels (odd channels) propagating from port 1 to port 2 can be circulated to port 3 with equivalent double-pass isolation. Since the device performs a bidirectional isolation function between any two adjacent ports, the odd wavelength channels, as shown in Figure 3.34A, therefore can be made to circulate from port 1→port 2→port 3→port 4 and back to port 1 while the even channels, as shown in Figure 3.34B, can be similarly made to propagate through port 1→port 4→port 3→port 2 before going back to port 1. Applications of such a device could be found in network monitoring and to provide an interface to interconnect bidirectional and unidirectional optical networks [74][77].

3.3.5 Microwave/millimetre wave signal processor

Besides optical signal processing functions, the fibre optical delay line structure is perhaps most commonly used as a microwave/millimetre signal processor. RF signal processing in the fibre optical domain utilizes the intrinsic advantages of optical fibres like high time-bandwidth product and low loss to overcome electronic bottleneck with conventional high-speed electronic signal processors. There has been increasing interest in using such fibre-based devices in fibre-fed broadband wireless networks, and various architectures have been proposed [e.g. 11-16]. As mentioned in section 3.2, many of the proposed schemes to date are incoherent systems where synthesis of optical beams based on low coherence source and/or large optical path difference are necessary to avoid optical interferometric intensity noise. This leads to the FSR of the filter being limited by the requirement that the shortest optical path difference be longer than the source coherence length. Proposed methods like the use of multiple sources or multimode lasers [16][78], though capable of achieving a large FSR, however impose a requirement on the transmission system.

The concept of the Hi-Bi fibre delay line filter structure applies equally to the RF frequency domain. Owing to the single-line cascaded Hi-Bi fibre structure, the environmental sensitivity typical of fibre-based optically coherent devices is greatly reduced. Furthermore, as detailed in previous sections, manipulation of the bipolar signal taps generated through the device architecture allows various frequency transfer responses, depending on the angular alignments θ_1, θ_2 and θ_3. The measurement setup using a Lightwave Component Analyser (LCA) for the characterization of the frequency response of the 2-section Hi-Bi delay line filter structure is as shown in Figure 3.35.

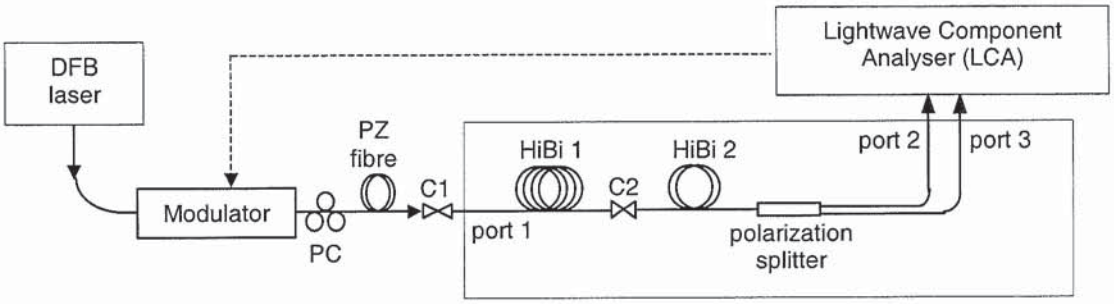

Figure 3.35 Measurement setup for the characterization of the frequency response of the 2-section Hi-Bi fibre delay line filter. PC: polarization controller, PZ fibre: polarizing fibre.

From (3.13), it is evident that the free spectral range of the filter structure depends strongly on the length of the fibre adopted. For a fibre of birefringence 5.1×10^{-4}, and with the system measurement range limited to <20GHz, fibre lengths on the order of at least 29.5m are required in order to observe the spectral features within the 20GHz measurement range. In the experiment, using available fibre lengths of 64.78m and 32.39m to form Hi-Bi 1 and Hi-Bi 2, filter responses with FSR in the range of 6GHz are achieved.

Similarly, when θ_1=45°; θ_2=0°; θ_3=45° and θ_1=45°; θ_2=90°; θ_3=45° the relative orientation between the birefringence axes of Hi-Bi fibre 1 and 2 were aligned and orthogonal respectively. These reconfigured the structure to a 2-tap RF notch filter with maximum tap time interval for the former and minimum tap time interval for the latter. Furthermore, taking note that the output axis of port 2 was orthogonal to that of port 3,

the set of output optical taps differed in the order of occurrence and the magnitude of the negated tap, based on (3.25) and (3.26). This resulted in complementary output response between port 2 and port 3. The measured and simulated (dotted) normalized complementary notch responses from the output ports when θ_1=45°; θ_2=0°; θ_3=45° are as shown in Figure 3.36 and Figure 3.37. The measured FSR was 6.1GHz.

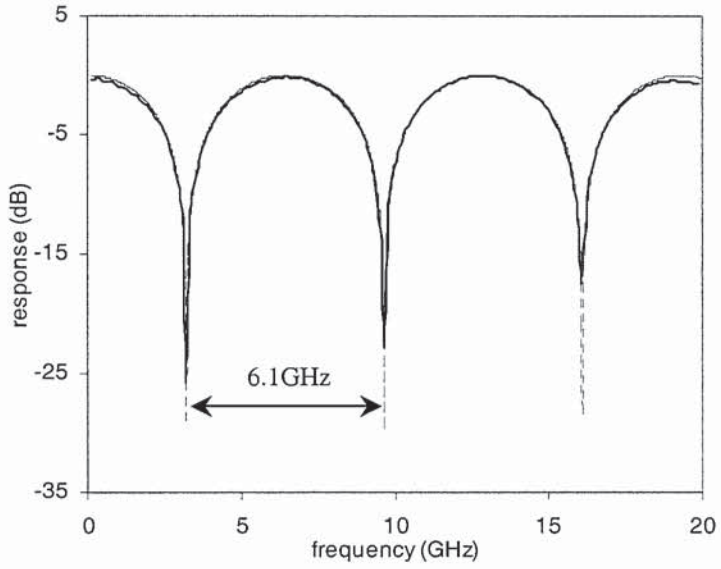

Figure 3.36 Measured (solid) and simulated (dotted) microwave notch responses from output port 2 when θ_1=45°; θ_2=0°; θ_3=45°.

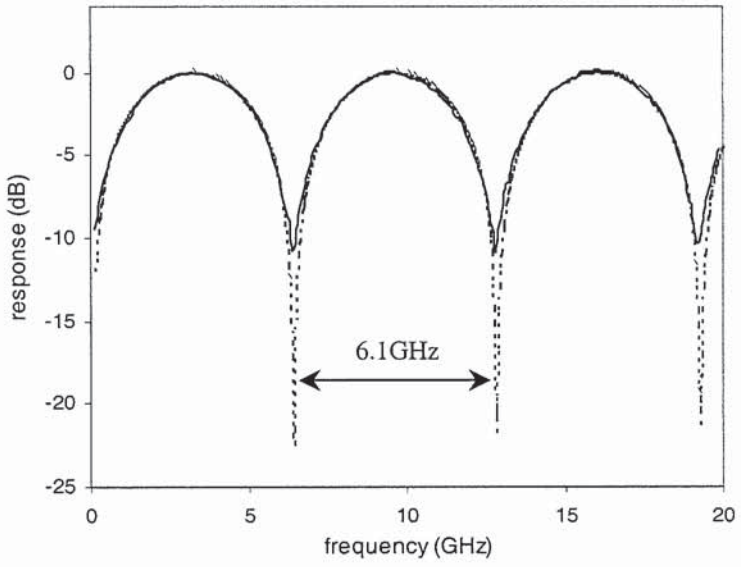

Figure 3.37 Measured (solid) and simulated (dotted) microwave notch responses from output port 3 when θ_1=45°; θ_2=0°; θ_3=45°.

Figure 3.38 and Figure 3.39 show the complementary output responses between port 2 and port 3. when θ_1=45°; θ_2=90°; θ_3=45°. Evidently due to the reduction in the unit time delay between the signal taps, the measured FSR widened to 18.2GHz. The null response at zero frequency achieved in Figure 3.37 and

Figure 3.39 were clear illustrations of the complex signal filtering functions based on this negative tap delay line filter scheme.

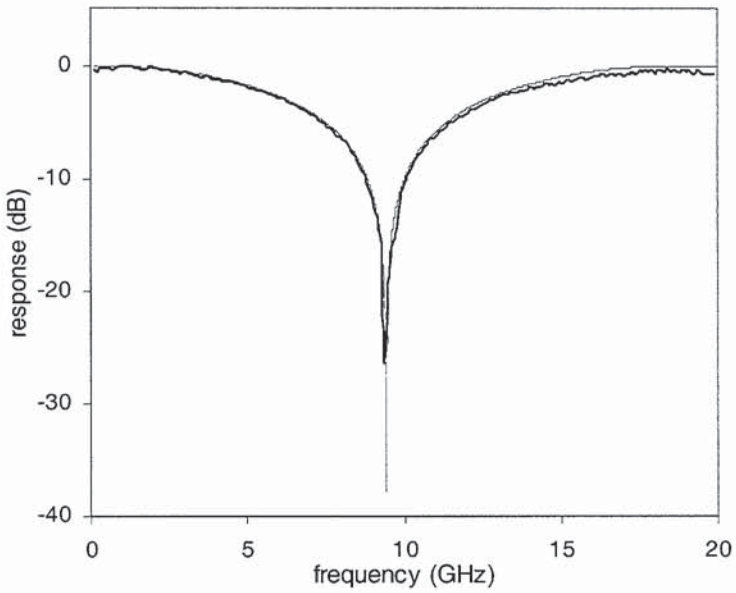

Figure 3.38 Measured (solid) and simulated (dotted) filter transfer responses at output port 2 when θ_1=45°; θ_2=90°; θ_3=45°.

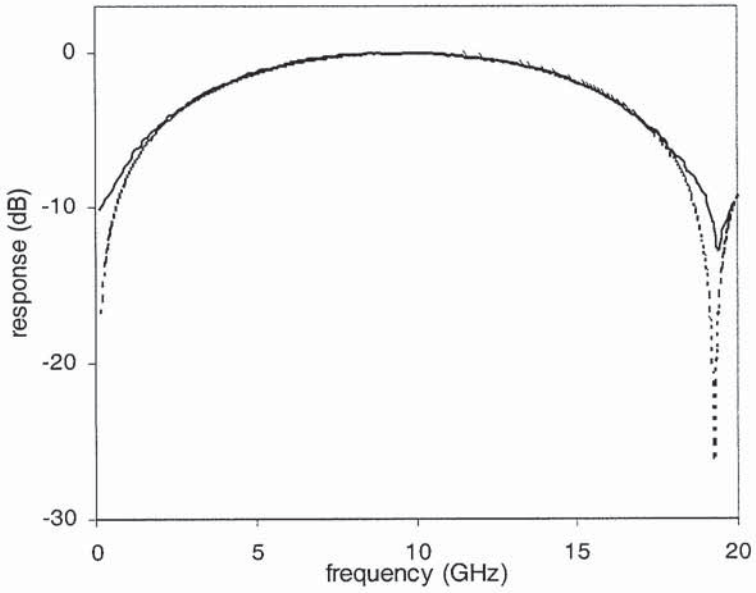

Figure 3.39 Measured (solid) and simulated (dotted) filter transfer responses at output port 3 when θ_1=45°; θ_2=90°; θ_3=45°.

By setting θ_1=75°; θ_2=58°; θ_3=45°, a low pass response with flattened passband was similarly realised as shown in Figure 3.40. Flattened passband width measured 4GHz with ripples <0.3dB was

achieved. Figure 3.41 shows the normalized complementary response obtained from output port 3 that corresponded to a high pass response.

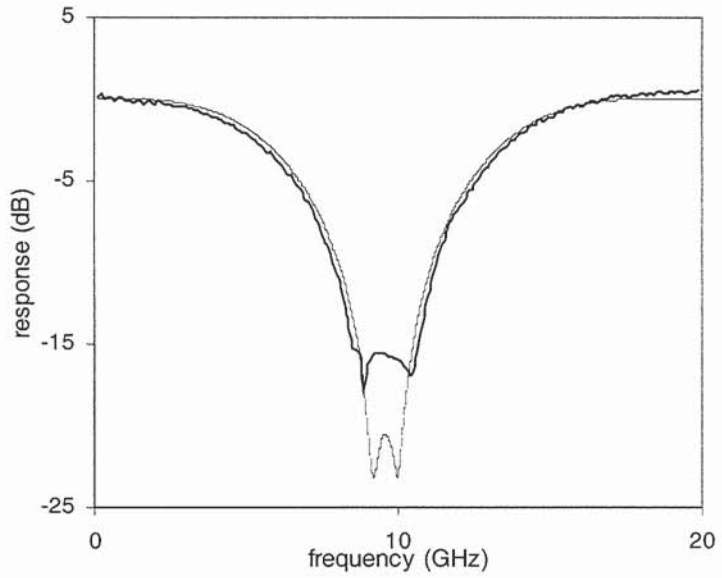

Figure 3.40 Measured (solid) and simulated (dotted) filter transfer responses at output port 2 when θ_1=75°; θ_2=58°; θ_3=45°.

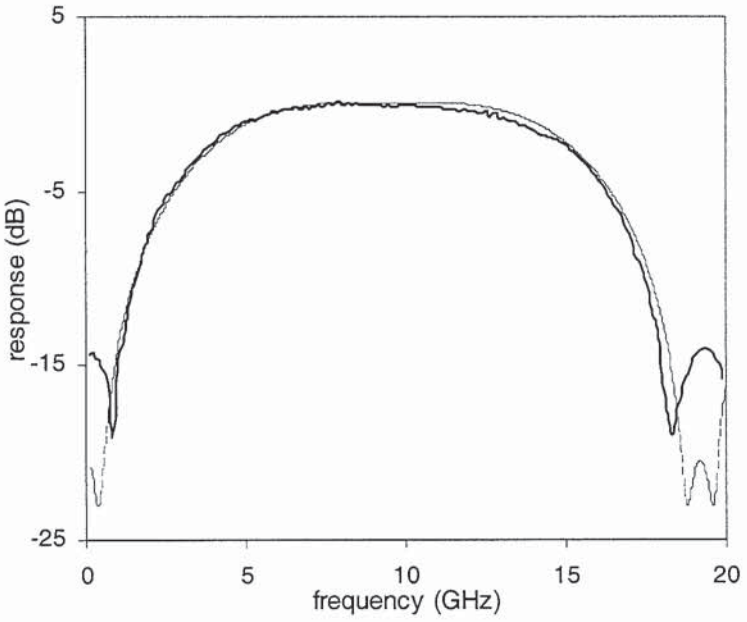

Figure 3.41 Measured (solid) and simulated (dotted) filter transfer responses at output port 3 when θ_1=75°; θ_2=58°; θ_3=45°.

3.4 Conclusions

Some of the key aspects of fibre optical delay line filter configurations have been outlined. In particular, the lattice structure delay line filter scheme and its analysis using matrix formulation have been discussed. Utilizing the non-interfering polarization modes in the Hi-Bi fibre, the coherent operation of a Hi-Bi fibre delay line filter has been demonstrated with greatly enhanced environmental stability. On the basis of such a Hi-Bi fibre delay line filter architecture, higher order lattice structure Hi-Bi fibre delay line filters have been proposed and demonstrated. More importantly, by taking advantage of the bipolar taps generated through the cascaded Hi-Bi fibre structure, complex signal processing operations like simultaneous complementary outputs and wavelength-interleaving nonreciprocal bidirectional filtering have been achieved. Based on a similar concept, complex microwave/millimetre wave signal processing operations have been further illustrated.

3.5 References

[1] B. Moslehi, J.W. Goodman, M. Tur, H.J. Shaw, "Fibre optic lattice signal processing", *Proc. IEEE*, 72, pp. 909, 1984.

[2] K.P. Jackson, S.A. Newton, B. Moslehi, M. Tur, C.C. Cutler, J.W. Goodman, H.J Shaw "Optical fibre delay-line signal processing", *IEEE Trans. Microwave Theory and Tech.*, MTT-33(3), pp.193-209, 1985.

[3] K. Wilner, A.P. van den Heuvel, "Fibre–optic delay lines for microwave signal processing", *Proc. IEEE*, 64, pp. 805, 1976.

[4] J.E. Bowers, S.A. Newton, W.V. Sorin, H.J. Shaw, "Filter response of single-mode fibre recirculating delay lines", *Electron. Lett.*, 18, pp. 110-111, 1982.

[5] M. Tur, J.W. Goodman, B. Moslehi, J.E. Bowers, H.J. Shaw, "Fibre optic signal processor with applications to matrix vector multiplication and lattice filtering", *Optics Lett.*, 7(9), pp. 463-465, 1982.

[6] C.T. Chang, J.A. Cassaboom, H.F. Taylor, "Fibre optic delay line devices for RF signal processing", *Electron. Lett.*, 13, pp. 678, 1977.

[7] K.P. Jackson, J.E. Bowers, S.A. Newton, C.C. Cutler, "Microbend optical fibre tapped delay line for gigahertz signal processing", *Appl. Phys. Lett.*, 41, pp.139, 1982.

[8] J. Capmany, M.A. Muriel, "A new transfer matrix formalism for the analysis of fibre ring resonators: compound coupled structures for FDMA demultiplexing", *J. Lightwave Technol.*, 8(12), pp. 1904-1919, 1990.

[9] L.F. Stokes, M. Chodorow, J. Shaw, "All single-mode fibre resonator", *Optics Lett.*, 7(6), pp. 288-290, 1982.

[10] K. Jinguji, M. Kawachi, "Synthesis of coherent two port lattice form optical delay line circuit", *J. Lightwave Technol.*, 13(1), pp. 73-82, 1995.

[11] D. Norton, S. Johns, C. Keefer, R. Soref, "Tunable microwave filtering using high dispersion fibre time delays", *IEEE Photon. Technol. Lett.*, 6(7), pp. 831-832, 1994.

[12] M.Y. Frankel, R.D. Esman, "Fibre-optic tunable microwave transversal filter", *IEEE Photon. Technol. Lett.*, 7(2), pp. 191-193, 1995.

[13] D.B. Hunter, R.A. Minasian, "Reflectively tapped fibre optic transversal filter using in-fibre Bragg gratings", *Electron. Lett.*, 31(12), pp. 1010-1012, 1995.

[14] D.B. Hunter, R.A. Minasian, "Microwaev optical filters using in-fibre Bragg grating arrays", *IEEE Microwave and Guided Wave Lett.*, 6(2), pp. 103-105, 1996.

[15] D. Pastor, J. Capmany, "Fibre optic tunable transversal filter using laser array and linearly chirped fibre grating", *Electron. Lett.*, 34(17), 1998.

[16] J. Marti, F. Ramos, R.I. Laming, "Photonic microwave filter employing multimode optical sources and wideband chirped fibre gratings", *Electron. Lett.*, 34(18), 1998.

[17] K.P. Jackson, G.G. Xiao, H.J. Shaw, "Coherent optical fibre delay line processor", *Electron. Lett.*, 22(25), pp.1335-1337, 1986.

[18] D.E.N Davies, G.W. James, "Fibre optic tapped delay line filter employing coherent optical processing", *Electron. Lett.*, 20, pp. 95-97, 1984.

[19] K. Sasayama, M. Okuno, K. Habara, "Coherent optical transversal filter using silica based single-mode waveguides", *Electron. Lett.*, 25(22), pp. 1508-1509, 1989.

[20] K. Sasayama, M. Okuno, K. Habara, "Coherent optical transversal filter using silica based waveguides for high speed signal processing", *J. Lightwave Technol.*, 9(10), pp. 1225-1230, 1991.

[21] K. Sasayama, M. Okuno, K. Habara, "Photonic FDM multichannel selector using coherent optical transversal fiter", *J. Lightwave Technol.*, 12(4), pp. 664-669, 1994.

[22] S. Sales, J. Capmany, J. Marti, D. Pastor, "Experimental demonstration of fibre-optic delay line filters with negative coefficients", *Electron. Lett.*, 31(13), pp. 1095-1096, 1995.

[23] F. Coppinger, S. Yegnanarayanan, P.D. Trinh, B. Jalali, "All-optical incoherent negative taps for phtooncis signal processing", *Electron. Lett.*, 33(11), 1997.

[24] X. Wang, L.Y. Chen, K.T. Chan, "All-optical incoherent negative tap fibre optic delay lines using injection locked FP laser diode", *Tech. Dig. LEOS*, vol. 1, WK2, pp. 229-230, 1998.

[25] X. Wang, K.T. Chan, "Tunable all-optical incoherent bipolar delay-line filter using injection locked Fabry-Perot laser and fibre Bragg gratings", *Electron. Lett.*, 36(24), 2000.

[26] J. Capmany, J. Cascón, J.L. Martín, S. Sales, D. Pastor, J. Martí, "Synthesis of fibre-optic delay line filters", *J. Lightwave Technol.*, 13(10), pp.2003-2012, 1995.

[27] W. Zhang, J.A.R. Williams, I. Bennion, "Optical fibre delay line filter free of limitation imposed by optical coherence", *Electron. Lett.*, 35(24), 1999.

[28] M. Sharma, H.Ibe, T. Ozeki, "Optical circuits for equalizing group delay dispersion of optical fibres", *J. Lightwave Technol.*, 12(10), pp. 1759-1765, 1994.
[29] L.R Chen, D.J.F. Cooper, P.W.E. Smith, "Transmission filters with multiple flattened passbands based on chirped Moiré gratings", *IEEE Photon. Technol. Lett.*, 10(9), pp. 1283-1285, 1998.
[30] B.J. Eggleton, G. Lenz, N. Litchinitser, D.B. Patterson, R.E. Slusher, "Implications of fibre grating dispersion for WDM communication systems", *IEEE Photon. Technol. Lett.*, 9(10), pp.1403-1405, 1997.
[31] G. Lenz, B.J. Eggleton, C.K. Madsen, C.R. Giles, G. Nykolak, "Optimal dispersion of optical filters for WDM systems", *IEEE Photon. Technol. Lett.*, 10(4), pp. 567-569, 1998.
[32] M. Ibsen, M.K. Durkin, M.J. Cole, R.I. Laming, "Optimised square passband fibre Bragg grating filter with in-band flat group delay response", *Electron. Lett.*, 34(8), pp. 800-802, 1998.
[33] X.F. Chen, C.C. Fan, Y. Luo, S.Z. X, S. Hu, "Novel flat multichannel filter based on strongly chirped sampled fibre Bragg grating", *IEEE Photon. Technol. Lett.*, 12(11), pp. 1501-1503, 2000.
[34] A.Y. Yan, R.J. Deri, M. Seto, R.J. Hawkins, "GaAs/GaAlAs asymmetric Mach-Zehnder demultiplexer with reduced polarization dependence", *IEEE Photon. Technol. Lett.*, 1(4), pp. 83-85, 1989.
[35] M.A. Scobey, R.M. Fortenberry, L.F Stokes, W.P. Kastanis, D.J. Derickson, "Thin film interference filters for 25GHz channel spacing", *Proc. Optical Fibre Communication Conference (OFC)*, ThC 5, pp. 398-399, 2002.
[36] J.C. Chon, C.H. Huang, J.R. Bautista, "Ultra small dispersion, low loss, flat-top, and all fibre DWDM and NWDM devices for high speed optical network applications", *Proc. European Conference Optical Communications (ECOC)*, pp. 103-104, 2000.
[37] C.H. Huang, H.L. Luo, S.L. Xu, P. Chen, "Ultra low loss, temperature insensitive 16-channel 100 GHz dense wavelength division multiplexers based on cascaded all-fibre unbalances Mach-Zehnder structure", *Proc. Optical Fibre Communication Conference (OFC)*, TuH 2-1, pp. 79-81, 1999.
[38] M. Kuznetsov, "Cascaded coupler Mach-Zehnder channel dropping filters for wavelength-division multiplexed optical systems", *J. Lightwave Technol.*, 12(2), pp. 226-230, 1994.
[39] B.J. Offrein, G.L. Bona, F. Horst, H.W.M. Salemink, R. Beyeler, R. Germann, "Wavelength tunable optical add-after-drop filter with flat passband for WDM networks", *IEEE Photon. Technol. Lett.*, 11(2), pp. 239-241, 1999.
[40] M. Kohtoku, S. Oku, Y. Kadota, Y. Shibata, Y. Yoshikuni, "200GHz FSR periodic multi/demultiplexer with flattened transmission and rejection band by using a Mach-Zehnder interferometer with a ring resonator", *IEEE Photon. Technol. Lett.*, 12(9), pp. 1174-1176, 2000.
[41] K. Oda, N. Takato, H. Toba, K. Nosu, "A wide band guided wave periodic multi/demultiplexer with a ring resonator for optical FDM transmission systems", *J. Lightwave Technol.*, 6(6), pp. 1016-1023, 1988.
[42] Y. Hida, Y. Hibino, "Ultra high density AWGs composed of super high Δ PLCs", *Proc. Optical Fibre Communication Conference (OFC)*, ThC6, pp. 399-401, 2002.
[43] M. Johnson, "Single-mode fibre birefringent filters", *Optics Lett.*, 5(4), pp. 142-144, 1980.
[44] Y. Yen, R. Ulrich, "Birefringent optical filters in single-mode fibre", *Optics Lett.*, 6(6), pp. 278-280, 1981.
[45] H.D. Ford, R.P. Tatam, "Birefringent-fibre Solc wavelength filters", *10th Optical Fibre Sensor Conference*, pp. 560-563, 1995.
[46] H.D. Ford, R.P. Tatam, "Narrowband wavelength division multiplexers using birefringent optical fibre", *Optics Comm.*, 98, 1-3, pp. 151-158, 1993.
[47] X.J. Fang, H.L. Ji, C.T. Allen, K. Demarest, L. Pelz, "A compound high order polarization independent birefringence filter using Sagnac interferometers", *IEEE Photon. Technol. Lett.*, 9(4), pp. 458-460, 1997.
[48] Y. Han, Q. Li, X.M. Liu, B.K. Zhou, "Architecture of high-order all fibre birefringent filters by the use of the Sagnac interferometer", *IEEE Photon. Technol. Lett.*, 11(1), pp. 90-92, 1999.
[49] B.J. Offrein, F. Horst, G.L. Bona, H.W.M. Salemink, R. Germann, R. Beyeler, "Wavelength tunable 1-from-16 and flat passband 1-from-8 add-drop filters", *IEEE Photon. Technol. Lett.*, 11(11), pp. 1440-1442, 1999.
[50] D.G. Falquier, J.L. Wagener, M.J.F. Digonnet, H.J. Shaw, "Polarized superfluorescent fibre source", *Optics Lett.*, 22(3), pp. 160-162, 1997.
[51] S. Ryu, Y. Horiuchi, "Novel chromatic dispersion measurement method over continuous gigahertz tuning range", *J. Lightwave Technol.*, 7(8), pp. 1177-1180, 1989.
[52] R.M. Fortenberry, "Enhanced wavelength resolution chromatic dispersion measurements using fixed sideband technique", *Proc. Optical Fibre Communication Conference (OFC)*, TuG8-1, pp.107-109, 2000.

[53] T. Mizuno, T. Kitoh, T. Saida, M. Oguma, T. Shibata, Y. Hibino, "Dispersionless interleave filter based on transversal form optical filter", *Electron. Lett.*, pp. 1121-1122, 2002.
[54] A. Zeng, X.G. Ye, J. Chon, F. Liang, "25GHz interleavers with ultra-low chromatic dispersion", *Proc. Optical Fibre Communication Conference (OFC)*, ThC 4, pp. 396-397, 2002.
[55] S. Cao, C. Lin, C. Yang, E. Ning, J. Zhao, G. Barbarossa, "Birefringent Gires-Tournois interferometer (BGTI) for DWDM interleaving", *Proc. Optical Fibre Communication Conference (OFC)*, ThC 3, pp. 395-396, 2002.
[56] T. Chiba, H. Arai, K. Ohira, H. Nonen, H. Okano, H. Uetsuka, "Novel architecture of wavelength interleaving filter with Fourier transform-based MZIs", *Proc. Optical Fibre Communication Conference (OFC)*, WB 5, 2000.
[57] M.O. van Deventer and O.J. Koning, "Unimpaired transmission through a bidirectional erbium-doped fibre amplifier near lasing threshold", *IEEE Photon. Technol. Lett.*, vol. 7(9), pp. 1078-1080, 1995.
[58] M.O. van Deventer and O.J. Koning, "Bidirectional transmission using an Erbium doped fibre amplifier without optical isolator", *IEEE Photon. Technol. Lett.*, vol. 7(11), pp. 1078-1080, 1995.
[59] M.O. van Deventer, "Power penalties due to reflection and Rayleigh backscattering in a single frequency bidirectional coherent transmission system", *IEEE Photon. Technol. Lett.*, 5(7), pp. 851-854, 1993.
[60] P.P. Bohn, S.K. Das, "Return loss requirements for optical duplex transmission", *J. Lightwave Technol.*, 5(2), pp. 243-254, 1987.
[61] R. Karl, P. Gysel, "Crosstalk penalties due to coherent Rayleigh noise in bidirectional optical communication systems", *J. Lightwave Technol.*, 9(3), 375-380, 1991.
[62] J.L. Gimlett, N.K. Cheung, "Effects of phase-to-intensity noise conversion by multiple reflections on gigabit-per-second DFB laser transmission systems", *J. Lightwave Technol.*, 25(20), pp. 1393-1394, 1989.
[63] J. Kani, M. Jinno, T Sakamoto, K. Hattori and K. Oguchi, "Bidirectional transmission to suppress interwavelength-band nonlinear interactions in ultrawide-band WDM transmission systems", *IEEE Photon. Technol. Lett.*, 11(3), pp.376-378, 1999.
[64] M.F. Ferreira, "Limitations imposed by stimulated Brillouin scattering on uni- and bi-directional transmission systems using active fibres", *Electron. Lett.*, 31, pp. 1182-1183, 1995.
[65] R. Waarts, A.Friesfm, F. Lichtman, H. Yafe, R. Braun, "Nonlinear effects in coherent multichannel transmission through optical fibres", *Proc. IEEE*, 78, pp. 1344-1368, 1990.
[66] F.W. Willems, J.C. van der Plaats, D.J. DiGiovanni, "EDFA noise figure degradation caused by amplified signal double Rayleigh scattering in erbium doped fibres", *Electron. Lett.*, 30(8), pp.645-646, 1994.
[67] J.L. Gimlett, M.Z. Iqbal, L. Curtis, N.K. Cheung, A. Righetti, F. Fontana, G. Grasso, "Impact of multiple reflection noise in Gbit/s lightwave systems with optical fibre amplifiers," *Electron. Lett.*, 25(20), pp. 1393-1394, 1989.
[68] S.K. Liaw, K.P. Ho, C.Lin, S. Chi, "Multichannel bidirectional transmission using a WDM MUX/DMUX pair and unidirectional in-line amplifiers", *IEEE Photon. Technol. Lett.*, 9(12), pp. 1664-1666, 1997.
[69] C.H. Kim, Y.C. Chung,"2.5Gb/s x 16 channel bidirectional WDM transmission system using bidirectional Erbium-doped fibre amplifier based on spectrally interleaved synchronized etalon filters", *IEEE Photon. Technol. Lett.*, 11(6), pp. 745-747, 1999.
[70] Y. Zhao, X.J. Zhao, J.H. Chen, F.S. Choa, "A novel bidirectional add/drop module using waveguide grating routers and wavelength channel match fibre gratings", *IEEE Photon. Technol. Lett.*, 11(9), pp. 1180-1182, 1999.
[71] T. W. Oh, J. H. Shin, H.D. Kim, C. H. Lee, M. S. Lee and B. Y. Kim, "Bidirectional erbium-doped fibre amplifier with non-reciprocal optical filter", *Electron. Lett.*, 37(5), pp.283-284, 2001.
[72] T. Ducellier, K. Tai, B. Chang, J. Xie, J. Chen, L. Mao, H. Mao and J. Wheeldon, "Bidirectional circulator: an enabling technology for wavelength interleaved bidirectional networks", *Proc. 26th European Conference Optical Communications (ECOC)*, Munich, PD3-9, 2000.
[73] M.S. Lee, I.K. Hwang, B.Y. Kim, "Bidirectional wavelength-selective optical isolator", *Electron. Lett.*, 37(14), 2001.
[74] K. Tai, B. Chang, J. Chen, H. Mao, T. Ducellier, J. Xie, L. Mao, J. Wheeldon, "Wavelength-interleaving bidirectional circulators", *IEEE Photon. Technol. Lett.*, 13(4), pp. 320-322, 2001.
[75] V. Annovazzi-Lodi, S. Donati, S. Merlo and A. Leona, "All-fibre faraday rotator made by a multiturn figure-of-eight coil with matched birefringence", *J. Lightwave Technol.*, 13(12), pp. 2349-2353, 1995.

[76] G. D. Peng and P. L. Chu, "Design and fabrication of birefringent splittable composite (BISPEC) fibre for polarisation-maintaining devices", *Electron. Lett.*, 30(8), pp. 666-667, 1994.
[77] K. Tai, Q.D. Guo, K.W. Chang, J. Chen, M. Xu, "4-port interleavers and fully circulating bi-directional circulators", *Proc. Optical Fibre Communication Conference (OFC)*, MK5-2, 2001.
[78] J. Marti, V. Polo, F. Ramos, D. Moodie, "Photonics tunable microwave filters employing electroabsorption modulators and wideband chrped fibre gratings", *Electron. Lett.*, 35(4), 1999.

Chapter 4: Fibre Bragg gratings

4.1 Overview

All-fibre filters attracted considerable research interest with the advent of fibre optic communication and fibre sensor systems [1]-[3]. Since the first demonstration of a UV-written fibre Bragg grating (FBG) through the side exposure technique [4], fibre gratings have developed into a critical component for many important technologies including fibre lasers, filters, dispersion compensators, gain flatteners as well as fibre sensors. Apart from its intrinsic merits like all-fibre geometry, low insertion loss and large operating bandwidth, the fibre Bragg grating distinguished itself from competing technologies in its versatility and flexibility. Numerous physical parameters in fibre Bragg gratings can be tailored at relative ease to achieve the desired transfer response. As a result, the fibre Bragg grating opens up a new horizon to a multitude of all-fibre device designs and applications. This chapter seeks to outline the key features and fabrication techniques of fibre Bragg gratings and its variants. Important characteristics of some special fibre Bragg grating structures are described. These grating structures form an integral part of the research work on the fibre-based devices described in subsequent chapters of this thesis.

4.2 Theory

The analysis of optical radiation in a distributed waveguide with periodic index perturbations has been carried out and detailed in various articles and texts e.g [5][6]. The coupled mode theory developed has since been a vital tool for analysing and obtaining quantitative information of the response of fibre grating structures. While different approaches based on coupled mode theory (e.g. numerical repetitions by integral forms of contradirectional coupled mode equations [7][8] and Riccati differential equation [9]) can effectively solve and describe grating filter characteristics of non-uniform periodicity, the transfer matrix technique (alternatively known as piece-wise uniform approach) for almost-periodic waveguide problems [10] has proved to be highly effective as well. The transfer matrix approach essentially divides the grating structure into short segments whose respective fundamental transfer matrices are determined. The characteristics of the compound grating structure can then be determined simply by multiplying these fundamental matrices together. Since each elementary transfer matrix is explicitly defined in terms of its phase, physical length and refractive index characteristics, the transfer matrix approach therefore provides a highly intuitive, straightforward analysis for various grating structures, in particular the phase-shifted fibre Bragg grating. Within the scope of this thesis, the evaluations of various transmission/reflection characteristics of fibre Bragg grating structures are based on this generalized transfer matrix formulation.

To simulate the wavelength transfer spectrum characteristics of fibre Bragg grating structures, we first consider the refractive index profile of a uniform fibre Bragg grating as shown in Figure 4.1. The refractive index profile of a uniform fibre Bragg grating along the spatial axis is assumed to vary

sinusoidally about an average refractive index n_{eff}. This index variation along spatial position, z, can be simply expressed by

$$n(z) = n_{eff} + n_1 \cos\left(\frac{2\pi}{\Lambda} z\right) \tag{4.1}$$

where n_1 denotes the peak index modulation and Λ is the grating period.

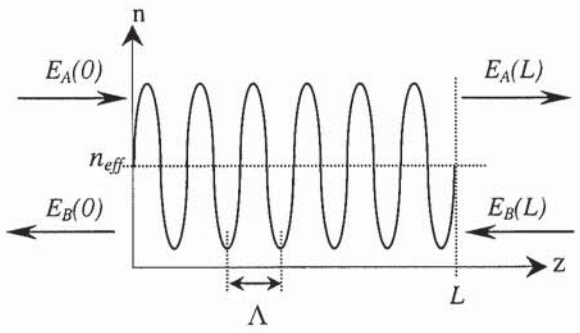

Figure 4.1 Diagram illustrating the refractive index profile of a uniform fibre Bragg grating. The total electric fields within the grating structure compose of forward and backward propagating waves.

Assuming the total electric field within the grating structure is a sum of forward and backward propagating waves, the basic coupled mode equations are given by [5]

$$\frac{\partial A(z)}{\partial z} = j\kappa B(z)\exp(-j2\Delta\beta z);$$
$$\frac{\partial B(z)}{\partial z} = -j\kappa A(z)\exp(j2\Delta\beta z) \tag{4.2}$$

where $A(z)$ and $B(z)$ denote the slowly varying amplitudes of the forward and backward travelling modes, κ is the coupling strength between the forward and backward propagating fields expressed as

$$\kappa = \frac{\pi n_1}{\lambda} \tag{4.3}$$

while $\Delta\beta$ denotes the detuning of the propagation constant

$$\Delta\beta = \beta - \frac{\pi}{\Lambda} \tag{4.4}$$

For $\Delta\beta$=0, we have, from (4.4), the Bragg wavelength $\lambda=\lambda_B$ given by

$$\beta = \frac{\pi}{\Lambda}$$
$$\frac{2n_{eff}\pi}{\lambda_B} = \frac{\pi}{\Lambda}$$
$$\lambda_B = 2n_{eff}\Lambda \tag{4.5}$$

and the Bragg wave vector β_B is given by

$$\beta_B = \frac{2n_{eff}\pi}{\lambda_B} \tag{4.6}$$

To solve (4.2) and (4.3), one expresses the forward and backward propagating E-fields as

$$E_A(z) = A(z)\exp(-j\beta z);$$
$$E_B(z) = B(z)\exp(j\beta z) \tag{4.7}$$

and based on (4.2)-(4.7), the solution to (4.2) is given by [6]

$$E_A(z) = [c_1\sinh(\gamma z) + c_2\cosh(\gamma z)]\exp(j\beta_B z)$$
$$E_B(z) = -\frac{\exp(-j\beta_B z)}{\kappa}[c_1(\Delta\beta\sinh(\gamma z) + j\gamma\cosh(\gamma z)) + c_2(\Delta\beta\cosh(\gamma z) + j\gamma\sinh(\gamma z))] \tag{4.8}$$

where

$$\gamma^2 = \kappa^2 - (\Delta\beta)^2 \tag{4.9}$$

c_1 and c_2 are arbitrary constants. Assuming the continuity conditions of forward and backward waves at the interfaces z=0 and at z=L, the E-fields in the grating structure, as shown in Figure 4.1, can be related by the matrix formulation given by

$$\begin{pmatrix} E_A(0) \\ E_B(0) \end{pmatrix} = [M_f]\begin{pmatrix} E_A(L) \\ E_B(L) \end{pmatrix} \tag{4.10}$$

where the matrix

$$M_f = \begin{bmatrix} M_{11} & M_{12} \\ M_{21} & M_{22} \end{bmatrix} \tag{4.11}$$

denotes the fundamental transfer matrix for the uniform Bragg grating structure. Through (4.8) to (4.10), the elements of the matrix are given by [6]

$$\begin{aligned} M_{11} &= \left[\cosh(\gamma z) - j\frac{\Delta\beta}{\gamma}\sinh(\gamma z) \right] \exp(-j\beta_B z) \\ M_{12} &= \left[-j\frac{\kappa}{\gamma}\sinh(\gamma z) \right] \exp(j\beta_B z) \\ M_{21} &= \left[j\frac{\kappa}{\gamma}\sinh(\gamma z) \right] \exp(-j\beta_B z) \\ M_{22} &= \left[\cosh(\gamma z) + j\frac{\Delta\beta}{\gamma}\sinh(\gamma z) \right] \exp(j\beta_B z) \end{aligned} \tag{4.12}$$

It is important to note that the fundamental matrix is valid only when the condition of dividing the grating structure satisfies $\Lambda \ll L$ for all grating segments [10]. This is generally satisfied since the envelope function over the grating structure is generally a slow varying function. Considering the continuity condition of the grating phase between i^{th} and $(i+1)^{th}$ grating segment, the phase condition at the interface between two adjacent segments must also satisfy

$$\phi_{start}^{i+1} = \phi_{end}^{i} = \phi_{start}^{i} + \frac{2\pi}{\Lambda_i} L_i = \phi_{start}^{i} + 2\beta_B L_i \tag{4.13}$$

where all the phase terms describe the phases of the grating itself and ϕ_{start}^{i} denotes the phase at the start of grating segment and vice versa. With the knowledge of the fundamental transfer matrices of the constituent segments, the resultant transfer matrix of the grating structure M_T can be determined simply by multiplying all the elementary matrices together as follows:

$$M_T = \prod_{i=1}^{N} M_i \tag{4.14}$$

where M_i denotes the fundamental transfer matrix for the i^{th} segment. The final transmission and reflection spectrum of the grating structure can be obtained from the elements of the final transfer matrix given by [6]

$$T = \left|\frac{E_A(z_n)}{E_A(0)}\right|^2 = \left|\frac{1}{M_{T11}}\right|^2 \; ; \; R = \left|\frac{E_B(0)}{E_A(0)}\right|^2 = \left|\frac{M_{T21}}{M_{T11}}\right|^2 \tag{4.15}$$

respectively.

4.3 Fibre Bragg grating fabrication techniques

A fibre Bragg grating is produced by exposing an optical fibre to a spatially varying UV intensity pattern. The fabrication techniques fall broadly into two categories: those that are holographic and those that adopt diffractive elements such as phase masks. The former technique divides a single UV beam into two paths, which interfere at the fibre through appropriate optical arrangements. This is illustrated in Figure 4.2. The UV interference pattern at the optical fibre photoinduced a spatial refractive index modulation with a period Λ given by

$$\Lambda = \frac{\lambda_{UV}}{2\sin\left(\frac{\theta}{2}\right)} \tag{4.16}$$

where θ denotes the angle between the two writing beams of wavelength λ_{UV}. Fibre Bragg grating fabrication through this method is highly versatile since the resultant grating periodicity Λ and therefore Bragg wavelength (λ_B) can be flexibly chosen by the angle at which the UV beams interfere at the fibre [11][12]. However, such interferometric technique imposes stringent requirements on the UV laser coherence, optical path difference control as well as stability of delivery optics arrangement against environmental perturbations. Furthermore, the grating length achievable through such fabrication technique is greatly limited by the size and uniformity of the interfering UV beams.

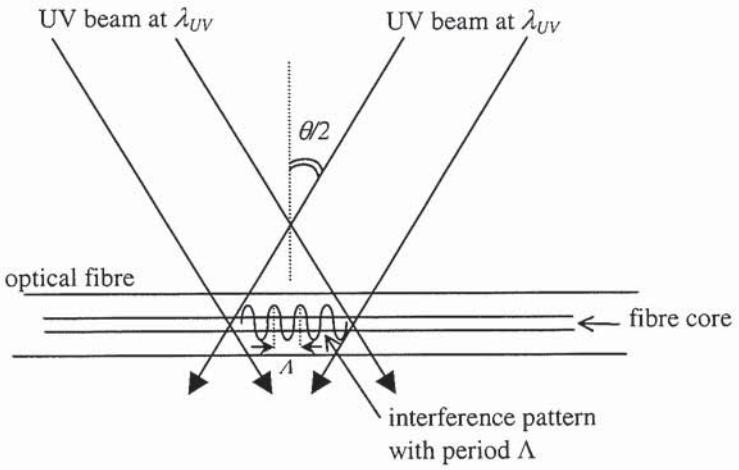

Figure 4.2 Diagram illustrating the holographic technique for the inscription of a fibre Bragg grating into the core of the optical fibre.

Towards easier inscription process of fibre Bragg gratings with high repeatability and more relax tolerances on the writing setup, the use of a diffractive element/phase mask has become the preferred method [13][14][15]. Used in transmission, the phase mask is a spatially periodic relief grating etched in a silica plate. The principle of operation is based on the diffraction of an incident UV beam into several orders. A deeply etched grating in the phase mask suppresses higher orders and controls the relative intensities. To fabricate uniform Bragg gratings using the phase mask, the zeroth order of the diffracted

beam from the phase mask is suppressed to a low value while the majority of the power is transmitted through the +1 and -1 orders only. The interference pattern formed by the transmitted orders is exposed onto the optical fibre at close proximity to create the desired grating periods. This fabrication process has proved to be efficient, highly repeatable and permits realisation of long gratings (on the order of several centimetres) [16][17] mainly limited by the useful aperture of the mask. As long as the mask and the fibre do not move relative to each other, the phase of the fringes created in the fibre is purely determined by the mask only, regardless of the position of the UV beam. Hence, by scanning an intense UV beam across the phase mask-fibre assembly, highly repeatable, effective and stable fabrication can be achieved. Furthermore, through changing the intensity of the writing beam, the strength of the grating structure can be modified at will along the fibre axis.

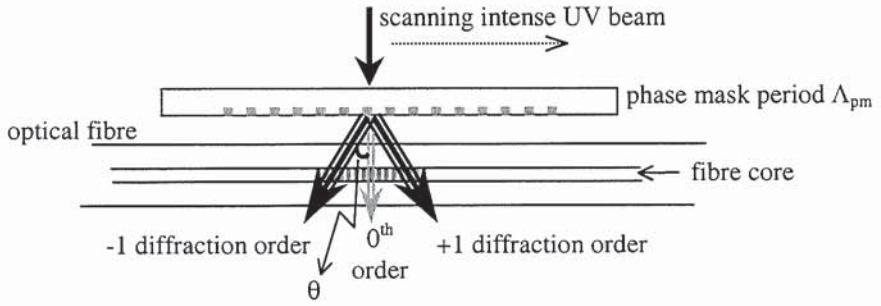

Figure 4.3 Diagram illustrating the fibre Bragg grating fabrication process through UV exposure with a phase mask. Note that the diagram is not drawn to scale.

Commercially available phase masks for fibre Bragg grating fabrication generally achieve an energy distribution of < 2% to the zeroth order. The rest of the energy is equally divided to the +1 and -1 orders with negligible amount to higher orders. Using the phase mask at normal incidence, the first order diffraction of the UV beam follows the general diffraction equation given by

$$\Lambda_{pm} = \frac{\lambda_{UV}}{\sin(\theta)} \tag{4.17}$$

where θ denotes the angle between the +1 (or-1) diffraction order and the 0th order. The interference pattern formed by the ±1 order beams at the fibre similarly photoinduces a spatial index modulation along the fibre axis with a period Λ_g (hence fibre Bragg grating period) that is related to the periodicity of the phase mask Λ_{pm} by

$$\Lambda_g = \frac{\lambda_{UV}}{2\sin(\theta)} = \frac{\Lambda_{pm}}{2} \tag{4.18}$$

Evidently, the fixed grating pitch on the phase mask will impose a strong restriction on the index modulation pattern photoinduced onto the optical fibre. Complex grating structures and variations to the

grating wavelength inscribed through the phase mask technique are not explicitly straightforward, even though techniques based on special dedicated phase mask [18], inclusion of magnification lens [19], and 'stretch-and-write' [20] method enabled some flexibility. To allow greater flexibility in the phase mask fabrication method, a moving fibre/phase mask scanning beam technique has been demonstrated [21][22]. By enabling a relative movement between the phase mask and the fibre during the writing scan, complex processes like phase shifts, Bragg wavelength shift, chirping, and apodization can be achieved depending on the relative motion introduced. Laser beam scanning is accomplished through the use of a highly stable frequency-doubled CW Argon laser operating at 244nm in conjunction with a translation stage onto which a mirror is mounted. High resolution and precision piezoelectric transducers (PZT) stages are attached either to the phase mask or fibre holders for sub-μm translation. Through the use of computer-controlled synchronization, relative movement between the fibre and the mask can be incorporated during the writing scan, allowing phase shifts to be created. Such a fabrication technique has allowed various complex grating structures like apodized gratings, multiple phase-shifted gratings and chirped gratings to be realised e.g. [23]-[25].

For all the research work described in this thesis, the fibre Bragg grating structures were fabricated using the scanning beam moving phase mask technique. Advanced grating fabrication techniques, namely, the sequential writing method [26][27] for realisation of arbitrary grating profiles are beyond the scope of this thesis. In the fabrication setup adopted, the PZT attached to the phase mask allowed a maximum translation of 10μm with an applied voltage of 10V. Through the use of computer control, relative shifts between the fibre and the phase mask on the order of a mask pitch period (order of 1μm) were achieved easily to create phase shifts with the fibre Bragg grating structures. The length of the phase mask limited the length of the grating achievable while the high power stability of the laser ensured uniformity in the exposure. Further discussions on some of the grating structures fabricated are detailed in the subsequent sections.

4.4 Characteristics of uniform fibre Bragg grating

The uniform fibre Bragg grating is one of the most basic forms of all fibre grating structures. As described in section 4.1, the theoretical simulation of the uniform fibre Bragg grating structure can be carried out using the transfer matrix approach. From (4.12) and (4.15), the reflectivity R of the grating is given by

$$R = \left|\frac{E_B(0)}{E_A(0)}\right|^2 = \left|\frac{M_{r21}}{M_{r11}}\right|^2 = \left|\frac{\left[j\frac{\kappa}{\gamma}\sinh(\gamma z)\right]\exp(-j\beta_B z)}{\cosh(\gamma z)-\left[j\frac{\Delta\beta}{\gamma}\sinh(\gamma z)\right]\exp(-j\beta_B z)}\right|^2 \tag{4.19}$$

When $\Delta\beta$ =0, this corresponds to the Bragg condition where the propagation constant β=β_B. This gives the familiar Bragg wavelength equation given by

$$\lambda_B = 2n_{eff}\Lambda \tag{4.20}$$

where n_{eff} is the mode effective index. More importantly, at the Bragg centre, maximum reflectivity is achieved given by

$$R = \tanh^2(\kappa z) \tag{4.21}$$

Clearly, when γz in (4.19) is an integer multiple of π, the grating will exhibit zero reflectivity. The locations of these zeroes describe the locations of the sidelobes in between them. The wavelength separation between the zeroes is given by [28]

$$\Delta\lambda = \frac{\lambda_B}{\pi n_{eff} L}\left[(\kappa L)^2 + N\pi^2\right]^{1/2} \tag{4.22}$$

where N is an integer, L is the length of the grating and the product κL, commonly quoted as a measure of the grating coupling strength, is known as the grating strength parameter. A useful measure of the grating spectral width (stopband width) is the wavelength separation between the first zeroes and conveniently defined as the full width first zeros (FWFZ) of the grating, simply given by

$$\Delta\lambda = \frac{\lambda_B}{\pi n_{eff} L}\left[(\kappa L)^2 + \pi^2\right]^{1/2} \tag{4.23}$$

Figure 4.4 shows the measured profile of a typical uniform fibre Bragg grating fabricated using the scanning beam phase mask technique. The length of the grating was 30mm and the measured grating peak

loss (i.e. grating strength) was 17.5dB (corresponding to κL = 2.69) with a FWFZ bandwidth of 0.072nm. The obtained data was in close agreement with the simulation result.

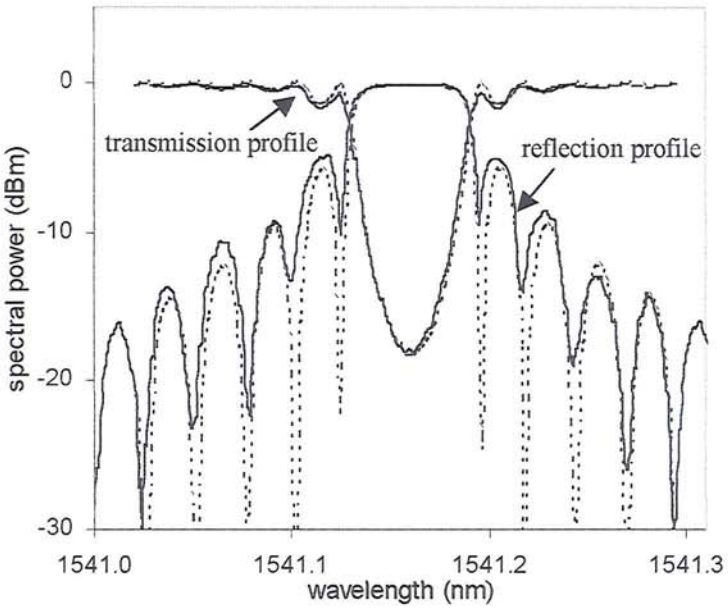

Figure 4.4 Measured (solid) and simulated (dotted) spectral profiles of a 30mm long uniform fibre Bragg grating.

Evidently, from (4.21), the strength of the uniform grating is a strong function of the coupling coefficient, κ, and the length of the grating, L. With increasing κL, the peak reflectivity increases, accompanied by increasing sidelobe levels and a broadening of the spectral width. Figure 4.5 and Figure 4.6 illustrate the comparisons of the FBG spectra fabricated with different lengths and UV exposure time (hence index modulation).

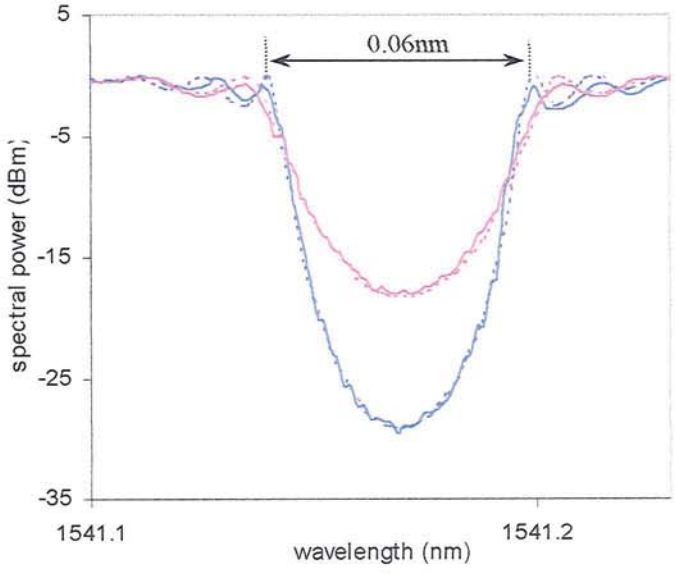

Figure 4.5 Measured (solid) and simulated (dotted) spectral profiles of two uniform FBGs of lengths 30mm and 45mm. The exposure time per unit length for each grating was identical at 2.5s/mm.

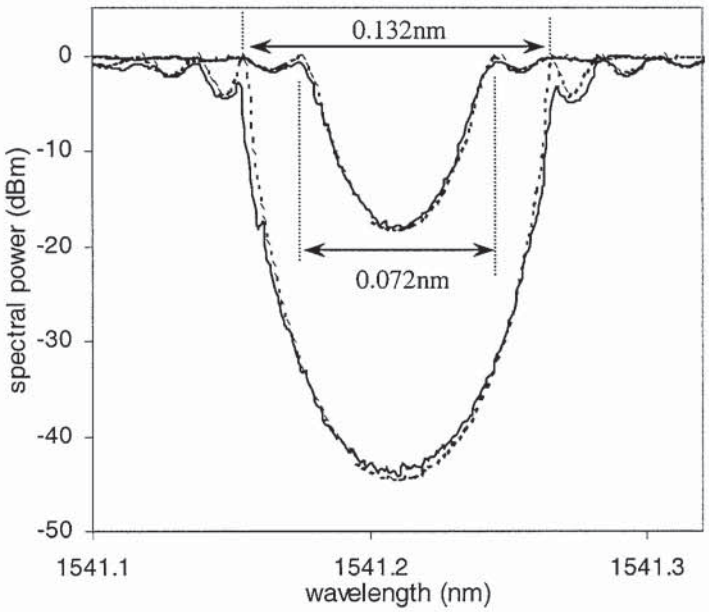

Figure 4.6 Measured (solid) and simulated (dotted) spectral profiles of two 30mm-long uniform FBGs of different coupling coefficients, achieved by altering the UV exposure time (scanning speed) during the fabrication process.

As shown in Figure 4.5, by increasing the grating length from 30mm to 45mm for a fixed UV intensity and scanning speed (hence exposure time per unit length), the grating strength increased from 17.5dB to 29dB with a corresponding decrease in the spectral width from 0.072nm to 0.06nm. For a fixed index modulation (hence coupling coefficient κ), the strength parameter κL increased to 4.04 due to the longer grating length. On the other hand, as shown in Figure 4.6, by increasing the exposure time per unit length (decreasing the scanning speed of the writing UV beam) during inscription of the 30mm long uniform FBG, the grating index modulation increased correspondingly. The increase in the coupling coefficient κ led to a similar increment in the strength parameter κL from κL=2.69 (κ=89.69m^{-1}) to κL=5.63 (κ=187.67m^{-1}). The grating peak loss measured 42.9dB (i.e. 25.4dB increase) with a corresponding stopband width measured 0.113nm (increment of 0.041nm). The continuous-wave UV laser intensity used in all cases was 90mW (beam width ~0.8mm) with an exposure time of 75s over the 30mm length for the former and increased, through reducing the scanning velocity, to 250s for the latter. Figure 4.7 highlights the relationship between the transmitted power at Bragg wavelength against grating length for various index modulations Δn = 4.4x10^{-5}, 8.3x10^{-5}, 9.2x10^{-5} (corresponding to coupling coefficients κ= 89.69m^{-1}, 169.21m^{-1}, 187.67m^{-1}). The relationship between the FWFZ bandwidth against the grating length under constant index modulation is depicted in Figure 4.8.

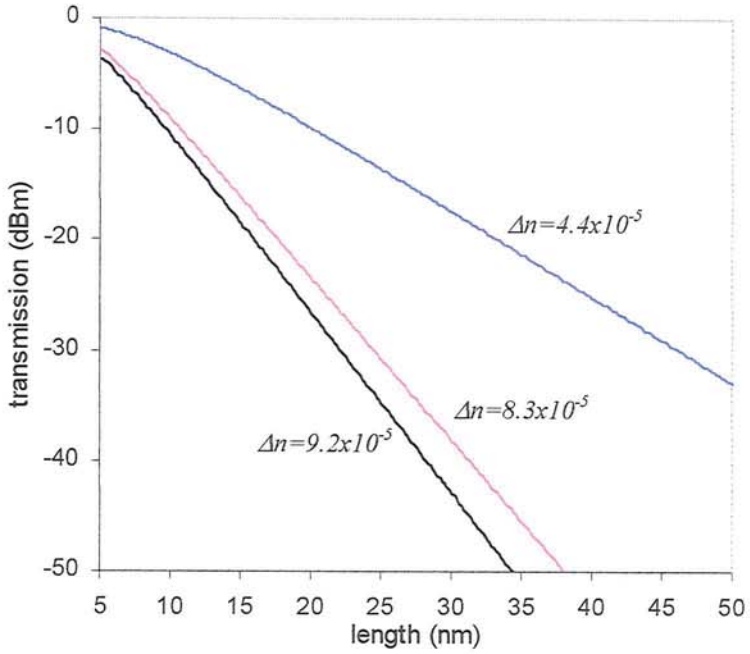

Figure 4.7 Relationship between transmitted power at Bragg wavelength against grating length for different index modulation Δn.

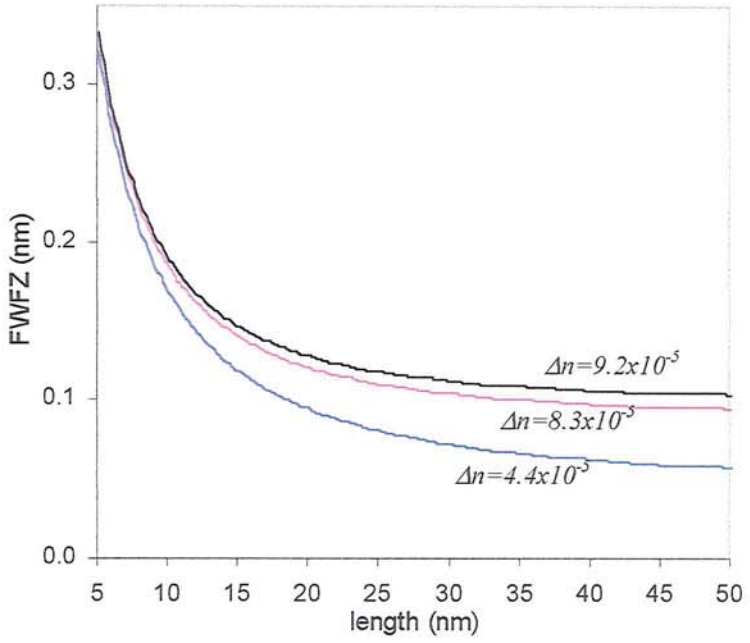

Figure 4.8 Relationship between grating FWFZ bandwidth against grating length for different index modulation Δn.

From Figure 4.7 and Figure 4.8, it is evident that two gratings of similar strength parameter κL can have distinctly different spectral stopband widths, depending on the length of the grating. This is illustrated in Figure 4.9 where two gratings of length 16mm and 30mm had comparable peak loss (reflectivity) but a distinct difference in the spectral width. The index modulation in the 16mm long grating was 8.3×10^{-5}

compared to $4.4x10^{-5}$ in the 30mm long grating. The ability to control the basic spectral characteristics of the fibre Bragg grating by simply varying the scanning speed and exposure length highlights the engineering simplicity of the fibre Bragg gratings. For a fixed set of fabrication conditions (UV intensity, fibre type, fibre strain, scanning velocity etc.), gratings of desired characteristics such as reflectivity and spectral bandwidth can be calibrated [14] and customized for specific applications. Such control proved to be essential for the realisation of special FBG filters and for active fibre grating devices like fibre lasers to be discussed in subsequent chapters.

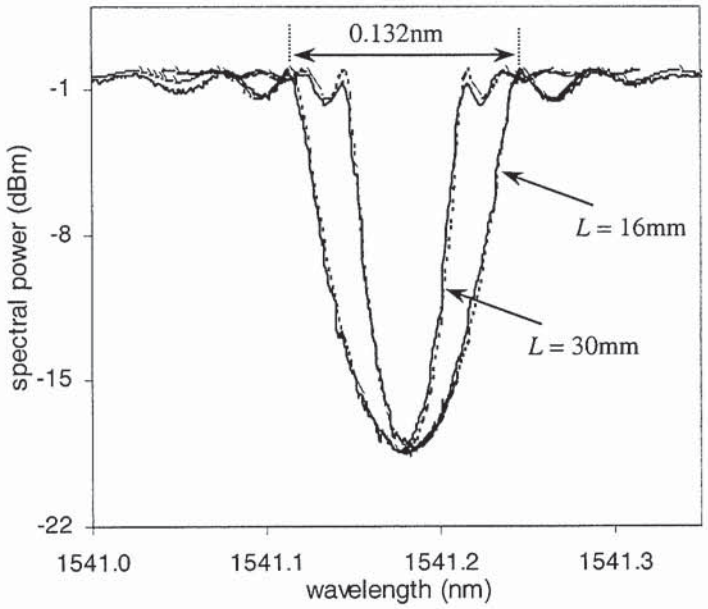

Figure 4.9 Superimposed measured (solid) transmission spectra of 2 uniform FBGs of length 30mm and 16mm. Despite the equivalent grating strength parameter κL= 2.69, the spectral bandwidths were distinctively different. The dotted traces are the simulated results.

4.4.1 Phase-shifted fibre grating

Despite the usefulness of uniform fibre Bragg gratings for narrowband in-fibre filtering applications, a large number of fibre grating structures for practical applications are in fact non-uniform grating structures. As mentioned, the optical properties of the grating structure can be adjusted by tailoring the grating parameters along the fibre axis. Among the commonly known variants of uniform fibre Bragg grating structures, the phase-shifted grating structure is perhaps the most well-known in passive filtering applications and in active devices like fibre lasers.

The interest in the phase-shifted fibre grating lies in the narrow transmission band within the stopband of its spectral response. Such a filter device has the advantage over a uniform fibre Bragg grating of giving the filter response in transmission. Narrowband transmission filtering using fibre Bragg gratings has been in the past realised in several forms. Early demonstrations included the use of a Moiré grating structure where 2 uniform fibre Bragg gratings of slightly different periods were superimposed together [29][30]. By limiting the length of the grating to be less than the index modulation envelope, one period of a Moiré grating was then equivalent to a π phase-shifted grating structure which exhibited a narrow resonance peak (transmission peak) at the Bragg centre. Other commonly adopted techniques to realise narrow linewidth bandpass filtering include the fibre grating resonator configurations [31]-[34]. These compound grating resonator structures achieve single or multiple narrow bandpass response through Vernier operation between the fibre grating cavities. Though flexible in design, such grating structures are generally more complex, less compact with greater demand in accuracy [35] and isolation to improve robustness against surroundings perturbations.

Compared to compound grating resonant structures or Moiré fibre gratings, phase-shifted fibre gratings realised through the incorporation of a discrete localized phase shift in a single uniform fibre Bragg grating are simple to tailor, easy to fabricate and are compact since they involve only a single fibre Bragg grating structure. The insertion of the phase shift opens up an extremely narrow transmission gap within the grating stopband and depending on various grating parameters such as the index modulation and the number of phase shifts within the structure, such phase-shifted gratings can effectively perform single or multiple narrowband wavelength selection as well as bandpass flattop filtering with steep extinction slopes.

Phase-shifted fibre gratings have a vast number of applications in optical communication systems [36][37]. Apart from filtering capabilities, the phase-shifted grating is perhaps most well known for its applications in fibre laser configurations [35][38]. In distributed feedback fibre (DFB) laser applications, the introduction of a π phase shift in the uniform grating structure breaks the threshold condition degeneracy for the two lowest order laser modes, enhancing single-mode fibre laser operation. The engineering simplicity of such DFB fibre lasers based on a phase-shifted fibre grating has led to the subsequent intense research interest into further optimisation and utilization of such high performance single-mode fibre-based optical sources.

To analyse the spectral response of the phase-shifted fibre grating structures by the transfer matrix technique, an equivalent phase-shift matrix of the form given by (4.23) is introduced:

$$M_{\phi} = \begin{bmatrix} \exp\left(-j\frac{\phi}{2}\right) & 0 \\ 0 & \exp\left(j\frac{\phi}{2}\right) \end{bmatrix} \tag{4.24}$$

where ϕ denotes the shift in the phase of the grating itself. For the case of a single phase-shifted fibre grating, the equivalent compound transfer matrix M_{psG} is hence given by:

$$M_{psG} = [M_f] \begin{bmatrix} \exp\left(-j\frac{\phi}{2}\right) & 0 \\ 0 & \exp\left(j\frac{\phi}{2}\right) \end{bmatrix} [M_f] \tag{4.25}$$

where the matrix M_f denotes the transfer matrix representation for a uniform fibre Bragg grating as defined in (4.12). Considering a uniform fibre Bragg grating of length 30mm and with a grating strength parameter of κL=4.7, the transfer response of the grating structure when a π phase shift is introduced in the middle of the grating structure is as shown in Figure 4.10.

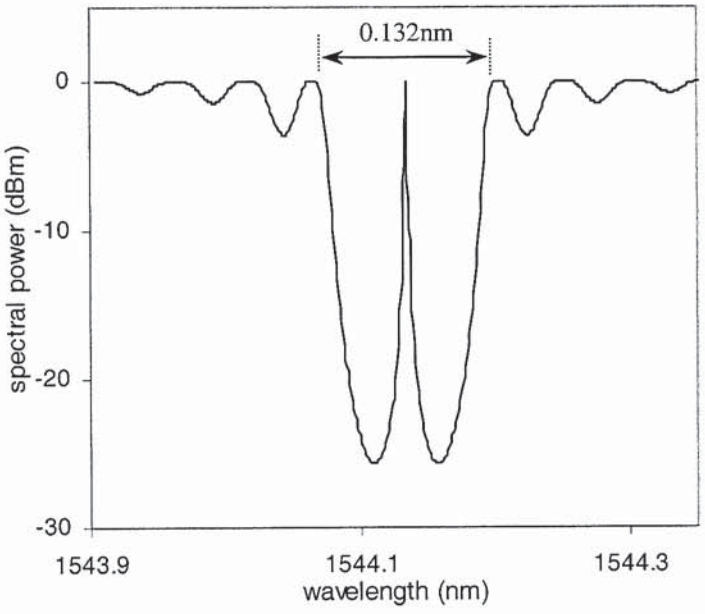

Figure 4.10 Simulated transmission profile of a π phase-shifted grating of length 30mm.

The extremely narrow transmission peak at the Bragg centre of the grating has a FWHM bandwidth on the order of < 1pm. The Lorentzian line shape transmission peak has a bandwidth that depends on the grating strength parameter. Increasing κL leads to a corresponding decrease in the passband width accompanied by the increase in spectral stop band [39]. Simulation results for the π phase-shifted grating at different κL (κL =4.7, 4.09, 3.48 and 2.87) are as shown in Figure 4.11.

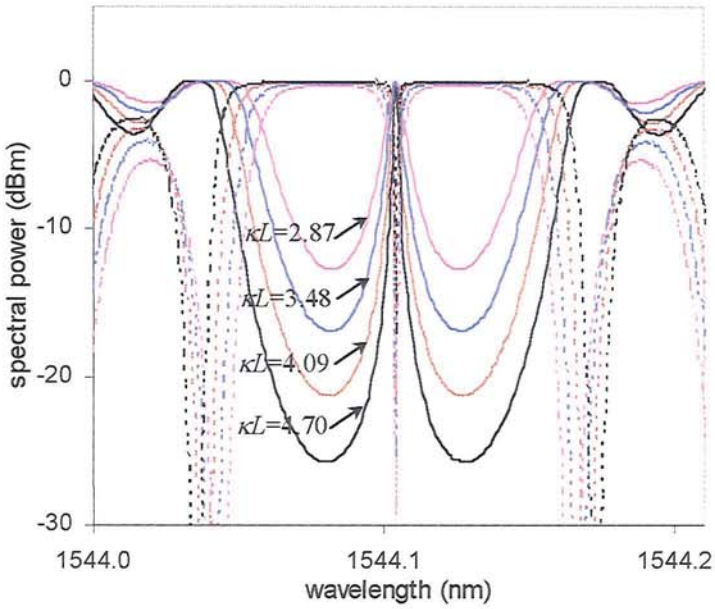

Figure 4.11 Superimposed π phase-shifted grating spectra of different κL. The dotted traces are the corresponding reflection spectra at each κL.

More importantly by introducing different amounts of phase shift into the grating structure, the position of the transmission peak relative to the grating stopband changes correspondingly. This is illustrated in Figure 4.12. Superimposed spectra of phase-shifted gratings with 0.56π, 0.78π, π, 1.22π and 1.44π phase shifts show relative transmission peak wavelength detuning of 14pm.

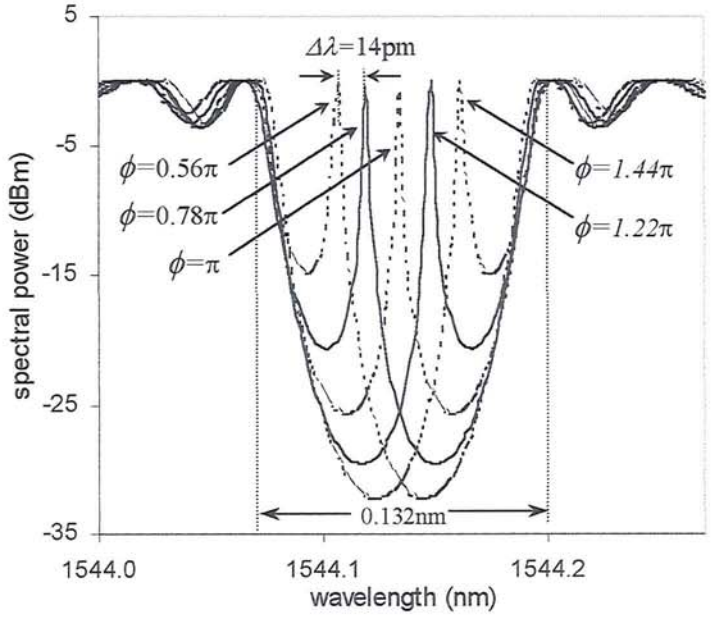

Figure 4.12 Superimposed spectra illustrating the variation of transmission peak position relative to the grating stopband at different induced phase shift.

The wavelength shift in the transmission peak associated with the variation in the induced phase shift is useful for phase-shifted fibre grating applications. One obvious example is the use of a single phase-shifted grating in the demultiplexing of multiwavelength channels [36] that are encompassed within the grating stopband width. The selected channel to be transmitted (dropped) is chosen by the amount of induced phase shift incorporated into the phase-shifted grating structure.

Established techniques to fabricate the phase-shifted fibre Bragg grating can be broadly classified into three categories: using a customized phase-shifted phase mask [40], post-processing techniques [39] and scanning beam moving phase mask/fibre techniques [21]. The use of a dedicated phase-shifted phase mask evidently enables reliable and highly repeatable fabrication though it limits the flexibility and incurs higher cost in making the specific required phase mask. The post-processing technique essentially involves irradiating a centre section of a uniform fibre grating with an intense uniform UV beam. Such UV trimming raises the refractive index of the processed region to disrupt the continuity of the original uniform FBG structure so as to create two gratings out of phase with each other. The phase shift induced, $\phi_{induced}$, is a function of the length of the post-processed region, L_{pp}, as well as the index increment incurred, Δn_{pp}, and can be expressed as

$$\phi_{induced} = (\Delta\beta)L_{pp} = \left(\frac{2\pi\Delta n_{pp}}{\lambda}\right)L_{pp} \tag{4.26}$$

Commonly carried out with real-time monitoring, the post-processing technique allows one to trim the induced phase shift to the desired value with ease. This technique is only limited when the grating length is too short compared to the order of the beam width (~0.8mm). Otherwise, this fabrication method is highly attractive for its simplicity, ease of control over the amount of induced phase shift and most important of all, requires no special phase mask or fabrication setup.

Towards a single-step fabrication technique, the scanning beam moving phase mask/fibre method provides the straightforward solution. Relative movement between the fibre and the phase mask during the writing scan similarly disrupts the uniform grating structure inscribed and the amount of disruption (measured in terms of relative movement induced) directly influences the amount of phase shift induced into the grating structure. In the experiment, a step voltage was applied to the PZT attached to the phase mask holder when the scanning beam reached the intended position for the insertion of the phase shift. The amount of relative movement introduced directly influences the amount of phase shift induced. Experimentally, for an applied voltage of 0.45V, a closely π phase-shifted grating was obtained as shown in Figure 4.13. By using step voltages of 0.4V and 0.5V, phase shifts of 0.88π and 1.11π were successfully incorporated into the grating structure as illustrated in Figure 4.14. All the measured spectral profiles were in good agreement with the simulation results.

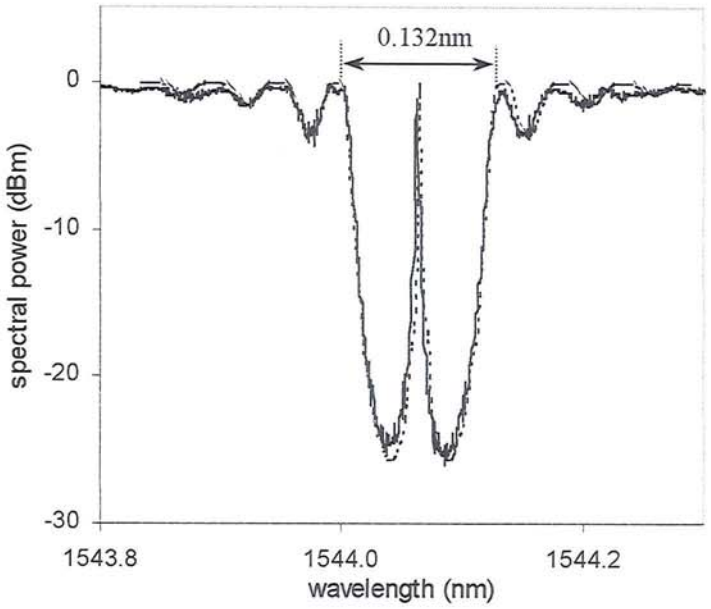

Figure 4.13 Measured (solid) and simulated (dotted) transmission spectra of a 30mm π phase-shifted fibre grating. Index modulation was $7.7x10^{-5}$. Transmission peak had a linewidth of <1pm and stopband width was 0.132nm.

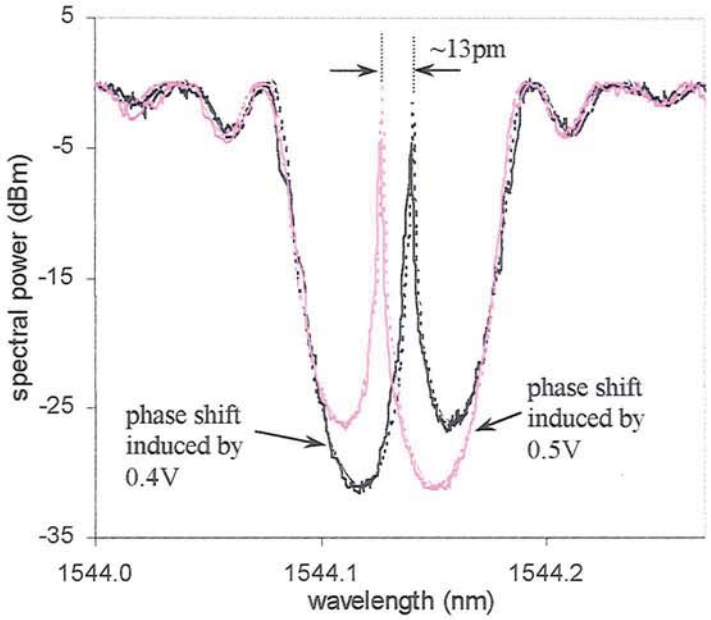

Figure 4.14 Measured (solid) and simulated (dotted) spectral profiles of two phase-shifted gratings created by using 0.4V and 0.5V step voltages during the fabrication process. Length of each grating was 40mm with index modulation $6.9x10^{-5}$.

The dependency of the transmission wavelength on the induced phase shift has led to a number of investigations to realise real-time variable phase shift in a uniform fibre grating structure so as to create a

tunable fibre grating transmission filter e.g. [41][42][43]. All these techniques take advantage of the fact that a perturbed region within a uniform fibre grating structure induces a phase shift and depending on the amount of external perturbation introduced, the spectral response of the phase-shifted grating structure response can be adjusted for specific applications. The subject of tunable fibre grating transmission filter is discussed in detail in Chapter 5 where a novel tuning mechanism is introduced.

It is interesting to compare the spectral profile of the uniform fibre Bragg grating to a π phase-shifted grating of identical coupling coefficient and physical length. Figure 4.15 shows the simulated and experimental results of a 30mm long uniform FBG fabricated under identical conditions used for the fabrication of the 30mm long π phase-shifted grating. The spectral bandwidth of the uniform fibre grating was measured to be 0.098nm with a peak loss of 35dB. The insertion of a π phase shift into the grating structure widened the spectral width to 0.132nm and lowered the peak notch about the Bragg wavelength to 25.7dB. Obtained results were in good agreement with the simulation results.

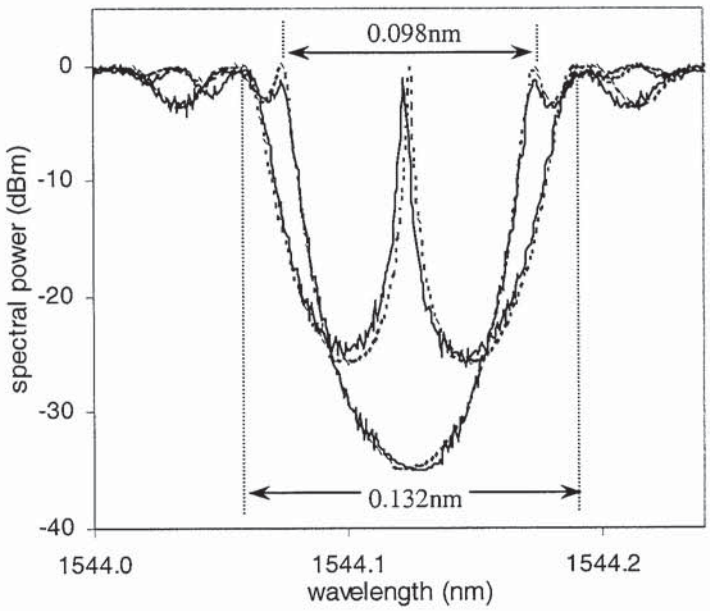

Figure 4.15 Comparison between a 30mm long uniform fibre Bragg grating and a 30mm long π phase-shifted grating of identical κL = 4.7 (i.e. index modulation of 7.7×10^{-5}). The dotted traces are the simulated results.

Following the realisation of a single phase-shifted fibre Bragg grating structure, it is a natural next step to investigate the realisation of multiple phase-shifted fibre grating structures [44]-[47]. Intense interest in multiple phase-shifted fibre gratings arises from the ability to tailor the transmission characteristics of the passband in these gratings. For some applications, the transmission band from the single phase-shifted grating structure is considered too narrow and its band edge slope too weak which consequently leads to a broad bottom level. Early demonstrations of double phase-shifted grating structures [44][45] showed 'improved' transmission band in terms of wider bandwidth and steeper side slope. The two phase shifts of π were inserted at locations L and $2L$ in a uniform fibre Bragg grating of length $4L$. A simulation result on

such a grating structure is as shown in Figure 4.16. The transmission profile of a single π phase-shifted grating of identical length and strength parameter is superimposed for comparison. In both cases, the grating length used was 40mm with index modulation of 6.9×10^{-5} (corresponding to $\kappa L = 5.62$). Comparing the transmission spectrum of the dual phase-shifted grating to that of the single π phase-shifted grating, the increase in the passband width was evident. The FWHM passband width in the doubly phase shifted grating was 7pm compared to 1pm for the single phase-shifted grating. Furthermore, for identical grating lengths and strength parameters, the introduction of addition phase shift increases the spectral width and sidelobes but lowers the extinction ratio. Further studies have highlighted that the insertion of a third phase-shift gives a more rectangular bandpass shape while increasing the phase shift number allows one to tailor this rectangular shape [45][46]. A bandpass response with negligible ripples (<0.01dB) can be achieved with optimisation of the distances between the phase shifts. For the case of a 3 phase-shifted grating structure with κL=5.62, using length ratios of 1: 2.18: 2.18: 1, a quasi-rectangular passband window with FWHM of 0.019nm can be obtained as shown in Figure 4.17. However, the increased number of phase shifts increases the sidelobes, spectral bandwidth and lowers the extinction ratio [47].

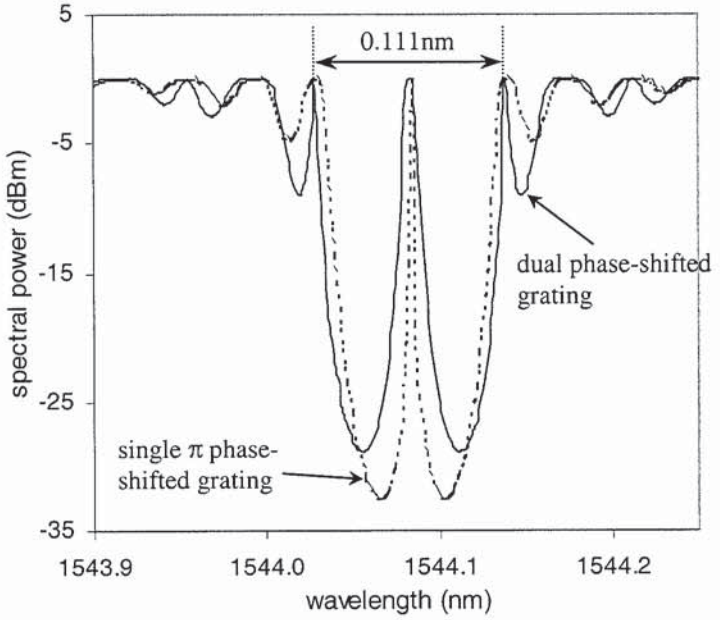

Figure 4.16 Simulated transmission profiles of a single π phase-shifted grating and a dual π phase-shifted grating. Both gratings had identical length and coupling strength. FWFZ bandwidth of the dual phase-shifted grating (measured 0.111nm) showed a slight increment compared to that of the single phase-shifted grating measured 0.107nm. Lengths of all gratings were 40mm with index modulation of 6.9×10^{-5}.

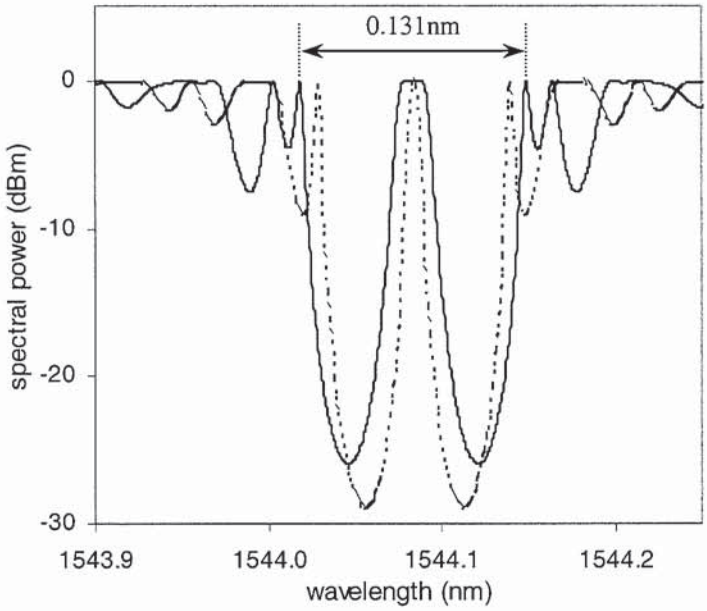

Figure 4.17 Simulated transmission spectrum (solid) of a three phase-shifted fibre grating structure of length 40mm and strength parameter κL = 5.62. Optimised length ratios between the phase shifts were 1: 2.18: 2.18: 1. Transmission spectrum (dotted) of the dual phase-shifted grating is superimposed for comparison.

It is important to note that to tune the transmission band in the multiple phase-shifted grating without distorting the spectral shape, it is vital to introduce an equal phase change to all phase shift regions. For the dual phase-shifted grating presented in Figure 4.16, the transmission band can be tuned by ±0.014nm through $\pm 0.22\pi$ change at each phase shift region. This is illustrated in Figure 4.18. Differential phase change incurred between the phase shift regions increases the transmission loss and increases passband ripple. Figure 4.19 illustrates the impact of differential phase change of 0.05π and 0.1π on the transmission response of the dual phase-shifted grating structure.

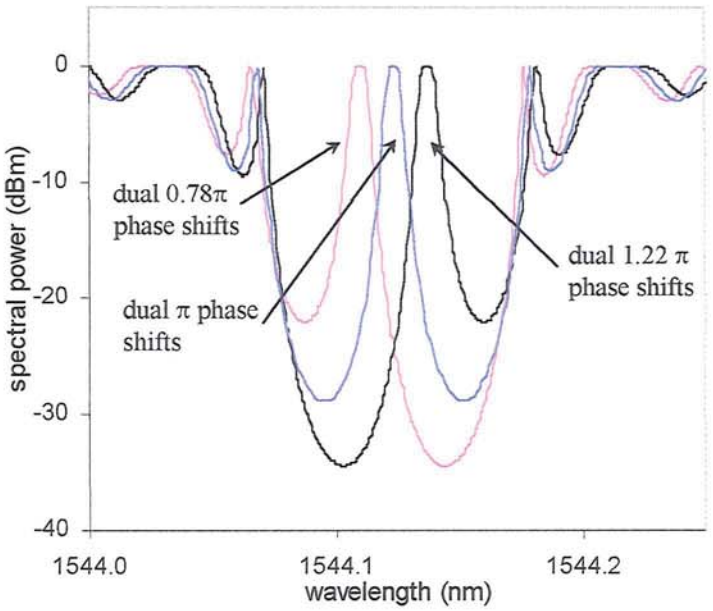

Figure 4.18 Spectral profiles of grating structures with dual 0.78π, π and 1.22π phase shifts respectively.

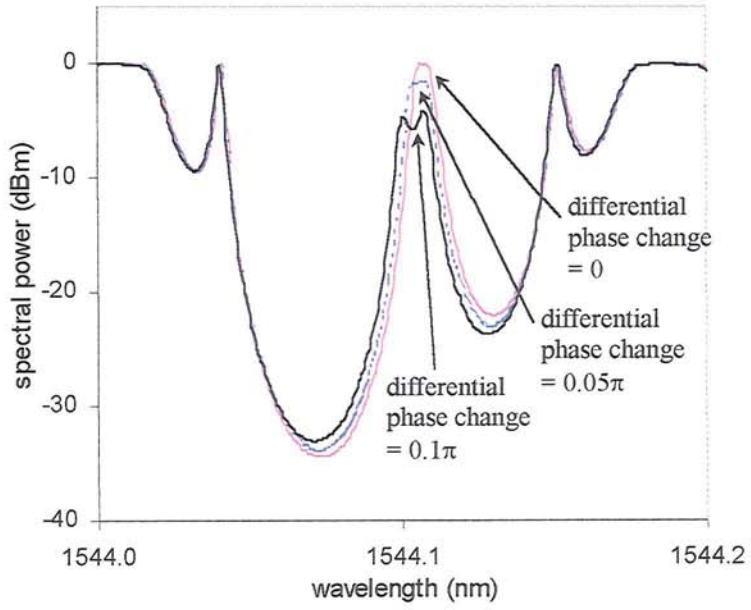

Figure 4.19 Spectral profiles illustrating the impact of differential phase changes in the dual phase-shifted grating structure.

4.4.2 Birefringence in fibre Bragg gratings

It is important to recognize the impact of fibre birefringence on the spectral characteristics of fibre grating structures. Despite the fact the amount of intrinsic birefringence in modern single-mode fibre (on the order of 10^{-8} to 10^{-7} over long distances) can be considered negligible in device applications, its effect on high finesses spectral features in fibre gratings (wavelength resolution on the order of few pm to tens of pm) however is significant. Furthermore, due to the fact UV photoinduced index change in fibres during grating formation can be anisotropic, effective birefringence in fibre grating structure hence plays an important role on the resultant spectral characteristics [47][40].

Compared to common grating characterization, special attention and additional apparatus are necessary to accurately define the spectral profile differences due to the effect of fibre birefringence. Considering the intrinsic birefringence of a conventional single-mode fibre for grating fabrication to be on the order of $1x10^{-7}$, the effective Bragg wavelength difference along the two polarization axes will therefore be on the order of $\Delta\lambda_{pol} = 2\Delta n_{bire}\Lambda = 0.1$ pm where Δn_{bire} denotes the effective fibre birefringence and Λ is the grating period. Using commercially available instrumentation such as tunable lasers and wavelength meters (wavemeters) functioning at 1pm resolution, standard grating characterization (within the context of this thesis) limits measurement of effective birefringence to the order of $1x10^{-6}$ and above. The experimental setup for such grating characterization is as shown in Figure 4.20.

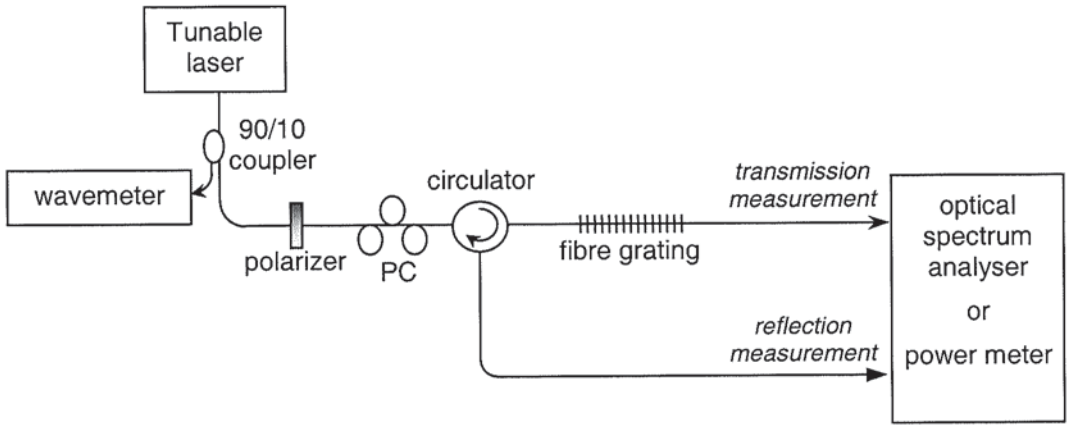

Figure 4.20 Experimental setup for high resolution (1pm) grating characterization to measure the effects of birefringence in the spectral profiles. PC: polarization controller.

Despite the high-resolution step-tuning achievable by the tunable laser, the use of a wavemeter in the experimental measurement system was necessary to ensure the absolute accuracy of the output wavelength (linewidth = 100kHz) to 1pm. A polarization controller (manually or electrically controlled) assisted the alignment of the linearly polarized measurement source (through the polarizer) to the principle axes of the grating structure. Although the output from the tunable laser was specified to be linearly polarized, its azimuth was found to deviate as the wavelength changes. Hence the use of a polarizer to define the input SOP orientation with respect to the principle axes of the grating structure was necessary. Based on the above measurement system setup, wavelength characterization to 1pm accuracy was achieved.

The most direct implication that fibre birefringence has on a uniform fibre Bragg grating is the Bragg wavelength shift when the state of polarization of the input light aligns with different principle propagation axes of the grating structure. Figure 4.21 illustrates again the superimposed spectral profiles of a uniform fibre grating measured along the two principle polarization axes.

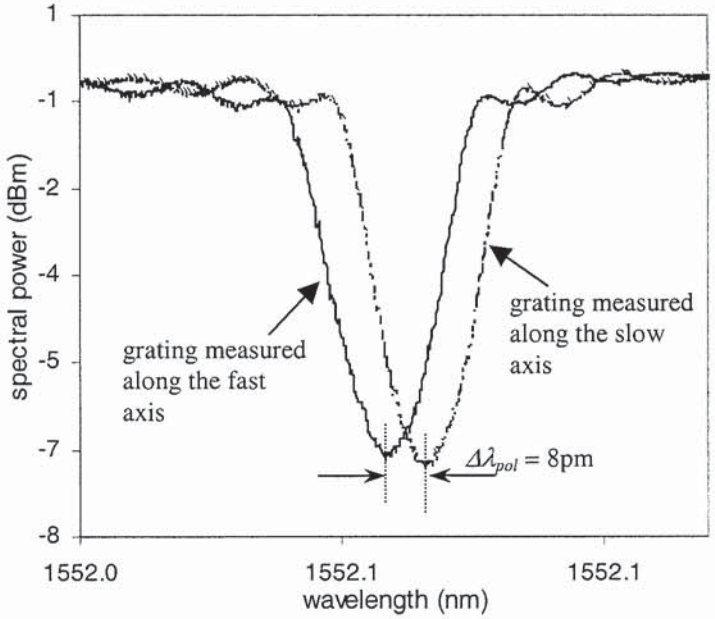

Figure 4.21 Superimposed transmission profiles of a uniform fibre Bragg grating measured along respective polarization axes. Birefringence-induced wavelength separation measured 8pm, corresponding to effective birefringence on the order of $7.5x10^{-6}$.

In this example, the UV scanning beam was intentionally offset from the fibre core to increase the UV-induced anisotropic index change along the grating length (L = 45mm). From the obtained results, the birefringence-induced Bragg wavelength shift measured 8pm corresponding to an effective birefringence of ~$7.5x\ 10^{-6}$ in the grating structure. Without intentional induced index anisotropy during fabrication, the birefringence effect was below the resolution achievable by the measurement setup. It is also important to note that the amount of UV induced birefringence, apart from the exposure geometry [49] (i.e. the UV intensity and the fabrication condition/alignment), was found to be a strong function of the fibre type as well. In the presence of sharp spectral features (on the order of 1pm), most notably from a phase-shifted grating structure, the effect of UV-induced birefringence in different fibres manifested clearly as illustrated by Figure 4.22 and Figure 4.23.

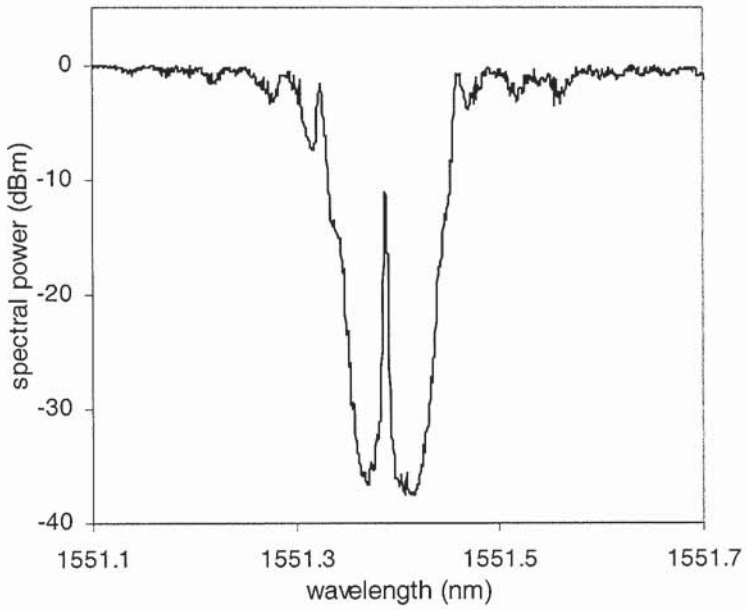

Figure 4.22 Transmission profile of a 40mm long π phase-shifted fibre grating written in standard fibre. Within the measurement resolution of the system setup, no birefringence-induced polarization splitting was observed in the transmission peak.

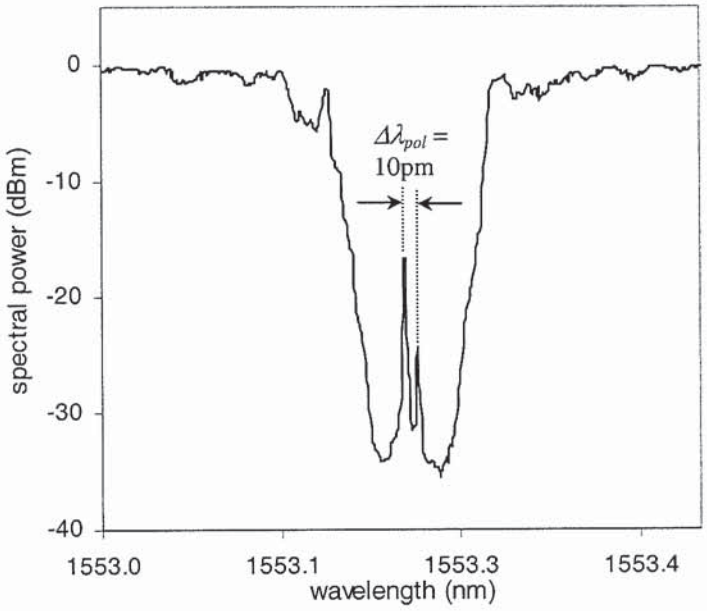

Figure 4.23 Transmission profile of an identical 40mm long π phase-shifted fibre grating written in Er/Yb fibre. Polarization splitting in the transmission peak was evident.

Since the fabrication conditions for the inscriptions of both grating structures were identical, it is evident that the fibre itself played a profound role on the amount of resultant birefringence in the grating structure. Fibre grating formation through side UV exposure potentially leads to uneven UV intensity distribution across the core of the fibre, in particular for highly photosensitive fibres (such as hydrogenated

B/Ge doped fibres). High UV absorption along one side of the fibre core effectively creates a UV intensity distribution across the fibre core, leading to anisotropic photoinduced index change. In conjunction with the fact the Er/Yb adopted in this example has a unique structural core/cladding where a photosensitive annulus is built around its core [50], the cross section UV intensity distribution was considerably more drastic compared to the case of a uniform photosensitive core. As a result, fibre gratings fabricated in such Er/Yb fibres exhibited birefringence-induced polarization-dependent spectral features. As shown in Figure 4.23, differential phase shift along the two polarization axes created polarization mode splitting at the transmission peak with wavelength spacing measured as 10pm. By varying the state of polarization of the input light, the heights of the two transmission peaks altered differentially. When the SOP of input light aligned with one or the other of the polarization axis, the transmission peak corresponding to the orthogonal propagation axis was extinguished. It is worth noting that the amount of induced birefringence can be increased further through UV offset post-processing. Exploitation of such birefringence features in phase-shifted gratings for fibre laser applications is discussed in Chapter 6.

Towards a more extreme case of birefringence effect on fibre grating characteristics is the inscription of FBGs into high birefringence fibre [51][52]. As detailed in Chapter 2, Hi-Bi fibre contains built-in physical asymmetry to induce large index anisotropy across the fibre core thereby creating a large birefringence. Since the effective core index along each polarization axis differs significantly (on the order of 10^{-4}), the typical transmission spectrum of a uniform fibre Bragg grating in Hi-Bi fibre manifests as two spectral stopbands corresponding to respective polarization axis. This is illustrated in Figure 4.24. The wavelength spacing, $\Delta\lambda_{pol}$, between the two polarization stopbands relates to the effective birefringence of the fibre Δn_{bire} by $\Delta\lambda_{pol} = 2\Delta n_{bire}\Lambda$ where Λ denotes the grating period. For the case depicted in Figure 4.24, the effective birefringence in the grating structure measured $3.9\text{x}10^{-4}$.

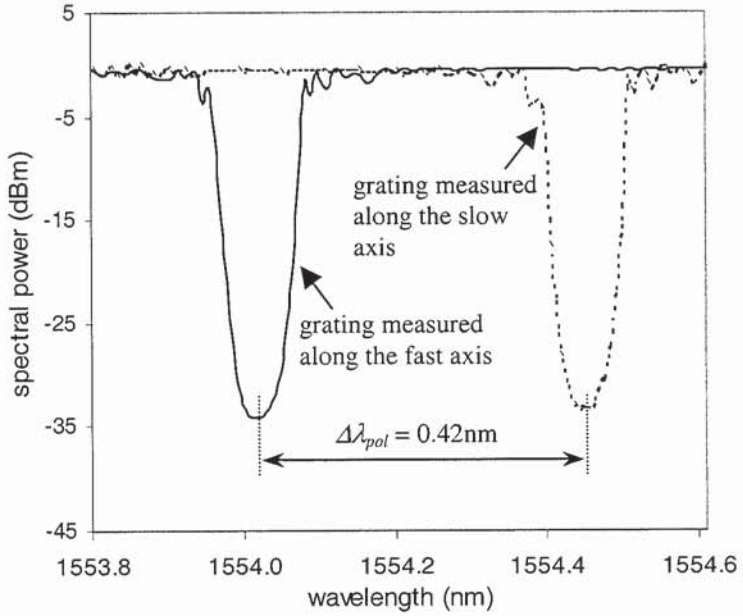

Figure 4.24 Transmission spectrum of a uniform fibre Bragg grating in Hi-Bi fibre measured along its polarization axes.

Evidently, a fibre Bragg grating in Hi-Bi fibre allows wavelength-selective polarization discriminating filtering. This is particularly useful for enforcing single polarization mode operation in fibre laser operations [53] and for generating polarization differential delay for polarization mode dispersion (PMD) compensation [54]. By adopting rare-earth doped Hi-Bi fibres (e.g. Er^{3+} doped fibres), fibre grating structures in such fibres can further realise active devices like fibre lasers with distinct polarization properties, determined by the fibre birefringence [55]. Novel applications of grating structures in Hi-Bi fibres for fibre laser configurations designed for microwave/millimetre wave photonics applications are illustrated in Chapter 6.

4.4.3 Superimposed fibre Bragg gratings

One of the key advantages of fibre grating technology compared to its semiconductor counterparts lies in its engineering simplicity and ease of fabrication. This is even more evident when one tries to grow several Bragg filters of various spectral characteristics at the same fibre position. Contrary to optical fibres, superimposing several Bragg gratings in planar waveguides [56]-[58] requires optimisation and stringent controls in the fabrication conditions. In many cases, the semiconductor material needs to be coated with a photoresist before being exposed successively by different fringe patterns, corresponding to different grating periods [59][56]. Due to the thresholding effect of the photoresist development and the characteristics of the etching process [59][57], the transfer of the superimposed fringe patterns into the semiconductor material is highly nonlinear [57]. In particular, the transfer of the exposure intensity to etch depth when using the dry-etching technique approximates a step function [57]. Consequently, nonlinearities arise and increase with increasing number of superimposed gratings. On the other hand, for a semiconductor waveguide, such as Ge-doped silica-on-silicon waveguides [60], which allows direct UV photoinscription (thereby eliminating the etching process), the nonlinearities in the superimposed grating structure arise as a result of the low nonlinear index saturation value (on the order of 3.5×10^{-4}). The saturation leads to intermodulation of gratings, as the fringes are superimposed, that results in the formation of a considerable number of undesired gratings (commonly known as spurious gratings), usually with non-negligible amplitudes [60]. The saturation nonlinear response decreases the amplitudes of the desired gratings while raising the spurious grating strength as more gratings are superimposed [60].

In optical fibre, the superimposition of several fringe patterns does not induce significant nonlinear effects due to the large available dynamic range of photoinduced index modulation in photosensitive fibres [61][62]. Early experimental demonstration of growing several gratings within the same fibre highlighted the availability of further photoinduced index modulation after the inscription of the first grating [63]. Such a grating structure is not only of considerable interest for providing a comb spectrum for spectroscopy and fibre optics communication applications [64][65]-[69], it can potentially serve as a single, compact sensor element for simultaneous measurement of more than one physical parameter in fibre optic sensor systems [70]. As a filter device, the superimposed fibre Bragg grating is highly suitable for multiplexing and demultiplexing signals and is desirable in applications where size is of concern. Apart from the ease of fabrication, it is worth noting that the advantageous characteristics like out-of-band losses, spectral width and even phase shifts of individual inscribed Bragg gratings can be maintained in the process of superimposition.

It is obvious that a superimposed fibre Bragg grating structure can be fabricated simply through multiple exposures of a section of the photosensitive optical fibre to spatial interference patterns of different periodicities. This can be achieved using an adjustable interferometric fabrication setup [61] or through the use of multiple phase masks with desirable periodicities. Towards a more economical solution with ease of implementation, fibre Bragg grating fabrications on pre-strained fibres were demonstrated [71][72]. By applying a longitudinal strain to the optical fibre, the Bragg condition varies linearly with the applied strain given by [71]

$$\frac{\Delta\lambda_B}{\lambda_B} = \frac{\Delta\Lambda}{\Lambda} + \frac{\Delta n}{n} = \frac{\partial l}{l} + \frac{1}{n}\frac{\partial n}{\partial s}\frac{\partial l}{l} = \left(1 + \frac{1}{n}\frac{\partial n}{\partial s}\right)\frac{\partial l}{l} \tag{4.27}$$

where λ_B denotes the Bragg wavelength, $\partial n/\partial s$ is the strain-optic coefficient of the fibre and $\partial l/l$ is the strain applied to the fibre of length l, leading a change in grating period of $\Delta\Lambda$ and $\Delta\lambda_B$ is the resultant Bragg wavelength shift. For typical glass properties [73], (4.26) simplifies to

$$\frac{\Delta\lambda_B}{\lambda_B} \sim 0.71\frac{\partial l}{l} = 0.71\frac{\Delta\Lambda}{\Lambda} \tag{4.28}$$

where $\frac{1}{n}\frac{\partial n}{\partial s} = -0.29$.

Hence, by applying a strain to the fibre prior to grating fabrication, the resultant Bragg gating wavelength can be varied. Based on the same context, superimposition of different Bragg wavelengths is then achieved by applying different strains to the fibre prior to each exposure. Considering a typical optical fibre strain limit of ~ 3% [72], the maximum wavelength spacing between two overwritten fibre Bragg gratings reaches >36nm.

Detailed analysis of superimposed fibre grating structures based on coupled mode theory [64] have highlighted some of the key performance characteristics and the corresponding determining grating parameters. In particular, key factors affecting the spectral characteristics of dual overwritten fibre grating structures are the grating length L and period difference $\Delta\Lambda$. When the period difference and grating length satisfy

$$L\Delta\Lambda \gg \frac{\Lambda_1\Lambda_2}{\pi} \tag{4.29}$$

where Λ_1 and Λ_2 denote respective grating periods, the reflection spectra of the two gratings are separated sufficiently such that the gratings are independent of each other. The transmission/reflection spectrum of the dual overwritten grating structure is then composed of two transmission/reflection bands located at the respective Bragg wavelength of individual grating.

Figure 4.25 shows the measured transmission spectrum of a dual overwritten uniform fibre Bragg grating structure fabricated in the experiment. The grating lengths were 30mm, superimposed at the same fibre position using identical UV intensity and scanning speed. The wavelength separation between the two gratings was 0.215nm corresponding to $\Delta\Lambda$=0.074nm. The grating structure satisfied (4.28) to yield two independent spectral stopbands at different Bragg wavelengths.

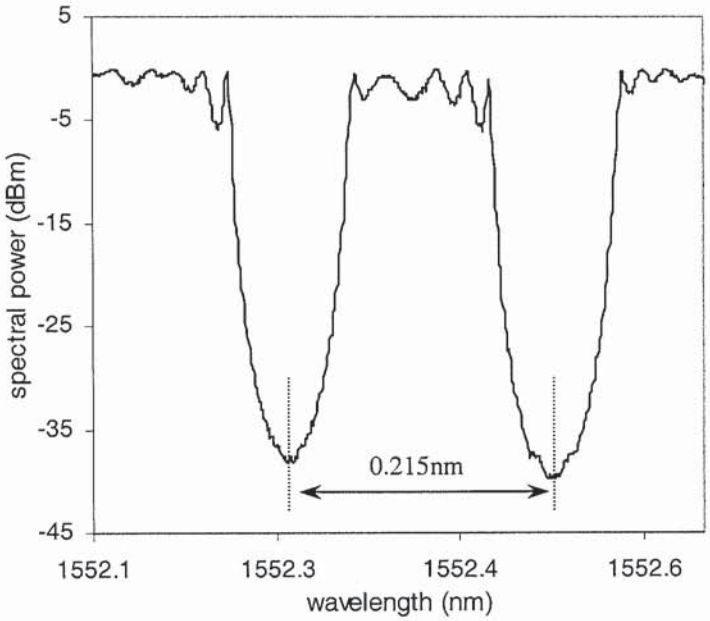

Figure 4.25 Measured transmission spectrum of a dual overwritten uniform fibre Bragg grating structure. Both gratings were of length =30mm.

The ability to overwrite fibre gratings without erasure of previous grating structure opens up a new horizon for realisation of more complex superimposed grating structures. Based on a similar concept, two phase-shifted grating structures satisfying (4.28) can be overwritten to create a dual, co-located π phase-shifted grating structure. The fabrication process for the superimposed phase-shifted grating structure is identical to that of the superimposed uniform FBG structure. The transmission spectrum of such a dual, co-located π phase-shifted grating structure is as shown in Figure 4.26.

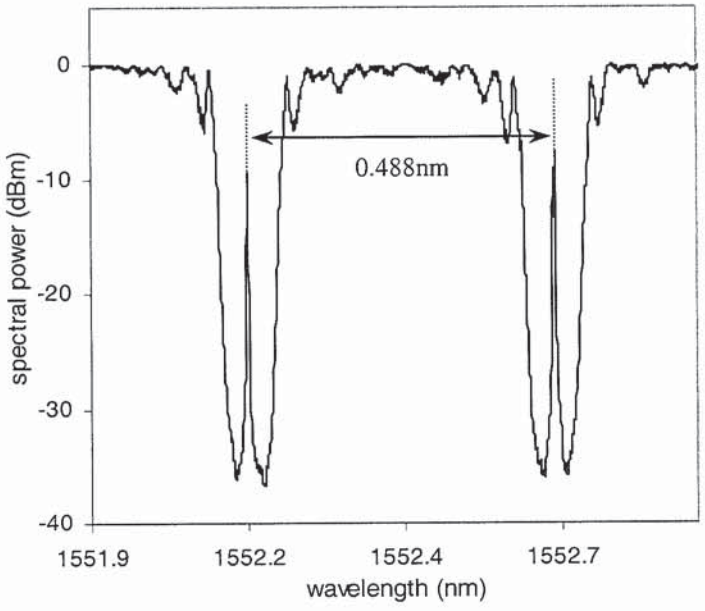

Figure 4.26 Transmission spectrum of a dual overwritten π phase-shifted fibre grating structure.

In the experiment, the length of individual π phase-shifted gratings was 40mm with induced index modulation Δn=7.4x10^{-5}. It is evident that the individual gratings remained independent of each other and retained their characteristic narrow transmission peak at the respective Bragg centres. It is interesting to note that comparing the spectral profile of the first grating before and after the inscription of the second overwritten structure, an observable amount of Bragg wavelength shift was detected. Such behaviour was similarly observed in [61] and had been attributed to the increase in the average photoinduced index when the second grating was superimposed at the same fibre position. The amount of additional induced average index increment depends on the UV exposure used for the fabrication of the second grating. For the case depicted in Figure 4.26, an additional average index growth of 6.5x10^{-5} was introduced to the first grating leading to a Bragg wavelength shift of 69pm. Hence for an applied strain to the fibre prior to the fabrication of the second superimposed fibre grating, the Bragg wavelength difference between the two superimposed grating did not follow (4.27) exactly, but offset by a positive constant depending on the additional induced average index. It is worth noting that system calibration taking into account induced index deviation can be achieved for the same UV intensity and exposure time for repeated fabrication.

Apart from its comb filtering function, the superimposed fibre grating structure, in conjunction with Hi-Bi fibre, presents yet another important device for fibre optic communications. Based on the merit of superimposed gratings to create spectral bands with desirable wavelength spacing and the polarization selectivity of FBG in Hi-Bi fibre, a superimposed fibre grating structure in Hi-Bi fibre enables polarization discriminating filtering (or even comb filtering) at specified wavelengths regardless of the intrinsic birefringence of the fibre. This concept is illustrated in Figure 4.27. As described in section 4.3.2, a uniform fibre grating inscribed into a Hi-Bi fibre presents two polarization discriminating spectral stopbands with wavelength spacing dictated by the intrinsic birefringence of the fibre. For a typical commercially available Hi-Bi fibre with birefringence on the order of 1x10^{-4} to 9x10^{-4}, the wavelength spacing achievable is limited to less than 2nm. This intrinsic birefringence also restricts the minimum wavelength spacing realisable through the inscription of a uniform fibre Bragg grating. Towards overcoming the limitations imposed by the fibre properties, the superimposed fibre grating concept is introduced. After the inscription of the first uniform fibre Bragg grating which manifests as two spectral stopbands along respective polarization axes, a second grating of appropriate wavelength separation from the first is fabricated to achieve the desired $\Delta\lambda_{pol}$ between λ_{1s} and λ_{2p}. In the experiment, as shown in Figure 4.27, the inscription of the first uniform fibre Bragg grating created spectral bands at λ_{1p} and λ_{1s} (along fast and slow axes of the fibre) with $\Delta\lambda_{pol(1s\text{-}1p)}$ = 0.418nm which corresponded to an effective birefringence of 3.9x10^{-4}. The second grating fabricated using the pre-strained fibre technique led to the formation of spectral bands λ_{2p} and λ_{2s}. Two separate sets of wavelength-selective, polarization discriminating filter bands were achieved between λ_{2s} and λ_{1p} ; λ_{2p} and λ_{1s} of wavelength spacings 0.15nm and 0.988nm respectively.

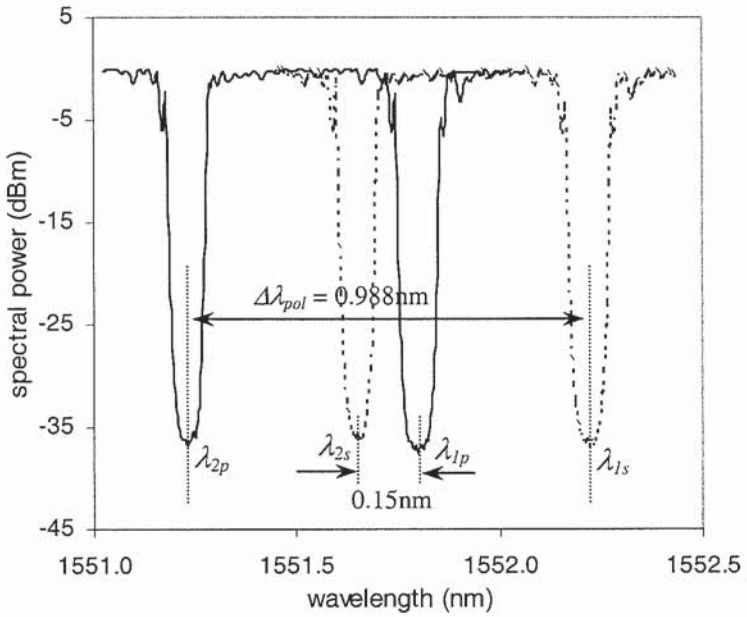

Figure 4.27 Transmission profiles of a superimposed uniform fibre Bragg grating structure in Hi-Bi fibre.

It is important to note that such a grating structure offers considerable wavelength separation range, $\Delta\lambda_{pol}$, not limited by grating/fibre parameters. Utilizing the prestrained fibre fabrication technique, wavelength spacing beyond 30nm can be achieved. In applications where simultaneous wavelength-selection and polarization discrimination are of importance, superimposed fibre grating structures in Hi-Bi fibres offer an elegant and easy solution. It is also worth noting that the distinct feature of superimposed fibre grating structure that differentiates itself from cascaded grating array or other forms of multiplexed grating structure lies in the fact that the two gratings, being physically co-located, experience identical external (environmental etc) perturbations under all circumstances. As a result, spectral characteristics, such as wavelength separation, can remain constant in the presence of external perturbations. A device architecture based on superimposed grating structure can hence enable common mode suppression to external disturbances without the need to isolate/condition individual gratings. On the basis of this intrinsic advantage, a superimposed grating structure can further be adopted in fibre grating monitoring purposes. The spectral characteristics of the superimposed grating effectively act as an indicator for the first inscribed grating. Bragg wavelength drift, chirping etc due to external perturbations manifest in identical magnitude in the spectral characteristics of both gratings. By adopting an appropriate, desirable spectral range for the superimposed grating, direct assessment of the status of the primary grating not possible in some applications can be achieved. This concept is applied to direct mode assessment and optimisation of linear cavity fibre laser configurations that are discussed in Chapter 7.

4.5 Conclusions

An overview of fibre Bragg grating technology has been outlined. A simulation technique for fibre Bragg grating structures based on the transfer matrix technique has been described and fibre Bragg grating fabrication based on the phase mask technique has been discussed. The important characteristics of uniform fibre Bragg gratings have been detailed and the relationships between the spectral response with various grating parameters like index modulation and grating length have been highlighted. The ease and ability to tailor the spectral characteristics of fibre Bragg grating structures have been highlighted. Furthermore, with little adjustment to the fabrication process, highly useful non-uniform fibre Bragg grating structures, namely phase-shifted fibre grating and superimposed grating structures have been realised. For the phase-shifted fibre grating, it has been noted that the transmission peak wavelength within the grating stopband depends on the amount of induced phase shift. More importantly, to prevent compromising transmission loss and passband ripples, attention must be paid to avoid differential phase change during the tuning of the dual phase-shifted grating structure. Fibre birefringence and its impact on the spectral characteristics of fibre gratings have been highlighted. In particular, birefringence-induced polarization mode splitting in phase-shifted fibre grating has been noted. The polarization mode splitting in the transmission peak of the spectral response of the phase-shifted grating has been found to be, apart from other factors, dependent on the fibre type as well. Lastly, the concept of superimposed fibre grating structures has been introduced. The concept has been applied to non-uniform grating structures to realise overwritten phase-shifted fibre gratings. More importantly, through combining the flexibility of superimposed grating with the polarization-selectivity of fibre Bragg grating in Hi-Bi fibre, a new concept of superimposed fibre grating structure in Hi-Bi fibre to enable widely/narrowly spaced polarization-discriminating filtering, not limited by fibre properties, has been demonstrated.

4.6 References

[1] T. Erdogan, "Fibre grating spectra", *J. Lightwave Technol.*, 15(8), pp. 1277-1294, 1997.

[2] C.R. Giles, "Lightwave applications of fibre Bragg gratings", *J. Lightwave Technol.*, 15(8), pp. 1391-1404, 1997.

[3] J.L. Archambault, S.G. Grubb, "Fibre gratings in lasers and amplifiers", *J. Lightwave Technol.*, 15(8), pp. 1378-1390.

[4] G. Meltz, W.W. Morey, W.H. Glenn, "Formation of Bragg gratings in optical fibres by a transverse holographic method", *Optics Lett.*, 14, pp. 823-825, 1989.

[5] A. Yariv, "Optical Electronics", Saunders College Publishing, 4th Edition, section 13.8, pp. 519-521, 1989.

[6] M.A. Rodriguez, M.S. Malcuit, J.J. Butler, "Transmission properties of refractive index-shifted Bragg gratings", *Optics Comm.*, 177, pp. 251-257, 2000.

[7] K.O. Hill, "A periodic distributed parameter waveguide for integrated optics", *Applied Optics*, 13(8), pp. 1853-1856, 1974.

[8] M. Matsuhara, K.O. Hill, "Optical waveguide band rejection filters: Design", *Applied Optics*, 13, pp 2886, 1974.

[9] H. Kogelnik, "Filter response of non-uniform almost periodic structures", *Bell System Technical Journal*, 55(1), pp. 109-126, 1976.

[10] M. Yamada, K. Sakuda, "Analysis of almost-periodic distributed feedback slab waveguides via a fundamental matrix approach", *Applied Optics*, 26(16), pp. 3474-3478, 1987.

[11] K Sugden, I Bennion, A Molony and N J Copner, "Chirped gratings produced in photosensitive optical fibre by fibre deformation during exposure", *Electron. Lett.* 30(5), pp. 440-442, 1994.

[12] K Byron, K Sugden, T Bricheno and I Bennion, "Fabrication of chirped Bragg gratings in photosensitive fibre", *Electron. Lett.*, 29(18), pp. 1659-1660, 1993.

[13] K.O. Hill, B. Malo, F. Bilodeau, D.C. Johnson, J. Albert," Bragg grating fabricated in monomode photosensitive optical fibre by UV exposure through a phase mask", *Applied Physics Lett.*, 62(10), 1993.

[14] D.Z. Anderson, V. Mizrahi, T. Erdogan, A.E. White, "Production of in-fibre grating using a diffractive element", *Electron. Lett.*, 29(6), pp. 566-568, 1993.

[15] B. Malo, D.C. Johnson, F. Bilodeau, J. Albert, K.O. Hill, "Single excimer pulse writing of fibre gratings by use of a zero-order nulled phase mask: grating spectral response and visualization of index perturbations", *Optics Lett.*, 18(15), pp. 1277-1279, 1993.

[16] J. Martin, F. Oulette, "Novel writing technique of long and highly reflective in-fibre gratings", *Electron. Lett.*, 30, pp. 811-812, 1994.

[17] H.N. Rourke, S.R. Baker, K.C. Byron, R.S. Baulcomb, S.M. Ojha, S. Clements, "Fabrication and characterization of long, narrowband fibre gratings by phase mask scanning", *Electron. Lett.*, 30(16), pp. 1341-1342, 1994.

[18] R. Kashyap, P.F. McKee, R.J. Campbell, D.L. Williams, "Novel method of producing all-fibre photo-induced chirped gratings", *Electron. Lett.*, 30, pp. 996-998, 1994.

[19] J.D. Prohaska, E. Snitzer, S. Rishton, V. Boegli, "Magnification of mask fabricated fibre Bragg gratings", *Electron. Lett.*, 29, pp. 1614-1615, 1993.

[20] K.C. Byron, H.N. Rourke, "Fabrication of chirped fibre gratings by novel stretch and write technique", *Electron. Lett.*, 31(1), pp. 60-61, 1995.

[21] M.J. Cole, W.H. Loh, R.I. Laming, M.N. Zervas, S. Barcelos, "Moving fibre/phase mask scanning beam technique for enhanced flexibility in producing fibre gratings with uniform phase mask", *Electron. Lett.*, 31(17), pp. 1488-1489, 1995.

[22] W.H. Loh, M.J. Cole, M.N. Zervas, S. Barcelos, R.I. Laming, "Complex grating structures with uniform phase mask based on the moving fibre-scanning beam technique", *Optics Lett.*, 20(20), pp.2051-2053, 1995.

[23] Sugden, L Zhang, J A R Williams, R W Fallon, L A Everall, K E Chisholm and I Bennion, "Fabrication and characterisation of bandpass filters based on concatenated chirped fibre gratings", *J. Lightwave Technol.*, 15(8), pp. 1424-1432, 1997.

[24] K E Chisholm, L A Everall, J A R Williams and I Bennion, "Comparison of theoretical and experimental performance of uniform period fibre grating apodisation functions", *Summer School on Photosensitivity in Optical Waveguides and Glasses*, Lake Lucerne, Switzerland, 1998.

[25] K E Chisholm, L A Everall, J A R Williams, L Zhang and I Bennion, "Apodised fibre Bragg grating arrays for quasi-distributed strain sensing", *11th IEEE Lasers and Electro-Optics Society Annual Meeting*, Orlando, Florida , WEE2, 1998.

[26] A. Asseh, H. Storøy, B.E. Sahlgren, S. Sandgren, R.A.H. Stubbe, "A writing technique for long fibre Bragg gratings with complex reflectivity profiles", *J. Lightwave Technol.,* 15, pp. 1419-1423, 1997.

[27] I. Petermann, B. Sahlgren, S. Helmfrid, A.T. Friberg, P.Y. Fonjallaz, "Fabrication of advanced fibre Bragg gratings by use of sequential writing with a continuous wave ultraviolet laser source", *Applied Optics*, 41(6), pp. 1051-1056, 2002.

[28] K Byron, K Sugden, T Bricheno and I Bennion, "Fabrication of chirped Bragg gratings in photosensitive fibre", *Electron. Lett.* 29 (18) , pp. 1659-1660, 1993.

[29] D.C.J. Reid, C.M. Ragdale, I. Bennion, D.J. Robbins, J. Buus, W.J. Stewart, "Phase shifted Moiré grating fibre resonators", *Electron. Lett.*, 26(1), pp.10-12, 1990.

[30] S. Legoubin, E. Fertein, M. Douay, P. Bernage, P. Niay, "Formation of Moiré grating in core of Germanosilicate fibre by trasverse holographic double exposure method", *Electron. Lett.*, 27(21), pp. 1945-1946, 1991.

[31] S.V. Chernikov, J.R. Taylor, R. Kashyap, "Coupled cavity erbium fibre lasers incorporating fibre grating reflectors", *Optics Lett.*, 18(23), pp. 2023-2025, 1993.

[32] J.C. Martin, M.P. Bernal, "Double ring and Fabry-Perot ring resonators: application for an optical fibre laser", *Applied Optics*, 33(21), pp. 4801-4806, 1994.

[33] Y.H. Jia, "Optical vernier filter with fibre grating Fabry-Perot resonators", *Applied Optics*, 34(27), pp. 6164-6167, 1995.

[34] B. Ortega, J. Capmany, D. Pastor, R.I. Laming, "Experimental demonstration of an ultraselective and tunable optical bandpass filter using a fibre grating and a Fabry-Perot", *Electron. Lett.*, 33(8), 1997.

[35] M.J. Guy, J.R. Taylor, R. Kashyap, "Single frequency erbium fibre ring laser with intracavity phase-shifted fibre Bragg grating narrowband filter", *Electron. Lett.,* 31(22), pp. 1924-1925, 1995.

[36] G.P. Agrawal, S. Radic, "Phase-shifted fibre Bragg gratings and their application for wavelength demultiplexing", *IEEE Photon. Technol. Lett.*, 6(8), pp. 995-997, 1994.

[37] A. Melloni, M. Chinello, M. Martinelli, "All-optical switching in phase-shifted fibre Bragg grating", *IEEE Photon. Technol. Lett.*, 12(1), pp. 42-44, 2000.

[38] J. T. Kringlebotn, J.-L. Archambault, L. Reekie, D. N. Payne, "Er^{3+} : Yb^{3+} codoped fibre distributed feedback laser", *Optics Lett.*, 19(24), pp. 2101-2103, 1994.

[39] J. Canning, M.G. Sceats, "π phase-shifted periodic distributed structures in optical fibres by UV post processing", *Electron. Lett.,* 30(16), pp. 1344-1345, 1994.

[40] R. Kashyap, P.F. Mckee, D. Armes, "UV written reflection grating structures in photosensitive optical fibres using phase-shifted phase masks", *Electron. Lett.*, 30(23), pp. 1977-1978, 1994.

[41] P. Torres, L.C.G. Valente, "Spectral response of locally pressed fibre Bragg grating", *Optics Comm.*, 208, pp. 285-291, 2002.

[42] D. Uttamchandani, A. Othonos, "Phase shifted Bragg gratings formed in optical fibres by post fabrication thermal processing", *Optics Comm.*, 127, pp. 200-204, 1996.

[43] L. Michaille, M.W. McCall, Yicheng Lai, J.A.R. Williams, "Analysis of single and multiple, non-permanent, tunable, birefringent spectral holes in a fibre Bragg grating stopband produced via uniaxial pressure", *Optics Comm.*, 222, pp. 1-8, 2003.

[44] F. Bakhti, P. Sansonetti, "Wide bandwidth, low loss and highly rejective doubly phase-shifted UV written fibre bandpass filter", *Electron. Lett.*, 32(6), pp. 581-582, 1996.

[45] R. Zengerle, O. Leminger, "Phase-shifted Bragg grating filters with improved transmission characteristics", *J. Lightwave Technol.*, 13(12), pp. 2354-2358, 1995.

[46] F. Bakhti, P. Sansonetti, "Design and realisation of multiple quarter wave phase shifts UV written bandpass filters in optical fibres", *J. Lightwave Technol.,* 15(8), pp. 1433-1436, 1997.

[47] L. Wei, J.W.Y. Lit, "Phase shifted Bragg grating filters with symmetrical structures", *J. Lightwave Technol.,* 15(8), pp. 1405-1409, 1997.

[48] R.J. Campbell, R. Kashyap, "Spectral profile and multiplexing of Bragg gratings in photosensitive fibre", *Optics Lett.*, 16(12), pp. 898-900, 1991.

[49] T. Erdogan, V. Mizrahi, "Characterization of UV-induced birefringence in photosensitive Ge-doped silica optical fibres", *J. Opt. Soc. Am. B*, 11(10), pp. 2100-2105, 1994.

[50] L. Dong, W.H. Loh, J.E. Caplen, J.D. Minelly, "Efficient single frequency fibre laser with novel photosensitive Er/Yb optical fibres", *Optics Lett.*, 22(10), pp.694-696, 1997.

[51] P. Niay, P. Bernage, T. Taunay, M. Douay, E. Delevaque, S. Boj, B. Poumellec, "Polarization selectivity of gratings written in Hi-Bi fibres by the external method", *IEEE Photon. Technol. Lett.*, 7(4), pp. 391-393, 1995.

[52] I. Abe, R.E. de Góes, J.L. Fabris, H.J. Kalinowski et al, "Production and characterization of refractive index gratings in high-birefringence fibre optics", *Optics and Lasers in Engineering*, 39(5-6), pp. 537-548, 2002.
[53] D. Pureur, M. Douay, P. Bernage, P. Niay, J.F. Bayon, "Single polarization fibre lasers using Bragg gratings in Hi-Bi fibres", *J. Lightwave Technol.*, 13(3), pp. 350-355, 1995.
[54] S. Lee, R. Khoaravani, J. Peng, V. Grubsky, D.S. Starodubov, A.E. Willner, J. Feinberg, "Adjustable compensation of polarization mode dispersion using a high-birefringence nonlinearly chirped fibre Bragg grating", *IEEE Photon. Technol. Lett.*, 11(10), pp. 1277-1279, 1999.
[55] W.H. Loh, J.P. de Sandro, G.J. Cowle, B.N. Samson, A.D. Ellis, "40GHz optical millimetre wave generation with a dual polarization distributed feedback fibre laser", *Electron. Lett.*, 33(7), pp. 594-595, 1997.
[56] A. Talneau, J. Charil, A. Ougazzaden, "Superimposed Bragg gratings on semiconductor material", *Electron. Lett.*, 32(20), pp. 1884-1885, 1996.
[57] G. Sarlet, G. Morthier, R. Baets, D.J. Robbins, D.C.J. Reid, "Optimisation of multiple exposure gratings for widely tunable lasers", *IEEE Photon. Technol. Lett.*, 11(1), pp. 21-23, 1999.
[58] V. Minier, A. Kévorkian, J.M. Xu, "Superimposed phase gratings in planar optical waveguides for wavelength demultiplexing applications", *IEEE Photon. Technol. Lett.*, 5(3), pp. 330-333, 1993.
[59] A. Talneau, C. Ougier, S. Slempkes, "Multiwavelength grating reflectors for widely tunable laser", *IEEE Photon. Technol. Lett.*, 8(4), pp. 497-499, 1996.
[60] X. Fu, M. Fay, J.M. Xu, "1x8 supergrating wavelength-division demultiplexer in a silica planar waveguide", *Optics Lett.*, 22(21), pp. 1627-1629, 1997.
[61] A. Othonos, X. Lee, R.M. Measures, "Superimposed multiple Bragg gratings", *Electron. Lett.*, 30(23), pp. 1972-1974, 1994.
[62] A. Arigiris, M. Konstantaki, A. Ikiades, D. Chronis, P. Florias, K. Kallimani, G. Pagiatakis, "Fabrication of high reflectivity superimpose multiple-fibre Bragg gratings with unequal wavelength spacing", *Optics Lett.*, 27(15), pp. 1306-1308, 2002.
[63] J. Lapierre, J. Bures, G. Checalier, "Fibre optic integrated interference filters", *Optics Lett.*, 7(1), pp. 37-39, 1982.
[64] J. Bao, X. Zhang, K. Chen, W. Zhou, "Spectra of dual overwritten fibre Bragg grating", *Optics Comm.*, 188, pp. 31-39, 2001.
[65] S. Doucet, R. Slavík, S. LaRochelle, "High finesse large band Fabry-Perot fibre filter with superimposed chirped Bragg gratings", *Electron. Lett.*, 38(9), 2002.
[66] R. Slavík, S. LaRochelle, "Large band periodic filters for DWDM using multiple superimposed fibre Bragg gratings", *IEEE Photon. Technol. Lett.*, 14(12), pp. 1704-1706, 2002.
[67] J. Azaña, P. Kockaert, R. Slavík, L. Chen, S. LaRochelle, "Generation of a 100GHz optical pulse train by pulse repetition rate multiplication using superimposed fibre Bragg gratings", *IEEE Photon. Technol. Lett.*, 15(3), pp. 413-415, 2003.
[68] L Zhang, K Sugden, I Bennion and A Molony, "Wide stopband chirped fibre Moiré grating transmission filters", *Electron. Lett.* 31(6), pp. 477-479, 1995.
[69] L A Everall, K Sugden, J A R Williams, I Bennion, X Liu, J S Aitchison, S Thoms and R M De La Rue, "Fabrication of multi-passband moiré resonators in fibres by dual phase mask exposure method", *Optics Lett.*, 22(19), pp. 1473-1475, 997.
[70] M.G. Xu, J.L. Archambault, L. Reekie, J.P. Dakin, "Discrimination between strain and temperature effects using dual-wavelength fibre grating sensors", *Electron. Lett.*, 30(13), pp. 1085-1087, 1994.
[71] R.J. Campbell, R. Kashyap, "Spectral profile and multiplexing of Bragg gratings in photosensitive fibre", *Optics Lett.*, 16(12), pp. 898-900, 1991.
[72] Q. Zhang, D.A. Brown, L. Reinhart, T.F. Morse, J.Q. Wang, G. Xiao, "Tuning Bragg wavelength by writing gratings on prestrained fibres", *IEEE Photon. Technol. Lett.*, 6(7), pp. 839-841, 1994.
[73] B.S. Kawasaki, K.O. Hill, D.C. Johnson, Y. Fuji, "Narrow band Bragg reflectors in optical fibres", *Optics Lett.*, 3(2), pp. 66-68, 1978.

Chapter 5: Optically tunable fibre grating filters

5.1 Overview

The evolution of transmission systems from point-to-point links to dynamically reconfigurable tunable networks produced a need for tunable devices. With the use of fibre grating technology in various fields, much effort has been put into controlling the fibre grating spectral profiles to enable adaptive operations. Several techniques for post-shaping the fibre grating responses have been demonstrated. In this chapter, a brief review of various reported fibre grating tuning mechanisms are outlined. Important issues for consideration in the realisation of an adaptive fibre grating structure are discussed. A novel fibre grating tuning mechanism utilizing the optical pump-induced thermal effects is presented. In particular, optically tunable phase-shifted fibre grating structures are illustrated based on the proposed technique. Experimental results on remotely, optically tunable single passband as well as multipassband fibre grating transmission filters are presented.

5.2 Fibre grating tuning mechanisms

In general, the spectral characteristics of fibre gratings can be tuned by exploiting the dependency of the refractive index to external perturbations like strain, temperature and transverse pressure. Initial interest in tunable fibre grating was to overcome its limitation of operating only at a fixed wavelength. Some important aspects of the tuning mechanisms include good repeatability, negligible hysterisis, high tuning efficiency and ease of implementation. Both mechanical and electrically controlled tuning mechanisms were demonstrated [1][2]. A number of techniques achieved tuning by varying the grating periodicity, most commonly by imposing a strain on the fibre. As illustrated in [2], a simple straining mechanism was created by embedding the fibre grating within a magnetostrictive substrate. With sufficient magnetic field applied to the substrate, the magnetostrictive material was stretched which consequently strained the fibre grating at the same time. Other ways to impose strain on fibres involved mechanical bending of the platform the fibre grating resided [3]. Tuning mechanisms based on bending structures allow more complex grating shaping to be achieved. As illustrated in [3], by attaching a uniform fibre grating onto a designed tapered cantilever bed, tunable chirping was achieved. This is particularly useful as a means to create an adjustable dispersion compensator highly desired in optical communication applications. On a similar basis, by varying the strain applied to the grating through flexing the cantilever appropriately, an adjustable multi-channel fibre bandpass filter based on a uniform fibre Bragg grating was realised [4]. Care should always be taken in these straining/bending techniques to reduce the amount of transverse strain coupled into the fibre. Such transverse strain coupling, particularly if nonsymmetrical around the fibre axis, can result in undesirable stress-induced birefringence during operation [3].

Towards a more compact structure, tunable fibre grating filters using cascaded piezoelectric transducers were demonstrated [5][6][7]. Miniature piezoelectric transducer (PZT) has the advantage of allowing greater spatial resolution (order of 1.4mm), thereby allowing greater control and variation on the

strain distribution to be imposed onto the fibre grating. More complex spectral shaping of the fibre grating, for example in [5], was achieved. The voltage required to drive PZT is generally high (tens of volts to > 100V) and the fibre grating needs to be attached carefully to the PZT segments. Flexibility of the bonding agent between the fibre and the PZT segments can lead to undesirable mechanical coupling. Furthermore, the rigidity of the bonding agent between the fibre and the tuning element/substrate can degrade with prolonged operating time.

To shape a fibre grating structure mechanically without the need to attach the grating structure permanently onto an external substrate, a transverse pressure technique has been adopted [8][9]. The effect of lateral force on the fibre changes the refractive index significantly and if the pressed region contains a fibre Bragg grating, it brings about a localized phase shift. Spectral profiling of a FBG through a pressure element has the advantage of not imposing permanent effects on the fibre (except when the fibre is physically damaged). As illustrated in [8], using a cylindrical pressure element, spatial resolution estimated to a few hundred micrometres was achieved and used to induce phase shifts in a uniform FBG. It is important to note that transverse pressure on an optical fibre generally leads to anisotropic index variations, thereby polarization dependent performance characteristics. The effects of lateral force on the fibre birefringence have been reported in studies related to sensing applications e.g. [10][11].

Apart from mechanically-induced spectral shaping of FBGs, the dependency of the refractive index on temperature offers an attractive means to alter the spectral profile of a fibre Bragg grating [12][13][14]. For a uniform fibre Bragg grating with uniform temperature distribution, the wavelength shift, $\Delta\lambda$, induced by temperature change of ΔT can be expressed by [12][15][16]

$$\frac{\Delta\lambda}{\lambda} = (\alpha + \xi)\Delta T \tag{5.1}$$

where α is the thermal expansion coefficient of silica (~$0.55\text{x}10^{-6}$ K^{-1}), ξ is the thermo-optic coefficient (~$1\text{x}10^{-5}$ K^{-1}) . Since the thermo-optic effect gives rise to an effect that is more than an order of magnitude larger than that due to thermal expansion, the origin of Bragg wavelength shift with temperature variation is largely attributed to thermal-induced index variation. To date, tunable fibre grating devices based on thermal effects adopt small-size thin film resistors placed at close proximity to the fibre grating structures [12]. For cases that adopt multiple thermal heads, thermal isolation between each heating element was necessary to minimize axial heat diffusion such that each element acted independently and performed independent variation to the local index [12]. Alternatively, resistive fibre coating to directly heat an intracore FBG can be adopted [13]. By applying uniform coatings of titanium and gold through processes such as magnetronsputter deposition e.g. [13], on-fibre thin film heaters that exhibited linear dependency with electrical power were achieved. By varying the thickness of the resistive coating, complex film profiles have been achieved to create phase-shifted gratings and superstructure gratings from uniform fibre Bragg gratings [14]. Compared to piezoelectric transducers, thermally-induced tuning mechanisms require lower driving voltage (below 10V). More importantly, such tuning mechanisms do not exhibit hysterisis in the induced index change and by ensuring uniform heating, they do not induce undesired birefringence effects during operation. Since the tuning mechanism does not involve physical contact, so avoiding wear, strain

/compression, with external material, thermal tuning has the additional advantage of avoiding physical degradation to the fibre grating over many operating cycles.

Thermally-induced transient resonance in a fibre Bragg grating was first demonstrated in [17] where a thin NiCr heating wire was used to form a tightly fitting loop (diameter ~250μm) around a uniform fibre Bragg grating. Controlled current passing through the wire thermally-induced a localized index change and effectively enabled a tunable single phase-shifted fibre grating structure. It was important to ensure the heating wire was tightly wrapped around the fibre grating because radially asymmetric heating can induce birefringence. A tunable transmission resonance/peak within the stop band of a fibre Bragg grating is potentially useful as an adjustable high finesse transmission filter in adaptive fibre sensors applications and reconfigurable optical communication networks [18]. However, as with all of the above-mentioned mechanical and thermal tuning schemes, the use of heating wire similarly belongs to the class of tuning schemes that rely on external perturbation mechanisms. The implementations of such schemes for remote/distant operation can be complex and costly. Together with the necessary electrical operation setup (like power supplies and wire leads) and/or mechanical structure, the resultant fibre grating device can become bulky, compromising the intrinsic small size nature of fibre-based devices. Furthermore, as mentioned above, care must always be taken to prevent induced index anisotropies that lead to undesirable birefringence effects during operation.

By exploiting the resonantly-enhanced nonlinearities in sections (few cm to ~2m) of highly doped Erbium or Ytterbium fibres, an interesting approach to realise a compact fibre grating tuning scheme has been demonstrated [19]-[22]. Compared to optical switches that rely on the weak Kerr nonlinearity in silica fibre [23], the resonant nonlinearity in rare-earth doped fibre requires significantly lower power-length product, using a few tens of mW·m or less [24][25]. The induced phase shifts associated with the index changes are attributed to the modifications of the electronic distributions of the rare-earth ions in the presence of an optical pump. As an example, consider a rare-earth doped fibre exhibiting an isolated absorption transition centred at λ_0. When an optical beam (optical pump) with a wavelength λ_p near λ_0 is launched into the fibre, the absorption of the pump photons excites electrons to a higher energy level (excited state). The changes in the electron distributions of the ground and excited states lead to a change in the refractive index for any signal with wavelength in the vicinity of λ_0. Over sufficiently long fibre and optical power, sizeable phase shift associated with index variation can be achieved [26]. Rare-earth doped fibres possess many absorption transitions in the visible and infrared spectrum. In commonly available rare-earth doped fibres with Er^{3+} and Yb^{3+}, nonlinear phase change with optical pump occurs favourably at the preferred telecommunication windows around 1300nm and 1550nm [21][27]. Over a length of the order of a metre and with a pump power of a few mW, the amount of phase shift produced exceeded π [24]-[25]. A tunable fibre grating transmission filter based on such nonlinear effect has the obvious advantage that the actual tuning mechanism lies within the fibre itself as clearly illustrated in [19].

It is important to note that if the signal wavelength is close to an absorption resonance, in the absence of the pump, the signal suffers a finite loss due to absorption from the ground state. In the presence of the pump, the ground state population decreases and the signal loss decreases. As a result, even though operating the signal wavelength close to the absorption resonance wavelength enables large phase change versus pump power ratio, it causes higher signal power variation with the input pump power. More

importantly, around an absorption or emission band, the refractive index is a strong function of wavelength. The Kramers-Kronig equations, which describe the relation between the spectral dependences of absorption and refractive index, indicate a refractive index variation at the signal wavelength between pump and unpumped states [27][28]. For a fixed absorbed pump power, the resonant-induced index variation, hence phase shift, shows a strong dependency on the signal wavelength. As highlighted in [27], the resonant-induced index change around 1536nm range showed a peak index variation of 0.3×10^{-6}. For a tunable narrowband transmission filter operating based on resonant nonlinearity of Er^{3+} doped fibre, undesirable spectral variations such as stopband broadening with the intensity of the pump beam was observed [19]. Even though operating at a wavelength far away from the pump reduces the absorption loss and the wavelength dependency of the induced phase shift, it compromises the efficiency of the system and consequently increases the required pump power for the desired induced phase change [26]. Such tunable fibre grating device schemes are therefore restricted by the fact the induced phase shift is a function of the pump and the signal wavelengths and undesirable spectral changes can occur when the pump or signal condition changes.

For rare-earth doped fibres, when the electronic relaxation of the dopants involves nonradiative processes under continuous optical pumping, a significant amount of heat is generated within the core of the fibre that leads to thermal-induced index change [29]. Depending on the dopants' spectroscopy, nonradiative relaxation can be dominant with much of the absorbed pump power being transformed into heat. Under such cases, thermal-induced phase shifts in doped fibres exceed resonantly enhanced nonlinearity significantly [29]. In particular, over short sections (on the order of a few cm) of rare-earth doped fibres, pump-induced index variation is predominantly thermal at an order of magnitude higher than that induced through electronic effects [30]. Pump-induced thermal effects in doped fibres due to nonradiative processes are generally considered detrimental in applications like fibre switches that are based on resonantly enhanced nonlinearity [29][31] and in fibre lasers and amplifiers [32][33][34].

In some commonly available fibres such as Er/Yb doped fibre and fibres doped with transition metal ions, a fraction of pump power is turned to heat due to nonradiative processes during the relaxation of the excited electrons. In fact, fibres doped with transition ions like cobalt and vanadium exhibit very strong thermal effects that mask any residual resonantly enhanced nonlinearity [35]. Since the interaction of the pump beam and the dopants is tightly confined within the core (cross section area $< 2 \times 10^{-4}$ mm^2) of the fibre, the steady state cross sectional temperature distribution profile is uniform [29][35] without undesired anisotropies, hence birefringence effects. More importantly, the thermal-induced index variation within the core is independent of the signal wavelength and therefore does not result in wavelength-dependent induced phase shift. With sufficiently high dopant concentration, the power-length product (on the order of a few mW·mm) to induce π radians phase shift is at least an order of magnitude lower than that based on resonant nonlinearity. Through combining such optically induced thermo-optic properties of doped fibres with passive FBG structures, practical and cost-effective means to design all-fibre, optically remote-controlled devices can be achieved.

In this part of the research work, a novel fibre grating transmission filter configuration based on pump-induced thermal effects is proposed and demonstrated. Tunable fibre grating devices utilizing pump-induced thermal effects possess the advantage that the tuning mechanism lies within the fibre itself. Without

the tedious task of performing resistive coating and the need to integrate electrical/mechanical setup, it enables a simple, miniature (since the required doped fibre is very short), remotely tunable fibre grating device configuration highly desirable in many applications.

5.3 Pump-induced thermal effect in Er/Yb doped fibre

Among commonly available rare-earth doped fibres, the Er/Yb doped fibre is particularly useful as a gain medium for realising single frequency fibre lasers. Its broad absorption band and more than 2 orders of magnitude of higher pump absorption than Er-doped fibre make them very attractive for constructing short fibre lasers. Typically, Er/Yb fibres can exhibit absorption ranging from 2 to 7dB/cm at 980nm resulting in tens of milliwatts pump power absorbed in the core over a very short fibre length.

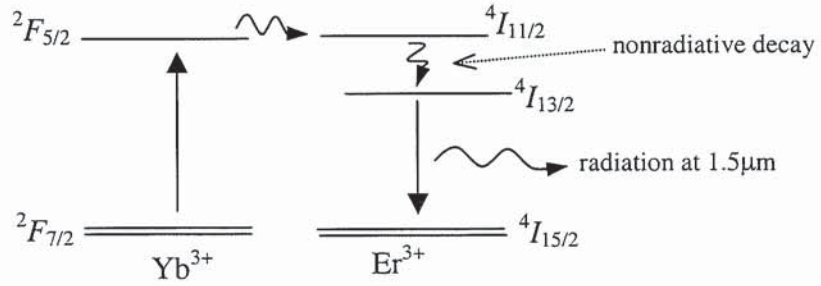

Figure 5.1 Relevant energy levels depicting the transfer of pump energy from Yb^{3+} system to the Er^{3+} system.

As shown in Figure 5.1, when an Er/Yb fibre is pumped, the Yb^{3+} ions are excited from the ground state to the $^3F_{5/2}$ manifold where nearly all the energy is transferred to the $^4I_{11/2}$ level of the Er^{3+} system [36]. The fast nonradiative decay to $^4I_{13/2}$ energy level then gives rise to a heating effect in the fibre. Considering the small volume of the core of a millimetre long fibre (~0.8×10^{-4} to 7×10^{-4} mm^3), the temperature rise is significant leading to a substantial thermal-induced index change, hence phase shift. Previous report on a 6mm long fibre Bragg grating written in a Er/Yb doped fibre (2dB/cm absorption at 980nm) highlighted a temperature rise of 38^0C within the core at 68mW pump power [33]. The thermal effect led to a wavelength shift of 0.32nm corresponding to a large index change of 2.9×10^{-4} (for a thermo-optic coefficient of $0.78\times10^{-5}/\ ^0$C).

5.4 Optically tunable single phase-shifted fibre grating transmission filter

To utilize the pump-induced thermal effect of Er/Yb doped fibre in a tunable fibre grating transmission filter, we first consider a fibre Bragg grating structure consisting of two uniform FBGs with a short section (~6mm) of fibre of uniform refractive index spliced in between. This is illustrated in Figure 5.2.

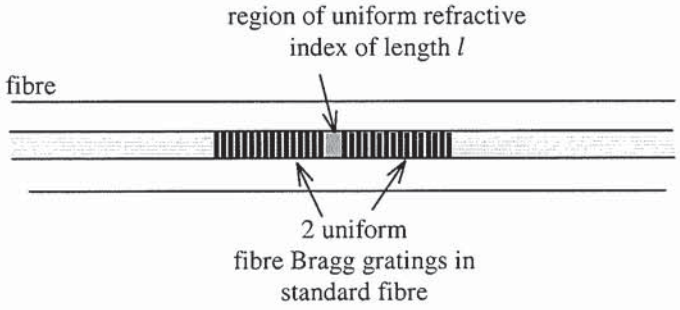

Figure 5.2 Diagram illustrating a fibre grating structure consisting of 2 uniform fibre Bragg gratings with a short section of fibre of uniform refractive index.

To simulate the transmission response of the grating structure using transfer matrix technique, an equivalent transfer matrix that accounts for the propagation through a medium of uniform refractive index, n, and length l is introduced as follows

$$M_l = \begin{bmatrix} \exp(-j\beta l) & 0 \\ 0 & \exp(j\beta l) \end{bmatrix} \tag{5.2}$$

where $\beta = \frac{2n\pi}{\lambda}$ denotes the propagation constant. Furthermore, to account for the transition between two regions of different refractive index, an equivalent transfer matrix matching the boundary condition at the interface between the two regions can be expressed as [37]

$$M_B = \begin{bmatrix} \frac{n_{01}+n_{02}}{2n_{01}} & \frac{n_{01}-n_{02}}{2n_{01}} \\ \frac{n_{01}-n_{02}}{2n_{01}} & \frac{n_{01}+n_{02}}{2n_{01}} \end{bmatrix} \tag{5.3}$$

where n_{01} and n_{02} denote the average refractive indices of the two regions. The transfer matrix, $M_{G\text{-}struct}$, representing the entire grating structure depicted in Figure 5.2 is simply the product of all the equivalent matrices of the elements of the grating structure and can be expressed by

$$M_{G-struct} = M_f \cdot M_B \cdot M_l \cdot M_B \cdot M_f \tag{5.4}$$

where M_f denotes the fundamental transfer matrix for the uniform fibre Bragg grating. Such a grating structure essentially forms a wavelength-selective Fabry-Perot resonator consisting of two out-of-phase gratings separated by a short cavity fibre of uniform refractive index. For a cavity length of 6mm and uniform FBGs of length 16mm with strength parameter κL =2.04 on each side, the simulated transmission profile of the fibre grating structure is as shown in Figure 5.3.

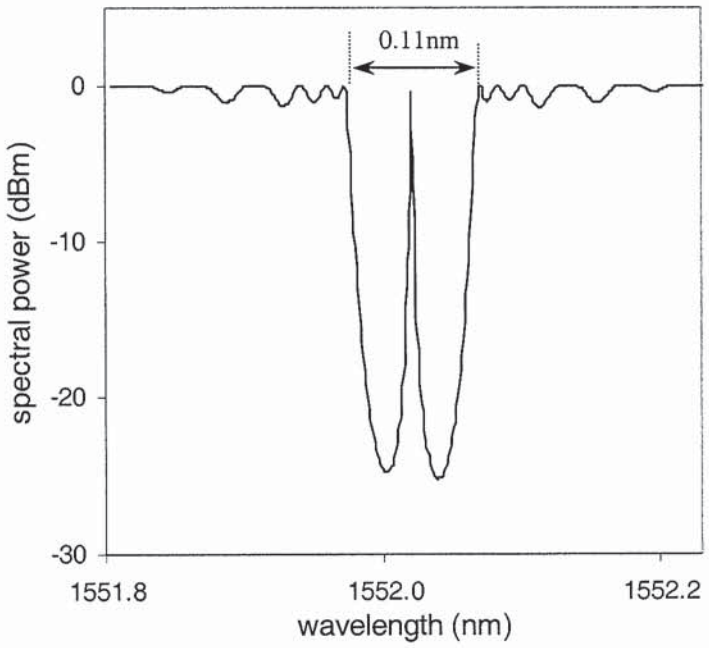

Figure 5.3 Simulated transmission profile of the fibre grating Fabry-Perot resonator structure. Cavity length was 6mm and uniform fibre Bragg gratings were of length 16mm each.

From Figure 5.3, the spectral response of the grating structure showed a dominant narrow transmission peak with a full width half maximum (FWHM) bandwidth <1pm within the grating stopband. The free spectral range of the grating response measured 0.056nm while the spectral stopband width measured 0.11nm. Due to the short cavity length, the resultant large FSR enabled a dominant resonance peak around the Bragg centre only. Such a spectral response resembled that of a single π phase-shifted grating structure described in section 4.4.1. The wavelength position of the transmission peak is a strong function of the refractive index of the cavity fibre. Variation of the cavity index changes the relative phase between the two uniform gratings causing a shift of the resonance mode structure. With increasing cavity refractive index, the transmission peak shifted towards longer wavelength. Such spectral variation with index increment is as shown in Figure 5.4.

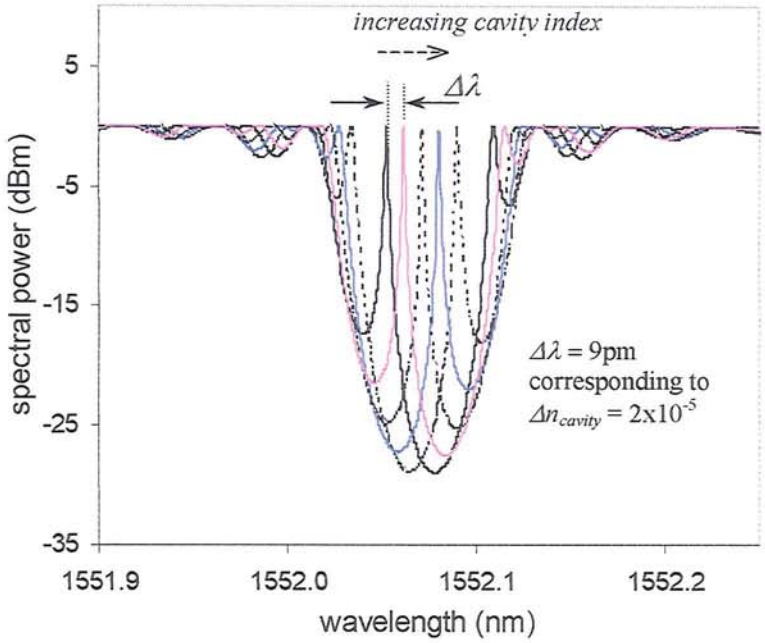

Figure 5.4 Superimposed transmission profiles of the simulated filter at different cavity refractive indices.

For every index increment of $2x10^{-5}$, the resonance peak shifted towards the longer wavelength side by 9pm. Over an index variation of $1.3x10^{-4}$, the resonance peak cycled across the spectral stopband corresponding to π phase shift. The dependency of the transmission peak wavelength on the cavity refractive index was exploited to realise a tunable narrowband fibre grating transmission filter. From the simulation results above, the required amount of index variation over 6mm section of fibre was on the order of $>1x10^{-4}$ to induce a π radians phase shift. Taking advantage of the large pump-induced thermal index variation in a short section of highly doped Er/Yb fibre, a novel optically tunable fibre grating transmission filter with the equivalent response of a single phase-shifted grating was hence realised.

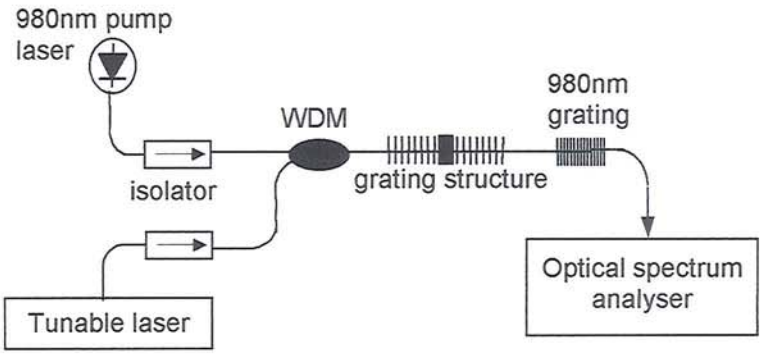

Figure 5.5 Experimental setup for the tunable single phase-shifted fibre grating structure.

In the experiment, a 6mm-long Er/Yb doped fibre (absorption at 979nm = 730dB/m and NA ~0.22) was spliced between two standard single-mode fibres (SMF) before hydrogenation. Uniform FBGs, each of

length 16mm and with strength parameter κL =2.07, were then written into the SMF on each side of the Er/Yb doped fibre to realise the equivalent single phase-shifted grating structure. The experimental setup for the operation and measurement of the grating structure is as shown in Figure 5.5. The 980nm FBG (90% reflectivity) in the setup was used to reflect the unabsorbed 980nm pump beam, thereby increasing the efficiency of the system. The transmission profile of the grating structure under different 980nm pump power was constantly monitored using a scanning tunable laser (calibrated to a wavemeter to 1pm resolution) synchronized to an optical spectrum analyser. The Er/Yb fibre region was sandwiched between polystyrene foam (heat conductivity = 0.36W/m·^{0}C) as a means to reduce the rate of heat loss from the doped fibre while the rest of the grating structure was thermally bonded to a Peltier element to help keep it at a constant temperature. Passive athermal coating/packaging, e.g. [38], otherwise can be adopted to further simplify the operation setup. The wavelength division multiplexer (WDM) was used to multiplex light at 980nm and 1550nm through the grating structure.

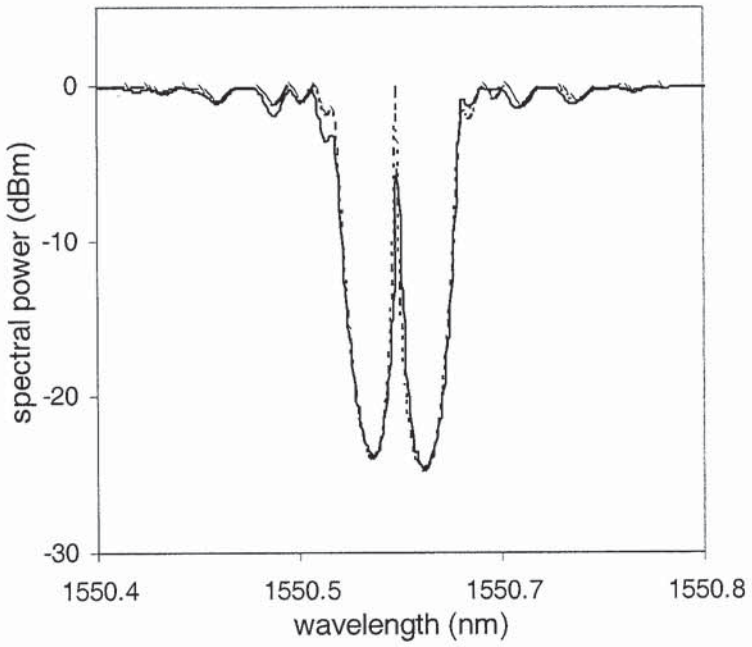

Figure 5.6 Measured (solid) and simulated (dotted) transmission profiles of the fibre grating transmission filter.

A measured transmission spectrum of the grating structure is as shown in Figure 5.6. The transmission peak had a FWHM bandwidth <3pm. Above the 980nm pump laser threshold, the transmission peak shifted towards higher wavelength proportionately with increasing pump power at a rate of ~7pm/mW as shown in Figure 5.7. Thermal effect in doped fibre induces phase shift via two means, namely, changing the index of refraction and by longitudinal expansion of the fibre. Since the thermo-optic effect is more than an order of magnitude larger than the effect of thermal expansion such that the second contribution amounts to less than 5% of the first one, in the remainder of the discussion, only the thermal index change is included. The overall thermal phase shift $\Delta\phi$ in the doped fibre of length l is hence defined by $\Delta\phi=(2\Delta n\pi l)/\lambda$ where λ denotes the wavelength, and Δn is the index change associated with temperature.

By matching the experimental data to the simulation results, the pump-induced index variation in the 6mm section of doped fibre was found to be 1.55×10^{-5}/mW. Over a pump power range between 1.5mW and 10mW, the transmission peak crossed the whole stopband of the grating, corresponding to $> \pi$ rad of phase change. The transmission extinction ratio measured using a narrowband probe signal was > 16dB with 1.5mW change in launched pump power. This isolation can be improved easily by increasing the strength of the uniform FBGs. Spectral profiles captured at 1.5mW pump power intervals indicated no wavelength-dependent phase variation. Furthermore, the induced phase shift exhibited a linear relationship with respect to the launched pump power as shown in Figure 5.8. To verify thermal phase shift as the key effect in the operation of the transmission filter, the grating structure was immersed in a water bath at 22^{0}C and there were no significant spectral changes with increasing pump power.

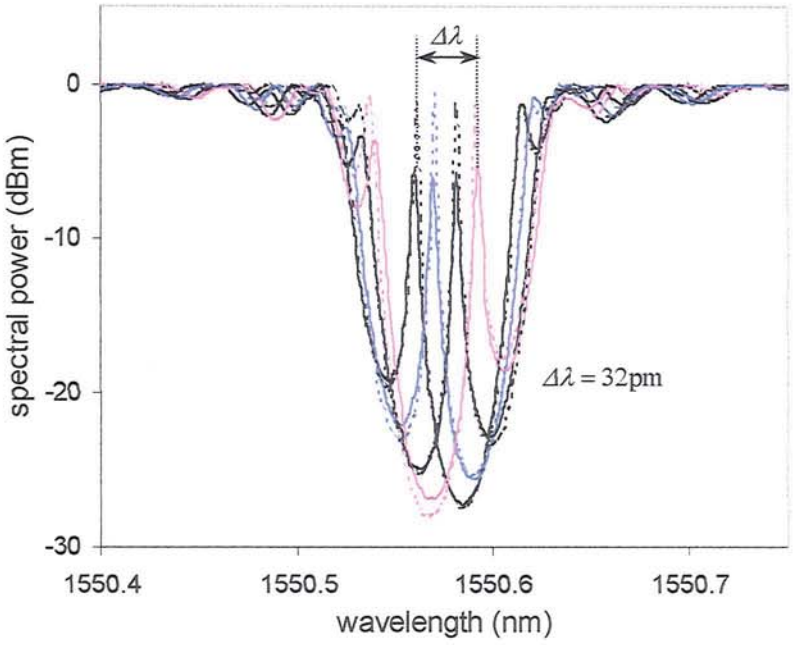

Figure 5.7 Superimposed transmission profiles of the tunable fibre grating structure measured at pump increment of 1.5mW. The dotted traces are the simulation results.

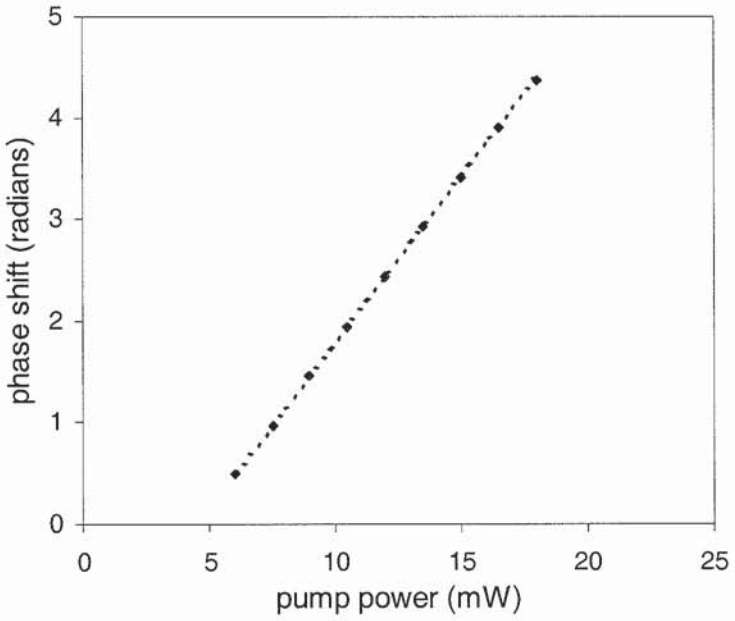

Figure 5.8 Diagram illustrating the linear variation of induced phase shift with launched pump power.

It is worth noting that the configuration exhibited no wavelength dependence or induced anisotropic effects during operation. Since the tuning mechanism does not introduce physical strain or wear on the fibre, the spectral characteristics were highly repeatable without hysterisis. With the control pump and signal wavelength propagating within the same fibre, the proposed configuration offers a simple and effective means to implement a miniature, remotely tunable fibre grating narrowband transmission filter.

To measure the temperature rise with pump power within the Er/Yb doped fibre, a 16mm-long uniform FBG was inscribed into the Er/Yb doped fibre and its Bragg wavelength shift with surrounding temperature was measured. Due to the low photosensitiviy of the Er/Yb doped fibre (even with hydrogenation) [39][40], the strength parameter achieved for the 16mm long uniform fibre Bragg grating was only κL=0.33 (i.e. index modulation of $1x10^{-5}$). Over a temperature range from 14^0C to 62^0C, the transmission profiles of the grating were captured at intervals of 6^0C with 1pm accuracy. Due to the low grating strength (peak transmission loss of only 0.5dB), the system noise (as a result of tunable laser output fluctuation as well as residual backreflections from the fibre connections) was evident. To improve the measurement results, each transmission profile was closely fitted to simulation to help deduce the Bragg wavelength. The superimposed measured (solid traces) and simulation (dotted traces) transmission profiles at different temperatures are as shown in Figure 5.9.

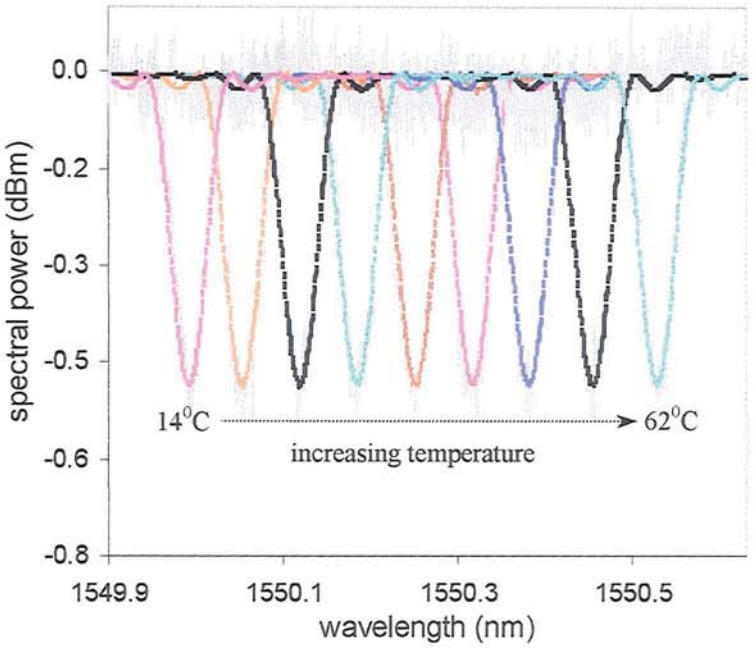

Figure 5.9 Measured (grey traces) and simulated transmission profiles of the 16mm uniform fibre grating in Er/Yb doped fibre at different temperatures.

From the results depicted in Figure 5.9, the Bragg wavelength shift with temperature was obtained and plotted out as shown in Figure 5.10. The obtained results indicated a gradient of 0.011nm/^{0}C which corresponded to a thermo-optic coefficient of 1.024×10^{-5}/^{0}C. Since the pump-induced index variation in the 6mm long doped fibre measured 1.55×10^{-5}/mW, it can be deduced that the pump-induced temperature rise within the doped fibre was 1.51^{0}C/mW, which is of the same order of magnitude but higher than the previous report [33] of 0.6^{0}C/mW due to the additional thermal insulation.

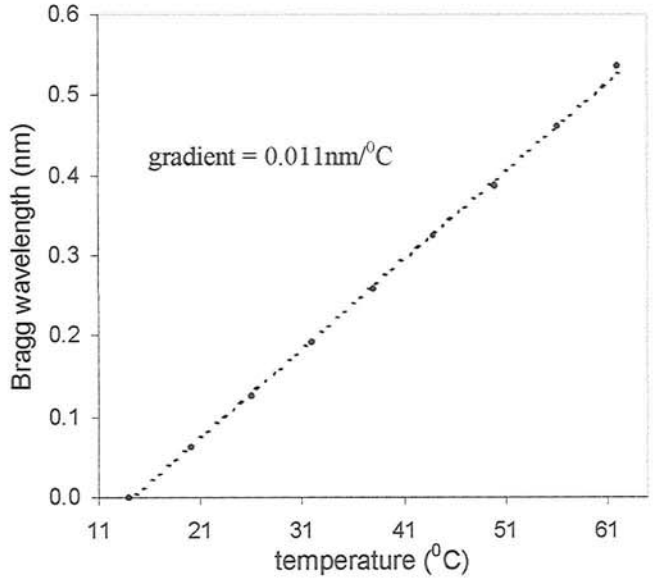

Figure 5.10 Bragg wavelength shift (relative to Bragg wavelength at 14^{0}C) versus temperature variation for the 16mm long uniform fibre Bragg grating in Er/Yb doped fibre.

5.5 Optically tunable dual phase-shifted fibre grating transmission filter

As highlighted in section 4.4.1, the insertion of a greater number of phase shifts within the uniform fibre grating structure enables a wider transmission passband with a more rectangular bandpass characteristic. From the previous section, it is clear that the introduction of a very short section of doped fibre in between two uniform fibre grating sections enables an equivalent single phase-shifted grating transmission response. In a similar fashion, the insertion of two very short sections of doped fibres within the uniform fibre Bragg grating structure enables an equivalent dual phase-shifted fibre grating structure. The proposed device configuration is as shown in Figure 5.11.

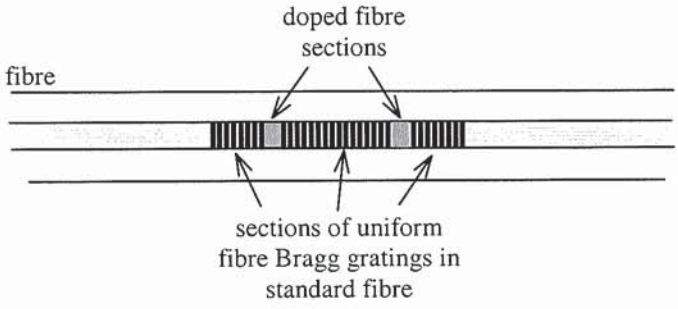

Figure 5.11 Fibre grating configuration incorporating two sections of doped fibres.

The equivalent dual phase-shifted fibre grating structure essentially consists of two identical doped fibre sections in between three sections of uniform FBGs. The two grating sections at each end of the structure are of equal length l_1 and the length of the centre grating, l_2 has a ratio $l_1 : l_2$ of 2 for optimum transmission bandpass response [41]. The transfer matrix representing the entire grating structure depicted in Figure 5.11 is similarly the product of all the equivalent matrices of the elements in the grating structure and can be expressed by

$$M_{G-struct} = M_{f1} \cdot M_B \cdot M_l \cdot M_B \cdot M_{f2} \cdot M_B \cdot M_l \cdot M_B \cdot M_{f1} \tag{5.5}$$

where matrices M_{f1} and M_{f2} denote the equivalent matrices for the uniform fibre Bragg gratings at the centre and at the ends of the structure respectively. A calculated transmission profile of the above grating structure is as shown in Figure 5.12. In the simulation, the length of each doped fibre section was 4.45mm and the length of the grating sections l_1 and l_2 were 7.5mm and 15mm respectively. The index modulations in all the grating section were 8×10^{-5}. The measured transmission peak had a FWHM bandwidth of 6pm.

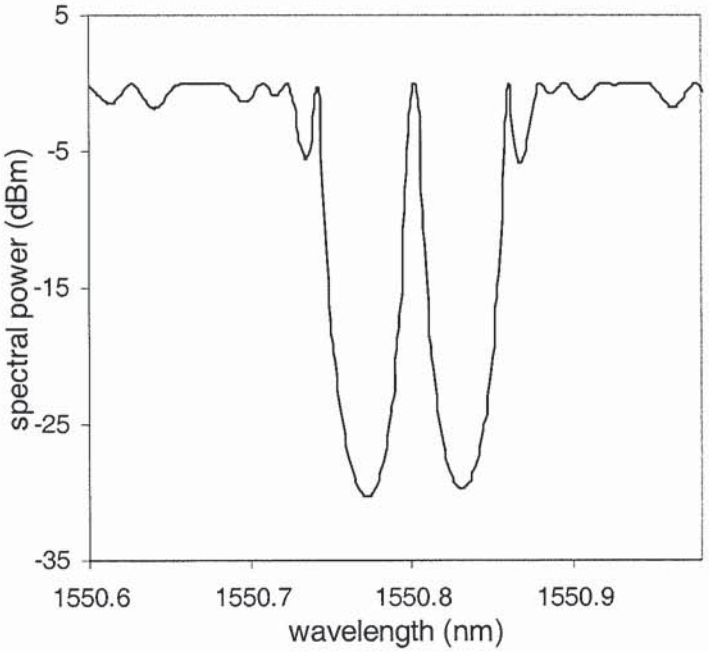

Figure 5.12 Simulated transmission profile of the equivalent dual phase-shifted fibre grating structure.

By increasing the refractive indices in both doped fibre sections, the transmission band shifted correspondingly towards longer wavelengths. For an index increment of $3x10^{-5}$ in each doped fibre section, the transmission peak shifted 14pm. Over an index variation of $1.8x10^{-4}$in each doped fibre section, the resonance peak cycled across the spectral stopband corresponding to π radians phase shift. The change in the wavelength position of the transmission band with variation in the refractive index of the dope fibre sections is as shown in Figure 5.13.

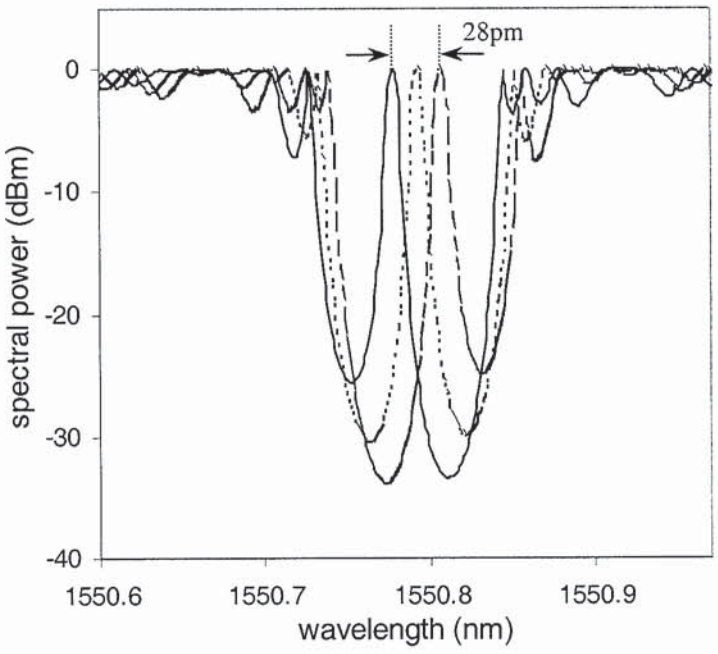

Figure 5.13 Transmission profiles of the grating structure as the refractive indices in the doped fibre sections varied.

The dependency of the transmission peak wavelength on the cavity refractive index similarly was exploited to enable a tunable fibre grating transmission filter. On the other hand, there were some important considerations in the actual implementation of the fibre grating device. As highlighted in section 4.4.1, the spectral variation of the dual phase-shifted grating structure is sensitive to the differential phase variation (i.e. index change) between the two doped fibre sections. Undesired spectral distortion occurs when the amount of index increment in the doped fibre sections differs and its impact is illustrated in Figure 5.14.

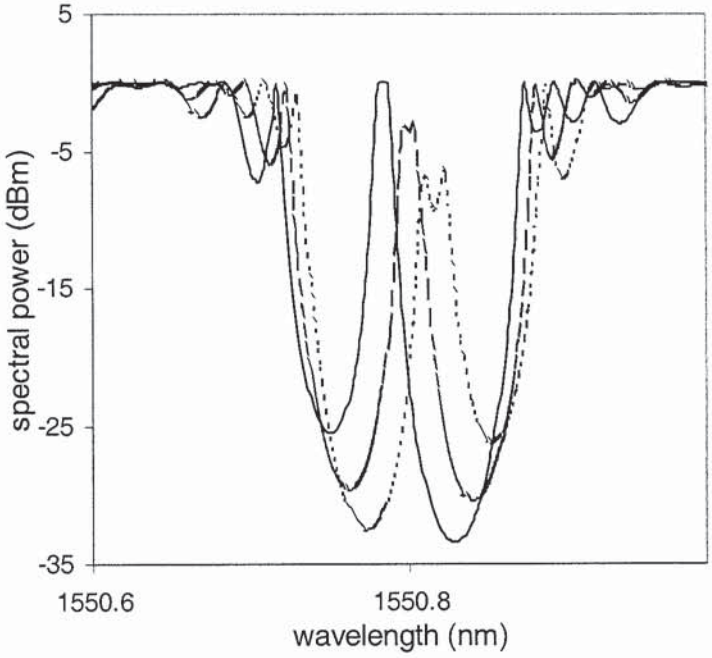

Figure 5.14 Simulated spectral distortions due to differential index increments between the two doped fibre sections in the tuning process of the grating structure.

In the simulation, the differential index increment between the 2 doped fibre sections for each tuning step was $1x10^{-5}$ and the escalating distortions of the transmission passband were evident. From a practical point of view, due to the large absorption of the Er/Yb doped fibre, the available amount of 980nm pump beam entering from one side of the grating structure can be significantly different between the two doped fibre sections. Differential pump-induced thermal effects will lead to different amount of induced phase shifts between the two sections. Consequently, the tuning of the transmission passband will be accompanied by significant distortions as shown in Figure 5.14.

Another important consideration in the practical implementation of the grating structure was the accuracy of the lengths achievable during the construction (splicing) of the device. Even though the uniform fibre grating parameters required can be fabricated with a high precision, it is unlikely, in practice, using conventional cleavers and fusion splicers that the sectional lengths of the spliced doped fibre sections have negligible length discrepancies. For a variation in fibre length Δl, the change in phase $\Delta\phi$ in a doped fibre section is defined by $\Delta\phi = (2n\pi\Delta l)/\lambda$. Simulation results indicated that for a small difference of 0.01mm between the two doped fibre sections of identical refractive indices, a drastic change in the spectral response occurred. The comparison between the spectral responses of the grating structure under this situation and that of the ideal case is as shown in Figure 5.15

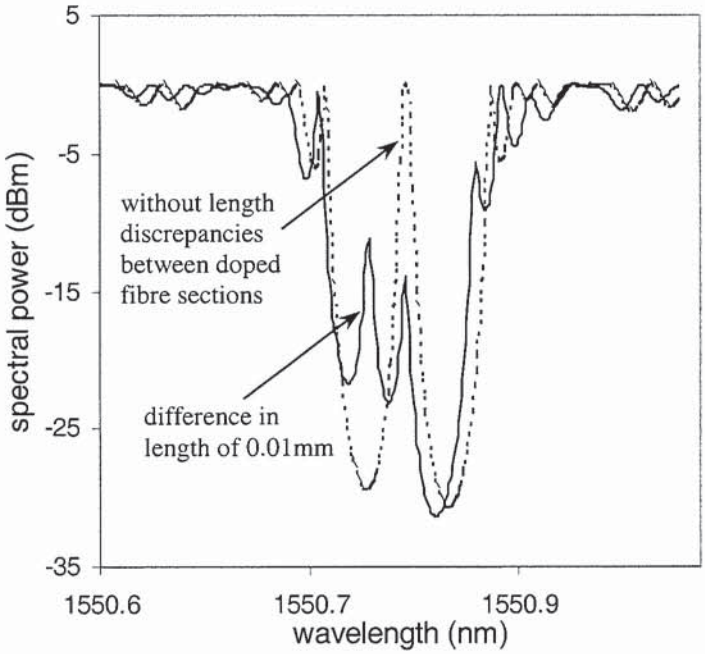

Figure 5.15 Simulated spectral profiles of the grating structure under the ideal situation (dotted) and the case (solid) where one of the doped fibre sections had a length discrepancy of 0.01mm.

Since the spectral distortion is attributed to the phase mismatch (as a result of length discrepancy) between the two doped fibre sections, it is obvious that post-fabrication phase compensation by UV trimming the doped fibre section/s can be adopted. For the example depicted in Figure 5.15, simulation results indicated that the required amount of UV induced index change over 4.5mm of the doped fibre was > $6x10^{-5}$. Due to the low photosensitivity of the Er/Yb doped fibre, the amount of UV induced index change is limited to < $2x10^{-5}$. To achieve the desired phase compensation, UV post-processing, hence phase trimming, over a very short section (~0.8mm) of standard fibre next to the doped fibre was alternatively adopted. Since the hydrogenated standard fibre is highly photosensitive, the required UV induced index increment (on the order of $3.1x10^{-4}$) can be achieved easily. By maintaining a short length post-processed region, negligible distortion to the grating structure will be incurred. The simulated spectral profile variation under such UV trimming process on the grating structure depicted in Figure 5.15 is as shown in Figure 5.16. The simulation considered a UV post-processing over 1mm section of the uniform fibre grating next to the doped fibre section. The required index change within the processed region to restore the ideal transmission response was $2.8x10^{-4}$.

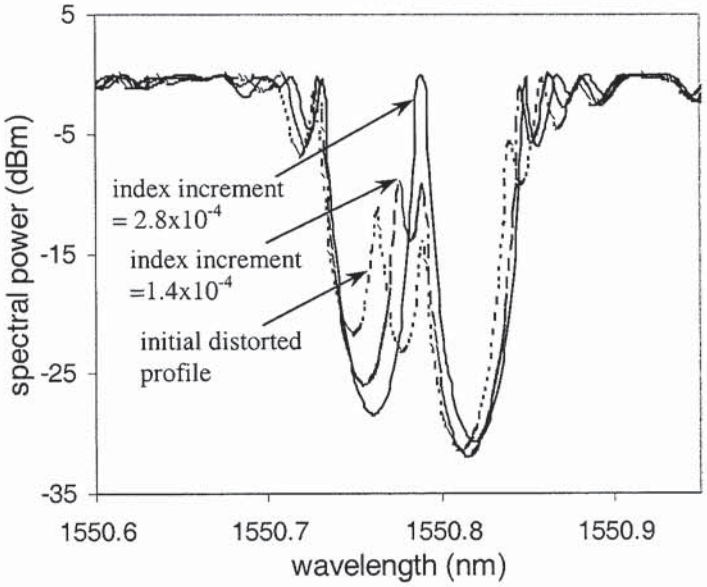

Figure 5.16 Spectral profile variations by UV post-processing over 1mm section of the fibre next to the doped fibre section. Compensation for phase mismatch between the two doped fibre sections was achieved.

To verify experimentally the feasibility of such UV trimming for phase compensation in the grating structure, a structure was produced consisting of two 4.5mm-long Er/Yb doped fibre sections spliced between three sections of standard single-mode fibres containing, respectively, gratings of lengths and strengths 7.5mm(κL ~1.31), 15mm(κL ~2.61) and 7.5mm(κL ~1.31).

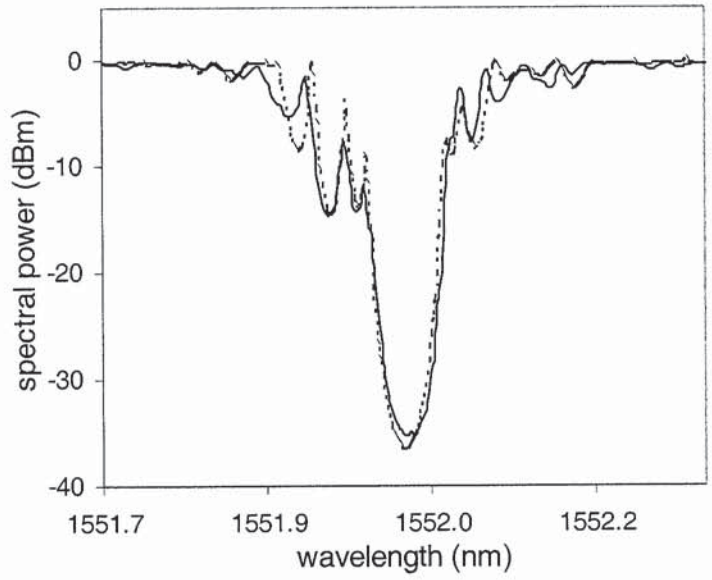

Figure 5.17 Measured (solid) and simulated (dotted) transmission profiles of the dual phase-shifted grating structure. Close fitting of the measured spectral response to the simulation result highlighted an effective difference in length of ~0.02mm between the doped fibre sections.

The resultant grating structure obtained exhibited phase mismatch between the doped fibre sections that led to significant spectral distortion as shown in Figure 5.17. By close fitting the simulation results to the measured data, the spectral distortion was attributed to an effective difference in length between the doped fibre sections of 0.02mm. By UV post-processing a short section of ~0.8mm (UV beam size) of the fibre next to one of the doped fibre sections, the ideal spectral response was restored expectedly as described above. Similarly, close fitting of the measured data to the simulation results suggested the index increment over the post-processed region was ~3.6×10^{-4}. The measured and simulated transmission profiles of the final grating structure is as shown in Figure 5.18.

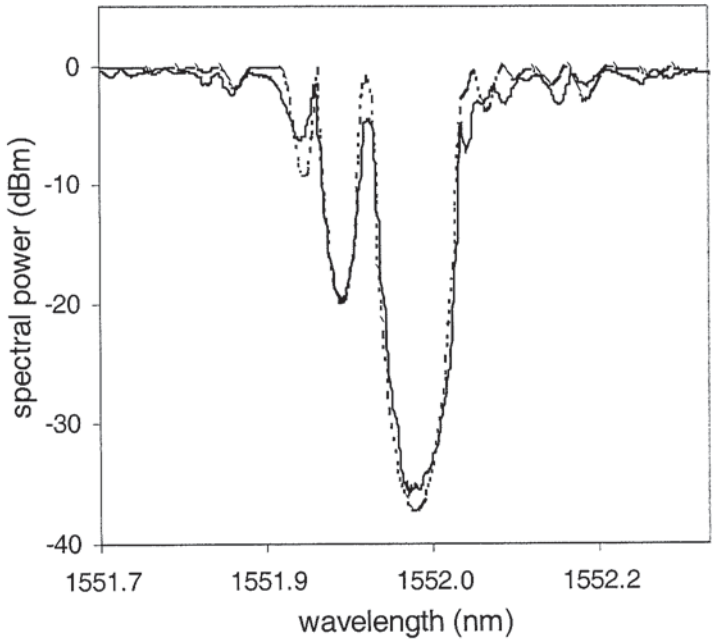

Figure 5.18 Measured (solid) and simulated (dotted) transmission profiles of the grating structure after UV post-processing.

Finally, to address the issue of spectral distortion due to differential pump-induced phase shifts between the doped fibre sections during operation, a bidirectional pumping scheme was proposed. To ensure the pump-induced phase shifts in both doped fibre sections are of equal magnitude, it is necessary to control the amount of pump beam entering individual doped fibre sections. As mentioned above, uni-directional pumping can lead to unequal amounts of 980nm beam absorptions between the doped fibre sections. The solution hence involved using an adjustable coupler to split the 980nm beam from the pump diode such that the grating structure was bidirectionally pumped from both ends. The pumping scheme ensured equalization of the pump-induced phase shifts in both doped fibre sections. The experimental setup for the operation of the dual phase-shifted grating structure is as shown in Figure 5.19.

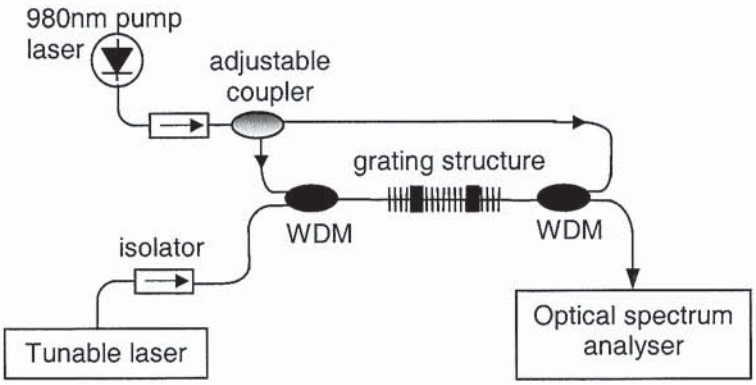

Figure 5.19 Experimental setup for the operation of the tunable dual phase-shifted fibre grating structure.

A measured transmission profile of the grating structure is shown in Figure 5.20. Evidently, the spectral response is equivalent to that of a dual phase-shifted fibre grating structure shown in Figure 4.16. Compared to the spectral profile of the single phase-shifted grating structure in Figure 5.6, the increase in the passband width was evident. The widened transmission peak had a FWHM bandwidth measured 8pm.

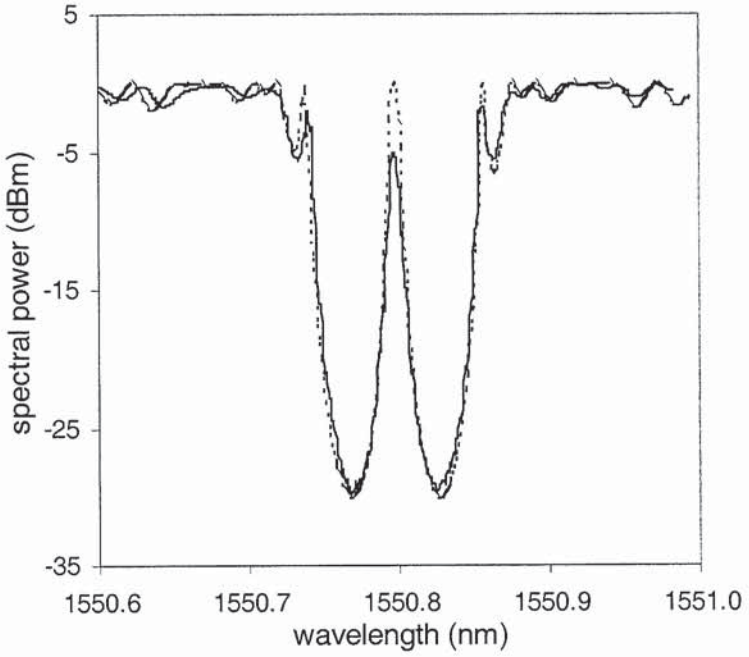

Figure 5.20 Measured (solid) and simulated (dotted) transmission profiles of the dual phase-shifted grating structure.

During operation, with increasing pump power, the transmission passband shifted towards the longer wavelength. The rate of wavelength shift with launched pump power measured 5pm/mW and corresponded to induced index variation of 0.85×10^{-5}/mW over each 4.5mm section of Er/Yb doped fibre. The transmission profiles at different pump powers are shown in Figure 5.21.

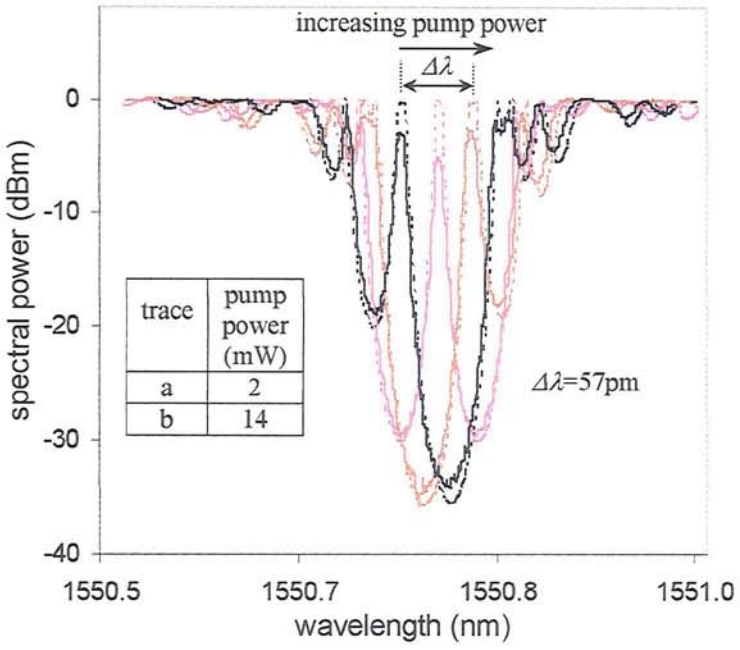

Figure 5.21 Transmission profiles of the grating structure at different pump powers.

Compared to the case of the single phase-shifted grating structure, the efficiency of the system was lower largely due to the greater number of sections of doped fibres as well as the absence of re-circulation of unabsorbed 980nm pump beam. Nevertheless, over a pump increment of 23mW, the bandpass peak crossed the stopband of the grating, achieving > π phase shift.

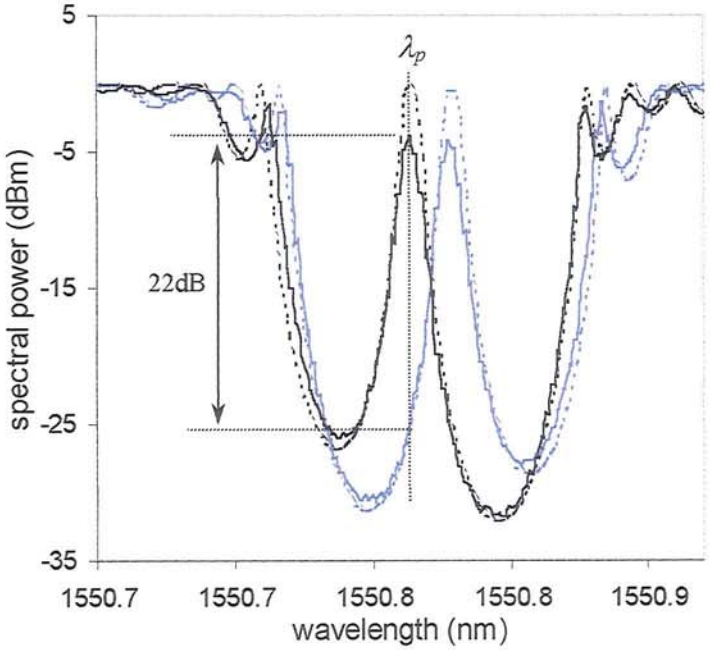

Figure 5.22 Measured (solid) and simulated (dotted) transmission profiles of the grating structure over a 3mW change in pump power.

Considering a passband operation at λ_p as shown in Figure 5.22, the transmission extinction ratio measured using a narrowband probe beam was > 21dB with 3mW change in pump power. Similarly, this transmission isolation can be improved easily by increasing the strength of the uniform gratings. It is important to note that the efficiency of the configuration can be improved further by using, for example, cobalt doped fibres under 720nm pump and vanadium doped fibres under 906nm pump [35] that exhibit light to heat conversion rate of > 55%. Furthermore due to the broad pump absorption bandwidth (>20nm) of these doped fibres, a number of the transmission filters, in tandem with respective FBG pump filters, can be individually addressed at different pump wavelengths. An adaptive/reconfigurable network of the transmission filters can hence be achieved.

5.6 Optically tunable multichannel passband filter

Multichannel passband filters have been an indispensable component in optical communication, in particular in WDM systems. Among various proposed filter architectures, the Fabry-Perot (FP) filter remains one of the most commonly adopted component configurations to process multiple wavelengths simultaneously [42][43]. Apart from their basic filtering operation, Fabry-Perot etalons are also employed in laser configurations as well as WDM systems channel monitoring schemes [44][45].

An all-fibre Fabry-Perot (FP) resonator can be constructed simply by fabricating two fibre gratings spaced apart by distance, d within an optical fibre. Depending on the spectral width of the fibre gratings and the effective cavity length, a finite number of narrowband transmission peaks arise within the stopband of the grating structure. The wavelength separation $\Delta\lambda_{FSR}$ (free spectral range, FSR) between these resonance peaks can be expressed by the well-known equation [46]

$$\Delta\lambda_{FSR} = \frac{\lambda^2}{2n_{cavity}l_{cavity}} \tag{5.6}$$

where n_{cavity} and l_{cavity} denote the effective cavity refractive index and length respectively. In a similar context, a fibre Fabry-Perot multichannel wavelength filter can be constructed by splicing a section (15mm) of Er/Yb doped fibre between two identical uniform FBGs. By doing so, the concept of the optically tunable fibre grating transmission filter can be extended to a multichannel passband filter scheme. The proposed filter device configuration is as shown in Figure 5.23.

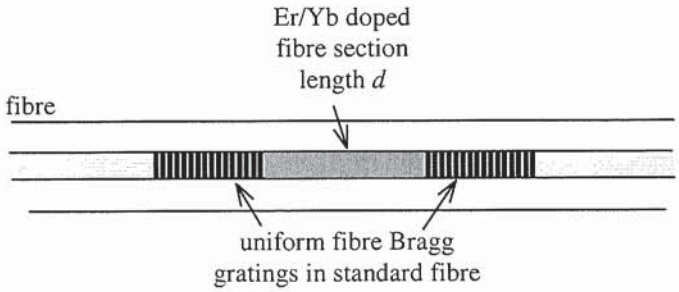

Figure 5.23 Proposed optically tunable multichannel fibre grating transmission filter.

In the extreme case where length d in Figure 5.23 is reduced to a very short section, the filter architecture reduces to that described in section 5.3. The short cavity length then leads to a large FSR such that the number of resonance peaks occurring within the narrow grating stopband is reduced to one as illustrated in Figure 5.3. However, in this case, for a length d=16mm and with uniform gratings of length 10mm each, the long cavity length leads to a FSR of 0.04nm such that multiple passbands reside within the spectral width of the grating as shown in Figure 5.24.

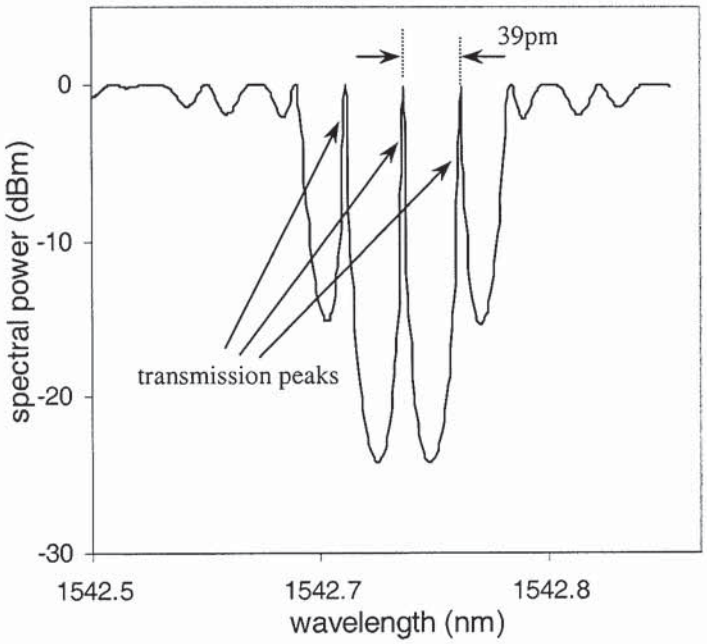

Figure 5.24 Simulated spectral response of the fibre grating multichannel transmission filter.

As the cavity index varies, the relative phase between the two uniform fibre gratings changes. Consequently, the resonance peaks within the grating stopband move towards longer wavelength as the index increases. It is also worth noting that the change in the FSR due to variation in the cavity refractive index is negligible, compared to the wavelength shift due to the induced phase shift. By differentiating (5.6) with respect to the cavity refractive index, the variation in the FSR, $\partial(\Delta\lambda_{FSR})$, can be expressed by

$$\frac{\partial(\Delta\lambda_{FSR})}{\partial n_{cavity}} = \frac{\partial}{\partial n_{cavity}}\left(\frac{\lambda^2}{2n_{cavity}l_{cavity}}\right) \tag{5.7}$$

$$\partial(\Delta\lambda_{FSR}) = \left(\frac{-\lambda^2}{2n_{cavity}^2 l_{cavity}}\right)\partial n_{cavity} \tag{5.8}$$

Based on (5.8), for an index increment on the order of 10^{-4}, the variation in the FSR is only of the order of 10^{-3}pm, which is much smaller than the resolution of the measurement setup (1pm). The induced phase shift $\Delta\phi$ due to index increment within the doped fibre of length d is given by

$$\Delta\phi = \frac{2\partial n_{cavity}\pi}{\lambda} d \tag{5.9}$$

and the wavelength shift $\partial\lambda_{shift}$ corresponding to the index change is given by

$$\partial\lambda_{shift} = \frac{\Delta\phi}{\pi}(\Delta\lambda_{FSR})$$

$$\Rightarrow \partial\lambda_{shift} = \frac{\partial n_{cavity}}{n_{cavity}} \cdot \frac{d}{l_{cavity}}\lambda \qquad (5.10)$$

From (5.10), for an induced index increment on the order of 10^{-5}, the wavelength shift is of the order of a few pm. Hence, the effect of FSR variation with induced index change in the doped fibre can be omitted throughout the discussion.

In the experiment, a 16mm long Er/Yb doped fibre was spliced between two standard SMF before hydrogenation. Uniform FBGs, each of length 10mm and with strength parameter κL =1.75, were then written into the SMF on each side of the doped fibre to realise the FP multipassband filter. The experimental setup was similar to that shown in Figure 5.5. Through a combination of insufficient cavity gain from the doped fibre section and the low reflectivity of the gratings (hence low resonance feedback), the resonator did not promote lasing operation. Instead, a multipassband wavelength-selective fibre grating FP filter was obtained.

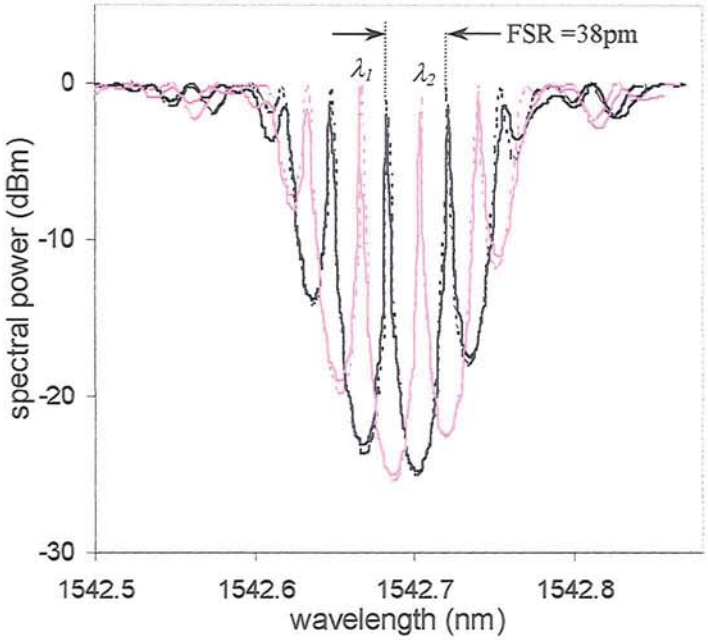

Figure 5.25 Measured (solid) and simulated (dotted) transmission profile variations over 2mW change in pump power.

Expectedly, as the pump power increased, the resonance peaks moved towards longer wavelength and continued to cycle within the grating stopband. Over a change in pump power of 3mW, the transmission passbands shifted by 19pm (half a free spectral range) that corresponded to induced index variation of $2.4\text{x}10^{-5}$. The measured and simulated transmission spectra are as shown in Figure 5.25. Considering operation channels at λ_1 and λ_2, the transmission extinction ratio measured >23dB with a 3mW change in pump power.

5.7 Conclusions

A brief review of some of the operating principles behind tunable fibre grating structures has been given. In particular, key limitations in tuning mechanisms based on external perturbation techniques have been highlighted. Towards a simple, compact and effective tuning mechanism for fibre grating structures, the optical pump-induced thermal effect in rare-earth doped fibres has been utilized. Based on the large optically-induced thermal index variations in very short sections of Er/Yb doped fibres, an optical pump controlled, remotely tunable fibre grating transmission filter configuration has been proposed and successfully demonstrated. Experimental results obtained from different device architectures, namely the single phase-shifted fibre grating, the dual phase-shifted fibre grating and the Fabry-Perot fibre grating multichannel filter, have illustrated high transmission extinction ratios and low power-distance products for the necessary induced phase changes. The proposed technique exhibits no wavelength dependence or induced anistropic effects during operation and is highly repeatable without hysterisis. Based on the results obtained, a simple and effective means to implement a miniature tunable fibre grating transmission filter has been illustrated.

5.8 References

[1] W.V. Sorin, P. Zorabedian, S.A. Newton, "Tunable single-mode fibre reflective grating filter", *J. Lightwave Technol.*, LT-5, (9), pp. 1199-1202, 1987.

[2] X.Z. Lin, Y. Zhang, H.L. An, H.D. Liu, "Electrically tunable single-mode fibre Bragg reflective grating", *Electron. Lett.*, 30(11), pp. 887-888, 1994.

[3] M.Le Blanc, S.Y. Huang, M.M. Ohn, R.M. Measures, "Tunable chirping of a fibre Bragg grating using a tapered cantilever bed", *Electron. Lett.*, 30(25), pp. 2163-2165, 1994.

[4] S. Li, K.T. Chan, J. Meng, W. Zhou, "Adjustable multi-channel fibre bandpass filters based on uniform fibre Bragg gratings", *Electron. Lett.*, 34(15), 1998.

[5] M.G. Xu, A.T. Alavie, R. Maaskant, M.M. Ohn, "Tunable fibre bandpass filter based on a linearly chirped fibre Bragg grating for wavelength demultiplexing", *Electron. Lett.*, 32(20), pp. 1918-1919, 1996.

[6] A.Iocco, H.G. Limberger, R.P. Salathé, L.A. Everall, K. Chisholm, J.A.R. Williams, I. Bennion, "Bragg grating fast tunable filter for wavelength division multiplexing", *J. Lightwave Technol.*, 17(7), pp. 1217-1221, 1999.

[7] T. Inui, T. Komukai, M. Nakazawa, "Highly efficient tunable fibre Bragg grating filters using multiplayer piezoelectric transducers", *Optics Comm.*, 190, 1-4, 2001.

[8] C.J.S. de Matos, P. Torres, L.C.G. Valente, W. Margulis, R. Stubbe, "Fibre Bragg grating (FBG) characterization and shaping by local pressure", *J. Lightwave Technol.*, 19(8), pp. 1206-1211, 2001.

[9] S. Savin, M.J.F. Digonnet, G.S. Kinko, H.J. Shaw, "Tunable mechanically induced long-period fibre gratings", *Optics Lett.*, 25, pp. 710-712, 2000.

[10] R.B. Wagreich, W.A. Atia, H. Singh, J.S. Sirkis, "Effects of diametric load on Bragg gratings fabricated in low birefringence fibre", *Electron. Lett.*, 32, pp. 1223-1224, 1996.

[11] M. LeBlanc, S.T. Vohra, T.E. Tsai, E.J. Friebele, "Transverse load sensing by use of pi-phase-shifted fibre Bragg grating", *Optics Lett.*, 24, pp. 1091-1093, 1999.

[12] S. Gupta, T. Mizunami, T. Shimomura, "Computer control of fibre Bragg grating spectral characteristics using a thermal head", *J. Lightwave Technol.*, 15(10), pp. 1925-1928, 1997.

[13] H.G. Limberger, N.H. Ky, D.M. Costantini, R.P. Salathé, C.A.P. Muller, G.R. Fox, "Efficient miniature fibre-optic tunable filter based on intracore Bragg grating and electrically resistive coating", *IEEE Photon. Technol. Lett.*, 10(3), pp. 361-363, 1998.

[14] A.K. Ahuja, P.E. Steinvurzel, B.J. Eggleton, J.A. Rogers, "Tunable single phase-shifted and superstructured gratings using micro fabricated on-fibre thin film heaters", *Optics Comm.*, 184, 119-125, 2000.

[15] S. Takahashi, S. Shibata, "Thermal variation of attenuation for optical fibres", *J. Non-crystalline solids*, 30, pp. 359-370, 1979.

[16] W.W. Morey, G. Meltz, W.H. Glenn, "Fibre optic Bragg grating sensors", *Proc. SPIE*, 1169, pp. 98-107, 1989.

[17] M. Janos, J. Canning, "Permanent and transient resonances thermally induced in optical fibre Bragg gratings", *Electron. Lett.*, 31(12), pp. 1007-1009, 1995.

[18] G.P. Agrawal and S. Radic, "Phase-shifted fibre Bragg gratings and their application for wavelength demultiplexing", *IEEE Photon. Technol. Lett.*, 6(8), pp. 995-997, (1994).

[19] M. Janos, J. Canning and M.G. Sceats, "Transient transmission notches induced in Er^{3+} doped optical fibre Bragg gratings", *Electron. Lett.*, 32(3), pp. 245-246, (1996).

[20] J.W. Arkwright, P. Elango, G.R. Atkins, T. Whitbread and M.J.F. Digonnet, "Experimental and theoretical analysis of the resonant nonlinearity in Ytterbium-doped fibre", *J. Lightwave Technol.*, 16(5), pp. 798-806, (1998).

[21] J.W. Arkwright, P. Elango, G.R. Atkins, T. Whitbread and M.J.F. Digonnet, "Nonlinear phase changes at 1310nm and 1545nm observed far from resonance in diode pumped Ytterbium doped fibre", *IEEE Photon. Technol. Lett.*, 8(3), pp. 408-410, 1996.

[22] J. Canning and M.G. Sceats, "Transient gratings in rare-earth doped phosphosilicate optical fibres through periodic population inversion", *Electron. Lett.*, 31(7), pp. 576-577, 1995.

[23] B.K. Nayer, N. Finlayson, N.J. Doran, S.T. Davey, D.L. Williams, J.W. Arkwright, "All-optical switching in a 200m twin-core fibre nonlinear Mach-Zehnder interferometer", *Optics Lett.*, 16(6), pp. 408-410, 1991.

[24] R.H. Pantell, R.W. Sadowski, M.J.F. Digonnet, H.J. Shaw, "Laser diode pumped nonlinear switch in erbium doped fibre", *Optics Lett.*, 17(14), pp. 1026-1028, 1992.

[25] P.L. Chu, B. Wu, "Optical switching in twin-core erbium doped fibres", *Optics Lett.*, 17(4), pp. 255-257, 1992.

[26] R.H. Pantell, M.J.F. Digonnet, R.W. Sadowski, H.J. Shaw, "Analysis of nonlinear optical switching in an Erbium doped fibre", *J. Lightwave Technol.*, 11(9), pp. 1416-1424, 1993.
[27] S.C. Fleming, T.J. Whitley, "Measurement of pump-induced refractive index change in Erbium doped fibre amplifier", *Electron. Lett.*, 27(21), pp. 1959-1961, 1991.
[28] E. Desurvire, "Study of complex atomic susceptibility of Erbium doped fibre amplifiers", *J. Lightwave Technol.*, 8(10), pp. 1517-1527, 1990.
[29] M.K. Davis, M.J.F. Digonnet, R.H. Pantell, "Thermal effects in doped fibres", *J. Lightwave Technol.*, 16(6), pp. 1013-1023, 1998.
[30] M. Janos, J. Arkwright, Z. Brodzeli, "Low power nonlinear response of Yb^{3+} doped optical fibre Bragg gratings", *Electron. Lett.*, 33(25), pp.2150-2151, 1997.
[31] M.J.F. Digonnet, R.W. Sadowski, H.J. Shaw, R.H. Pantell, "Resonantly enhanced nonlinearity in doped fibres for low power all-optical switching: A review", *Optical Fibre Technol.*, 3, pp. 44-64, 1997.
[32] D.C. Hanna, M.J. McCarthy, P.J. Suni, "Thermal considerations in longitudinal pumped fibre and miniature bulk lasers", *Proc. Fibre Laser sources and Amplifiers, Proc. SPIE*, 1171, pp. 160-166, Boston, MA, 1990.,
[33] Y.Z. Xu, H.Y. Tam, S.Y. Liu, M.S. Demokan, "Pump-induced thermal effects in Er-Yb fibre grating DBR lasers", *IEEE Photon. Technol. Lett.*, 10(9), pp. 1253-1255, 1998.
[34] D.C. Brown, H.J. Hoffman, "Thermal, stress and thermo-optic effects in high average power double-clad silica fibre lasers", *IEEE J. Quantum Electron.*, 37(2), pp. 207-217, 2001.
[35] M.K. Davis, M.J.F. Digonnet, "Measurements of thermal effects in fibres doped with cobalt and vanadium", *J. Lightwave Technol.*, 18(2), pp. 161-165, 2000.
[36] W.L. Barnes, S.B. Poole, J.E. Townsend, "Er^{3+}- Yb^{3+} and Er^{3+} doped fibre lasers", *J. Lightwave Technol.*, 7, pp. 1461-1465, 1989.
[37] M.A. Rodriguez, M.S. Malcuit, J.J. Butler, "Transmission properties of refractive index-shifted Bragg gratings", *Optics Comm.*, 177, pp.251-257, 2000.
[38] T. Iwashima, A. Inoue, M. Nishimura and Y. Hattori, "Temperature compensation technique for fibre Bragg gratings using liquid crystalline polymer tubes", *Electron. Lett.*, 33(5), pp. 417-419, (1997).
[39] L. Dong, W.H. Loh, J.E. Caplen, J.D. Minelly, "Efficient single frequency fibre laser with novel photosensitive Er/Yb optical fibres", *Optics Lett.*, 22(10), pp.694-696, 1997.
[40] J.T. Kringlebotn, J.L. Archambault, L. Reekie, J.E. Townsend, G.G. Vienne, D.N. Payne, "Highly efficient low noise grating feedback Er^{3+}:Yb^{3+} codoped fibre laser", *Electron. Lett.*, 30(12), pp.972-973, 1994.
[41] F. Bakhti, P. Sansonetti, "Wide bandwidth, low loss and highly rejective doubly phase-shifted UV written fibre bandpass filter", *Electron. Lett.*, 32(6), pp. 581-582, 1996.
[42] B. Ortega, J. Capmany, J.L. Cruz, "Wavelength division multiplexing all-fibre hybrid devices based on Fabry-Perot and gratings", *J. Lightwave Technol.*, 17(7), pp. 1241-1247, 1999.
[43] G.E. Town, K. Sugden, J.A.R. Williams, I. Bennion, S.E. Poole, "Wide band Fabry-Perot-like filters in optical fibre", *IEEE Photon. Technol. Lett.*, 7(1), pp. 78-80, 1995.
[44] J.C. Martín, M.P. Bernal, "Double ring and Fabry-Perot ring resonators: application for an optical fibre laser", *Applied Optics*, 33(21), pp. 4801-4806, 1994.
[45] M. Iodice, G. Cocorullo, F.G. Della Corte, I. Rendina, "Silicon Fabry-Perot filter for WDM systems channels monitoring", *Optics Comm.*, 183, pp. 415-418, 2000.
[46] J. Stone, D. Marcuse, "Ultrahigh finesse fibre Fabry-Perot interferometers", *J. Lightwave Technol.*, LT4(4), pp. 382-385, 1986.

Chapter 6: Fibre lasers

6.1 Overview

Utilizing fibres in optical communication systems presents the problem of obtaining a high efficiency coupling between the fibre and the optical source. One elegant solution to this issue is to incorporate the laser source as an integral part of the fibre using distributed feedback structures from periodic perturbations of index of refraction [1]. With the advancement in fibre grating technology and the development of high concentration rare-earth doped fibres [2], a class of active fibre devices highly compatible with single-mode fibre systems are hence realised. These solid-state lasers within the optical fibre, commonly known as fibre lasers, possess various output performance merits (e.g. narrow optical linewidth and low intensity noise) and inherit advantages like low loss and engineering simplicity inherent to the fibre grating structures [3]. As a result, fibre lasers are widely adopted in optical communication systems and are considered potential alternatives to their semiconductor counterparts. In this chapter, the key features and fabrications of rare-earth doped fibre lasers are outlined. In particular, the distributed feedback (DFB) fibre laser configuration is discussed and the effect of fibre birefringence on the operation of the fibre laser are highlighted. Based on the performance characteristics of the DFB fibre lasers, novel concepts to enable optical generation of high frequency signals with high spectral purity are illustrated.

6.2 Rare-earth doped fibre lasers

The initial development of fibre amplifiers and lasers was closely linked to the advancement in rare-earth doped single-mode optical fibres [4]. Specifically for telecommunication applications, ions like Nd^{3+} and Er^{3+} were identified for their emissions at around 1.3μm and 1.5μm respectively [5]. Early demonstrations of Nd^{3+} and Er^{3+} fibre lasers [6] highlighted the potential and the ease with which low threshold single-mode fibre lasers can be constructed. The availability of semiconductor pump laser diodes with high output power [7] then made possible Er^{3+} fibre amplifiers and lasers as very practical devices that coincided with the desired third optical transmission window at 1.5μm. Much of the key absorption and fluorescence characteristics of Er^{3+} doped fibres have been detailed in section 2.2.5 and the basic spectroscopy is essentially derived from a three-level transition. Lasing action in the Er^{3+} doped fibre is obtained on the $^4I_{13/2} - {}^4I_{15/2}$ transition and the low threshold requirement was highlighted in some of the earliest works on Er^{3+} fibre lasers e.g. [6][8]. Several pump wavelengths are available to populate the upper laser state $^4I_{13/2}$ in Er^{3+} fibre laser but results soon indicated that pumping at 980nm offers the advantage of operating in a region free of pump excited state absorption [9] as well as higher gain efficiency and lower noise characteristics compared to other pump wavelengths [10][11][12][13]. With the subsequent improvement to various aspects [14]-[18] of Er^{3+} doped fibre through codoping with Yb^{3+}, efficient and compact fibre laser configurations were realised [19][20].

Apart from the development in rare-earth doped fibres for high performance lasers and amplifiers applications, efforts to improve the output spectral characteristics of fibre lasers also initiated intense research activities. In particular, narrow linewidth, single longitudinal mode output is of great interest in a number of applications such as coherent communication and wavelength division multiplexed (WDM) communication systems. Early fibre laser configurations generally adopted a conventional Fabry-Perot cavity [13][21] in which a number of resonance modes were allowed to oscillate. This led to a broad lasing linewidth and power instabilities associated with mode competitions and mode hoppings. Through the incorporation of wavelength-selective elements such as bulk diffraction gratings [6] or external air-spaced étalons formed by the fibre and the output mirror surfaces [22], significant reduction of the output linewidth was achieved and highlighted the fact that line-narrowing of the fibre laser does not reduce its efficiency. Towards an all-fibre device, high reflectivity, integral fibre grating was adopted to provide the wavelength discriminating feedback [23][24]. These fibre gratings were formed by corrugations etched onto a side polished fibre [25]. The fibre laser configuration reduced significantly the linewidth of the output from a few nm to less than 0.05nm. These devices, however, still oscillated with tens of longitudinal modes. To effectively limit the number of oscillating modes within the reflection spectrum of the fibre grating, the fibre cavity length was reduced to increase the axial mode spacing of the laser cavity. Based on a combination of narrowband fibre gratings and a short highly-doped cavity, a truly single longitudinal mode fibre laser configuration has been achieved [26].

The development of fibre grating structures written by intense UV light into the core of optical fibres inevitably has a strong influence on the design and realisation of narrow linewidth single frequency fibre lasers. Fibre grating technology enables the non-invasive fabrication of highly spectrally selective feedback elements directly into the fibre core, leading to extremely low loss resonators. Utilizing two intra-core fibre Bragg gratings for cavity feedback and longitudinal mode discrimination, a robustly single-mode, narrow linewidth, low threshold Er^{3+} doped fibre laser has been illustrated [27]. The ability to inscribe fibre gratings directly into the Er^{3+} doped germanoaluminosilicate fibre core, has allowed great flexibility in the design of the fibre laser cavity. By adjusting parameters such as grating bandwidth, grating strength, and cavity length, desired modal discrimination during operation can be achieved. More importantly, due to the low cavity loss, the resonator can be made much shorter and with greater finesse [28] such that the cavity mode spacing becomes comparable to the grating bandwidth. As a result, fibre lasers can be robustly single-mode and extremely resistant to mode hopping even under the influence of external perturbations such as heating of the gratings [28]. Long-term bit error rate transmission tests further illustrated the potential of fibre lasers as a promising alternative to semiconductor DFB lasers for high-speed communication applications [29].

To increase the fibre laser output power, high dopant concentration was often needed to compensate for the short cavity length that was necessary to maintain stable single-mode operation. As mentioned in section 2.5.5, fibre lasers adopting high concentration erbium-doped fibre often suffered from sustained self-pulsation associated with saturable absorbers formed by Er^{3+} ion clusters within the doped fibre [30]-[32]. To avoid such impairment on long-term transmission operation, short cavity fibre lasers using low concentration Er^{3+} fibre (a few 100ppm) were necessary [33]. Such a configuration led to inadequate pump absorption and low output power on the order of 100-200μW. One solution to increase the

output power was by using the residual pump power to pump an Erbium doped fibre amplifier following the fibre laser [29][34]. The integrated fibre master oscillator power amplifier (MOPA) enabled effective gain in excess of 25dB to achieve an output power on the order of tens of mW. However, in these cases, the amplified spontaneous emission from the amplifier increased the output noise as well.

Efforts to improve the efficiency of short cavity fibre laser configurations led to the use of Er/Yb doped fibre as the gain medium [19][20]. By reducing the intra-cavity splice losses, Er/Yb fibre grating feedback laser with a cavity length on the order of a few cm can reach output power on the order of mW with 100mW 980nm pump power. Unlike Er^{3+} fibre lasers [27][28], the fibre gratings had to be spliced to the doped fibre because Er/Yb fibre cannot be made both efficient and photosensitive [20]. To avoid compromising the efficiency of the fibre laser, attention was required to reduce the intra-cavity splice losses.

Towards a low loss, intra-cavity fibre grating feedback, single-mode Er/Yb fibre laser configuration, a novel photosensitive Er/Yb fibre was realised [35]. As detailed in section 2.5.5, the fibre contains a photosensitive B/Ge/Si annulus around the Er/Yb core to enable fibre Bragg grating (FBG) formation. Photoinduced index change on the order of 10^{-3} can be achieved and despite the reduced field overlap between the grating and the guided optical field, effective index changes $>10^{-4}$ had been demonstrated [35][36]. With the photosensitive Er/Yb fibre, uniform fibre gratings can be fabricated directly into a short section of the doped fibre to create a highly spectrally-selective low loss resonator. More importantly, with the versatility and flexibility of fibre grating structures, a multitude of fibre laser configurations based on different fibre grating structures (such as phase-shifted gratings [37] or twin reflection gratings [38]) can be realised to enable specific output characteristics for desired applications. To date, this form of photosensitive Er/Yb fibre remains the enabling technology behind various compact, efficient Er/Yb fibre laser structures [39][40].

6.3 Distributed feedback (DFB) fibre laser

Among various fibre laser configurations, the distributed feedback (DFB) fibre laser is one of the most commonly adopted fibre laser architectures for single frequency operation. Distributed feedback structures and the corresponding laser action have been analysed in various literature studies [1][41]-[43]. Compared to conventional laser structures utilizing cavity mirrors, distributed feedback structures provide the optical feedback via backward Bragg scattering from the periodic perturbations of the refractive index of the laser medium itself [41]. This form of feedback mechanism is distributed throughout the length of the periodic structure and in the presence of a gain medium within the periodic structure, the condition for oscillation occurs [41].

Based on [41]-[43], it is well known that a distributed feedback laser utilizing a uniform grating structure leads to a symmetric resonance mode spectrum with respect to the Bragg frequency and that there is no resonance at the Bragg centre wavelength. The two lowest order resonance modes spaced symmetrically about the Bragg wavelength will reach lasing threshold first and the laser structure will oscillate in two modes. No real mode can exist in the DFB structure at the Bragg wavelength [41][44]. Experimental demonstrations of such lasing operation in fibre lasers with uniform fibre grating structures can be found in [44][45]. Energy exchange between the two oscillating modes was observed [45]. To enable single-mode operation of a DFB laser, a single pass optical phase shift of $\pi/2$ (i.e. π phase shift for the grating structure) is introduced into the grating such that the round trip phase condition is satisfied at the Bragg wavelength [46]. Under such conditions, the introduction of the phase shift in the uniform grating structure breaks the threshold condition degeneracy for the two lowest order laser modes. A resonance mode at the Bragg wavelength arises and undergoes strongest feedback and lowest required threshold gain. The threshold gain difference between this main longitudinal mode and the side modes is the largest, thereby giving enhanced single-mode operation [43]. In a similar fashion, based on the π phase-shifted fibre grating structure, robustly single-mode DFB fibre lasers were realised [45][47].

6.3.1 Distributed feedback fibre laser operation

The ability to inscribe high quality π phase-shifted grating structures (section 4.3.1) in doped fibres facilitated the realisation of single longitudinal mode DFB fibre lasers. Since the laser cavity essentially consists of a π phase-shifted fibre grating structure, the transmission profile can be characterized and the typical spectral profile of the cavity resonance structure of a π phase-shifted DFB fibre laser fabricated in the experiment is shown in Figure 6.1.

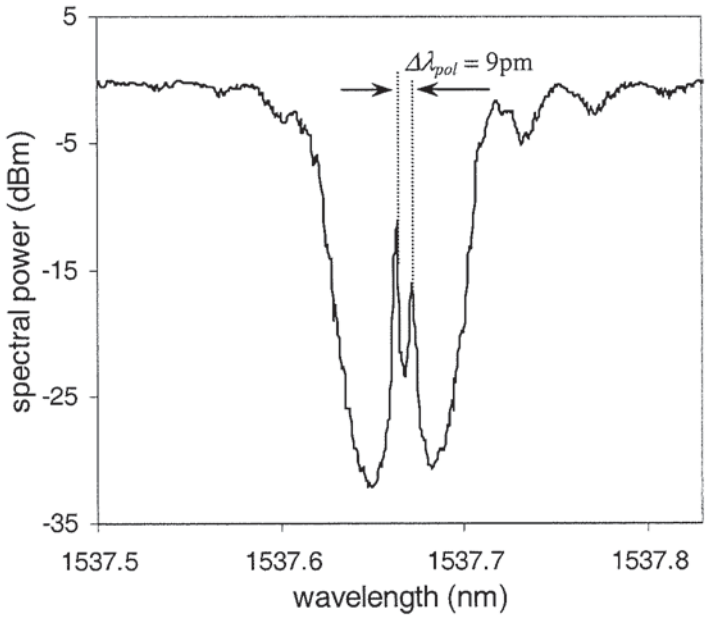

Figure 6.1 Typical transmission profile of the phase-shifted DFB fibre laser cavity.

The fibre grating structure inscribed into the Er/Yb fibre was 45mm long with refractive index modulation of $6x10^{-5}$ (i.e. κL = 5.5). The phase shift was induced by post-processing over a 1mm central section of the grating. Ideally, the DFB fibre laser structure containing the π phase-shifted grating exhibits a narrow transmission peak, which defines the lasing wavelength, in the middle of the grating stopband. As illustrated in Figure 6.1 (and highlighted in section 4.4.2), due to both intrinsic and UV-induced fibre birefringence, differential phase shifts along the two polarization axes created polarization mode splitting at the transmission peak of the phase-shifted grating. As a result, during laser operation, the single longitudinal mode phase-shifted DFB fibre laser actually operated in two eigenpolarization modes [35][44][47] corresponding to the two resonance peaks in the phase-shifted grating structure [48][49][50]. Due to the difference in the resonant wavelength, the two polarization modes can beat to form a polarization mode beating (PMB) signal at the receiver end, generally a microwave signal on the order of a few hundred MHz to ~ 2GHz, depending on the amount of birefringence within the fibre grating structure.

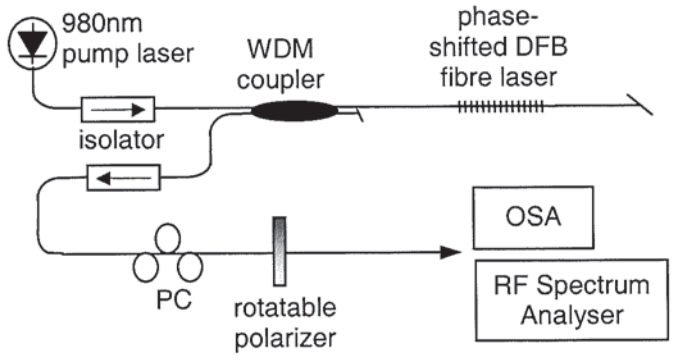

Figure 6.2 Operational setup for the phase-shifted DFB fibre laser. WDM coupler: 980nm/1550nm wavelength division multiplexer, PC: polarization controller, OSA: optical spectrum analyser.

Figure 6.2 shows the experimental setup for the operation of the phase-shifted DFB fibre laser. The fibre laser, placed on an aluminium plate without temperature control, was pumped by a 980nm laser diode with a maximum pump power of 60mW. The pump light coupled into the fibre laser through the 980nm/1550nm wavelength division multiplexer (WDM). The fibre laser was spliced at one end to the WDM coupler and the other end was angle cleaved and submerged into index matching gel to prevent optical backreflections from destabilizing the fibre laser. The output from the fibre laser after a 1550nm isolator was fed through a manually-controlled polarization controller (PC) and a polarizer before being characterized by the optical spectrum analyser (OSA) and the RF spectrum analyser. The fibre laser output registered by the OSA at maximum pump power is as shown in Figure 6.3.

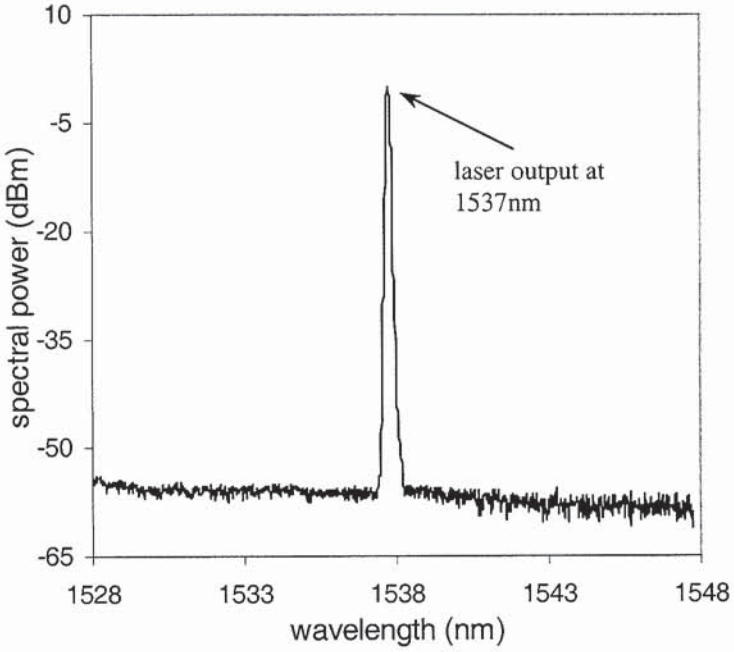

Figure 6.3 Optical output spectrum of the phase-shifted DFB fibre laser.

Due to the limited resolution of the OSA (0.1nm), the measured optical linewidth of the output spectrum of the fibre laser was broadened. Furthermore, due to the close proximity of the polarization modes (9pm), the dual-polarization mode operation was not resolvable on the OSA. On the other hand, using a RF spectrum analyser, the PMB signal generated by the two polarization modes was captured and is shown in Figure 6.4.

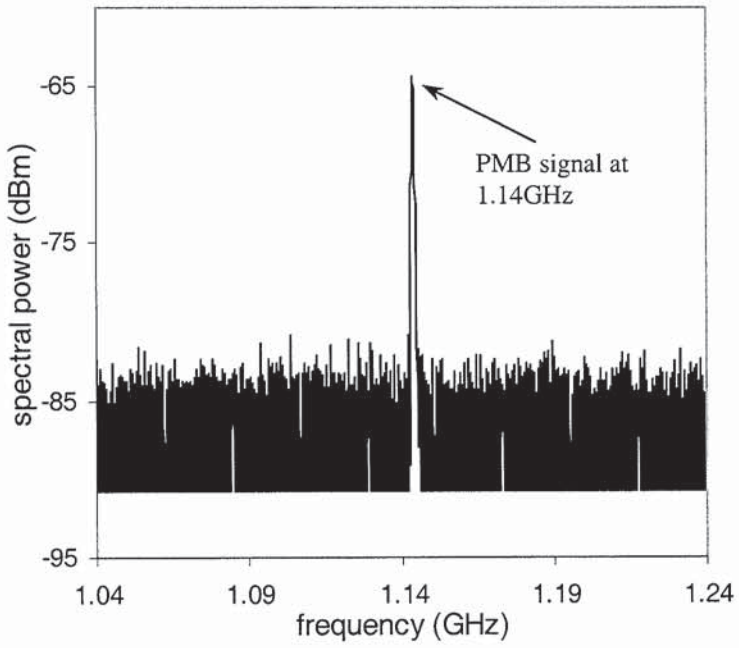

Figure 6.4 Polarization mode beating signal from the phase-shifted DFB fibre laser.

It is interesting to note that the polarization mode separation in the output of the fibre laser, which is the feature of our interest, can be examined from the passive cavity resonance spectral profile. The wavelength separation between the polarization transmission peak, $\Delta\lambda_{pol}$, is related to the birefringence, Δn, by [51]

$$\frac{\Delta\lambda_{pol}}{\lambda_B} = \frac{\Delta n}{n_{eff}} \tag{6.1}$$

and the obtained PMB frequency Δf_{pol} is simply given by

$$\Delta f_{pol} = \frac{c}{\lambda_B^2}\Delta\lambda_{pol} \tag{6.2}$$

where c is the speed of light. Based on the measurement as shown in Figure 6.1, the polarization mode splitting at the transmission peak has a wavelength separation of 9pm, subjected to 1pm measurement resolution. At λ_B=1537nm, this wavelength separation corresponded to 1.143GHz, which is in close agreement with the experimental result obtained. The effective birefringence in the DBF fibre laser cavity was calculated to be ~8.5×10^{-6} which was of the same order of magnitude as [52].

The existence of dual polarization modes in the operation of phase-shifted DFB fibre lasers is generally considered an undesired side effect. The beat noise from the dual-polarization mode operation limits its applications in optical communication and spectroscopy systems. Various efforts to resolve this issue in DFB fibre lasers have been carried out [48]-[50][52][53]. On the other hand, the birefringence

properties in fibre lasers make such devices attractive as polarimetric fibre sensors where changes in the birefringence in the laser cavity in response to external perturbations directly translate into a change in the PMB frequency [51][54][55]. In the following sections, a different application for dual-polarization mode DFB fibre lasers in the field of fibre-radio communication systems is proposed and demonstrated. Taking advantage of the polarization mode characteristics in the fibre lasers as well as the versatility of fibre grating structures, novel fibre laser configurations to enable optical generation of microwave and millimetre wave signals of high spectral purity are illustrated.

6.4 Optical generation of high frequency signal

As discussed in Chapter 1, wireless communication systems employing optical fibre distribution networks (i.e. fibre-radio systems) have been considered as an effective means to meet the future demand for broadband services such as interactive multimedia, video on demand, and mobile systems [56]. To reduce the complexity and to enable these systems in a low cost manner, it is advantageous that the radio wave signals are generated and transported by optical means to antenna units where they are radiated and distributed to customers [57]. Such distribution networks can exploit the inherent advantages of optical fibres, such as low loss and wide bandwidth characteristics, and optical amplifiers can be utilized to provide gain for both the optical carriers as well as the radio wave signals. Apart from applications in the future broadband wireless photonics networks, optical generation of radio frequency (RF) signals is also attractive for a wide range of applications like Lidar-radar [58], phased array antennas [59] and near-field optical microscopy [60].

The enabling technology for generation of high frequency signals ranging from gigahertz (GHz) to terahertz (THz) directly in the optical domain has been the focus of much research. Various techniques have been proposed with strong emphasis on the ability to attain millimetre wave (mm-wave) signal (on the order of tens of GHz) generation. Despite the availability of fast photodiodes, which make possible optical distribution of mm-wave signals in the fibre radio systems, the photodiode speeds are not matched by the direct modulation bandwidth of semiconductor lasers [61]. Furthermore, mm-wave modulation using currently available optical sources and optical modulators is not straightforward and generally requires drive electronics of considerable sophistication [62]. Among various techniques currently employed, an effective and favoured technique is to use heterodyning between two lasers whose frequencies differ by the required microwave/millimetre-wave frequency, and which are mixed at a photodetector (square-law detector) to produce the desired electrical beat signal. Optical heterodyning offers the highest degree of flexibility in terms of the accessible frequency range and offers the prospect of high efficiency and insensitivity to chromatic dispersion in optical fibres [63]. Simply relying on the frequency separation of the two lasers, heterodyning potentially offers ease of implementation and operation. Optical mixing of two laser sources also has the advantage over other generation techniques of giving higher RF power [64]. This is due to the fact the optical power is concentrated only in the two needed optical waves and the beating between the two optical waves generate a difference signal with 100% modulation depth [65][66]. It is particularly advantageous for fibre-radio network applications to use optical heterodyning since it reduces base station hardware complexity and overcomes limitations on transmission imposed by fibre chromatic dispersion [57].

To heterodyne two lasers for the generation of high spectral purity beat signal, it is necessary to maintain a high degree of coherence between the two lasers. The total optical field of two laser modes can be expressed by,

$$E = E_1 e^{j(\omega_1 t+\phi_1)} + E_2 e^{j(\omega_2 t+\phi_2)} \tag{6.3}$$

where $\omega_{1,2}$ represent the two optical frequencies and $\phi_{1,2}$ the phase noises for the corresponding modes. Photocurrent, I, generated by direct detection of the optical field defined by (6.3) is proportional to $E \cdot E^*$ and is given by,

$$I \propto E_1^2 + E_2^2 + 2E_1E_2\cos\left[(\omega_1 - \omega_2)t + (\phi_1 - \phi_2)\right] \tag{6.4}$$

The difference of the two optical frequencies produces a beat signal located in the microwave/millimetre wave domain. Generally $\phi_{1,2}$ are high frequency noise components and are uncorrelated if the two modes originate from different lasing cavities. The difference between them is a high frequency noise source, which consequently leads to a large linewidth of the generated beat signal. This phase noise, however, is very small provided the two modes are phase-locked (i.e. highly correlated) to each other.

Considerable efforts using different techniques to enable two highly correlated, phase-locked laser sources separated by the desired frequency spacing have been carried out. Most notably, mode injection locking technique between two or three lasers has been widely adopted to correlate the noises of the lasers used in the heterodyning [67][68]. Based on the principle of injection locking [69], the technique relies on coupling of two oscillators (lasers) so that the frequency and the phase characteristics of one laser (Master laser) or its harmonics (generated by optical modulation) is imposed onto one or more of the longitudinal modes of the other lasers (slave lasers). It is important to note that such schemes generally require a high frequency synthesizer (ranging from a few GHz up to 20GHz) and RF amplifiers and the locking range is sensitive to the injected optical power and state of polarization from the master laser [65][70][71]. An alternative approach based on harmonic generation in intensity or frequency modulators has also been demonstrated [61][62]. Extracting two higher order sidebands at multiples of the modulation frequency from the output of a modulator, high spectral purity beat frequency was achieved despite the relatively broad linewidth of the input DFB laser light. Proper biasing is critical in these schemes and optical filtering is necessary to suppress unwanted optical components generated in the process [61][62]. Furthermore, a large extension of the frequency range through employing higher harmonics requires more complex modulator configuration [72]. In a similar fashion, a high frequency heterodyne signal can also be formed between two extracted optical modes from a frequency comb spectrum generated by, for example, a pulse source [66][73]. Similarly, such schemes require high frequency signal generators and optical filterings and in some cases require incorporating nonlinear fibre optic media for spectrum expansion to generate the required frequency comb [73].

To overcome the frequency instability and phase noise of the generated beat signal by heterodyning two uncorrelated laser sources, other techniques involving the use of feedback loops such as optical phase

lock loops (OPLL) [74][75][76] to correlate the optical modes were carried out. Practical limitation of the shortest loop delay time achievable imposes a stringent requirement on the linewidth of the optical sources used in the configuration. Similar to all of the above-mentioned heterodyne schemes, the technique also requires high frequency synthesizers and additional electronic infrastructures that can limit its wide spread practical deployment within the fibre-radio network.

With the objective of developing a simple and potentially low cost device for the optical generation of high spectral purity RF signals, the concept of dual-mode laser source in the form of a dual-mode semiconductor laser diode was developed [64][77]. Even though phase-locking by applying an electrical drive signal at a subharmonic of the beat frequency may be necessary, these schemes represent the most direct approach in optical heterodyning for generation of high frequency RF beat signal.

Apart from their obvious fibre compatibility and fabrication simplicity, phase-shifted DFB fibre lasers typically exhibit extremely narrow optical linewidths on the order 10kHz [45] with good frequency stability against temperature fluctuations and without mode hopping. Propelled by improvements to fibre grating technology and the developments in rare-earth doped fibres, fibre lasers can be attractive potential candidates not only for optical WDM communication systems but also for applications in the optical generation of high frequency RF signals. In the following sections, a different approach towards optical generation of microwave wave signals based on a phase-shifted DFB fibre laser is demonstrated. The proposed technique utilizes the tendency of phase-shifted DFB fibre laser to operate in dual polarization modes to generate two highly correlated optical modes for heterodyning. Tuning mechanisms based on fabrication conditions, temperature and transverse pressure are illustrated. More interestingly, a unique DFB fibre laser configuration has been proposed and demonstrated to achieve high spectral purity beat frequency at millimetre wave regime and beyond. In all cases, the device configurations utilize the flexibility and engineering simplicity of fibre grating based lasers. The proposed fibre-laser-based RF signal generators retain their all-fibre configurations and more importantly, do not require external instruments such as high frequency synthesizers, RF amplifiers or feedback loops.

6.4.1 Optical generation of microwave signal based on a phase-shifted DFB fibre laser

The phase-shifted DFB fibre laser has the tendency to operate in dual polarization modes, generally with a wavelength separation of a few hundred MHz to <2 GHz, corresponding to birefringence on the order of $< 1.4 \times 10^{-5}$ at 1550nm. It is worth noting that the two lasing polarization modes are essentially from an identical laser cavity. More importantly, phase perturbations that arise due to environmental factors are imposed simultaneously onto both laser components and the two beating modes exhibit strong common-mode rejection of phase noise [62]. As a result, the two lasing modes are highly correlated and based on (6.4), heterodyning the two optical modes leads to a beat frequency of low phase noise and of very narrow linewidth [67].

In the experiment, a 45mm long π phase-shifted DFB fibre was fabricated and placed within a temperature controller which contained a Peltier device providing a temperature control with a precision better than 0.1^{0}C. The experimental setup for the operation of the fibre laser was identical to that shown in Figure 6.2. The output of the fibre laser measured on a scanning Fabry-Perot interferometer with a free spectral range of 8GHz is shown in Figure 6.5. Evidently, the fibre laser delivered dual-polarization mode

output with a wavelength spacing ~ 1.1 GHz. The corresponding PMB signal was obtained after passing the output through a polarizer and the recorded spectrum is shown in Figure 6.6. Tuning the polarization controller or the polarizer enabled one or the other polarization mode (and the PMB signal) to be eliminated, as shown in Figure 6.7, confirming that the lasing modes corresponded to the orthogonal polarization modes. By lowering the resolution bandwidth of the RF spectrum analyser, the high spectral purity of the generated PMB signal was clearly demonstrated. It is important to note that the measurement of the true linewidth of the beat signal was limited by slow drift in the microwave signal and the much longer measurement time of the RF spectrum analyser at high resolution. Nevertheless, measurement based on a lower resolution of 1kHz showed that the linewidth of the beat signal was <1kHz as shown in Figure 6.8.

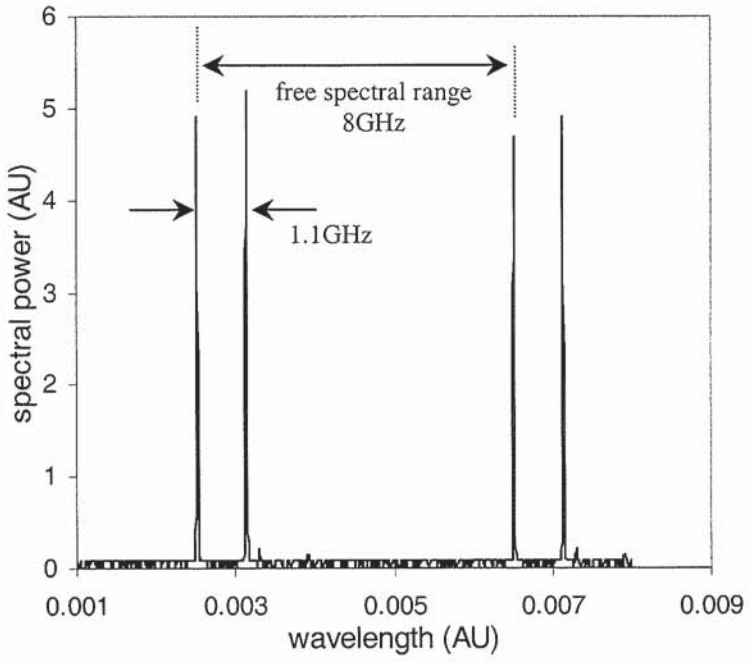

Figure 6.5 Output spectrum of the phase-shifted DFB fibre laser observed on the scanning Fabry-Perot interferometer. The free spectral range of the interferometer was 8GHz.

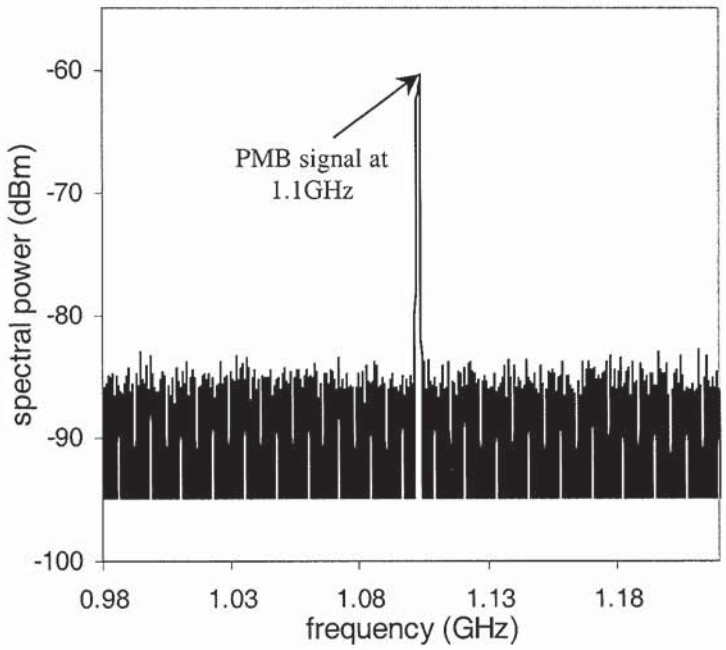

Figure 6.6 Beat signal generated by the phase-shifted DFB laser measured on the RF spectrum analyser.

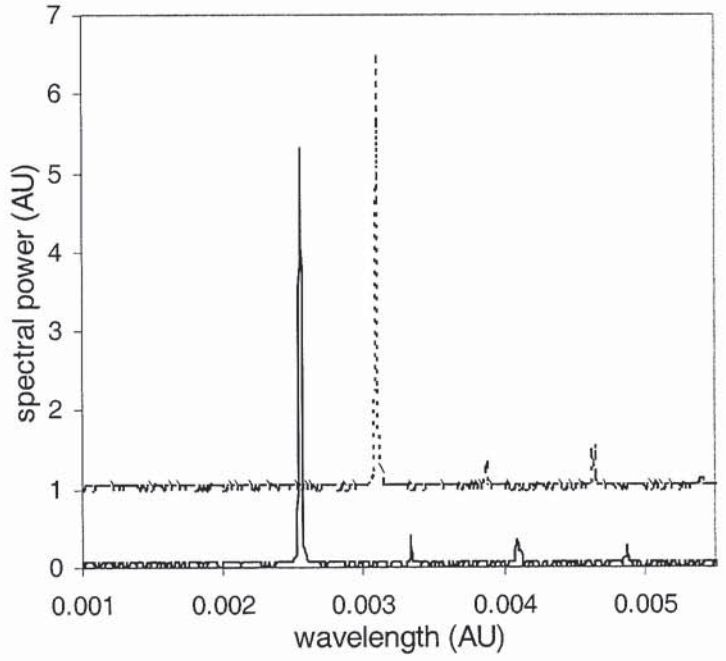

Figure 6.7 Individual polarization modes observed through the scanning Fabry-Perot interferometer when the polarizer at the output of the fibre laser was adjusted. The superimposed spectra are vertically offset for clarity.

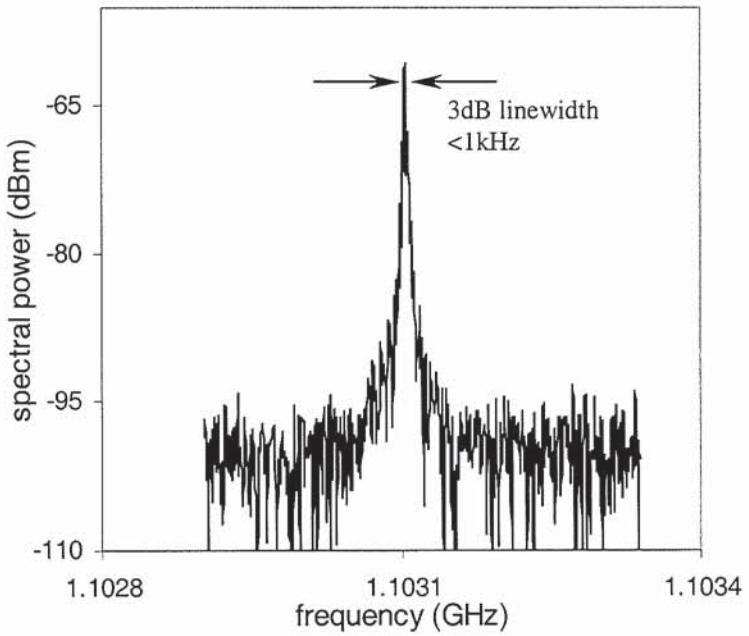

Figure 6.8 Measured PMB signal generated by the fibre laser. The 3dB linewidth of the beat signal measured <1kHz.

The linewidth of the measured beat signal was comparable to reported schemes based on other heterodyne techniques. The result shown in Figure 6.8 also attests to the high degree of coherence between the two lasing polarization modes from the π phase-shifted DFB fibre laser [67]. The spectral purity of the beat signal achieved without the need for high frequency RF synthesizer, feedback loops or any other electronics further exemplified the potential of using π phase-shifted DFB fibre lasers as optical microwave signal generators. Based on [50], it is worth noting that the polarization mode spacing in the fibre laser is predominantly determined by the birefringence in the UV-induced phase shift region of the grating structure. Hence, by increasing the induced birefringence in the phase shift region, the polarization mode spacing can be increased. To take advantage of this, a UV offset post-processing technique was proposed and validated.

In the experiment, identical fabrication conditions as used for the previous π phase-shifted DFB fibre laser were adopted. A 45mm long uniform fibre Bragg grating was inscribed into an identical Er/Yb fibre, followed by UV post exposure over a ~1mm central section of the grating. The only difference in the fabrication was that the UV beam was intentionally offset from the core of the fibre in order to create a larger UV-induced birefringence at the phase shift region. The transmission profiles of the fibre lasers fabricated with and without UV offset post-processing are superimposed for comparison as shown in Figure 6.9.

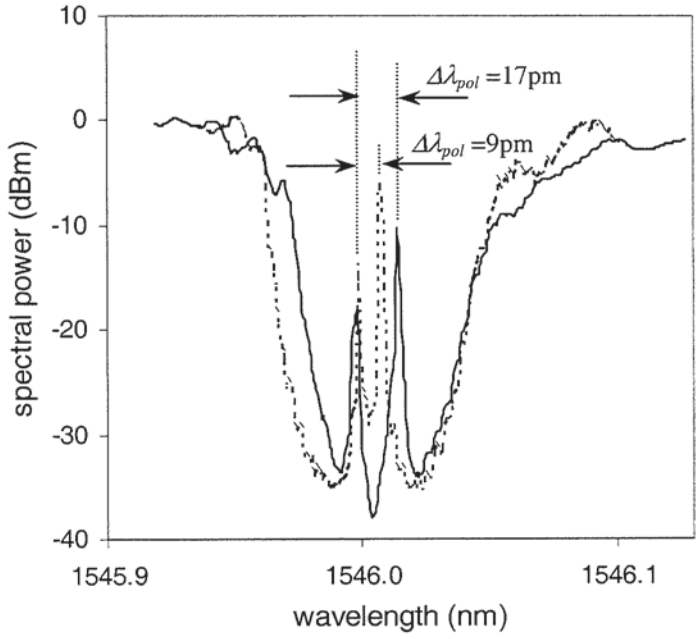

Figure 6.9 Superimposed transmission profiles of two π phase-shifted DFB fibre lasers fabricated under normal post-processing condition (dotted trace) and with UV offset post-processing (solid trace).

With 1pm resolution measurement, it is evident that a significant increase in the birefringence in the phase shift region of the grating structure was achieved. Conventional UV post-processing induced an effective polarization mode separation of 9pm. The UV offset post-processing, on the other hand, led to a polarization mode separation measured at 17pm. Due to the increase in the wavelength separation between the polarization modes, the fibre laser generated an equivalent beat signal of higher frequency. The superimposed RF spectra obtained from the two lasers are shown in Figure 6.10.

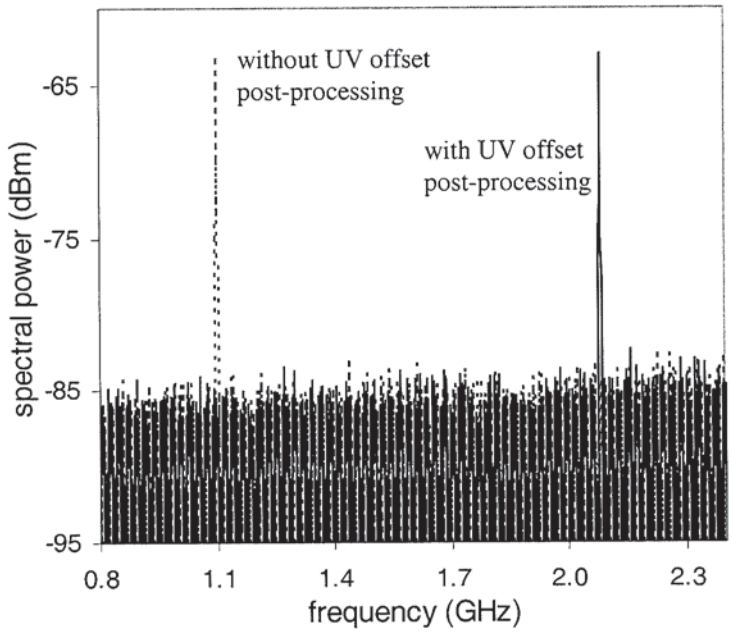

Figure 6.10 Superimposed RF spectra from the two fibre lasers.

The beat signal produced from the previous fibre laser was 1.1GHz while the second laser produced a beat note at 2.09GHz. The results agreed with the transmission peak separations as shown in Figure 6.9 and it was evident that the beat frequency doubled due to the effect of the UV offset post-processing. More importantly, the measured linewidth of the beat signal at 2.09GHz was <1kHz (limited by the measurement setup and resolution) confirming that the fabrication technique did not compromise the effectiveness of the device for microwave signal generation.

As the application of transverse force or temperature variation changes the linear birefringence in the π phase-shifted grating [78], we utilized the variation of the beat frequency with both of these parameters as means to introduce tuning of the microwave signal generated. Over a temperature variation of 25°C, the beat signal varied over 28MHz in a linear fashion as shown in Figure 6.11. Furthermore, by applying transverse force onto the fibre laser cavity, large tuning of the beat frequency was achieved. At a transverse force of 60N, the recorded beat frequency exhibited an increase of 690MHz as shown in Figure 6.12. Both techniques offer effective means to fine tune the microwave signal generated from the phase-shifted DFB fibre laser during operation with sensitivities ~ -1.13MHz/^{0}C and ~11.5MHz/N respectively.

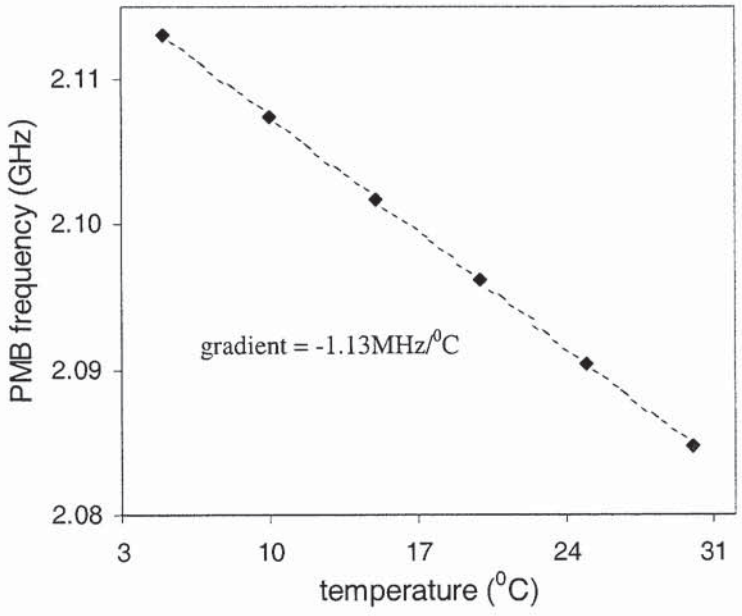

Figure 6.11 PMB frequency tuning with temperature.

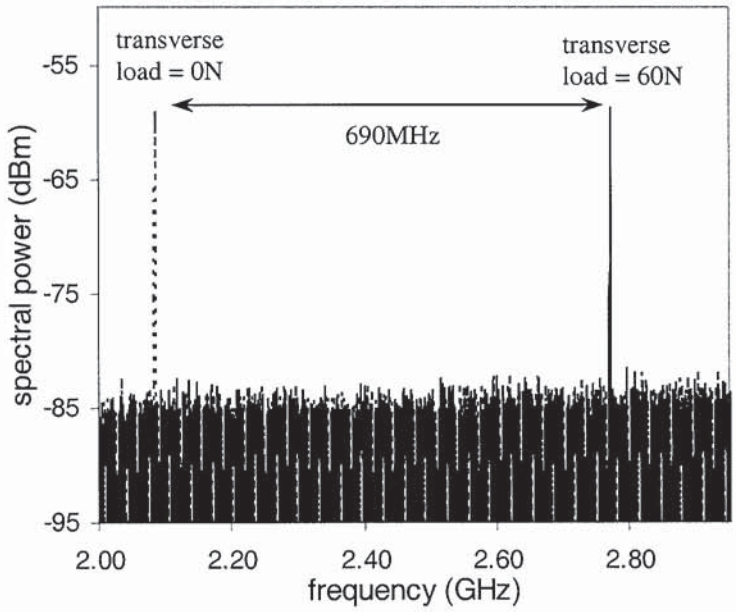

Figure 6.12 Beat frequency tuning by transverse force. Effective shift under 60N measured 690MHz.

Based on the results obtained, it is evident that the dual-mode operation from a single fibre laser cavity can enable two highly correlated lasing modes, necessary for optical generation of narrow linewidth heterodyne signal. For applications where a simple, compact device structure is of practical importance, dual-mode fibre laser configurations hence provide a simple technique to meet this requirement.

6.4.2 Optical generation of millimetre wave signal based on a co-located dual DFB fibre laser

The frequency separation between the polarization modes of the fibre laser is dependent upon the amount of birefringence within the fibre grating structure. The amount of UV-induced birefringence can reach 5%-8% of the total UV-induced index change [79]. Experimentally, as shown in the previous section, this represents achievable UV-induced birefringence generally on the order of $2x10^{-5}$ for strong induced index change of $4x10^{-4}$ within the fibre. The corresponding polarization mode splitting, and thus the PMB signal achievable, from (6.2), is less than 3GHz (polarization mode wavelength separation ~ 21pm). For applications in fibre-radio systems, the millimetre wave frequency regime around 30 to 70GHz is required due to various favourable reasons such as frequency allocation, low spectral congestion, and the inherent advantage of the small size of transmitting and receiving apparatus [70]. Dual-polarization phase-shifted DFB fibre lasers that are based on UV-induced birefringence in conventional gain fibres are therefore not able to meet the requirement.

Evidently, the straightforward solution to increase markedly the amount of fibre birefringence in the fibre laser cavity is to adopt Hi-Bi rare-earth doped fibres [80]. Hi-Bi rare-earth doped fibres exhibit birefringence on the order of $5x10^{-4}$ and, thus, are able to yield polarization mode spacing up to tens of GHz. However, it is important to note that the Hi-Bi fibre DFB fibre laser configuration essentially remains dependent on the physical properties of the gain fibre. The PMB signal generated by the laser is

predetermined by the intrinsic birefringence of the rare-earth doped fibre. Wide range tuning, not easily achievable, will be necessary to generate beat signals at frequencies that do not correspond to the birefringence of the fibre. Hence, optical millimetre wave generation based on this kind of fibre laser configuration has limited flexibility in creating beat signals at customized/desired frequencies.

Optical heterodyning of two laser modes from the same fibre laser cavity is an effective means to generate a very narrow linewidth beat signal without phase-locked feedback control due to the common mode suppression of phase noise. Based on this concept and to overcome the limitations imposed by fibre characteristics, we proposed an alternative fibre laser configuration based on a dual, co-located phase-shifted grating structure (i.e. co-locating two DFB fibre laser cavities) for generating heterodyne signals in millimetre wave regime and beyond. The fibre laser generates dual optical modes that are highly correlated to enable a narrow linewidth heterodyne beat signal at any frequency depending on the wavelength separation between the two fibre laser grating structures (phase-shifted gratings) during fabrication. Similarly, the fibre laser does not require expensive high frequency synthesizers, amplifiers or feedback loops to suppress uncorrelated phase noises in the lasing modes. Notably, the wavelength spacing between the lasing modes is purely determined by the fibre grating parameters only. Furthermore, we emphasize the simplicity and flexibility of the fabrication process while retaining the advantages associated with fibre lasers for optical generation of high frequency radio wave signals.

The proposed dual co-located phase-shifted DFB fibre laser configuration essentially builds on the concept of the superimposed fibre grating structure. As highlighted in section 4.4.3, two fibre Bragg grating structures can be superimposed onto one another with relative ease during fabrication. Furthermore, when the period difference and grating length satisfy (4.28) in Chapter 4 given by

$$L\Delta\Lambda \gg \frac{\Lambda_1\Lambda_2}{\pi} \tag{4.28}$$

where Λ_1 and Λ_2 denote the respective grating periods, $\Delta\Lambda$ is the period difference and L is the grating length, the spectra of the two gratings are separated sufficiently such that the gratings are independent of each other. The spectrum of the dual overwritten grating structure is then the superposition of the individual grating spectra located at the respective Bragg wavelengths. More interestingly, without the need for further modification to the fabrication conditions, we have demonstrated in section 4.4.3 that two phase-shifted fibre gratings, satisfying (4.28), can also be overwritten to create a dual co-located phase-shifted grating structure. By inscribing the superimposed phase-shifted grating structure into an active fibre (Er/Yb doped fibre), a dual co-located phase-shifted DFB fibre laser configuration is achieved.

In the experiment, a 40mm long π phase-shifted FBG was first inscribed into the Er/Yb doped fibre using a phase mask with period Λ_{mask} = 1069nm. The fibre was adhered firmly at its ends to a translation stage to allow a strain to be applied to the fibre. By real-time monitoring the spectrum of the first grating, the fibre was strained 0.02% so that a wavelength shift of 0.26nm, corresponding to $\Delta\Lambda$ = 0.09nm, was obtained. A second phase-shifted grating was then produced under the exact same conditions. The total fabrication time for the device was < 5min and the resultant profile of the laser cavity measured using a tunable laser with resolution of 1pm is shown in Figure 6.13. It is evident that the spectral profiles of each

phase-shifted grating in the overwritten structure remain independent. The wavelength spacing between the transmission peaks of each grating measured 0.26nm and birefringence-induced polarization mode splitting ($\Delta\lambda_{bire}$ ~ 9pm i.e. birefringence ~ $8.5\text{x}10^{-6}$) was observed in both gratings.

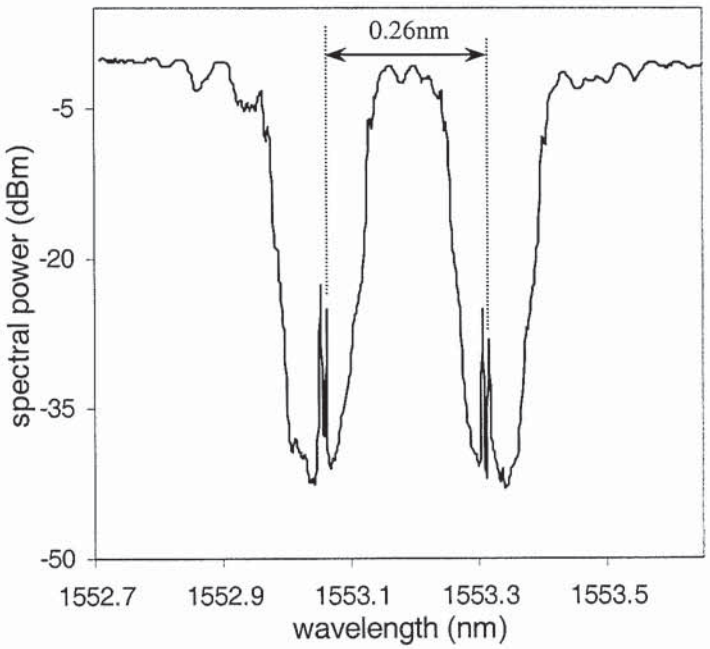

Figure 6.13 Spectral profile of the dual co-located DFB fibre laser structure. Birefringence-induced polarization mode splitting was evident each grating.

The operational setup of the fibre laser was identical to that shown in Figure 6.2. During operation, the optical output spectrum of the fibre laser obtained on the optical spectrum analyser revealed dual-mode operation with wavelength spacing measured ~0.26nm, corresponding closely to the passive measurement. The captured spectrum is shown in Figure 6.14.

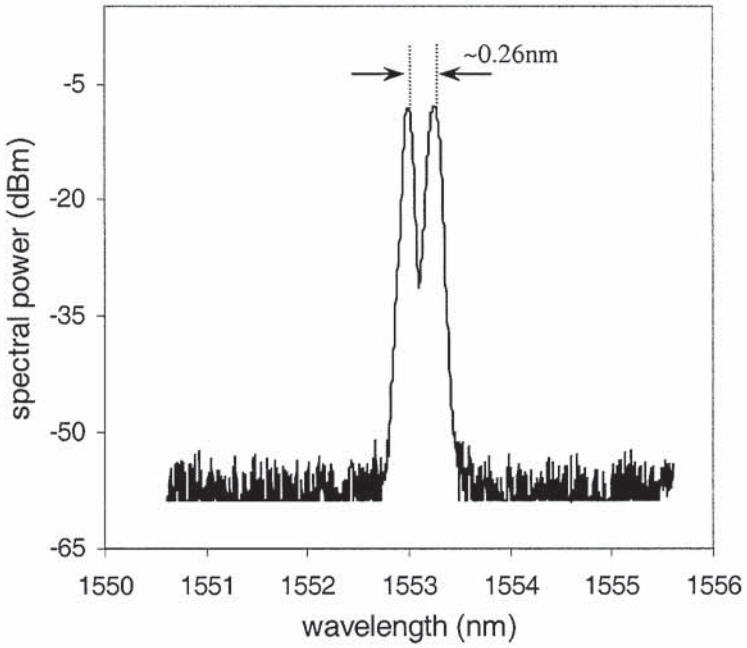

Figure 6.14 Optical output spectrum of the fibre laser. Resolution 0.1nm.

Evidently, there is a natural tendency for each laser cavity to lase in both polarization modes, thereby introducing mode competition and mode hopping. Within the resolution of the optical spectrum analyser (0.1nm), the polarization modes cannot be resolved although output power fluctuations were clearly visible. By observing the beat signals generated by the output modes of the fibre laser on the RF spectrum analyser, the output operation characteristics of the fibre laser can be deduced.

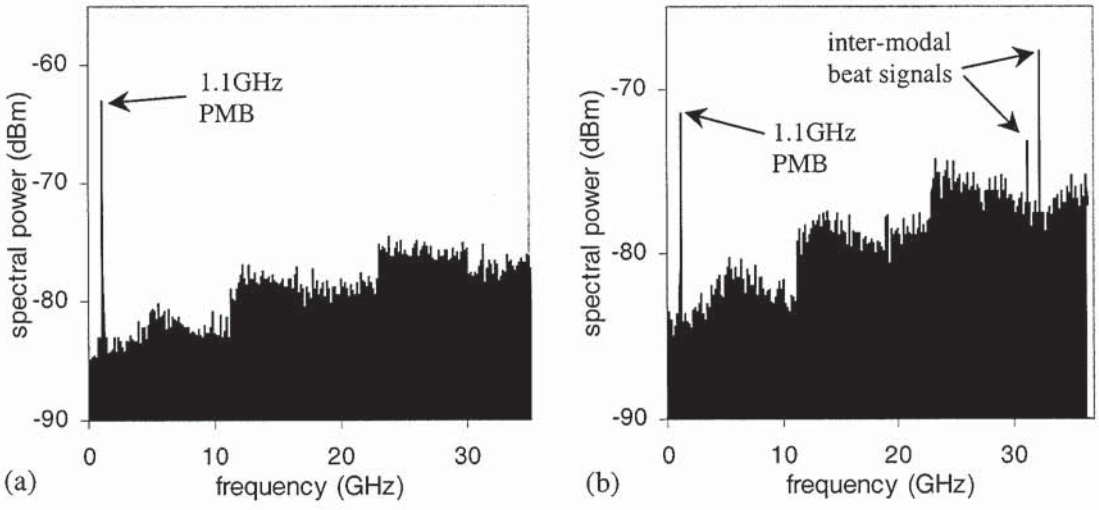

Figure 6.15 Beat signal spectra from the output of the fibre laser. Inconsistent occurrences of the beat signals highlighted the operation of the fibre laser was unstable.

Variations in the beat signal spectrum highlighted instability of the lasing modes due to mode competition between the two lasing cavities. Figure 6.15a shows the PMB signal observed at a particular instance in time during the fibre laser operation. The beat note at ~1.1GHz corresponded to the frequency

separation between two polarization modes within one laser cavity. The absence of beat signals at higher frequencies over the entire measurement range indicated the absence of inter-modal beating between oscillating modes from different cavities. Prolonged operation of the fibre laser showed that the oscillating modes were not stable and random occurrences of lasing modes from both laser cavities were obtained. The existence of lasing modes from both laser cavities introduced inter-modal beating signals at high frequencies (~32GHz) corresponding to the wavelength spacing of ~0.26nm between the laser cavities. This is illustrated in the beat signal spectrum in Figure 6.15b.

To achieve stable dual-mode operation from the fibre laser configuration, each laser cavity must oscillate with one polarization mode only. More importantly, the lasing modes from the two cavities must be mutually orthogonal to avoid mode competition. To achieve stable dual-polarization mode operation from the co-located dual DFB fibre laser configuration, a novel self-injection locking mechanism was introduced into the fibre laser structure. Injection locking is a technique for coupling two oscillators so that their frequencies and phases are highly correlated [81]. As applied to laser systems, this technique enables a low power laser (denoted as master laser) with desirable frequency properties to impose its frequency and mode structure onto a higher power laser (denoted as slave laser) whose spectral properties would otherwise not be so good. The use of injection locking in fibre lasers has been demonstrated [82]-[85] and the frequency range, commonly known as locking bandwidth, in which such injection locking occurs for the DFB fibre laser is given by [83]

$$\Delta f_{lock} = \frac{4c\kappa \exp(-\kappa L)}{2n\pi} \sqrt{\frac{P_{master}}{P_{slave}}} \tag{6.5}$$

where c is the speed of light, P_{master} is the injected laser power, P_{slave} is the slave laser power, κ is the coupling coefficient of the grating and L is the length of the fibre laser. Considering a DFB fibre laser with κ =120m^{-1} and L=40mm, the locking bandwidth is found to be 130MHz when $P_{master} = P_{slave}$. For practical applications, such an injection locking technique is not useful because it requires an external laser source and the allowable margin for frequency deviation between the master laser and the slave laser is too narrow. On the other hand, injection locking in fibre lasers is particularly effective in suppressing dual-polarization mode operation to enable stable single frequency, single polarization operation [83]-[85]. The concept relies on introducing polarization-selective optical feedback, derived from the fibre laser itself. Taking note that fibre lasers actually lase in both directions, the laser output at one end can be fed into a wavelength-selective and polarization-selective optical feedback device composed of, for example, a narrowband FBG and an inline polarizer [83]. This self-injection mechanism enhances the polarization mode that aligns with the feedback light and suppresses the orthogonal polarization mode. Since the optical feedback originates from the laser cavity itself, polarization self-injection locking is immune from frequency deviations and shown to enable highly stable, single-polarization mode operations in DFB fibre lasers [85].

To enable stable dual-polarization mode operation from the dual DFB fibre laser configuration, we first introduced a new approach towards realising polarization-discriminating, self-injection locking based on the superimposed fibre Bragg grating structure in Hi-Bi fibre. In contrast with the case of single polarization self-injection locking of a conventional dual-polarization DFB fibre laser, the optical feedback

scheme in this configuration requires two mutually orthogonal, self-injection locking mechanisms to enable the desired dual-polarization mode of operation. It is also essential to maintain common mode suppression of phase noise in the fibre laser configuration with the integrated optical feedback path. The use of an in-line polarizer was not feasible since the polarizer transmits only a single polarization. To enable simultaneous polarization injection feedbacks into the respective co-located DFB fibre laser cavities at the appropriate wavelengths, superimposed uniform fibre Bragg gratings in Hi-Bi fibre offer an elegant solution.

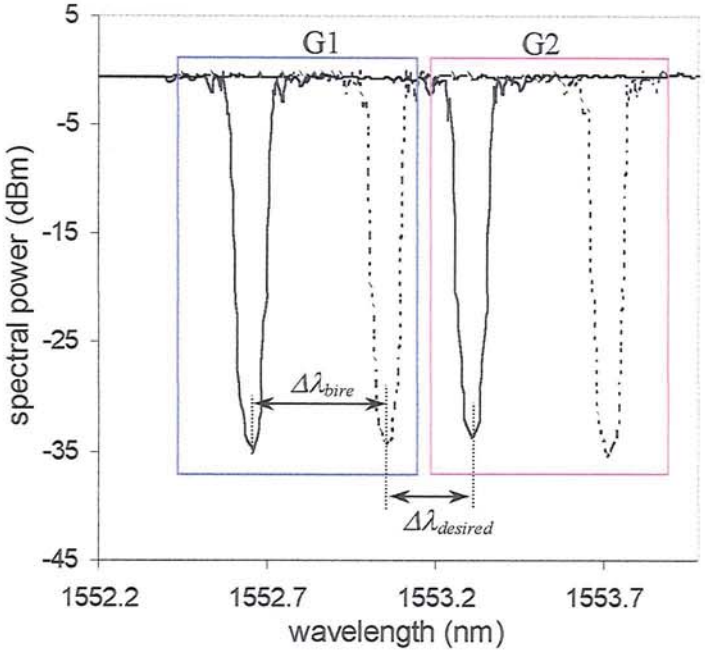

Figure 6.16 Transmission spectra of the superimposed uniform fibre Bragg grating structure in Hi-Bi fibre measured along orthogonal polarization axes. The solid trace corresponds to the measured profile along the fast axis while the dotted trace corresponds to the slow axis. $\Delta\lambda_{bire}$ is the polarization wavelength separation due to intrinsic fibre birefringence.

As illustrated in section 4.4.3, a dual overwritten uniform fibre grating structure in Hi-Bi fibre combines the merits of the superimposed grating structure and the polarization-selectivity of gratings in Hi-Bi fibre to enable polarization-discriminating filtering at specified wavelengths and polarizations. Based on this concept, a superimposed uniform fibre Bragg grating structure in Hi-Bi fibre, therefore, is able to perform polarization-discriminating optical reflections at desired wavelengths along orthogonal polarization axes. As shown in Figure 6.16, the superimposed transmission profiles of the dual overwritten uniform fibre Bragg grating structure consisted of polarization-selective and wavelength–selective stopbands from individual gratings denoted by G1 and G2. The wavelength spacing between the two uniform fibre Bragg gratings was controlled during fabrication to create spectral stopbands at desired Bragg wavelengths regardless of the intrinsic birefringence of the fibre. By matching the wavelength spacing $\Delta\lambda_{desired}$ to the wavelength separation between the co-located fibre laser cavities, an optical feedback device for the dual-wavelength, orthogonal polarization self-injection feedback scheme was realised. The superimposed transmission profiles of the dual co-located DFB fibre laser and the Hi-Bi grating structure are shown in Figure 6.17.

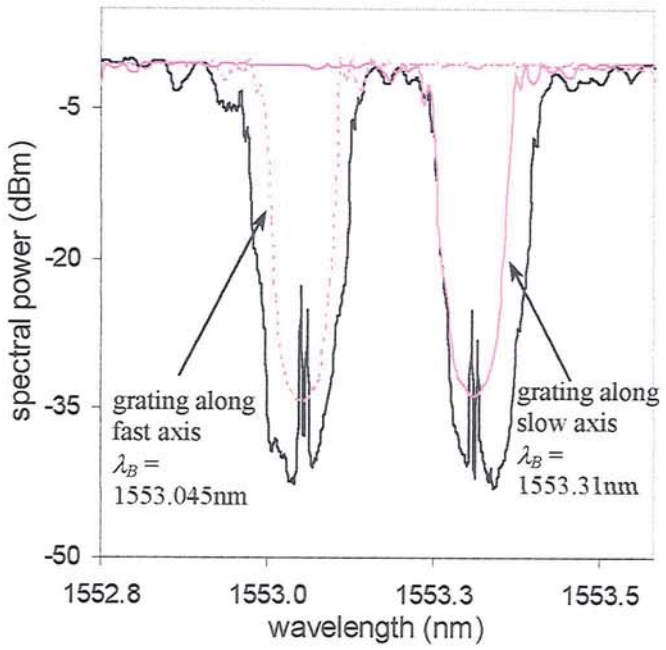

Figure 6.17 Superimposed transmission profiles of the dual co-located DFB fibre laser and the dual overwritten Hi-Bi fibre grating structure.

The Hi-Bi grating stopband centred at λ_B = 1553.045nm will reflect light along the fast axis to enable self-injection locking of the fibre laser cavity to operate on the polarization mode along identical axis. Similarly, the grating stopband along the slow axis centre at λ_B =1553.310nm coincided with the second fibre laser cavity to enable optical feedback and self-injection locking of the polarization mode along the slow axis only. Consequently, this mechanism will enable dual-polarization mode operation by forcing each DFB laser cavity to operate in one mutually orthogonal polarization mode only. The experimental setup of the fibre laser structure is as shown in Figure 6.18.

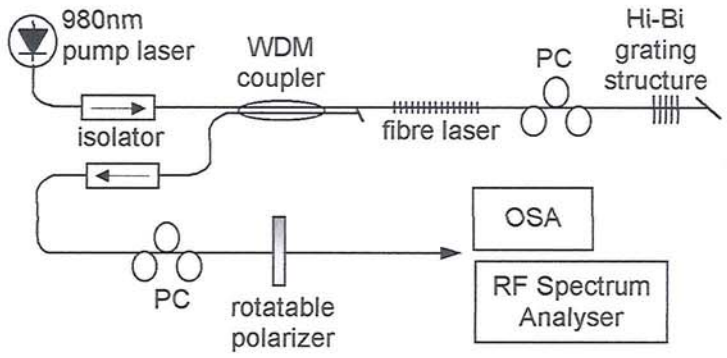

Figure 6.18 Operational setup for the co-located dual DFB fibre laser with self-injection locking feedback.

During operation, to reduce the effects of environmental perturbations, the fibre laser was placed in a temperature controller containing a Peltier device. The 27mm long Hi-Bi fibre grating was spliced to the end of the fibre laser and a polarization controller (PC) was placed in the feedback path to align the

polarization axes between the fibre laser and the grating. The optical output spectrum of the fibre laser revealed dual-mode operation with wavelength spacing measured at 0.26nm, corresponding closely to the passive measurement. As shown in Figure 6.19, tuning the polarizer enabled one or other of the two optical frequencies to be eliminated, indicating that they corresponded to the orthogonal polarization states. The output signal after the polarizer was then fed directly to a high-speed photodetector and the resulting electrical spectrum monitored on the RF spectrum analyser. The absence of any polarization mode beating (PMB) signal up to 3GHz on the RF spectrum analyser indicated that one polarization mode from each DFB laser cavity contributed to the dual-mode output. The fibre laser operation was stable with maximum differential power of < 0.25dBm due to polarization-dependent gain. On the higher frequency range, an electrical beat signal was measured at 32.5GHz, with an estimated linewidth of less than 1kHz. The obtained RF spectra are as shown in Figure 6.20 and Figure 6.21.

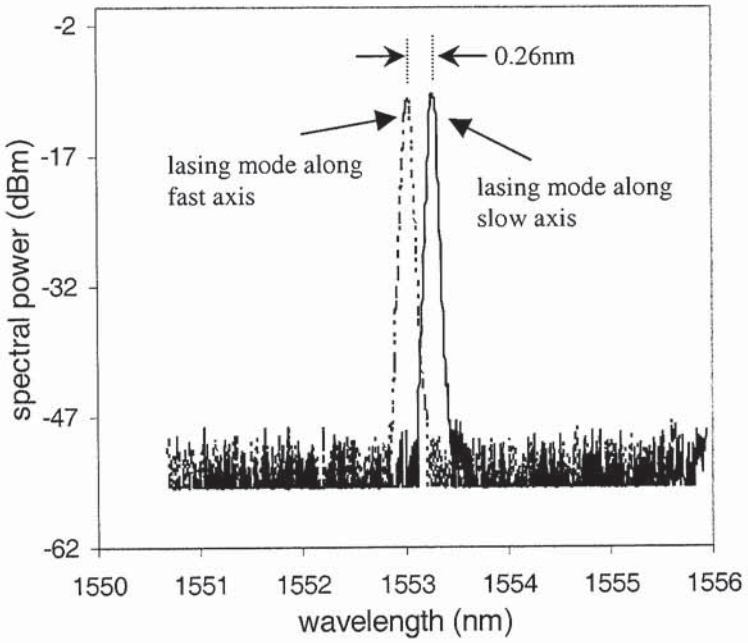

Figure 6.19 Optical output spectrum indicating dual-polarization mode operation.

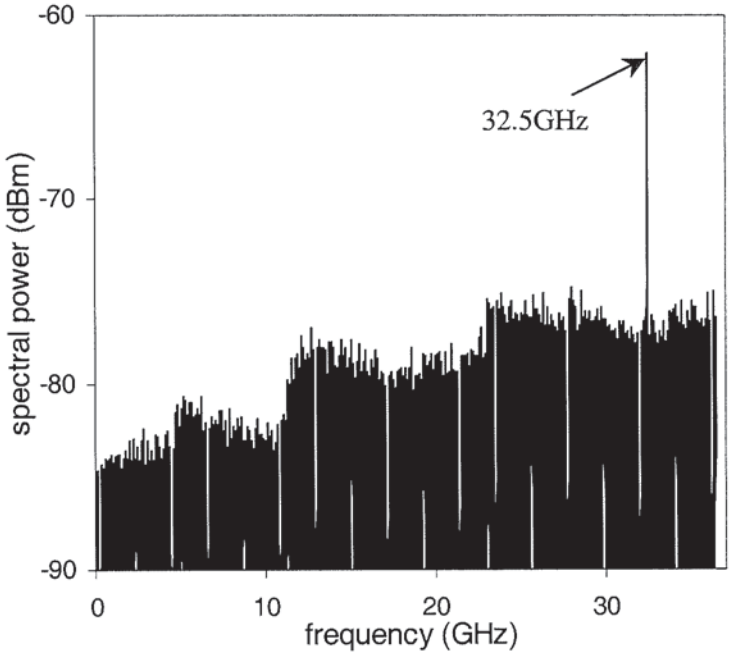

Figure 6.20 RF spectrum showing a single beat signal at 32.5GHz. The absence of beat signal at lower frequencies verified that one polarization mode from each laser cavity constituted the dual-mode output.

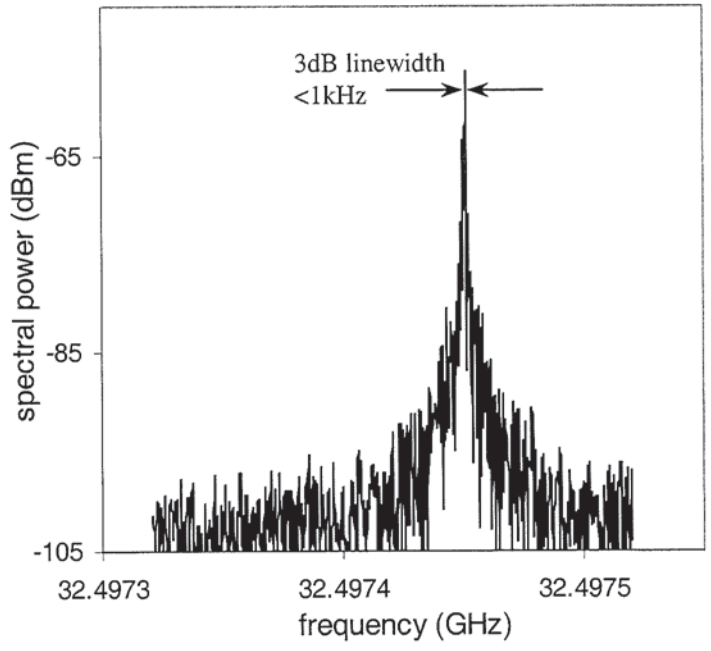

Figure 6.21 Beat signal at 32.5GHz showing linewidth <1kHz (measurement resolution 1kHz).

The narrow linewidth millimetre wave beat signal obtained highlighted the low phase noise present in the fibre laser device. Both the dual DFB fibre laser structure and the Hi-Bi fibre grating consisted of superimposed grating structures. The distinct feature of the superimposed fibre grating that differentiates itself from cascaded grating array or other forms of multiplexed grating structure lies in the fact the two

gratings, physically co-located, experience identical external perturbations under all circumstances. As a result, spectral wavelength separation can be made to remain constant in the presence of external perturbations. Device architectures based on the superimposed grating structure hence enable common mode suppression to external disturbances without the need to isolate/condition individual gratings. Despite the overall increase in length of the fibre laser structure with the self-injection locking scheme, the feedback paths for both laser cavities were within a single fibre. As a result, the overall configuration did not significantly compromise common mode suppression of phase noise in the beat signal generated.

The operation of the fibre laser was straightforward and with better stabilization of the laser, possibly with active feedback control, a 3dB beat linewidth of the order of a few Hertz should be possible. We emphasize the simplicity of the fabrication process, the flexibility achievable and the all-fibre nature of the configuration. The fabrication involves straightforward inscriptions of two phase-shifted gratings and uniform fibre Bragg gratings in conventional round-core active/standard fibres. Within the mechanical strength limitation of the fibre (~3%), wavelength separation of the order of tens of GHz (i.e tens or hundreds of pm) is easily achievable utilizing a prestrained fibre fabrication technique. As an example, an identical fibre laser configuration with wavelength separation 0.75nm was realised and the transmission profile of the laser structure is shown in Figure 6.22. A matching Hi-Bi fibre grating was fabricated for the self-injection feedback and the superimposed spectral profiles of the laser with the Hi-Bi grating is shown in Figure 6.23.

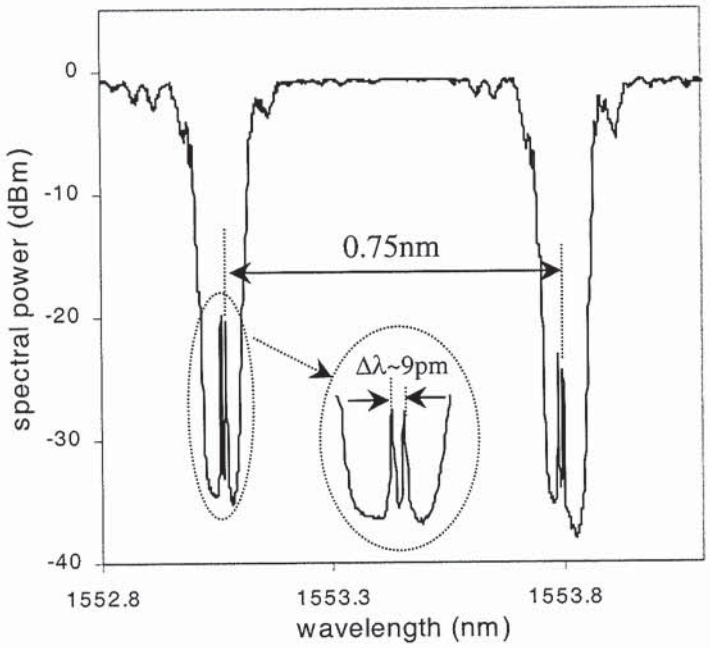

Figure 6.22 Transmission spectrum of the co-located dual DFB fibre laser with 0.75nm separation between the two laser cavities. Inset highlights the existence of polarization mode splitting with wavelength spacing measured 9pm.

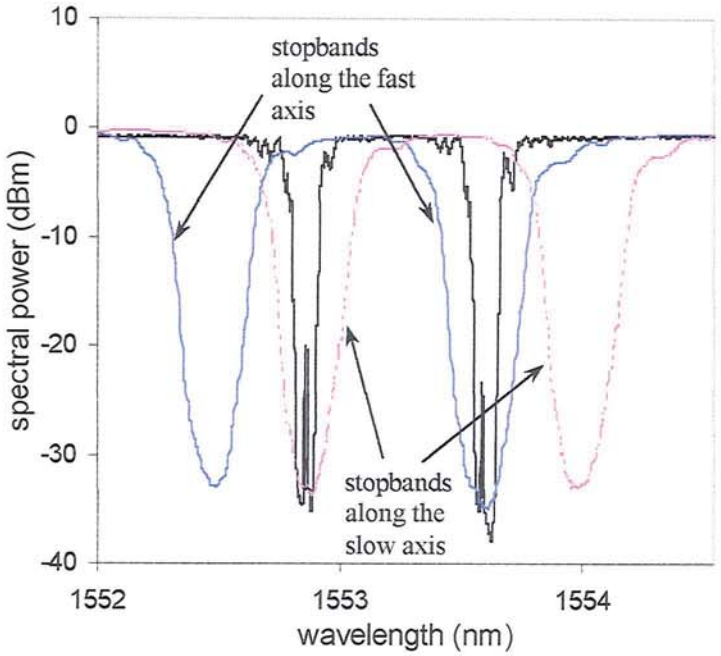

Figure 6.23 Superimposed spectra of the fibre laser and the matching Hi-Bi fibre grating for optical feedback in the self-injection locking path.

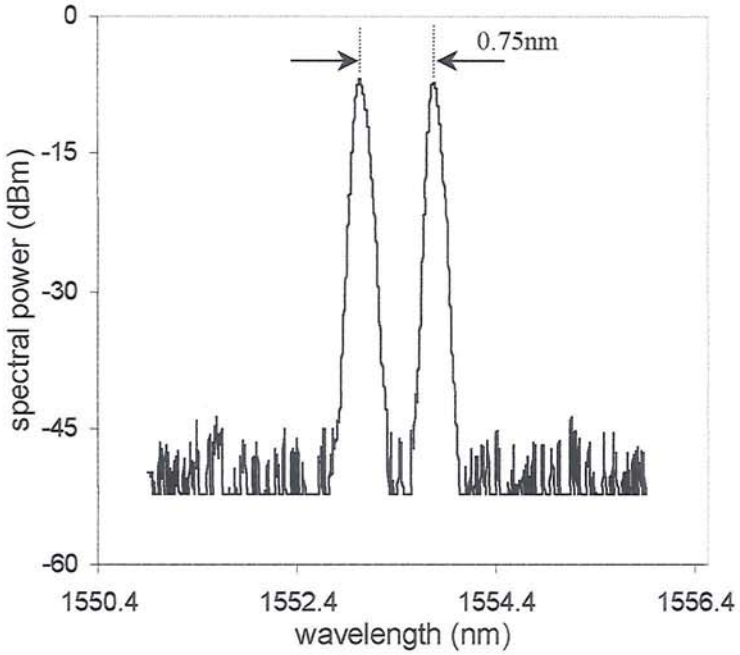

Figure 6.24 Optical output spectrum of the fibre laser. Wavelength separation measured 0.75nm as expected.

During operation, the fibre laser exhibited dual-polarization mode operation with wavelength separation of 0.75nm as expected. The corresponding heterdodyne signal formed by the lasing modes reached, in theory, 93.2GHz which was beyond the measurement range of our setup. The captured optical

output spectrum is shown in Figure 6.24. It is worth noting that using a second phase mask of appropriate periodicity to fabricate the second grating, frequency separation into the THz range (i.e. a few nm) can be easily achieved in this fibre laser configuration. Due to its dual-polarization output, the co-located dual DFB fibre laser has a potential advantage in the relative ease by which one polarization state can be selectively phase modulated before heterodyning. Phase shifts imposed on the millimetre wave signal by such means can be attractive for phased array antenna applications [59]. Furthermore, in contrast with reported dual longitudinal mode fibre grating laser schemes [38][86], output power equalization can be readily achieved by a single polarizer at the output. Apart from fibre-radio system applications, the proposed fibre laser device is also highly applicable as a dual-wavelength optical source for WDM optical communication systems. Compared to coupled cavity fibre laser structures [38][87] for the generation of dual-mode output, the proposed fibre laser configuration compares favourably in terms of its structural simplicity, ease of fabrication, flexibility in the wavelength separation achievable and most importantly, enabling common mode suppression of phase noise without the need for additional high frequency electronic devices or complex feedback controls.

6.5 Conclusions

A brief review of rare-earth doped fibre lasers has been given. In particular, the passive spectral profiles and operating characteristics of π phase-shifted DFB fibre lasers have been highlighted. The ability of a π phase-shifted DFB fibre laser to generate dual-polarization mode operation has been utilized for generating high spectral purity, narrow linewidth microwave heterodyne signal without the use of any costly RF electronic equipment. Based on the results obtained, the effectiveness of dual-mode operation from one fibre laser cavity for common mode suppression of phase noise between the lasing modes has been highlighted. To increase the beat frequency generated, a new technique based on asymmetric UV post-processing in phase-shifted DFB fibre lasers has been proposed and demonstrated. Frequency tuning based on transverse loading and thermal conditioning have been further employed. Towards optical generation of high frequency signals at millimetre wave regime and beyond, a novel co-located dual DFB fibre laser configuration has been proposed and demonstrated. Based on the merits of superimposed fibre grating structures, the proposed fibre laser configuration featured advantages like engineering/structural simplicity, ease of implementation and operation and high flexibility in the wavelength separations achievable. Similarly, high spectral purity millimetre wave signals with <1kHz linewidths have been obtained without the need for high frequency synthesizers and complex feedback controls due to common mode suppression of phase noise between the two lasing modes. Results obtained have illustrated that the fibre laser configurations offer potentially low cost, compact and simple alternatives to optical generation of very narrow linewidth microwave/millimetre wave signals.

6.6 References

[1] G. Evans, T. Wilcox, "Mode coupling and distributed feedback lasers in periodic fibre waveguides", *IEEE J. Quantum Electron.*, QE13(4), pp. 145-152, 1977.

[2] B.J. Ainslie, "A review of the fabrication and properties of Erbium doped fibres for optical amplifiers", *J. Lightwave Technol.*, 9(2), pp. 220-227, 1991.

[3] G. Meltz, W.W. Morey, W.H. Glenn, "Formation of Bragg gratings in optical fibres by a transverse holographic method", *Optics Lett.*, 14(15), pp. 823-825, 1989.

[4] S.B. Poole, D.N. Payne, R.J. Mears, M.E. Fermann, R.I. Laming, "Fabrication and characterization of low loss optical fibres containing rare-earth ions", *J. Lightwave Technol.*, LT4(7), pp. 870-876, 1986.

[5] B.J. Ainslie, S.P. Craig, S.T. Davey, "The absorption and fluorescence spectra of rare-earth ions in silica based monomode fibre", *J. Lightwave Technol.*, 6(2), pp. 287-291, 1988.

[6] L. Reekie, R.J. Mears, S.B. Poole, D.N. Payne, "Tunable single-mode fibre lasers", *J. Lightwave Technol.*, LT4(7), pp. 956-960, 1986.

[7] A. Larsson, S.Forouhar, J. Cody, R.J. Lang, P.A. Andrekson, "A 980nm pseudomorphic single quantum well laser for pumping erbium doped optical amplifiers", *Topical Meet. Amplifiers and Applications*, Monterey, CA, WA2, 1990.

[8] R.J. Mears, L. Reekie, S.B. Poole, D.N. Payne, "Low threshold tunable CW and Q-switched fibre laser operating at 1.55μm", *Electron. Lett.*, 22, pp. 159-160, 1986.

[9] R.I. Laming, S.B. Poole, E.J. Tarbox, "Pump excited state absorption in erbium doped fibres", *Optics Lett.*, 13(12), pp. 1084-1086, 1988.

[10] R.I. Laming, M.C. Farries, P.R. Morkel, L. Reekie, D.N. Payne et al, "Efficient pump wavelengths of erbium doped fibre optical amplifier", *Electron. Lett.*, 25, pp.12-14, 1989.

[11] M. Yamada, M. Shimizu, T. Takeshita, M. Okayasu, M. Horiguchi, S. Uehara, E. Sugita, "Er^{3+} doped fibre amplifier pumped by 0.98μm laser diodes", *IEEE Photon. Technol. Letters*, 1(12), pp. 422-424, 1989.

[12] M. Yamada, M. Shimizu, M. Okayasu, T. Takeshita, M. Horiguchi, Y. Tachikawa, E. Sugita, "Noise characteristics of Er^{3+} doped fibre amplifiers pumped by 0.98 and 1.48μm laser diodes", *IEEE Photon. Technol. Letters*, 2(3), pp. 205-207, 1990.

[13] W.L. Barnes, P.R. Morkel, L. Reekie, D.N. Payne, "High quantum efficiency Er^{3+} fibre lasers pumped at 980nm", *Optics Lett.*, 14(18), pp. 1002-1004, 1989.

[14] J.E. Townsend, W.L. Barnes, K.P. Jedrzejewski, "Yb^{3+} sensitised Er^{3+} doped silica optical fibre with ultrahigh transfer efficiency and gain", *Electron. Lett.*, 27(21), pp.1958-1959, 1991

[15] W.L. Barnes, P.R. Morkel, L. Reekie, D.N. Payne, "Er^{3+}-Yb^{3+} and Er^{3+} doped fibre lasers", *J. Lightwave Technol.*, 7(10), pp. 1461-1465, 1989.

[16] D.C. Hanna et al, "Efficient operation of an Yb^{3+} sensitised Er fibre laser pumped in the 0.8μm region", *Electron. Lett.*, 24, pp. 1068-1069, 1988.

[17] M. Ding, P.K. Cheo, "Effects of Yb:Er-codoping on suppressing self-pulsing in Er-doped fibre lasers", *IEEE Photon. Technol. Lett.*, 9(3), pp.324-326, 1997

[18] H.L. An, X.Z. Lin, H.D. Liu, "Intensity noise suppression by Ytterbium codoping in heavily erbium doped fibre lasers with partly clustered erbium ions", *Optics Lett.*, 25(24), pp. 1747-1749, 2000.

[19] J.T. Kringlebotn, P.R. Morkel, L. Reekie, J.L. Archambault, D.N. Payne, "Efficient diode pumped single frequency Erbium:Ytterbium fibre laser", *IEEE Photon. Technol. Lett.*, 5(10), pp.1162-1164, 1993.

[20] J.T. Kringlebotn, J.L. Archambault, L. Reekie, J.E. Townsend, G.G. Vienne, D.N. Payne, "Highly efficient low noise grating feedback Er^{3+}:Yb^{3+} codoped fibre laser", *Electron. Lett.*, 30(12), pp.972-973, 1994.

[21] Y. Kimura, M. Nakazawa, "Lasing characteristics of Er^{3+} doped silica fibres from 1553 up to 1603nm", *J. Applied Physics*, 64(2), pp. 516-520, 1988.

[22] M.S. O'Sullivan, J. Chrostowski, E. Desurvire, J.R Simpson, "High power narrow linewidth Er^{3+} doped fibre laser", *Optics Lett.*, 14(9), pp. 438-440, 1989.

[23] I.M. Jauncey, L. Reekie, R.J. Mears, C.J. Rowe, "Narrow linewidth fibre laser operating at 1.55μm", *Optics Lett.*, 12(3), pp. 164-165, 1987.

[24] I.M. Jauncey, L. Reekie, R.J. Mears, D.N. Payne, C.J. Rowe, D.C.J. Reid, I. Bennion, C. Edge, "Narrow linewidth fibre laser with integral fibre grating", *Electron. Lett.*, 22(19), pp. 987-988, 1986.

[25] I. Bennion, D.C.J. Reid, C.J. Rowe, W.J. Stewart, "High reflectivity monomode fibre grating filters", *Electron. Lett.*, 22(6), pp. 341-343, 1986.

[26] I.M. Jauncey, L. Reekie, J.E. Townsend, D.N. Payne, "Single longitudinal mode operation of an Nd^{3+} doped fibre laser", *Electron. Lett.*, 24(1), pp. 24-26, 1988.
[27] G.A. Ball, W.W. Morey, W.H. Glenn, "Standing wave monomode erbium fibre laser", *IEEE Photon. Technol. Lett.*, 3(7), pp. 613-615, 1991.
[28] J.L. Zyskind, V. Mizrahi, D.J. DiGiovanni, J.W. Sulhoff, "Short single frequency Erbium doped fibre laser", *Electron. Lett.*, 28(15), pp. 1385-1387, 1992.
[29] V. Mizrahi, D.J. DiGiovanni, R.M. Atkins, S.G. Grubb, Y.K. Park, Jean-Marc P. Delavaux, "Stable single-mode erbium fibre grating laser for digital communication", *J. Lightwave Technol.*, 11(12), pp. 2021-2025, 1993.
[30] J.L. Wagener, P.F. Wysocki, M.J.F. Digonnet, H.J. Shaw, "Effects of concentration and clusters in erbium doped fibre lasers", *Optics Lett.*, 18(23), pp. 2014-2016, 1993
[31] F.Sanchez, P.L.Boudec, P.L.François, G.Stephan, "Effects of ion pairs on the dynamics of erbium-doped fibre lasers", *Physics Review*, 48, 1993.
[32] H.L.An, E.Y.B. Pun, H.D. Liu, X.Z.Lin, "Effects of ion clusters on the performance of a heavily doped erbium doped fibre laser", *Optics Lett.*, 23(15),pp. 1197-1199, 1998.
[33] J.L. Zyskind, J.W. Sulhoff, P.D. Magill, K.C. Reichmann, V. Mizrahi, D.J. DiGiovanni "Transmission at 2.5Gbits/s over 654km using an erbium doped fibre grating laser source", *Electron. Lett.*, 29(12), pp.1105-1106, 1992.
[34] G.A. Ball, C.E. Holton, G. Hull-Allen, W.W. Morey, "60mW 1.5μm single frequency low noise fibre laser MOPA", *IEEE Photon. Technol. Lett.*, 6(7), pp. 192-194, 1994.
[35] L. Dong, W.H. Loh, J.E. Caplen, J.D. Minelly, K. Hsu, L. Reekie, "Efficient single frequency fibre laser with novel photosensitive Er/Yb optical fibres", *Optics Lett.*, 22(10), pp.694-696, 1997.
[36] K. Hsu, W.H. Loh, L. Dong, C.M. Miller, "Efficient and tunable Er/Yb fibre grating lasers", *J. Lightwave Technol.*, 15(8), pp. 1438-1441, 1997.
[37] W.H. Loh, R.I. Laming, "1.55μm phase-shifted distributed feedback fibre laser", *Electron. Lett.*, 31(17), pp. 1440-1442, 1995.
[38] S.V. Chernikov, R. Kashyap, P.F. McKee, J.R. Taylor, "Dual frequency all fibre grating laser source", *Electron. Lett.*, 29(12), pp. 1089-1091, 1993.
[39] L.B. Fu, M. Ibsen, J. Nilsson, D.J. Richardson, D.N. Payne, "Erbium-Ytterbium L-band fibre DFB laser pumped at 1534nm", *Proc. European Conference Optical Communications (ECOC)*, We2.6.6, Rimini, Italy, 2003.
[40] L. Fu, M. Ibsen, M. Mokhtar, M. Gunning, D. Richardson, D. Payne, "Wideband compression tuned all fibre DFB laser: Analysis and characterisation", *Proc. Optical Fibre Communication Conference (OFC)*, Atlanta, TuL3, 2003.
[41] H. Kogelnik, C.V. Shank, "Coupled wave theory of distributed feedback lasers", *J. Appl. Physics*, 43(5), pp. 2327-2335, 1972.
[42] M. Sargent III, W.H. Swantner, J.D. Thomas, "Theory of a distributed feedback laser", *IEEE J. Quantum Electron.*, QE16(4), pp. 465-472, 1980.
[43] K. Utaka, S. Akiba, K. Sakai, Y. Matsushima, "λ/4 shifted InGaAsP/InP DFB lasers", *IEEE Quantum Electron.*, QE22(7), pp. 1042-1051, 1986.
[44] J.T. Kringlebotn, J.L. Archambault, L. Reekie, D.N. Payne, "Er^{3+}:Yb^{3+} codoped fibre distributed feedback laser", *Optics Lett.*, 19(24), pp.2101-2103, 1994.
[45] M. Sejka, P. Varming, J. Hubner, M. Kristensen, "Distributed feedback Er^{3+} doped fibre laser", *Electron. Lett.*, 31(17), pp. 1445-1446, 1995.
[46] H.A. Haus, C.V. Shank, "Antisymmetric taper of distributed feedback lasers", *IEEE Quantum Electron.*, QE12(9), pp. 532-539, 1976.
[47] W.H. Loh, R.I. Laming, "1.55μm phase-shifted distributed feedback fibre laser", *Electron. Lett.*, 31(17), pp. 1440-1442, 1995.
[48] Z.E. Harutjunian, W.H. Loh, R.I. Laming, D.N. Payne, "Single polarisation twisted distributed feedback fibre laser", *Electron. Lett.*, 32(4), pp. 346-348, 1996.
[49] H. Storøy, B. Sahlgren, R. Stubbe, "Single polarisation fibre DFB laser", *Electron. Lett.*, 33(1), 1997.
[50] J.L. Philipsen, M.O. Berendt, P. Varming, V.C. Lauridsen, J.H. Povlsen, J. Hübner, M. Kristensen, B. Pálsdóttir, "Polarisation control of DFB fibre laser using UV-induced birefringent phase-shift", *Electron. Lett.*, 34(7), 1998.
[51] G.A. Ball, G. Meltz, W.W. Morey, "Polarimetric heterodyning Bragg grating fibre laser sensor", *Optics Lett.*, 18(22), pp. 1976-1978, 1993.
[52] S. Yamashita, G.J. Cowle, "Single polarization operation of fibre distributed feedback (DFB) lasers by injection locking", *J. Lightwave Technol.*, 17(3), pp. 509-513, 1999.

[53] W. Fan, B. Chen, X. Li, L. Chen, Z. Lin, "Stress-induced single polarization DFB fibre laser", *Optics Comm.*, 204, pp. 157-161, 2002.
[54] H.K. Kim, S.K. Kim, H.G. Park, B.Y. Kim, "Polarimetric fibre laser sensors", *Optics Lett.*, 18(4), pp. 317-319, 1993.
[55] H.K. Kim, S.K. Kim, B.Y. Kim, "Polarization control of polarimetric fibre laser sensors", *Optics Lett.*, 18(17), pp. 1465-1467, 1993.
[56] R. Heidemann, G. Veith, "mm-wave photonic technologies for Gbit/s-wireless-local-loop", *Proc. OECC*, Chiba, Japan, pp. 310-311, 1998.
[57] L. Noël, D. Wake, D.G. Moodie, D.D. Marcenac, L.D. Westbrook, D. Nesset, "Novel techniques for high capacity 60-GHz fibre radio transmission systems", *IEEE Trans. Microwave Theory and Tech.*, 45(8), pp. 1416-1423, 1997.
[58] Y. Li, A.J.C. Vieira, S.M. Goldwasser, P.R. Herczfeld, "Rapidly tunable millimetre wave optical transmitter for lidar-radar", *IEEE Trans. Microwave Theory and Tech.*, 49(10), pp. 2048-2053, 2001.
[59] W. H. Loh and C. L. Tang, "Polarisation modulation for optical microwave applications in phased array antennas", *IEEE Photon. Technol. Lett.*, 3(5), 1991
[60] S.K. Han, M.E. Ali, S.D. Jung, K.Y. Kang, H.R. Fetterman, "Application of near field optical fibre probes to millimetre wave optical heterodyne", *IEEE Trans. Microwave Theory and Tech.*, 47(7), pp. 1381-1384, 1999.
[61] P.A. Davies, A.P. Foord, K.E. Razavi, "Millimetre wave signal generation by optical filtering of frequency modulated laser spectra", *Electron. Lett.*, 31(20), pp. 1754-1756, 1995.
[62] J.J. O'Reilly, P.M. Lane, "Fibre supported optical generation and delivery of 60GHz signals", *Electron. Lett.*, 30(16), pp. 1329-1330, 1994.
[63] H. Schmuck, "Comparison of optical millimetre wave concepts with regard to chromatic dispersion", *Electron. Lett.*, 31(21), pp. 1848-1849, 1995.
[64] C.R. Lima, D. Wake, P.A. Davies, "Compact optical millimetre wave source using a dual mode semiconductor laser", *Electron. Lett.*, 31(5), pp. 364-366, 1995.
[65] R.P. Braun, G. Grosskopf, R. Meschenmoser, D. Rohde, F. Schmidt, G. Villino, "Microwave generation for bidirectional broadband mobile communications using optical sideband injection locking", *Electron. Lett.*, 33(16), 1997.
[66] D. Novak, R.S. Tucker, "Millimetre wave signal generation using pulsed semiconductor lasers", *Electron. Lett.*, 30(17), pp. 1430-1431, 1994.
[67] L. Goldberg, A.M. Yurek, H.F. Taylor, J.F. Weller, "35GHz microwave signal generation with an injection locked laser diode", *Electron. Lett.*, 21(18), pp. 814-815, 1985.
[68] Y.J. Wen, H.F. Liu, D. Novak, Y. Ogawa, "Millimetre wave signal generation from a monolithic semiconductor laser via subharmonic optical injection", *IEEE Photon. Technol. Lett.*, 12(8), pp. 1058-1060, 2000.
[69] H.W. Yen, M.K. Barnoski, "Optical injection locking and switching of transistor oscillators", *Appl. Phys. Lett.*, 32, pp. 182-184, 1978.
[70] Z. Ahmed, H.F. Liu, D. Novak, M. Pelusi, Y. Ogawa, D.Y. Kim, "Low phase noise millimetre wave signal generation using a passively modelocked monolithic DBR laser injection locked by an optical DSBSC signal", *Electron. Lett.*, 31(15), pp. 1254-1255, 1995.
[71] L. Noel, D. Marcenac, D. Wake, "Optical millimetre wave generation technique with high efficiency, purity and stability", *Electron. Lett.*, 32(21), 1996.
[72] J. O'Reilly, P. Lane, "Remote delivery of video services using mm-wave and optics", *J. Lightwave Technol.*, 12(3), pp. 369-375, 1994.
[73] T. Yamamoto, H. Takara, S. Kawanishi, "270-360GHz tunable beat signal light generator for photonic local oscillator", *Electron. Lett.*, 38(15), 2002.
[74] R.T. Ramos, A.J. Seeds, "Delay, linewidth and bandwidth limitations in optical phase-locked loop design", *Electron. Lett.*, 26(6), 1990.
[75] R.T. Ramos, A.J. Seeds, "Fast heterodyne optical phase lock loop using double quantum well laser diodes", *Electron. Lett.*, 28(1), pp. 82-83, 1992.
[76] M. Hyodo, M. Watanabe, "Optical generation of millimetre wave signals up to 110GHz by phase locking of two external cavity semiconductor lasers", *Electron. Lett.*, 38(25), 2002.
[77] D. Wake, C.R. Lima, P.A. Davies, "Optical generation of millimetre wave signals for fibre radio systems using a dual mode DFB semiconductor laser", *IEEE Trans. Microwave Theory and Tech.*, 43(9), pp. 2270-2276, 1995.
[78] M. LeBlanc, S.T. Vohra, T.E. Tsai, E.J. Friebele, "Transverse load sensing by use of pi-phase shifted fibre Bragg grating", *Optics Lett.*, 24(16), pp. 1091-1093, 1999.

[79] T. Erdogan, V. Mizrahi, "Characterization of UV-induced birefringence in photosensitive Ge-doped silica optical fibres", *J. Opt. Soc. Am.*, 11(10), pp. 2100-2105, 1994.
[80] W.H. Loh, J.P. de Sandro, G.J. Cowle, B.N. Samson, A.D. Ellis, "40GHz optical millimetre wave generation with a dual polarization distributed feedback fibre laser", *Electron. Lett.*, 33(7), pp. 594-595, 1997.
[81] C.D. Nabors, A.D. Farinas, T. Day, S.T. Yang, E.K. Gustafson, R.L. Byer, "Injection locking of a 13W CW Nd:YAG ring laser", *Optics Lett.*, 14(21), pp. 1189-1191, 1989.
[82] B. Meziane, F. Sanchez, G.M. Stephan, P.L. François, "Feedback induced polarization switching in a Nd-doped fibre laser", *Optics Lett.*, 19(23), pp. 1970-1972, 1994.
[83] S. Yamashita, K. Hsu, "Single frequency, single polarization operation of tunable miniature Erbium:Ytterbium fibre Fabry-Perot lasers by use of self-injection locking", *Optics Lett.*, 23(15), pp. 1200-1202, 1998.
[84] S. Yamashita, K. Hsu, T. Murakami, "High performance single frequency fibre Fabry-Perot laser (FFPL) with self-injection locking", *Electron. Lett.*, 35(22), pp. 1952-1953, 1999.
[85] S. Yamashita, G.J. Cowle, "Single polarization operation of fibre distributed feedback (DFB) lasers by injection locking", *J. Lightwave Technol.*, 17(3), pp. 509-513, 1999.
[86] S. Taccheo, G. Sorbello, G. Della Valle, P. Laporta, G. Karlsson, F. Laurell, W. Margulis, S. Cattaneo, "Generation of micro- and THz-waves at 1.5μm by dual frequency Er:Yb laser", *Electron. Lett.*, 37(24), 2001.
[87] R. Kashyap, S. V. Chernikov, and J. R. Taylor, "Fibre laser and beat frequency sources based on fibre gratings for microwave and ultrafast processing", *International J. Optoelectron.*, 11(2), pp.87-92, 1997.

Chapter 7: Mode assessment and optimisation of fibre laser operation

7.1 Overview

Single longitudinal mode fibre lasers are currently finding a wide range of applications in fibre sensor and optical communication systems. In particular, narrow linewidth operations of fibre lasers by the incorporation of mode-selective elements such as fibre Bragg gratings (FBG) are useful for Dense Wavelength Division Multiplexed (DWDM) communication systems, optical metrology and high-resolution spectroscopy applications [1]. For these applications, the oscillating frequency of the fibre laser must be well defined and stabilized. In fibre sensor applications, the precision of the wavelength-encoded optical sensors is in many cases limited by the accuracy by which the optical frequency of the interrogating source can be controlled or stabilized [2]. Therefore, apart from a proper fibre laser cavity design, considerable efforts have been put into monitoring and enhancing longitudinal mode stability during operation [3][4]. In this chapter, a brief review of some of the wavelength stabilization techniques for fibre lasers is outlined. The importance of cavity mode condition monitoring is highlighted. Based on a superimposed cavities structure, a unique cavity mode condition monitoring and optimisation scheme is presented. Illustration of the proposed scheme in the operation of a distributed Bragg reflector (DBR) fibre laser is presented. Extension of the proposed concept to the DFB fibre laser is further demonstrated.

7.2 Stabilization of fibre grating laser operation

Since the early demonstration of a narrow linewidth single longitudinal mode fibre laser operation [5], fibre gratings have been particularly attractive for line-narrowing fibre lasers since they provide a route towards compact integrated all-fibre laser devices. The use of fibre Bragg gratings for cavity feedback and mode selectivity are attractive for their engineering simplicity, reproducibility and convenient wavelength selectivity during manufacturing. When properly designed, the fibre grating lasers enforce single longitudinal mode operations, making them plausible alternatives to semiconductor laser technology as optical sources [6][7]. Various fibre laser configurations, notably the distributed feedback fibre laser (as described in the previous chapter) and the distributed Bragg reflector (DBR) fibre laser have been proposed and demonstrated. Single-mode operation is maintained, in general by two mechanisms. Firstly, the narrow cavity feedback spectral bandwidth of the fibre grating structure limits the number of longitudinal modes within the gain profile. Secondly, within the cavity resonance mode structure, the differential losses between the dominant mode and the neighbouring modes are sufficient to keep all but the dominant mode below lasing threshold [6][8]. On the other hand, the steady state lasing operation of the fibre laser has been known to be easily perturbed by ambient effects [9][2][10] since the fibre grating structures that constitute the fibre laser cavity are sensitive to thermal and mechanical disturbances. Most notably, the pump-induced thermal effects, as highlighted in section 5.3, can cause large thermally-induced index changes and introduce phase

variations in the grating structures [4]. Due to the large pump absorption in rare-earth doped fibres, the temperature rise within the fibre laser cavity is significant and unevenly distributed along the cavity. The resultant thermo-optic effect then leads to Bragg wavelength shift and grating chirp which detune the cavity resonance mode structure. Consequently, the output performance deteriorates and exhibits mode hopping with pump power variation [10]-[13]. Without proper monitoring and countermeasures, the pump-induced thermal detuning can even inhibit lasing operation [10][13].

To alleviate the pump-induced thermal effect and the associated temperature distribution in the fibre laser cavity, the heat dissipation rate along the fibre laser was increased by placing the laser on an aluminium block or by inserting the fibre laser into a metal ferrule [14][15]. To stabilize the output wavelength, techniques using fibre interferometer or gas cell were generally adopted [15]-[19]. In all reported cases, the stabilization schemes essentially only monitor and maintain the obtained output frequency. Furthermore, stabilization schemes based on gas cells may be limited in their operating wavelengths by the distribution of the absorption lines [16]. The interferometric technique, on the other hand, requires stringent environmental isolation and stabilization of the fibre interferometer during operation. The sensitivity of the laser to ambient effects is ultimately reduced to that of the residual sensitivity of the locking interferometer. Above all, these schemes alleviate pump-induced thermal effects by simply increasing the heat conductivity of the fibre laser through an external heat sink material. Without feedback control, direct thermal conditioning through heat dissipation may not be sufficient to counter fast, wide environmental excursions and pump power variations. The laser performance remains dependent on the thermal properties or conditions surrounding it and without feedback control can lead to over-cooling or under-cooling situations.

In contrast with fibre lasers, wavelength stabilization and mode optimisation have been proposed and incorporated in semiconductor laser technology to ensure high reliability and to achieve optimised output performance [20]-[26]. These monitoring and feedback mechanisms stabilize not only the Bragg frequency but also the cavity mode conditions. For optimised single-mode operation, the mode monitoring and feedback schemes ensure the lasing mode and the Bragg wavelength coincide, thus maximizing the output side mode suppression ratio (SMSR) and ensure operation away from a mode hop condition [21][23]. Consequently, the laser operation is highly robust against ambient effects and exhibits high performance integrity during tuning operation. To date, such direct cavity mode condition monitoring and optimisation schemes have remained a missing key element in fibre laser systems. For applications involving wavelength tuning, cavity mode condition monitoring and feedback controls are vital to prevent operating near the onset of mode hopping and to ensure performance integrity over the operation band. Similar to semiconductor lasers, it is important during tuning of the fibre laser cavity to match the wavelength shift between the Bragg frequency and cavity modes wavelengths [26]-[28]. Any mismatch due to non-uniform tuning or pump-induced thermal effect can lead to mode hopping or performance degradation [12]. To the best of our knowledge, longitudinal mode stabilization schemes reported to date only address long-cavity-length fibre laser structures [29][30]. These techniques generally involve incorporating one or multiple subcavities and the cavity mode condition monitoring requires additional filters or modulators to enable its operation and derivation of error signals [29][30]. Active stabilization schemes implemented by means of modulating the fibre laser output followed by phase detection have also been illustrated [31]-[33]. The proposed scheme

[31] involved probing the laser cavity with a signal obtained by modulating a fraction of the laser output at a frequency equivalent to the mode spacing (or integer multiples of it). The required feedback signal was then derived by taking the difference of the phase responses of the sidebands of the probe signal. Evidently, apart from the need to place a phase modulator into the laser cavity, such a stabilization configuration may be limited by the bandwidths of the modulator and detector required, in particular for wide cavity mode spacing. To eliminate the need to integrate into the cavity an additional modulator, methods based on dithering the cavity wavelength-selective filter have been demonstrated [32][33]. Besides a potential issue with parasitic modulation of the laser output frequency [32][33], such stabilization schemes require careful optimisation of the modulation depth for optimal performance. More importantly, as with all of these mode stabilization techniques, the proposed scheme compromised the simplicity of fibre laser configuration and increased the complexity of the cavity structure. The need to employ various filters and optical components limit their applications where a simple, compact device structure is of practical importance. Despite the ability to sustain robust single-mode operations, these stabilization mechanisms essentially only insure the lasing mode is far from a mode hop condition during operation. This does not necessary imply the best performance in terms of, for example, maximum SMSR and lowest threshold.

To date, pump-induced thermal effects remain an important issue in the operation of DFB and DBR fibre laser configurations [34][35]. Mode assessment and feedback mechanisms for suppression of mode hopping, frequency stabilization and mode optimisation are still major goals to be achieved in these useful fibre laser structures. It is worth noting that the optimisation of fibre laser conditions is increasingly important, in particular, for high power fibre lasers as indicated by previous studies [36]. In fact, careful management of thermal effects in fibre lasers can determine the efficiency and success of scaling-up efforts [36] and feedback schemes can play an important role. In the following sections, a novel technique for direct cavity mode condition monitoring and optimisation of linear-cavity fibre lasers during operation is presented. The proposed technique is particularly suitable for short-cavity-length fibre grating laser configurations and does not require incorporation of addition components into the laser cavity. For illustration, optimisation for the single-mode operation of a highly doped Er/Yb DBR fibre laser and a DFB fibre laser for DWDM applications are presented.

7.3 Cavity mode assessment and optimisation scheme based on superimposed fibre laser cavities structure

It has been demonstrated that for a dual overwritten fibre grating laser structure, the spectrum of the individual cavities (denoted as primary cavity and secondary cavity) can remain independent of each other [37][38]. As detailed in Chapter 6, physically co-located, superimposed fibre laser operations exhibit common mode suppression of environmental perturbations to enable low phase noise, narrow linewidth heterodyne signal generations. Based on the fact that the perturbations incurred in the laser structure are imposed simultaneously onto both cavities, the spectral variations incurred in both fibre laser grating structures are hence identical. The amount of spectral changes, thereby cavity resonance mode conditions, can be obtained from either of the two grating structures. In fact, the overwritten cavities mutually mirror each other's cavity mode condition variations under all circumstances. By designing the superimposed

secondary grating structure 1) at a spectral location away from the peak gain region and 2) with a lower grating coupling strength (κL) such that its lasing threshold is not reached, the secondary cavity will remain passive during operation and serves to mirror the mode conditions in the active primary cavity only. The high finesse resonance peaks in the passive grating structure allow continuous, accurate and even remote wavelength and mode condition monitoring to a very high accuracy and resolution. Determination of whether the laser is near a mode-hop or detuned from the Bragg centre is achieved by examining this correlated passive secondary cavity. Utilizing the spectral information of the secondary structure, an error signal is generated by the deviation of Bragg centre and resonance peaks' positions from the desired optimum and a truly cavity mode conditioning feedback mechanism is realised. The proposed structure essentially exploits the concept and simplicity of superimposed fibre grating structures and is applicable to all linear cavity configurations. It is particularly advantageous for short structural length designs since it does not require integration of any additional components into the laser cavity. It does not compromise the simplicity of the fibre laser configuration or increase markedly the complexity of the cavity and its operation. With the knowledge of the exact operation regime of the fibre laser, it is then possible to optimise the lasing mode and to enable robust applications over varying pump powers and environmental conditions.

7.3.1 Optimisation of a DBR fibre laser operation

The distributed Bragg reflector (DBR) fibre laser configuration [6] is one of the most commonly adopted single-mode fibre laser configuration for a wide range of communication, sensor and spectroscopy applications. The laser configuration in its elementary form comprises of a length of rare-earth doped fibre enclosed by two fibre Bragg grating reflectors. This simple resonator configuration is illustrated in Figure 7.1.

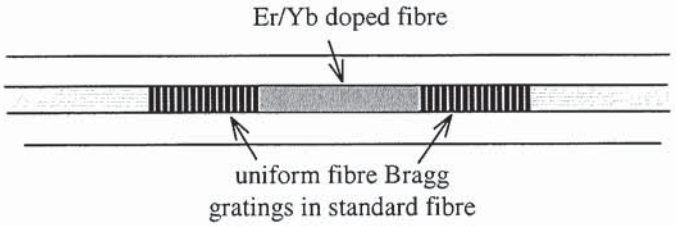

Figure 7.1 Linear DBR fibre laser configuration.

Each fibre Bragg grating is characterized by a reflectivity spectrum which has a peak reflectivity and an associated bandwidth. These intra-core Bragg reflectors function as both cavity feedback and mode discriminators. The resultant overlapped spectral bandwidth of the two gratings determines the wavelength range in which oscillations can occur in the resonator. For a fixed cavity length and within the resultant spectral bandwidth, a number of resonance modes satisfy the roundtrip phase condition (i.e. multiples of 2π) [21]. Each resonance mode corresponds to a potential lasing mode and as the laser gain increases through optical pumping, the mode with the lowest threshold begins lasing operation and dominates as the cavity main mode. The wavelength separation between the resonance modes in the laser cavity is simply given by

$$\Delta\lambda_{FSR} = \frac{\lambda^2}{2nL} \tag{7.1}$$

where λ denotes the average wavelength, n is the effective cavity refractive index and L is the effective cavity length. Single-mode operation in the DBR fibre laser configuration is achieved when the differential losses between the dominant mode and the neighbouring modes are sufficient to keep all but the dominant mode below lasing threshold [39]. The condition for single-mode operation is dependent on both the gain and the loss for the two lowest loss cavity modes [39][40]. Since the gain medium is considered homogenous and constant over the narrow grating bandwidth, the gain is essentially constant for both modes [40]. Mode discrimination must therefore result from the cavity loss mechanism. Due to the use of fibre Bragg gratings for cavity feedback, a differential loss as a function of wavelength is naturally imposed on the cavity [40]. Two neighbouring longitudinal modes will therefore see different cavity losses. Due to the low propagation loss in the fibre and the low grating insertion loss, the primary loss mechanism in the DBR fibre laser cavity is given by [30]

$$\gamma = -ln[R_1(\lambda)R_2(\lambda)] \tag{7.2}$$

where $R_1(\lambda)$ and $R_2(\lambda)$ are the reflectivity functions of the fibre Bragg gratings. Using a short cavity length, based on (7.1), the free spectral range of the resonance modes increases and only a few longitudinal modes have frequencies within the gain bandwidth of the grating (hence laser cavity). Consequently, for a narrowband steep-slope fibre grating reflection spectrum, this implies an increase in the differential losses between the dominant and neighbouring modes and therefore enhances mode discrimination. The loss in the laser cavity, given by (7.2), is minimum at the Bragg grating line centre. Analogous to the semiconductor DBR laser, the required pump is minimum when the cavity mode and the reflection peaks of the DBR mirrors are aligned. Locking to such a minimum ensures stable single-mode operation since it maximizes mode discrimination and improves output performances like SMSR.

The stability of the single-mode operation of the DBR fibre laser configuration is compromised when the lasing mode is detuned and the cavity losses of the neighbouring modes decrease, relative to the increasing cavity loss of the dominant mode, to the point that multimode operation regime is reached [39][40]. Ideally, the dominant lasing mode of the DBR fibre laser is located at the Bragg grating line centre for optimised performance [41][22][21]. Deviation from the Bragg centre degrades the output performance (increases the lasing threshold, reduces SMSR) and leads to mode hopping when the differential loss between the two lowest loss modes is insufficient to maintain single-mode operation. At the point when the losses are approximately equal, the laser will mode hop one free spectral range up/down in frequency [39]. The stability of the single-mode operation hence relies on sustaining the fibre optical path length since thermal, acoustic and mechanical perturbations can easily create a small optical path length variation of $\lambda/2n$ to shift the resonance one free spectral range [40]. More importantly, it is vital to maintain the dominant resonance mode at the Bragg centre for optimised performance [23][25]. It is, hence, necessary to monitor

both the cavity mode conditions and Bragg frequency to enable optimised single-mode operation from the DBR fibre laser [24].

Figure 7.2 illustrates the transmission profile of a DBR fibre laser cavity fabricated in the experiment. The laser structure consisted of two 25mm long uniform FBGs (Bragg wavlength =1535.5nm, strength parameter κL ~2.1) in standard fibre and a 30mm length of highly doped Er/Yb fibre (absorption at 979nm =730dB/m) as the gain medium. As highlighted in Figure 7.2, within the stopband width of the uniform fibre gratings, a number of resonance frequencies satisfying the round trip phase condition manifested as resonance peaks. Each resonance peak in the laser cavity corresponded to a potential lasing longitudinal mode. The resonance mode closest to the Bragg centre will experience the lowest threshold, and thus become the dominant lasing mode.

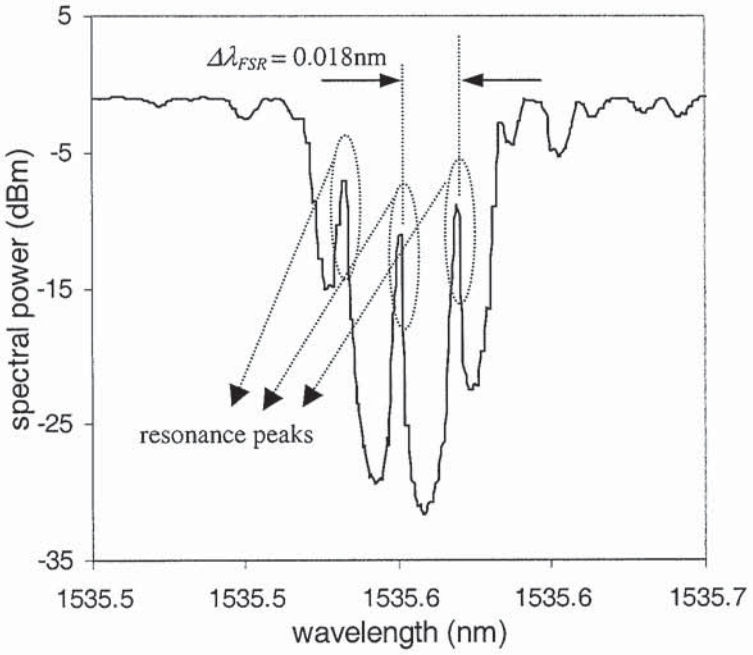

Figure 7.2 Measured transmission profile of a DBR fibre laser cavity.

At the same physical location, an identical secondary grating structure with grating parameters of Bragg wavelength =1566.9nm, κL ~1.4 was fabricated. The schematic diagrams depicting the realisation of such a fibre laser structure are illustrated in Figure 7.3.

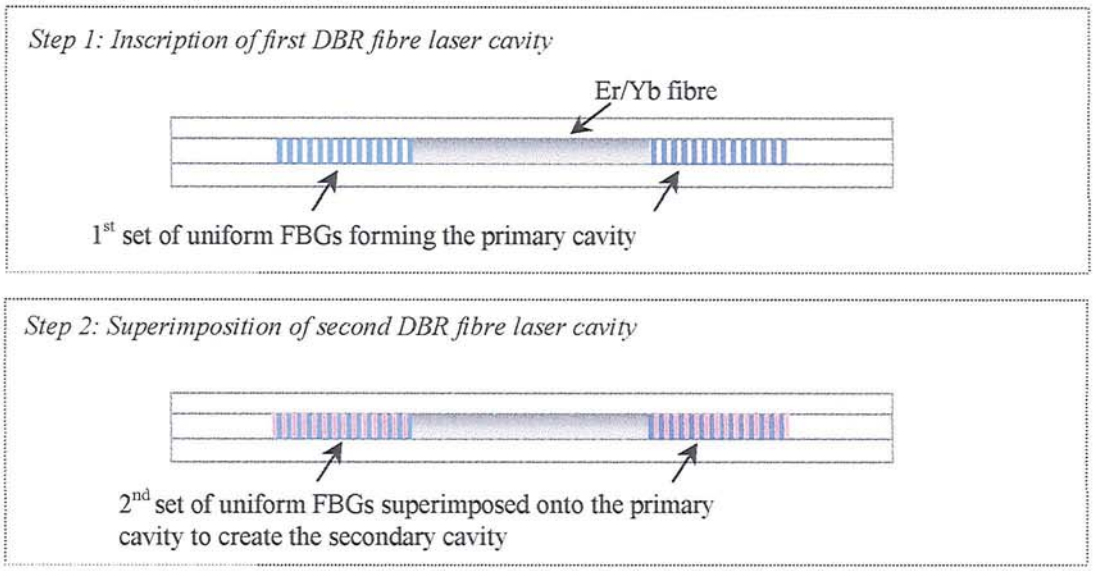

Figure 7.3 Schematic diagrams illustrating the realisation of superimposed fibre laser cavities structure.

The spectral profile of the superimposed secondary cavity was measured and shown in Figure 7.4. Due to the weaker grating strength enclosing the secondary cavity, the peak loss of the transmission spectrum was less than that of the primary laser cavity shown in Figure 7.2. The spectral profile similarly exhibited resonance peaks corresponding to resonance frequencies that satisfied the round trip phase condition in the secondary grating structure. Due to the difference in the Bragg frequency, the initial resonance mode structure of the secondary cavity differed from that of the primary cavity.

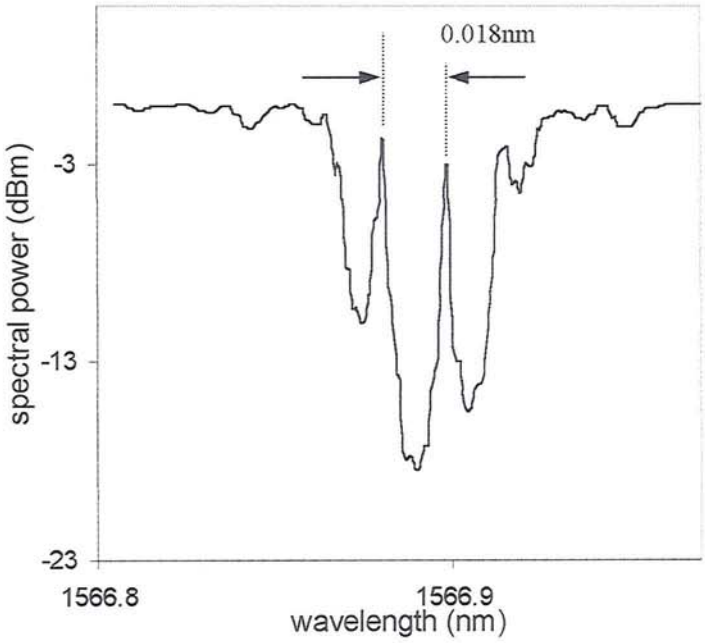

Figure 7.4 Measured transmission profile of the superimposed secondary grating cavity.

Below the lasing threshold, as the pump power increased, the resonance peaks shifted continuously within the Bragg grating spectrum due to pump-induced thermo-optic effects in the Er/Yb fibre. The

refractive index variations with pump power measured ~$0.6x10^{-5}$/mW in both cavities. More importantly, the thermally-induced index variations affected simultaneously the resonance mode structures in both cavities. The spectral profiles of the secondary grating structure served to mirror the exact mode condition variations in the primary laser cavity. This is illustrated in Figure 7.5.

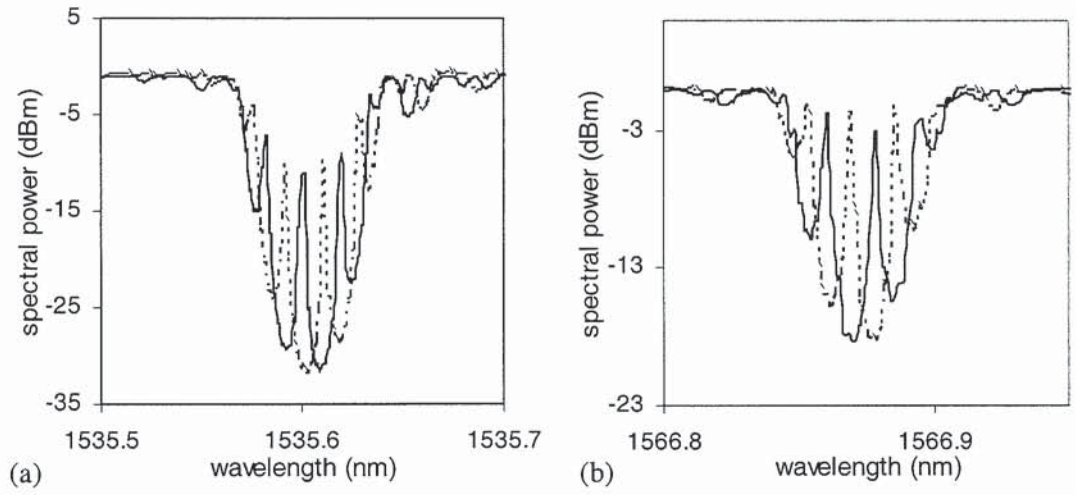

Figure 7.5 Spectral profile variations, due to pump-induced thermal effect in the Er/Yb fibre cavity, manifested in both (a) the primary and (b) the secondary cavities.

Over a pump power variation of 2mW (below the lasing threshold), the resonance mode structure in the primary cavity shifted by 9pm (~half a FSR) corresponding to an index variation of $1.2x10^{-5}$. Despite the initial difference in the resonance structure, the variations in the resonance peaks in both cavities due to perturbations remained consistent to one another. Expectedly, the resonance peaks in the secondary structure similarly shifted towards longer wavelength by 9pm (limited by 1pm measurement resolution), again corresponding to index variation in the cavity of $1.2x10^{-5}$. Evidently, the spectral information of the secondary cavity can effectively serve to indicate the cavity mode conditions in the primary cavity.

Under small resonator optical path length perturbations, the resonance modes of the resonator will shift under the Bragg grating spectrum and the free spectral range will not vary significantly [40]. In a similar context, the resonance modes in the cavity can therefore be controlled by inducing a small optical path length variation in the cavity fibre through straining. Based on the DBR fibre laser configuration described above, for a cavity fibre of length 30mm, simulation results indicated that the required induced length variation to cause the resonance mode structure to shift half a FSR (i.e. 9pm) was 0.27μm. The spectral variation due to the induced cavity strain is illustrated in Figure 7.6. Using a piezoelectric transducer (PZT) of length 7mm, the required strain was therefore 0.004% which was easily achievable in practice.

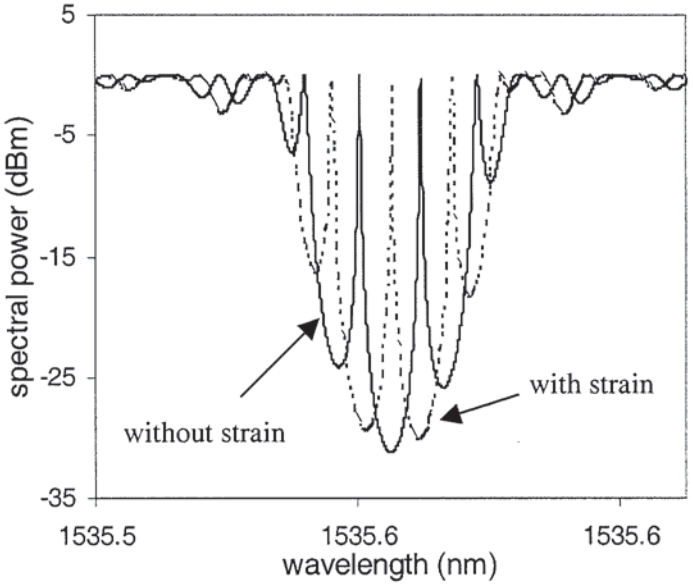

Figure 7.6 Simulated transmission profiles of the DBR fibre laser structure when the cavity fibre was subjected to an induced length variation of 0.27μm.

Experimentally, a short PZT (7mm long) was adhered to the Er/Yb fibre as a means to alter the cavity mode conditions. Over an applied voltage range of 0 to 6.24V, the PZT induced the required strain of 0.004% to shift the primary laser cavity modes by half a free spectral range as shown in Figure 7.7a. As expected, identical variations to the resonance mode structure in the secondary cavity were experienced as shown in Figure 7.7b. Furthermore, the amount of wavelength shift in the resonance peak varies linearly with applied PZT voltage.

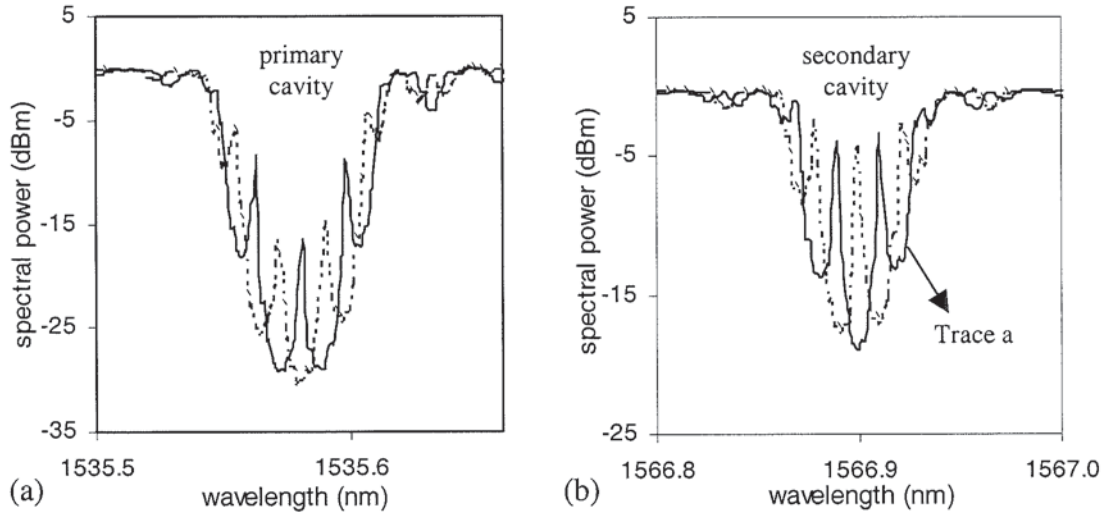

Figure 7.7 Passive spectral profiles of (a) the primary cavity and (b) the secondary cavity subjected to an induced strain of 0.004% on the cavity length.

The results further verified the functionality of the secondary passive structure as a means to mirror variations in the primary laser cavity. One can correlate the spectrum of the secondary cavity to that of the primary cavity. In particular, by maintaining the spectral profile indicated as Trace a in Figure 7.7b, the dominant longitudinal mode of the primary laser cavity will reside at the Bragg grating line centre, enhancing single-mode operation with optimised performance. It is important to note that direct measurement of the spectral profiles of the primary cavity during lasing operation is not feasible as the lasing mode saturates the detector and obscures spectral features around it. This will be illustrated in the latter part of this section.

It is worth noting that the Bragg wavelength selection for the superimposed secondary cavity is not of critical importance to the operation of the DBR fibre laser since the secondary cavity remains passive during operation and only serves to mirror the mode conditions in the active primary cavity. To reduce the gain in the secondary cavity during operation, its Bragg wavelength is chosen to be far away from the gain peak of Er^{3+} (~1535nm). In conjunction with gratings of weak feedback strength (i.e. reflectivity), the secondary cavity will not reach lasing threshold and remains passive during operation. The latter plays a more important role on inhibiting lasing operation in the secondary cavity. Hence, the Bragg wavelength selection of the secondary cavity is not critical.

The operational setup of the fibre laser is shown in Figure 7.8. For demonstration, only a straightforward approach was adopted for the feedback control mechanism in this work. A fast scanning tunable laser (max.100nm/sec, 1pm resolution, calibrated by the wavemeter) and a high-speed detector were used to probe real-time the spectral profile of the passive secondary grating structure during laser operation. A computer acquired the spectral data from the detector and applied control signals to the PZT drivers to alter the cavity mode conditions. Optical filters A and B were used to isolate the probe signal and the fibre laser output respectively. No special attention was necessary to isolate any part of the entire setup from ambient perturbations.

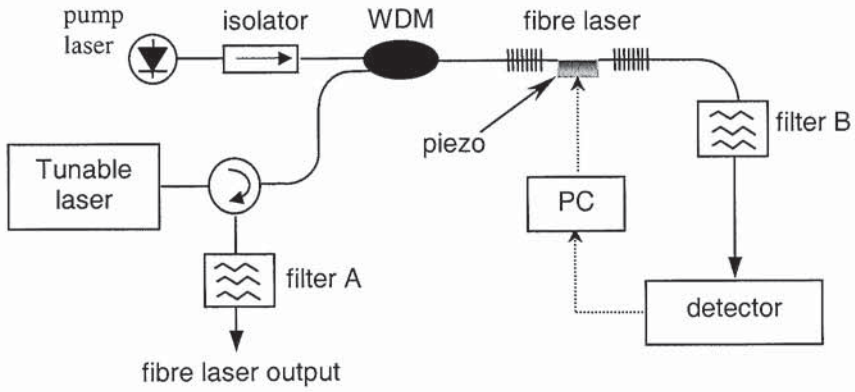

Figure 7.8 Experimental setup for the operation of the DBR fibre laser.

In the experiment, lasing operation only occurred from the primary cavity expectedly as shown in Figure 7.9. The spectral profiles of the primary and secondary cavities prior to operation are shown in Figure 7.10a (solid trace) and Figure 7.10b (solid trace) respectively. Without feedback control, as the pump power

increased from 0mW to 50mW, the resonance peaks shifted continuously within the Bragg grating spectrum due to the pump-induced thermo-optic effects in the Er/Yb fibre which were measured to be ~0.6×10^{-5}/mW in both cavities. As shown in Figure 7.10a (dotted trace), direct spectral characterization of the active primary cavity during operation was not feasible as the lasing mode saturated the detector and obscured the spectral features around it. Resonance mode structure in the passive secondary cavity depicted in Figure 7.10b (dotted trace), however, remained clearly resolved.

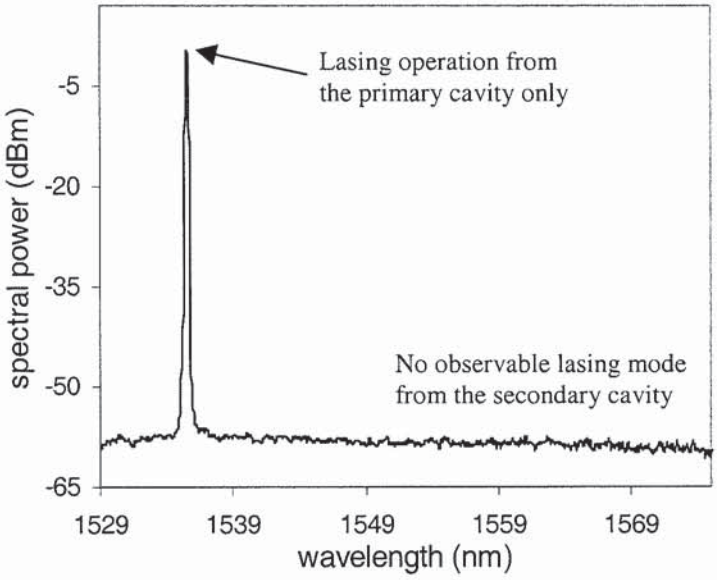

Figure 7.9 Optical output spectrum of the DBR fibre laser. Lasing operation from the primary cavity was observed only.

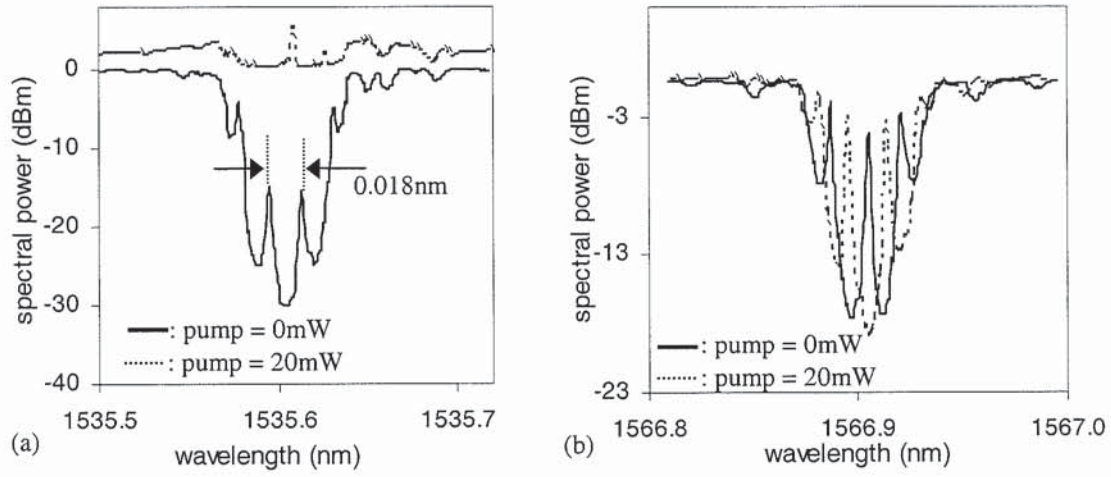

Figure 7.10 Spectral profiles of the (a) primary fibre laser cavity and (b) secondary cavity at different pump powers.

Due to the increasing thermally-induced index with pump power, the dominant lasing mode was constantly detuned away from the Bragg centre while the sidemodes moved in as exemplified in Figure 7.5. When two resonance modes experienced the same reflectivity (placed symmetrically about the Bragg

frequency), they acquired the same threshold gain and mode hopping occurred [41][21]. Consequently, with increasing pump power, the fibre laser exhibited transitions from single-mode to multimode operation exemplified by occurrences of an intermodal beat signal at 2.3GHz (corresponding to intermodal spacing of 0.018nm) as shown in Figure 7.11 inset. Over the entire pump power range, output power instability associated with mode competition as shown in Figure 7.11 (dotted trace) and mode-hopping were encountered together with wavelength fluctuations of >18pm over the entire pump power range.

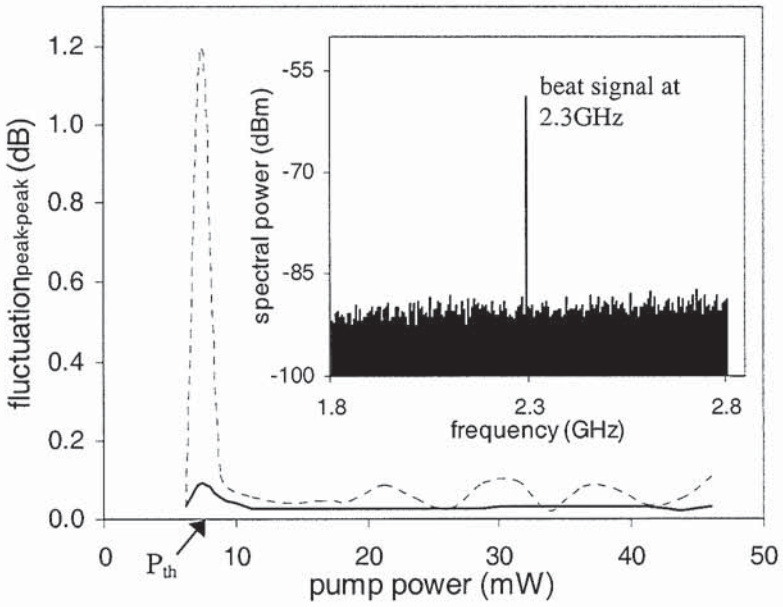

Figure 7.11 Output power fluctuations with (solid) and without (dotted) mode optimisation feedback controls. Inset shows the resultant inter-modal beat signal when the fibre laser was operating in multimode regime. P_{th} : threshold power =6mW.

A simple feedback control based on detecting the deviations of the resonance peaks from its optimal positions in the secondary cavity was implemented. The optimum secondary cavity resonance mode structure was such that the dominant resonance mode in the primary cavity aligned with the Bragg centre and as highlighted in Figure 7.7, this corresponded to the spectral profile indicated by Trace (a). Based on a straightforward approach, the resonance modes' wavelengths in the optimum secondary cavity were taken as references. During operation, the deviations of the resonance modes from these references in the secondary cavity generated the error signal for the feedback mechanism to alleviate the detuning of the dominant lasing mode with increasing pump power. As illustrated in Figure 7.12, output power fluctuation associated with the multimode operation regime was suppressed as the PZT, with increasing applied voltage, altered the cavity path length to restore the desired cavity mode condition. With the mode optimisation feedback control, stable single-mode operation was obtained over the entire pump power range. As shown in Figure 7.11 (solid trace), power fluctuation of <0.05dB was achieved without the occurrence of mode-hopping. Furthermore, fluctuation in the output power near threshold was significantly decreased and showed an order of magnitude improvement in stability compared to the case without feedback control. Output wavelength deviation measured over the entire pump power range was <1pm (limited by the measurement setup).

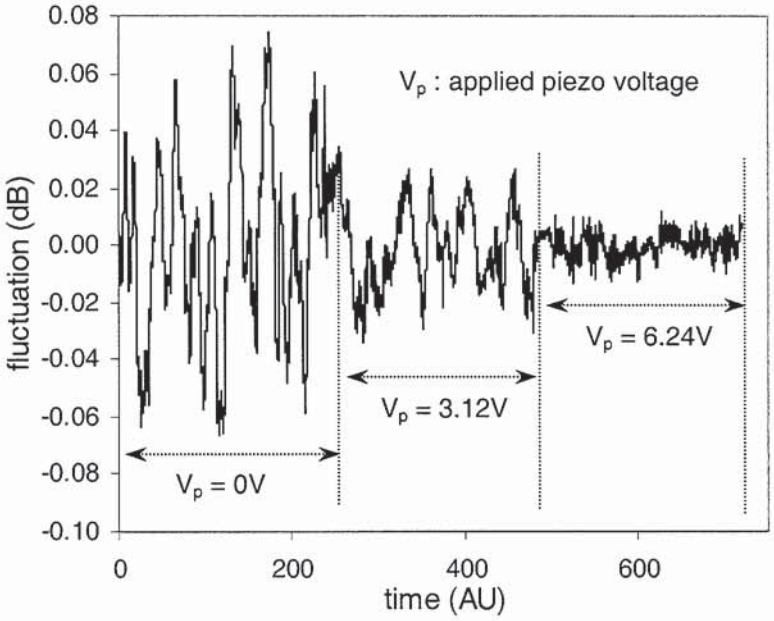

Figure 7.12 Output power fluctuation variations with optimising piezo voltages.

It is worth noting that one can potentially adopt a single interrogation and feedback system for multiple fibre lasers through a 1xN optical switch as shown in Figure 7.13. Since the proposed scheme is based on interrogating the passive superimposed secondary cavity, remote wavelength and mode condition monitoring, in principle, can be achieved conveniently. Towards a cost-effective interrogation scheme, a number of ways are under investigation. Most notably, a passive interrogation technique based on quadrature phase detection [42] can potentially allow one to detect index changes in the resonance cavity and thereby the cavity resonance mode conditions. Such a scheme only requires a conventional broadband source, narrowband uniform fibre Bragg gratings and photodiodes.

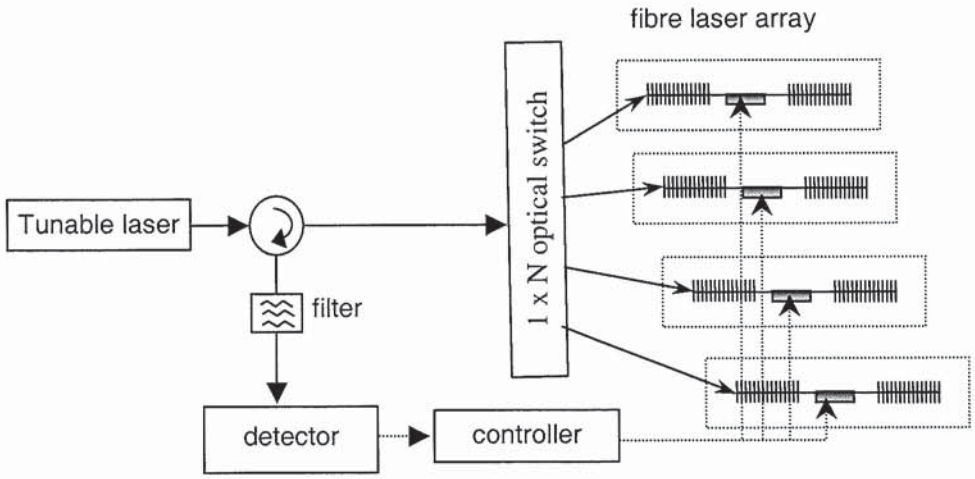

Figure 7.13 Schematic diagram depicting the use of one interrogation and optimisation system for multiple fibre lasers though a 1x N optical switch.

7.3.2 Optimisation of a DFB fibre laser operation

An important feature of the proposed scheme lies in its suitability for short, linear-cavity fibre laser configurations since the only modification to the laser grating structure is a non-invasive inscription of a superimposed grating cavity. As highlighted in Chapter 6, the distributed feedback (DFB) fibre laser configuration (a linear-cavity type) is one of the most elegant ways to achieve robust single longitudinal mode operation [43][44]. One of the advantages of DFB fibre laser over the DBR fibre laser configuration is the use of a single fibre grating (phase-shifted grating) for feedback and wavelength determination [45]. The introduction of the phase shift in the uniform grating structure breaks the threshold condition degeneracy for the two lowest order laser modes. A resonance mode at the Bragg wavelength arises and undergoes strongest feedback and lowest required threshold gain. The threshold gain differences between this main longitudinal mode and the side modes are the largest thereby giving enhanced single-mode operation [45][46].

Ideally, the spectral profile of a DFB fibre laser structure, consisting of a FBG incorporating a π phase shift, exhibits a narrow transmission peak, which defines the lasing wavelength, in the middle of the grating stopband. Essentially, as detailed in Chapter 6, the DFB fibre laser is realised by inscribing a π phase-shifted grating into a length of active fibre (e.g. Er/Yb doped fibre). Optimum laser operation is theoretically reached when the optical phase shift within the grating structure reaches the value of $\pi/2 + N(\pi)$ where N is an integer [46][47] and the corresponding resonance peak in the spectral profile resides at the Bragg centre. Perturbations to the resonance mode structure due to phase shift deviation, Bragg wavelength shift and/or grating chirp can all influence the lasing mode significantly [47][48]. Previous studies have also highlighted the dependencies of the fibre laser performance on the ambient conditions and the pump power [14][46][48]. Large detuning of the grating structure can also further inhibit lasing operation [43][46].

In general, there are two key sources of distortions to the DFB fibre laser grating structure. Firstly, in particular to DFB fibre lasers made using the post-processing fabrication technique [49], the residual hydrogen at the phase shift region is lower compared to the rest of the grating structure due to longer UV exposure. In the annealing process, the phase shift induced deviates from its original value of π due to reduced index drift at the phase shift region compared to the rest of the grating structure [50]. Since the phase shift in the grating structure relates to the wavelength position of the resonance peak within the grating stopband [51], consequently the resultant resonance mode of the DFB fibre laser no longer aligns with the Bragg centre for optimised operation. The second source of distortion to the DFB fibre laser grating structure, as in the case of the DBR fibre laser, is the pump-induced thermo-optic effect in the active fibre during operation. Apart from introducing a temperature gradient along the laser cavity, thus causing a grating chirp, it has been observed that a localized heat spot at the phase-shifted region is also created which further introduces a phase shift deviation during operation [14][52]. The combination of these distortions to the cavity grating spectral characteristics lead to lower output performance and a strong dependence on the input pump power.

Based on the similar concept described in section 7.3.1, by superimposing a secondary grating structure onto the primary DFB fibre laser cavity, a mode assessment and optimisation scheme for the DFB fibre laser was carried out. In the experiment, a 45mm long DFB fibre laser structure (Bragg wavelength 1545.8nm, κL ~6.1) was first fabricated in an Er/Yb fibre (230dB/m absorption at 980nm). At the same physical location, an identical secondary structure with grating parameters Bragg wavelength 1569.5nm, κL

~3.2 was fabricated. The phase shift was induced by UV post-processing over a 0.7mm central section of the grating. Prior to the experiment, the measured spectral profile of the DFB fibre laser cavity after fabrication is as shown in Figure 7.14a. The π phase-shifted grating structure forming the fibre laser cavity yielded a resonance mode at the Bragg centre, corresponding to the optimal condition for laser operation. However, after the thermal annealing process, as compared to its initial profile, the measured spectral characteristics of the primary fibre laser cavity shown in Figure 7.14b illustrated a detuned transmission peak. The amount of phase deviation was measured to be ~0.15π radians and was consistent in both cavities. The corresponding index deviation at the phase-shifted region (i.e. the post-processed region) was ~$1.7\text{x}10^{-4}$.

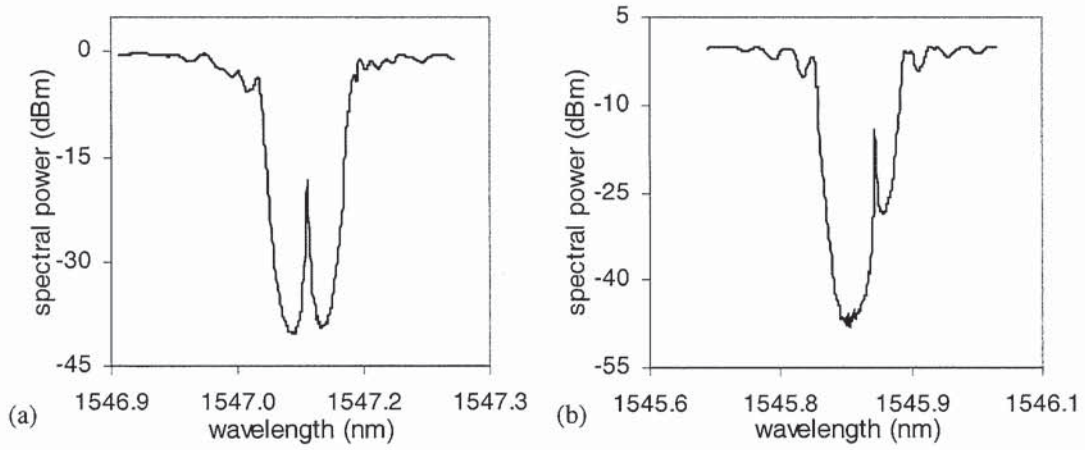

Figure 7.14 Spectral profiles of the primary DFB fibre laser cavity (a) after fabrication process and (b) after the thermal annealing process.

The operational setup for the fibre laser is as shown in Figure 7.15. Similarly, a fast scanning tunable laser (max.100nm/sec, 1pm resolution) calibrated by the wavemeter, and a high-speed detector were used to probe real-time the spectral profile of the passive secondary grating structure during laser operation. The fibre laser was mounted on a 50mm long thin metal plate with temperature gradient (hence heat dissipation rate) along the cavity controlled by two Peltiers on each end of the plate. A thin copper filament wire with one end thermally bonded to a third Peltier was placed over the phase shift region to thermally adjust the phase deviation. A computer acquired the spectral data from the detector and applied control signals to the Peltier drivers to alter temperatures around the fibre laser, and thereby cavity mode conditions. Optical filters A and B were used to isolate the probe signal and the fibre laser output respectively.

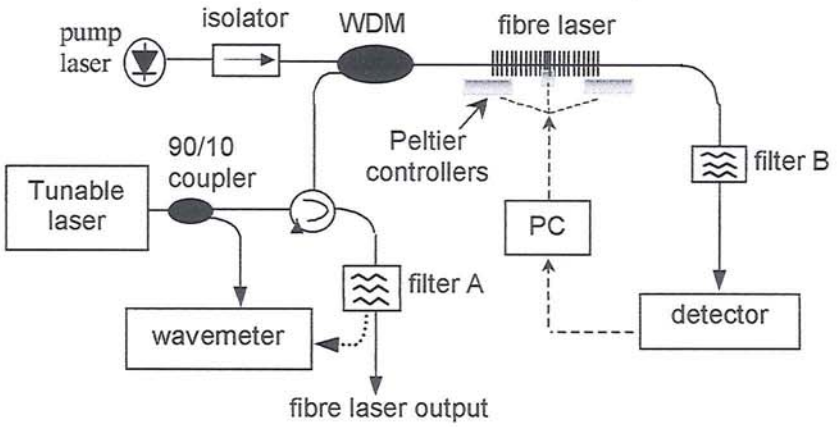

Figure 7.15 Experimental setup for the operation of the DFB fibre laser with the mode optimisation scheme.

It is interesting to note that by suspending the fibre laser in air, no lasing operation was obtained. Apart from the phase shift deviation incurred in the thermal annealing process, pump-induced thermal effects in the Er/Yb fibre further distorted the grating structure, as exemplified by the measured and close-fitted simulated spectral profiles of the primary cavity at 16mW and 28mW (Figure 7.16). Based on the fitted simulation data, it was deduced that an exponential temperature distribution occurred along the fibre laser cavity with a peak temperature difference of 14^{0}C at 28mW. The temperature gradient however decreased beyond 28mW as the pump distribution along the laser improved.

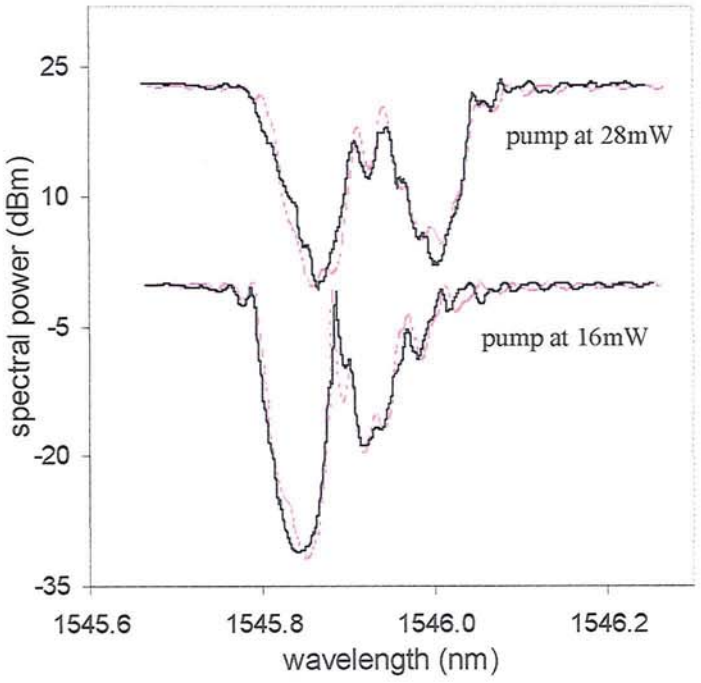

Figure 7.16 Pump-induced thermal effects on the spectral profiles of the DFB fibre laser grating structure. The close fit of the measured data (solid) to the simulated profile (dotted) indicated an exponential temperature distribution along the laser cavity.

With the thermal conditioning feedback scheme in operation, the optimised spectral profiles of the primary and the secondary cavities are as shown in Figure 7.17 Trace a and inset respectively. The control mechanism detected the expansion in the grating stopband (i.e. chirping) and applied a cooling gradient along the cavity by the two Peltiers on each end of the plate. Since the phase shift in the grating structure is related to the wavelength position of the resonance peak within the grating stopband [49], the thin copper filament wire thermally optimised the deviation in the phase shift by monitoring the variation of the resonance peak from the Bragg centre. Note that due to the fact the two cavities centred at different Bragg wavelengths and that the induced phase shift is a function of the wavelength, the transmission peak positions hence differed for the two cavities for the same amount of induced index. Nevertheless, the feedback control maintained the secondary cavity spectral profile, thereby stabilizing and optimising the resonance mode in the primary cavity during operation. Above threshold, lasing operation occurred only from the primary laser cavity expectedly as shown in Figure 7.18. Direct spectral characterization of the active primary cavity while lasing was not feasible as the lasing mode saturated the detector and obscured the spectral features of the cavity response as shown in Figure 7.17 Trace b. The resonance mode structure in the passive secondary cavity however remained highly resolved.

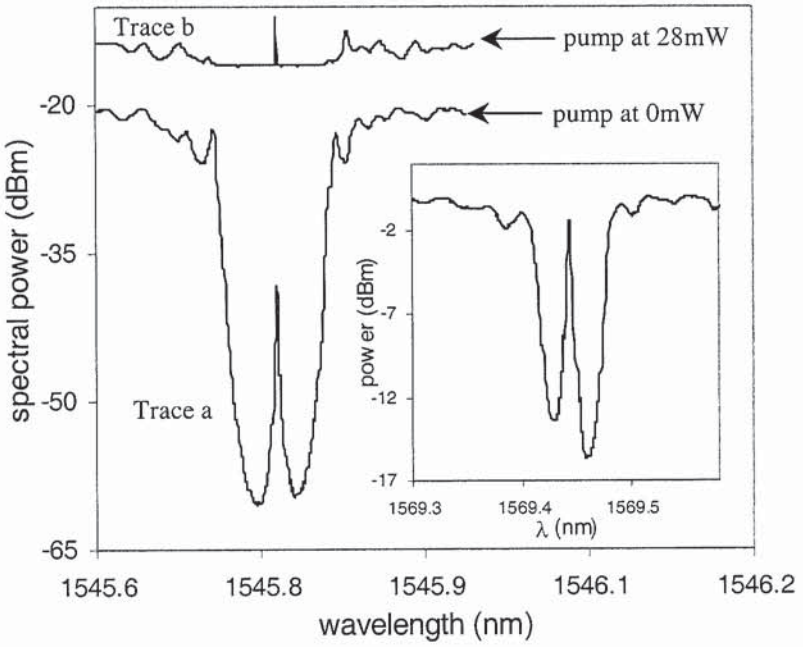

Figure 7.17 Spectral profiles of the DFB fibre laser under the mode assessment and optimisation scheme.

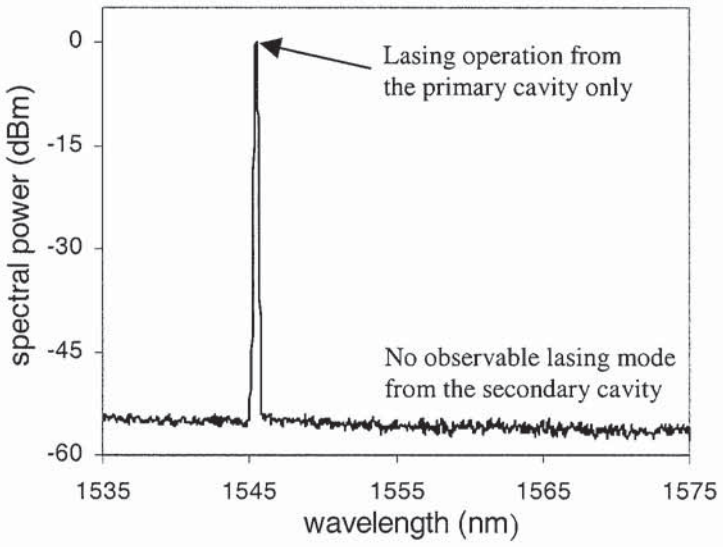

Figure 7.18 Optical output spectrum of the DFB fibre laser. Lasing operation from the primary cavity was observed only.

The fibre laser delivered 1mW output at 52mW pump power with a slope efficiency of ~3% (Figure 7.19 Trace a) limited by the fibre properties. Output wavelength deviation measured over the entire pump power range was <1pm (limited by the measurement setup). Using a fixed thermal condition (optimised for 52mW pump power only), the detuning of the laser cavity as the pump decrease as manifested by the increase in threshold and the change in the slope efficiency as shown in Figure 7.19 Trace b. More importantly, in the absence of optimisation, the fibre laser delivered only 0.37mW at 52mW pump power with a slope efficiency of 1.2% as shown in Figure 7.19 Trace c. Furthermore, the threshold increased by 4mW and a wavelength drift of 27pm over the entire pump power range was measured. Spectral information from the secondary cavity indicated both the localized heat-induced index change at the phase shift region of $\sim 5 \times 10^{-5}$ and an overall Bragg wavelength shift of 25pm accounted for the wavelength drift.

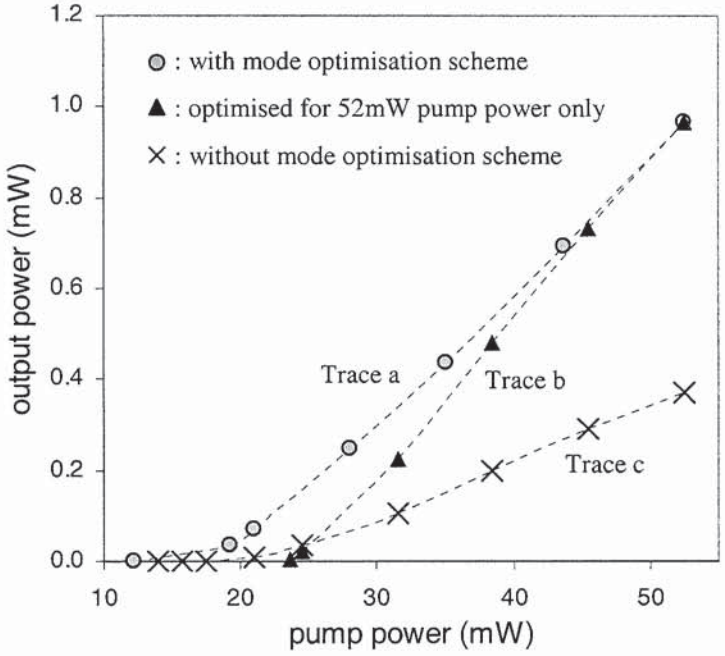

Figure 7.19 Output efficiency curves of the DFB fibre laser with and without mode optimisations.

It is worth noting that the fluctuation of a laser output power caused by resonant pump power perturbation is inversely proportional to the lifetime of the photons in the laser cavity [53]. In fact, the cavity photon density fluctuation is approximated by [53]

$$\frac{q_m}{q_0} \propto \frac{1}{\tau_c}\frac{R_m}{R_{po}} \tag{7.3}$$

where q_m denotes the amplitude of the cavity photon density fluctuation, q_0 denotes the steady state photon density, R_m is the amplitude of the pump power perturbation at the relaxation oscillation frequency, R_{p0} is the steady state pump rate and τ_c is the photon lifetime. In the DFB fibre laser, the cavity photon lifetime is related to the threshold gain coefficient g_{th} given as [54]

$$\tau_c = \frac{n}{c g_{th}} \tag{7.4}$$

Furthermore, the threshold gain coefficient can be approximated by [54]

$$g_{th} \approx 4\kappa \exp(-\kappa L) \tag{7.5}$$

Based on (7.3) to (7.5), it can be deduced that the cavity photon lifetime is dependent on the coupling coefficient experienced by the resonance mode. For an optimised lasing condition, the resonance mode aligns with the Bragg frequency and experiences highest cavity finesses and strongest feedback (i.e. largest

grating coupling κL) [55]. Detuning of the grating structure due to thermal effect lowers the cavity finesse experienced by the resonance mode and the output performance and cavity photon lifetime decrease. From (7.3), it can be deduced that the relative intensity noise (RIN) performance of the DFB fibre laser will deteriorate. Experimentally, as shown in Figure 7.20, comparing the RIN measurement at 40mW pump power, it was evident that the optimised fibre laser exhibited a 6dB improvement in noise performance accompanied by an increase in the relaxation oscillation frequency of 192kHz.

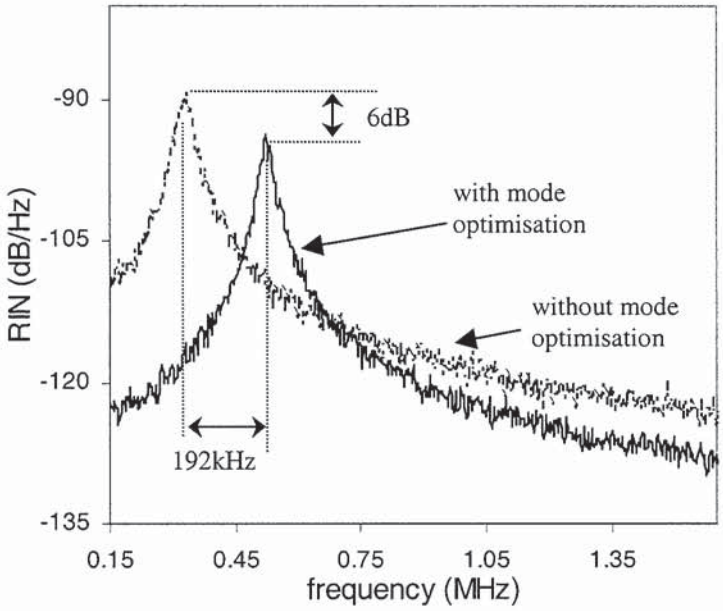

Figure 7.20 Comparison of the relative intensity noise (RIN) of the fibre laser output with and without mode optimisations.

7.4 Conclusions

Some of the common wavelength monitoring and longitudinal mode stabilization schemes for fibre lasers have been outlined. The lack of cavity mode assessment and optimisation control for fibre lasers, in particular linear-cavity configurations for enhanced output performance, has been highlighted. Pump-induced thermal effects during operation and differential index variations in the grating cavity due to the thermal annealing process have been shown to have drastic impacts on the fibre laser output performance. To address the need for a cavity mode assessment and optimisation scheme in short-cavity-length, linear fibre laser configurations, a mode condition monitoring and feedback scheme based on superimposed cavities structure has been proposed and demonstrated. The proposed optimisation method utilized the concept and simplicity of superimposed fibre grating structures to enable direct, real-time cavity mode assessment in linear-cavity fibre laser configurations. Based on the obtained information of the cavity mode conditions, feedback controls using PZT/Peltiers to optimise the resonance mode of the fibre lasers have been illustrated. Stable, optimised single longitudinal mode operation has been achieved in a DBR fibre laser, despite under strong influence of the pump-induced thermal effect. To illustrate the feasibility of the proposed scheme to other short length linear-cavity fibre laser configurations, stabilization and optimisation of a DFB fibre laser operation have been demonstrated. Based on the results obtained, the importance of cavity mode conditioning feedback for optimised performance such as low threshold, highest SMSR and better RIN performance has been highlighted.

7.5 References

[1] R.J. Foster, N. Langford, A. Gloag, L. Zhang, J.A.R. Williams, I. Bennion, "Narrow linewidth operation of an Erbium fibre laser containing a chirped Bragg grating etalon", *J. Lightwave Technol.*, 15(11), pp. 2130-2135, 1997.

[2] E. Rønnekleiv, "Frequency and intensity noise of single frequency fibre Bragg grating lasers", *Optical Fibre Technol.*, 7, pp. 206-235, 2001.

[3] J. Hernandez-Cordero, V.A. Kozlov, T.F. Morse, "Highly accurate method for single-mode fibre laser wavelength measurement", *IEEE Photo. Technol. Lett.*, 14(1), pp. 83-85, 2002.

[4] M. Svalgaard, S.L. Gilbert, "Stability of short, single-mode erbium doped fibre lasers", *Applied Optics*, 36(21), pp. 4999-5005, 1997.

[5] I.M. Jauncey, L. Reekie, J.E. Townsend, D.N. Payne, C.J. Rowe, "Single longitudinal mode operation of an Nd^{3+}doped fibre laser", *Electron. Lett.*, 24(1), pp.24-25, 1988.

[6] G.A. Ball, W.W. Morey, W.H. Glenn, "Standing wave monomode Erbium fibre laser", *IEEE Photon. Technol. Lett.*, 3(7), pp. 613-615, 1991.

[7] V. Mizrahi, D.J. DiGiovanni, R.M. Atkins, S.G. Grubb, Y.K. Park, Jean-Marc P. Delavaux, "Stable single-mode erbium fibre grating laser for digital communication", *J. Lightwave Technol.*, 11(12),pp. 2021-2025, 1993.

[8] G.A. Ball, W.H. Glenn, W.W. Morey, P.K. Cheo, "Modeling of short, single frequency fibre lasers in high gain fibre", *IEEE Photon. Technol. Lett.*, 5(6), pp. 649-651, 1993.

[9] G.A. Ball, G. Hull-Allen, C. Holton, W.W. Morey, "Low noise single frequency linear fibre laser", *Electron. Lett.*, 29, pp. 1623-1625, 1993.

[10] Y.Z. Xu, H.Y. Tam, S.Y. Liu, M.S. Demokan, "Pump induced thermal effects in Er-Yb fibre grating DBR lasers", *IEEE Photon. Technol. Lett.*, 10, pp. 1253-1255, 1998.

[11] L. Dong, W.H. Loh, J.E. Caplen, J.D. Minelly, K. Hsu, L. Reekie, "Efficient single frequency fibre laser with novel photosensitive Er/Yb optical fibres", *Optics Lett.*, 22(10), pp.694-696, 1997.

[12] K. Hsu, W.H. Loh, L. Dong, C.M. Miller, "Efficient and tunable Er/Yb fibre grating lasers", *J. Lightwave Technol.*, 15(8), pp. 1438-1441, 1997.

[13] W.H. Loh, B.N. Samson, L. Dong, G.J. Cowle, K. Hsu, "High performance single frequency fibre grating based Erbium-Ytterbium codoped fibre lasers", *J. Lightwave Technol.*, 16(1), pp. 114-118, 1998.

[14] O. Hadeler, E. Rønnekleiv, M. Berendt, M. Zervas, "Temperature distribution along DFB fibre lasers", *IEE Optical Fibre Grating Colloquium*, Aston University, Birmingham, 1999.

[15] W.S. Man, Y.Z. Xu, H.Y. Tam, M.S. Demokan, "Frequency instability in Er/Yb fibre grating lasers due to heating by nonradiative transitions", *IEEE Photon. Technol. Lett.*, 11(11), pp. 1390-1392, 1999.

[16] W.H. Chung, H.Y. Tam, M.S. Demokan, P.K.A. Wai, C. Lu, "Frequency stabilization of DBR fibre grating laser using interferometric technique", *IEEE Photon. Technol. Lett.*, 13(9), pp. 951-953, 2001.

[17] G.A. Cranch, "Frequency noise reduction in erbium doped fibre Bragg grating lasers using active electronic feedback", *Proc. Optical Fibre Sensor Conference (OFS)*, vol. 1, WB5, pp. 293-296, 2002.

[18] R. Larose, D. Stepanov, C. Latrasse, M. Têtu, F. Ouellette, M.A. Guguay, "Simple frequency tuning technique for locking a single-mode erbium-doped fibre laser to the centre of molecular resonances", *Electron. Lett.*, 30, pp. 791-793, 1994.

[19] S.L. Gilbert, "Frequency stabilization of a tunable erbium-doped fibre laser", *Optics Lett.*, 16(3), pp. 150-152, 1991.

[20] S.L. Woodward, I.M.I. Habbab, T.L. Koch, U. Koren, "The side mode suppression ratio of a tunable DBR laser", *IEEE Photon. Technol. Lett.*, 2(12), pp. 854-856, 1990.

[21] I.M.I. Habbab, L.J. Cimini Jr, "A new DBR laser structure for improved side mode suppression", *IEEE Photon. Technol. Lett.*, 3(8), pp. 700-702, 1991.

[22] S.L. Woodward, T.L. Koch, U. Koren, "A control loop which ensures high side mode suppression ratio in tunable DBR laser", *IEEE Photon. Technol. Lett.*, 4(5), pp. 417-419, 1992.

[23] S.L. Woodward, V. Mizrahi, T.L. Koch, U. Koren, P.J. Lemaire, "Wavelength stabilization of a DBR laser using an in-fibre Bragg filter", *IEEE Photon. Technol. Lett.*, 5(6), pp. 628-630, 1993.

[24] H. Ishii, F. Kano, Y. Yoshikuni, H. Yasaka, "Mode stabilization method for superstructure-grating DBR laser", *J. Lightwave Technol.*, 16(3), pp. 433-442, 1998.

[25] G. Sarlet, G. Morthier, R. Baets, "Wavelength and mode stabilization of widely tunable SG-DBR and SSG-DBR lasers", *IEEE Photon. Technol. Lett.*, 11(11), pp. 1351-1353, 1999.

[26] N. Fujiwara, T. Kakitsuka, F. Kano, H. Okamoto, Y. Kawaguchi, Y. Kondo, Y. Yoshikuni, Y. Tohmori, "Mode-hop-free wavelength-tunable distributed Bragg reflector laser", *Electron. Lett.*, 39(7), 2003.

[27] G.A. Ball, W.W. Morey, "Continuously tunable single-mode erbium fibre laser", *Optics Lett.*, 17(6), pp. 420-422, 1992.

[28] G.A. Ball, W.W. Morey, "Compression-tuned single-frequency Bragg grating fibre laser", *Optics Lett.*, 19(23), pp. 1979-1981, 1994.

[29] R.J. Forster, N. Langford, "Longitudinal mode control of a narrow-linewidth fibre laser by use of the intrinsic birefringence of the fibre laser", *Optics Lett.*, 21(20), pp. 1679-1681, 1996.

[30] S.K. Kim, G. Stewart, W. Johnstone, B. Culshaw, "Mode-hop-free single longitudinal mode erbium doped fibre laser frequency scanned with a fibre ring resonator", *Applied Optics*, 38(24), pp. 5154-5157, 1999.

[31] H. Sabert, "Active stabilization of single-mode operation in a fibre laser", *Electron. Lett.*, 29(11), pp. 1004-1005, 1993.

[32] H. Sabert, "Suppression of mode jumps in a single-mode fibre laser", *Optics Lett.*, 19(2), pp. 111-113, 1994.

[33] A. Gloag, N. Langford, K.McCallion, W. Johnstone, "Continuously tunable single-frequency erbium ring fibre laser", *J. Opt. Soc. Am. B*, 13(5), pp. 921, 1996.

[34] L.B. Fu, M. Ibsen, J. Nilsson, D.J. Richardson, D.N. Payne, "Erbium-Ytterbium L-band fibre DFB laser pumped at 1534nm", *Proc. European Conference Optical Communications (ECOC)*, We2.6.6, Rimini, Italy, 2003.

[35] C. Spiegelberg et al, "Compact 100mW fibre laser with 2kHz linewidth", *Proc. Optical Fibre Communication Conference (OFC)*, PD45, 2003.

[36] D.C. Brown, H.J. Hoffman, "Thermal, stress, and thermo-optic effects in high average power double-clad silica fibre lasers", *IEEE J. Quantum Electron.*, 37(2), pp.207-217, 2001.

[37] J. Bao, X. Zhang, K. Chen, W. Zhou, "Spectra of dual overwritten fibre Bragg grating", *Optics Comm.*, 188, pp. 31-39, 2001.

[38] Y. Lai, W. Zhang, J.A.R. Williams, I. Bennion, "An optical millimeter wave fibre laser", *Proc. Optical Fibre Communication Conference (OFC)*, Atlanta, TuL5, 2003.

[39] G.A. Ball, W.H. Glenn, W.W. Morey, P.K. Cheo, "Modeling of short, single-frequency, fibre lasers in high gain fibre", *IEEE Photon. Technol. Lett.*, 5(6), pp. 649-651, 1993.

[40] G.A. Ball, W.H. Glenn, "Design of a single-mode linear cavity Erbium fibre laser utilizing Bragg reflectors", *J. Lightwave Technol.*, 10(10), pp. 1338-1343, 1992.

[41] S.L. Woodward, I.M.I. Habbab, T.L. Koch, U. Koren, "The side mode suppression ratio of a tunable DBR laser", *IEEE Photon. Technol. Lett.*, 2, pp. 854-856, 1990.

[42] M. Dahlem, J.L. Santos, L.A. Ferreira, F.M. Araújo, "Passive interrogation of low finesse Fabry-Perot cavities using fibre Bragg gratings", *IEEE Photon. Technol. Lett.*, 13(9), pp.990-993, 2001.

[43] J.T. Kringlebotn, J.L. Archambault, L. Reekie, D.N. Payne, "Er^{3+}:Yb^{3+} codoped fibre distributed feedback laser", *Optics Lett.*, 19(24), pp.2101-2103, 1994.

[44] W.H. Loh, R.I. Laming, "1.55μm phase-shifted distributed feedback fibre laser", *Electron. Lett.*, 31(17), pp. 1440-1442, 1995.

[45] K. Utaka, S. Akiba, K. Sakai, Y. Matsushima, "λ/4 shifted InGaAsP/InP DFB lasers", *IEEE Quantum Electron.*, QE22(7), pp. 1042-1051, 1986.

[46] A. Asseh, H. Storoy, J.T. Kringlebotn, W. Margulis, B. Sahlgren, S. Sandgren, R. Stubbe, G. Edwall, "10cm Yb^{3+} DFB fibre laser with permanent phase shifted grating", *Electron. Lett.*, 31(12), pp. 969-970, 1995.

[47] H. Storoy, B. Sahlgren, R. Stubbe, "Single polarization fibre DFB laser", *Electron. Lett.*, 33(1), 1997.

[48] H. Kogelnik, C.V. Shank, "Coupled-wave theory of distributed feedback lasers", *J. Appl. Phys.*, 43(5), 1972.

[49] J. Canning, M.G. Sceats, "π phase shifted periodic distributed structures in optical fibres by UV post processing", *Electron. Lett.*, 30(16), pp. 1344-1345, 1994.

[50] B. Malo, J. Albert, K.O. Hill, F. Bilodeau, D.C. Johnson, "Effective index drift from molecular hydrogen diffusion in hydrogen-loaded optical fibres and its effect on Bragg grating fabrication", *Electron. Lett.*, 30(5), 1994.

[51] J.L. Philipsen, M.O. Berendt, P. Varming, V.C. Lauridsen, J.H. Povlsen, J. Hübner, M. Kristensen, B. Pálsdóttir, "Polarisation control of DFB fibre laser using UV-induced birefringent phase-shift", *Electron. Lett.*, 34(7), 1998.

[52] E. Rønnekleiv, M. Ibsen, M.N. Zervas, R.I. Laming, "Characterization of fibre distributed-feedback lasers with an index-perturbation method", *Applied Optics*, 38(21), pp. 4558-4656, 1999.

[53] M. Ding, P.K. Cheo, "Analysis of Er-doped fibre laser stability by suppressing relaxation oscillation", *IEEE Photon. Technol. Lett.*, 8(9), pp. 1151-1153, 1996.
[54] S. Yamashita, G.J. Cowle, "Single polarization operation of fibre distributed feedback (DFB) lasers by injection locking", *J. Lightwave Technol.*, 17(3), pp. 509-513, 1999.
[55] S. W. Løvseth, E. Rønnekleiv, "Fundamental and higher order mode thresholds of DFB fibre lasers", *J. Lightwave Technol.*, 20(3), pp. 494-501, 2002.

Chapter 8: Thesis conclusions

8.1 Summary

This thesis has discussed some of the key characteristics of single-mode optical fibre and related technologies, namely, optical fibre delay line filters and fibre Bragg gratings, as well as a number of novel fibre devices, based on these technologies, potentially applicable in next generation broadband photonics communication systems. Among the technological challenges to the realisation of future broadband photonics communication networks, two key areas of research, namely, the optical generation and distribution of radio frequency signals over fibres, and the fibre optic signal processing of optical and radio frequency signals, have been identified and constituted the main focus of studies in this research.

An overview of the intrinsic advantages of single-mode optical fibres and some of its key characteristics relevant to device architectures has been given. In particular, fibre birefringence and its impact on the transfer responses of fibre-based devices have been highlighted. Two special fibre types, namely, the high birefringence (Hi-Bi) fibre and the Er/Yb doped fibre have been studied and subsequently formed the basis of the novel fibre devices realised in this research.

The key concepts behind the optical fibre delay line filter have been reviewed and its analysis based on matrix formulation has been discussed. Utilizing the non-interfering polarization modes in the Hi-Bi fibre, the coherent operation of a Hi-Bi fibre delay line filter with greatly enhanced environmental stability has been demonstrated. On the basis of such a Hi-Bi fibre delay line filter architecture, unique higher order lattice structure Hi-Bi fibre delay line filters have been proposed and demonstrated. Complex signal processing operations like simultaneous complementary outputs and wavelength-interleaving nonreciprocal bidirectional filtering have been achieved by taking advantage of the bipolar taps generated through the cascaded Hi-Bi fibre structure. Desirable characteristics such as ease of implementation, reconfigurable transfer function, negligible chromatic dispersion, and low insertion loss have been illustrated in the proposed configurations. Based on a similar concept, complex microwave/millimetre wave signal processing operations have been further achieved. An intuitive approach, based on a series of cross-sectional views and ray arrows, to analyse the filter transfer responses has also been demonstrated.

An overview of the key features and the fabrication techniques of fibre Bragg gratings (FBG) has been given. The straightforward simulation technique for fibre Bragg grating structures based on the transfer matrix method has been described. The ease and ability to tailor the spectral characteristics of the FBG structures have been highlighted and non-uniform fibre Bragg grating structures, namely, phase-shifted fibre gratings and superimposed grating structures have been realised. Characteristics of the phase-shifted fibre grating structures, in particular birefringence-induced polarization splitting, have been described and important issues concerning the tuning of the transmission band of the phase-shifted fibre grating to avoid compromising loss and passband ripples have been discussed. The concept of the superimposed uniform fibre Bragg grating structure has been extended to non-uniform grating structures to realise a unique overwritten phase-shifted fibre grating structure. More importantly, through combining the flexibility of

superimposed gratings with the polarization-selectivity of fibre Bragg grating in Hi-Bi fibre, a new concept of using a superimposed fibre grating structure in Hi-Bi fibre to enable widely/narrowly spaced polarization-discriminating filtering, not limited by fibre properties, has been achieved. These superimposed fibre grating structures subsequently formed an integral part of the research work on fibre lasers described in this thesis.

A brief review of some of the operating principles behind tunable fibre grating structures has been given. Towards a simple, compact and effective tuning mechanism for fibre grating structures, a novel technique based on the optical pump-induced thermal effects in rare-earth doped fibres has been proposed and illustrated. Experimental demonstrations on three different device architectures, namely, the single phase-shifted fibre grating, the dual phase-shifted fibre grating and the Fabry-Perot fibre grating multichannel filter, have been carried out. Desirable features such as high transmission extinction ratios, high repeatability without hysterisis, pump/signal wavelength independent, no induced anisotropic effects, and low power-distance products for the necessary induced phase changes have been achieved. Results obtained have highlighted the effectiveness and simplicity of the proposed mechanism for implementing miniature, optically tunable fibre grating transmission filters.

A brief review of rare-earth doped fibre lasers has been given. In particular, the passive spectral profiles and operation characteristics of π phase-shifted DFB fibre lasers have been highlighted. The ability of a π phase-shifted DFB fibre laser to generate dual-polarization mode operation has been utilized for generating high spectral purity, narrow linewidth microwave heterodyne signal without the use of any costly high frequency electronic equipment. Based on the results obtained, the effectiveness of dual-mode operation from one fibre laser cavity for common mode suppression of phase noise between the lasing modes has been highlighted. To increase the beat frequency generated, a new technique based on asymmetric UV post-processing in phase-shifted DFB fibre lasers has been proposed and demonstrated. Frequency tuning based on transverse loading and thermal conditioning have been further employed. Towards optical generation of high frequency signals at millimetre wave regime and beyond, a novel co-located dual DFB fibre laser configuration, based on the proposed superimposed phase-shifted fibre grating structure, has been realised. Distinct features such as engineering simplicity, ease of implementation/operation, and high flexibility in the frequencies attainable, have been achieved in the proposed fibre laser configuration. High spectral purity millimetre wave signals with <1kHz linewidths have been obtained without the need for high frequency synthesizers and complex feedback controls due to the common mode suppression of phase noise between the two lasing modes. Results obtained have highlighted the potential of these fibre laser configurations as low cost, compact and simple alternatives to optical generation of very narrow linewidth microwave/millimetre wave signals.

Lastly, the issues of wavelength monitoring and longitudinal mode stabilization for fibre lasers have been discussed. The lack of cavity mode assessment and optimisation control for fibre lasers, in particular linear-cavity configurations, for enhanced output performance has been highlighted. Pump-induced thermal effects during operation and differential index variations in the grating cavity due to the thermal annealing process have been shown to have drastic impacts on the fibre laser output performance. To address the need for a cavity mode assessment and optimisation scheme in short-cavity-length, linear fibre laser configurations, a mode condition monitoring and feedback scheme based on superimposed cavities structure has been proposed and demonstrated. The proposed optimisation method utilized the

concept and simplicity of superimposed fibre grating structures to enable direct, real-time cavity mode assessments. In conjunction with the cavity mode condition monitoring, feedback controls using PZT/Peltiers to optimise the resonance modes of the fibre lasers have been illustrated. Stable, optimised single longitudinal mode operation has been achieved in a DBR fibre laser, despite under the strong influence of the pump-induced thermal effect. To illustrate the feasibility of the proposed scheme to other short-length linear-cavity fibre laser configurations, stabilization and optimisation of a DFB fibre laser operation have been demonstrated. Based on the results obtained, the importance of cavity mode conditioning feedback in fibre lasers for optimised performance has been highlighted.

8.2 Suggested future works

In the course of this research, the effectiveness and various advantages of the Hi-Bi fibre delay line filter configurations have been clearly illustrated. On the basis of its fibre-based configuration, the filter scheme can potentially enable bidirectional, nonreciprocal wavelength-interleaving amplification by adopting Hi-Bi rare-earth doped fibres. Contrary to all reported schemes, such a Hi-Bi fibre delay line amplifier architecture will not require additional cascaded unidirectional amplifiers or circulars to enable high performance, low noise figure, bidirectional amplification. Furthermore, since the wavelength-selective element in the filter configuration consists of high birefringence fibres, and the spectral responses depend strongly on the birefringence of the fibres adopted, the physical size and simplicity of the filter configuration can be further improved with photonics crystal fibres that exhibit very high birefringence. To enable tunable spectral responses, the sensitivity of Hi-Bi fibre to transverse force applied at 45^0 azimuth to its birefringence axes can be utilized. Controlled variations to the applied transverse forces onto the Hi-Bi fibre delay line filter structure can potentially enable free spectral range adjustments as well as wavelength shiftings.

The use of superimposed fibre laser cavities structure for cavity mode condition monitoring and optimisation has been proposed and realised. Its feasibility has been demonstrated by a straightforward approach using a scanning tunable laser to interrogate the deviations of the resonance peaks/spectral stopbands from its optimal positions. Towards a more cost-effective interrogation scheme, a passive interrogation technique based on quadrature phase detection can be adopted. Such a scheme only requires a conventional broadband source, narrowband uniform fibre Bragg gratings and photodiodes. By detecting the index changes in the secondary resonance cavity, the resonance mode conditions can be deduced and feedback schemes based PZT/Peltiers can be similarly used to optimise the lasing mode. The concept of this cavity mode condition assessment and optimisation scheme can be further integrated into the proposed fibre laser configurations used for optical generation of radio frequency signals. The high-resolution cavity mode condition monitoring and optimisation can potentially enhance the stability of the dual-mode operation of the fibre lasers, thereby the beat frequency generated.

The effectiveness of combining the optically induced thermo-optic properties of doped fibres with passive fibre Bragg grating structures has been illustrated in the course of this research. Such fibre grating device configuration enables a practical and cost-effective means to design all-fibre, optically remote-controlled devices. Apart from uniform fibre grating structures, the proposed scheme can be extended to other grating types such as superimposed fibre gratings, chirped gratings as well as sampled fibre grating

structures. By exploiting the versatility and flexibility of various non-uniform fibre grating structures, a variety of useful, tunable, wavelength-selective filters for signal processing in fibre sensors and optical fibre communication systems can be achieved. Interestingly, the proposed tuning mechanism can be extended to structures where the fibre gratings are fabricated into the doped fibres. The spectral features of such fibre gratings can be optically varied by a combination of the change in the pump power and the pump wavelengths. The corresponding variations in the dispersion characteristics of these grating devices can be exploited for appropriate applications. Such remotely tunable fibre devices will be highly desirable in optical fibre communication systems in applications like chromatic dispersion compensations. Last but not least, the pump-induced thermal index variations in doped fibres can be also utilized in coupled fibre grating cavity configurations. Such fibre grating structures will therefore exploit the spectral features of coupled cavities (based on Vernier effects) and the advantages of optically remote-controlled mechanism offered by the use of the doped fibres.

Apart from the intense research activities on various enabling fibre-based devices, there is also continuing research interest on the system implementation aspects of the future photonics communication network. A vast number of research works on millimetre-wave broadband radio-over-fibre communication systems based on different transmission techniques, modulation schemes as well as detection methods have been investigated, with common objectives such as low cost, wide coverage, practicability, scalability etc. It is of interest to construct an experimental fibre-radio transmission system utilizing a combination of novel techniques and fibre devices proposed in this thesis. Remote delivery of millimetre wave signals using the proposed fibre laser configurations can be evaluated in the transmission system. Fibre grating devices and Hi-Bi fibre delay line filters can be incorporated and their system performances can be investigated. Since the proposed millimetre wave fibre laser delivers dual-polarization mode output, polarization modulation technique can be considered. Issues with system degradation due to chromatic and polarization mode dispersion effects can be analysed. Applications of optical networking concepts such as wavelength division multiplexing (WDM) to such wireless photonics communication systems can be further investigated.

Appendix

Author's publications

[1] Yicheng Lai, W. Zhang and J.A.R. Williams, "All fibre multichannel flattop filter based on coherent fibre delay line structure", *Electron. Lett.*, 38 (10), pp. 473-474, 2002.

[2] Yicheng Lai, W. Zhang, J.A.R. Williams and I. Bennion, "A novel dual complementary output optical fibre transversal filter for DWDM applications", *15th IEEE Lasers and Electro-Optics Society Annual Meeting (LEOS)*, Glasgow, UK, ThE1, pp. 659-660, 2002.

[3] Yicheng Lai, W. Zhang and J.A.R. Williams, "A novel all fibre microwave transversal filter with complementary outputs", *Proc. International Topical Meeting on Microwave Photonics (MWP)*, Awaji, Japan, P2-1, pp. 173-176, 2002.

[4] Yicheng Lai, W. Zhang, J.A.R. Williams and I. Bennion, "Optical Multichannel Flattop Filter with Complementary Outputs for DWDM Applications", *1st International Conference on Optical Communications and Networks (ICOCN)*, Singapore, 13D3, pp. 163-166, 2002.

[5] Yicheng Lai, W. Zhang and J.AR. Williams, "Microwave photonic response based on nonlinear response of chirped fibre grating", *Institute of Physics International Conference on Optoelectronics (Photon)*, Cardiff, OP2.2.5, pp. 14-15, 2002.

[6] Yicheng Lai, W. Zhang and J.A.R. Williams, "Bidirectional nonreciprocal wavelength-interleaving coherent fibre transversal filter", *Proc. 5th Pacific Rim Conference on Lasers and Electro-Optics (CLEO/PR)*, Taipei, Taiwan, W4J, 2003.

[7] Yicheng Lai, W. Zhang and J.A.R. Williams, "Bidirectional nonreciprocal wavelength-interleaving coherent fibre transversal filter", *IEEE Photon. Technol. Lett., to be published,* 2004.

[8] W. Zhang, Yicheng Lai, C. Lu, J.A.R. Williams, L. Zhang and I. Bennion, "A fibre grating DFB laser for generation of optical microwave Signal", *Opt & Laser Tech.*, 32(5), pp. 369-371, 2000.

[9] Yicheng Lai, C. Lu, W. Zhang, J.A.R. Williams, L. Zhang and I. Bennion, "Generation of microwave signal with very narrow linewidth from a dual mode fibre DFB laser", *Applied Optics and Opto-Electronics Conference*, Loughborough, UK, BG.1.11, pp. 23-24, 2000.

[10] Yicheng Lai, W. Zhang and J.A.R. Williams, "Optical generation of tunable microwave signal from a dual mode fibre grating DFB laser", *International Topical Meeting on Microwave Photonics (MWP)*, Long Beach, Califonia, Tu 4.2, pp. 101-103, 2001.

[11] Yicheng Lai, W. Zhang and J.A.R. Williams, "Dual mode fibre grating DFB laser and its application in optical generation of tunable microwave signal", *Institute of Physics Meeting on Applied Photonic Processing*, London, UK, P2, pp.11-12, 2001.

[12] Yicheng Lai, W. Zhang and J.A.R. Williams, "High frequency signal generation for fibre radio application based on a novel fibre laser structure", *7th IEEE High Frequency Postgraduate Student Colloquium (HFPSC)*, London, UK, S4-P3, 2002. [***BEST PAPER AWARD***]

[13] Yicheng Lai, W. Zhang, J.A.R. Williams and I. Bennion, "An optical millimetre wave fibre laser", *Conference on Optical Fibre Communications (OFC)*, Atlanta, USA, TuL 5, pp. 238-239, 2003.

[14] Yicheng Lai, W. Zhang and J.A.R. Williams, "Optical generation of millimetre wave signal using a co-located dual distributed feedback fibre laser", *1st International Conference on Optical Communications and Networks (ICOCN)*, Singapore, 13G3, pp. 223-226, 2002.

[15] L. Michaille, M.W. McCall, Yicheng Lai and J.A.R. Williams, "Analysis of single and multiple, non-permanent, tunable, birefringent spectral holes in a fibre-Bragg grating stop-band produced via uni-axial pressure", *Optics Comm.*, 222 (1-6), pp. 1-8, 2003.

[16] X. Chen, Yicheng Lai, K. Zhou, L. Zhang and I. Bennion, "Axially displaced nonoverlapping parallel grating structure in conventional multimode fibre", *Institute of Physics Meeting on In-Fibre Gratings and Special Fibres*, P11, Stoneleigh, Warwickshire, 2003.

[17] Yicheng Lai, W. Zhang, L. Zhang, J.A.R. Williams and I. Bennion, "Optically tunable fibre grating transmission filters", *Optics Lett., to be published,* 28(24), 2003.

[18] Yicheng Lai, W. Zhang, J.A.R. Williams and I. Bennion, " An optical pump controlled tunable phase shifted fibre grating transmission filter ", *Conference on Optical Fibre Communications (OFC)*, Atlanta, USA, MF32, pp. 238-239, 2003.

[19] Yicheng Lai, W. Zhang, J.A.R. Williams and I. Bennion, "Application of superimposed grating structures for optimisation of fibre laser performance", *Institute of Physics Meeting on In-fibre Gratings and Special Fibres (Photonex)*, Stoneleigh, Warwickshire, P9, 2003.
[20] Yicheng Lai, W. Zhang and J.A.R. Williams, "Direct cavity assessment and mode optimisation technique for DFB fibre laser", *Electron. Lett.*, 39(21), pp. 1518-1519, 2003.
[21] Yicheng Lai, W. Zhang, J.A.R. Williams and I. Bennion, "Direct real-time cavity mode assessment and optimization technique for fibre lasers", *IEEE Photon. Technol. Lett., to be published*, 2004.
[22] Yicheng Lai, W. Zhang and J.A.R. Williams, "Optimization of DFB fibre laser performance based on a superimposed cavities structure", *Proc. 5th Pacific Rim Conference on Lasers and Electro-Optics (CLEO/PR)*, Taipei, Taiwan, TH1I, 2003.
[23] Yicheng Lai, W. Zhang, J.A.R. Williams and I. Bennion, "A novel cavity mode assessment technique for fibre lasers" *Proc. 29th European Conference on Optical Communications (ECOC/IOOC), Rimini, Italy, We2.6.4, 2003.*
[24] D. Zhao, X. Shu, W. Zhang, Yicheng Lai and I. Bennion, "Stable dual-wavelength oscillation of an Er-doped fibre ring laser at room temperature", *Fibre and Integrated Optics*, 21(6), pp. 465-470, 2002.
[25] D. Zhao, X. Shu, W. Zhang, Yicheng Lai, L. Zhang and I. Bennion, "Stable dual-wavelength oscillation of an erbium-doped fibre ring laser at room temperature", *SPIE Proc. of High-Power Lasers and Applications II (Photonics Asia)*, Shanghai, China, 4914, pp. 493-497, 2002.
[26] D. Zhao, Yicheng Lai, X. Shu, L. Zhang and I. Bennion, "Supermode-noise supression using a nonlinear Fabry-Perot filter in a harmonically mode-locked fibre ring laser", *Appl. Phys. Lett.*, 81(24), pp. 4520-4522, 2002.
[27] D. Zhao, Yicheng Lai, X. Shu, L. Zhang and I. Bennion, "Supermode-noise supression using a nonlinear Fabry-Perot filter in a harmonically mode-locked fibre ring laser", *Proc. 28th European Conference on Optical Communications*, Copenhagen, Denmark, P1.18, 2002.
[28] Yicheng Lai, G F Qiu, W Zhang, L Zhang, I Bennion and K.T.V. Grattan, "Simultaneous measurement of temperature and strain by combining active fibre with fibre gratings", *Measurement & Control*, 34(6), pp. 172-174, 2001.
[29] Yicheng Lai, F. Qiu, W. Zhang, L. Zhang, I. Bennion and K.T.V. Grattan, "Amplified spontaneous emission-based technique for simultaneous measurement of temperature and strain by combining active fibre with fibre gratings", *Rev. Sci. Instr.*, 73(9), pp. 3369-72, 2002.
[30] Yicheng Lai, G.F. Qiu, W. Zhang, L. Zhang, I. Bennion and K.T.V. Grattan, "Simultaneous measurement of temperature and strain by combining active fibre with fibre gratings", *Sensors & their applications (XI/ISMCR)*, London, UK, S5-P3, pp.135-139, 2001.
[31] P.C. Won, J. Leng, Yicheng Lai and J.A.R. Williams, "Determination of Localised Temperature Changes using a Chirped Fibre Bragg Grating", *16th International Conference on Optical Fibre Sensors (OFS)*, Nara, Japan, Tu4-3, pp. 244-247, 2003.
[32] P.C. Won, J. Leng, Yicheng Lai and J.A.R. Williams, "Distributed temperature sensing based on a chirped fibre Bragg grating", *Institute of Physics Meeting on In-fibre Gratings and Special Fibres (Photonex)*, Stoneleigh, Warwickshire, P4, 2003.
[33] Yicheng Lai, W. Zhang, J.A.R. Williams, K. Sugden and I. Bennion, "Accurate differential group delay measurement of narrowband fibre devices with immunity to environmental perturbation", *15th IEEE Lasers and Electro-Optics Society Annual Meeting (LEOS)*, Glasgow, UK, ThU1, pp. 811-812, 2002
[34] Yicheng Lai, W. Zhang, J.A.R. Williams, K. Sugden and I. Bennion, "Characterisation of differential group delay of fibre devices with high resolution and enhanced immunity to environmental perturbation", *Electron. Lett.*, 39(1), pp. 26-28, 2003.

Author's patents

[1] Yicheng Lai, W. Zhang, J.A.R. Williams, "Generating electronic carrier signals in the optical domain", EP1343227, US2003219257, WO03075420.
[2] Yicheng Lai, W. Zhang, J.A.R. Williams, "Optical filters having coupled birefringent polarisation maintaining waveguides", GB2377504.
[3] Yicheng Lai, W. Zhang, J.A.R. Williams, I. Bennion, "Bidirectional nonreciprocal optical filter and optical devices incorporating it", European patent application 03252806.9.